

X-660-76-53

PREPRINT

NASA TM X-71097

**PROCEEDINGS OF THE SYMPOSIUM ON
THE STUDY OF THE SUN AND
INTERPLANETARY MEDIUM IN THREE
DIMENSIONS**

(NASA-TM-X-71097) PROCEEDINGS OF THE
SYMPOSIUM ON THE STUDY OF THE SUN AND
INTERPLANETARY MEDIUM IN THREE DIMENSIONS
(NASA) 345 p HC \$10.00

CSCI 03B

N76-24119
THRU
N76-24135
Unclas

G3/92 27466

MARCH 1976



GODDARD SPACE FLIGHT CENTER
GREENBELT, MARYLAND

PROCEEDINGS

of the

SYMPOSIUM ON THE STUDY OF THE SUN
AND INTERPLANETARY MEDIUM
IN THREE DIMENSIONS

held at

GODDARD SPACE FLIGHT CENTER

on

MAY 15-16, 1975

under the sponsorship of

NASA ESA

AMERICAN ASTRONOMICAL SOCIETY

AMERICAN GEOPHYSICAL UNION

The proceedings were edited by

L. A. FISK
Laboratory for High Energy Astrophysics
Goddard Space Flight Center
Greenbelt, Maryland

W. I. AXFORD
Max-Planck Institute for Aeronomy
Katlenburg-Lindau, Germany

March 1976

PREFACE

On May 15-16, 1975, a symposium was held at the Goddard Space Flight Center on the Study of the Sun and Interplanetary Medium in Three Dimensions. The symposium brought together more than 200 scientists from the U. S. and Europe to discuss the importance of exploring the interplanetary medium, and viewing the Sun over a wide range of heliographic latitudes. Among the topics discussed were the missions that NASA and ESA are currently considering for possible flight out of the ecliptic plane, and the likely scientific returns of these missions in the areas of solar, interplanetary and cosmic-ray physics. The symposium was sponsored by NASA and ESA, and was a topical meeting of the American Astronomical Society and the American Geophysical Union.

In this proceedings an attempt has been made to provide a complete summary of the content of the symposium. J. A. Simpson has kindly summarized the various options for out-of-the-ecliptic missions. The speakers who addressed the likely scientific returns from these missions have in most cases provided detailed summaries of their remarks. In cases where a full summary was not available, an abstract has been provided. In addition, K. C. Hsieh has kindly provided an article on direct measurements of neutral gas out of the ecliptic. Time was not available at the symposium for presentation of these interesting ideas.

The organizing committee of the symposium is very grateful to the authors, all of whom have busy schedules, for providing detailed summaries of their talks. We would also like to express our sincere appreciation to Mrs. Sandy Schraeder and Mrs. Martha Harding for their invaluable help in organizing the symposium.

A list of all the speakers at the symposium, and their topics is given in Appendix A to this proceedings. A list of all the attendees at the symposium is provided in Appendix B.

L. A. Fisk
W. I. Axford

TABLE OF CONTENTS

	Page
Some Introductory Remarks	1
CHAPTER I - THE MISSIONS	
Experiments Out of the Solar System Ecliptic Plane: An Introduction to the Execliptic Mission; J. A. Simpson	10 ^{D1}
An Alternative Option to the Dual-Probe Out-of- Ecliptic Mission Via Jupiter Swingby; G. Colombo, D. A. Lautman and G. Pettengill	37 ^{D2}
CHAPTER II - SOLAR PHYSICS	
Out-of-Ecliptic Studies of Coronal Holes and Their Relation to the Solar Wind; R. W. Noyes	48 ^{D3}
Solar Magnetic Fields and the Corona; G. Newkirk, Jr.	59 ^{D4}
3-D Solar Radioastronomy and the Structure of the Corona and the Solar Wind; J. L. Steinberg and C. Caroubalos	65 ^{D5}
CHAPTER III - SOLAR WIND	
IPS Observations of the Solar Wind Speed Out of the Ecliptic; W. A. Coles and B. J. Rickett	84 ^{D6}
Latitudinal Properties of the Solar Wind from Studies of Ionic Comet Tails; J. C. Brandt	95
Implications of Saito's Coronal Density Model on the Polar Solar Wind Flow and Heavy Ion Abundances; W. C. Feldman	108
Thermal Properties of the Solar Wind at High Lati- tudes; M. D. Montgomery	138 ^{omit}
CHAPTER IV - INTERPLANETARY MAGNETIC FIELDS	
The Large-Scale Magnetic Field in the Solar Wind; L. F. Burlaga and N. F. Ness	142
Three-Dimensional Aspects of Interplanetary Shock Waves; G. L. Siscoe	166

(Continued)

(Continued)

TABLE OF CONTENTS

	Page
CHAPTER V - SOLAR AND GALACTIC COSMIC RAYS	
Cosmic-Ray Transport Theory and Out-of-the-Ecliptic Exploration; J. R. Jokipii	188
Cosmic-Ray Modulation in Three Dimensions; J. J. Quenby	210
Cosmic-Ray Access at Polar Heliographic Latitudes; H. J. Völk	217
Solar Cosmic-Ray Measurements at High Heliocentric Latitudes; K. A. Anderson	231
Coronal Propagation: Variations with Solar Longi- tude and Latitude; G. Wibberenz	261
CHAPTER VI - INTERPLANETARY DUST/INTERSTELLAR NEUTRAL GAS	
Investigation of Interplanetary Dust from Out-of- Ecliptic Space Probes; H. Fechtig, R. H. Giese, M. S. Hanner and H. A. Zook	298
A Means of <u>In Situ</u> Measurements of Neutral H and He on an Out-Of-the-Ecliptic Mission; K. C. Hsieh	321
APPENDIX A - THE PROGRAM	329
APPENDIX B - ATTENDEES	333

Some Introductory Remarks

Over the years studies of the Sun and interplanetary medium have occupied the attention of a sizeable fraction of the space community, and have constituted a considerable portion of NASA and ESA's efforts in space science. And rightly so. We attempt in this subject to understand our local environment in space.

With our continuous and in some cases in situ observations, we also provide in this subject detailed testimony as to what physical processes are possible on a star and in an astrophysical plasma. Our studies of the solar environment thus influence our thinking as to what is possible in other astrophysical settings. In some cases the influence is quite direct. For example, the solar wind should exhibit many of the properties of stellar winds. Shock waves in interplanetary space may resemble those in interstellar space. The behavior traits of cosmic rays propagating in the interplanetary magnetic field should be similar to those of cosmic rays in the galaxy. And so on.

All of the spacecraft that NASA and ESA have flown to study the Sun and interplanetary medium, however, have been limited in one major respect. None of these spacecraft have penetrated off the equatorial plane of the Sun by more than about $\pm 10^\circ$ in heliographic latitude. We have thus sampled particle emission from the Sun, or interstellar matter

impinging on the solar cavity (e.g. galactic cosmic rays), only over a narrow range of latitudes. The look-angle for studying photon emission from the Sun is similarly limited.

This latitude limitation would not be serious, of course, if we had any expectation that conditions in the solar environment were invariant with latitude. However, even the most cursory of examinations of a white light photograph of a solar eclipse reveals a strong latitude dependence for conditions in the corona. Sun-spot and flare activity is known to be concentrated in the mid-latitude regions on the Sun. Interplanetary scintillation studies suggest that the flow of the solar wind is faster and more turbulent over the solar poles, than it is in the equatorial plane (See Coles and Rickett, in this proceedings). The expected Archimedes spiral pattern of the interplanetary magnetic field may cause the ratio of thermal to magnetic pressure of the solar wind to vary strongly with latitude, thus resulting in a plasma over the poles which has substantially different properties from the local solar wind. This same field pattern may let low energy galactic cosmic rays (< 100 MeV) penetrate unopposed into the region of the solar poles, whereas such particles are excluded from the inner solar system near earth. And the list goes on.

We are thus forced to conclude that, to date, spacecraft exploration of the interplanetary medium, and measurements of the Sun which are look-angle dependent, have studied a non-representative sample of our total solar environment.

We have studied in only two dimensions, what is a three-dimensional structure. We have not sampled the full variety of astrophysical conditions that are available to direct measurements in our local environment. Thus, we have not adequately broadened the base of knowledge that we can use for deciding what is possible in other astrophysical settings.

An Out-of-the-Ecliptic (O/E) Mission, in which the interplanetary medium is explored, and the Sun is viewed over a wide range of heliographic latitudes, will provide the measurements that can help replace our current parochial view, with a more accurate assessment of our local environment in space.

The Current Status of the O/E Mission

At the time of the publishing of these proceedings, NASA and ESA are engaged in a Phase A study of an O/E mission, which could be launched in the early 1980's. Two possible missions, a primary and a backup, are currently under consideration. In the primary mission two spacecraft are to be launched simultaneously by the shuttle, with the Interim Upper Stage (IUS) - 4 stage booster. The spacecraft, which would be similar in design to Pioneers 10 and 11, would then fly to Jupiter. There, one of the spacecraft would be targeted so that after encounter it passes up out of the ecliptic plane and over the north pole of the Sun. The other spacecraft would be targeted so that it passes over the south solar pole. Following their polar passes, each of the space-

craft would return to the ecliptic plane, and then would fly up over the opposite solar pole. In the backup mission, one spacecraft is launched from the shuttle /IUS - 2 stage. This spacecraft is targeted at Jupiter to pass over one of the solar poles, return to the ecliptic plane, and then fly up over the opposite solar pole. In both missions the spacecraft can obtain high heliographic latitudes (80°).

The major advantages to the primary mission are:

(i) It will provide simultaneous measurements of conditions in the northern and southern hemispheres of the Sun. (ii) The total science payload (both spacecraft) carried in this mission is large (60 kg). (iii) The two spacecraft passing by Jupiter will provide an interesting opportunity to distinguish spatial from temporal effects in the Jovian magnetosphere. Indeed, this mission may provide the only opportunity in the foreseeable future when two spacecraft are simultaneously near Jupiter. The advantage for the backup mission is, of course, in cost. It costs less than the primary mission, and yet it still provides a survey of conditions at high heliographic latitudes.

In the primary mission, it is planned that ESA would build one of the spacecraft, and NASA, the other. In the backup mission, the spacecraft would be provided by ESA. In both missions, NASA would provide the launch vehicle and the RTG power supplies.

The Phase A study will be completed in the spring of

1976. After this time, NASA and ESA will decide whether or not to proceed with a joint O/E mission. A decision can be expected in the summer of 1976 as to whether a Phase B study of one of these mission options (or some other option) will be undertaken.

Details on the primary and backup mission, as well as on other options for O/E missions, can be found in the review paper that J. A. Simpson has kindly written for this proceedings. It should be noted also that a particularly interesting variation on the O/E mission is discussed in the proceedings in the paper by G. Colombo, D. A. Lautman, and G. Pettingill. In this variation, one of the two spacecraft in the two-spacecraft, Jupiter-swingby mission is a solar probe, which after encounter with Jupiter is directed back at the Sun along a nearly rectilinear path. Accurate measurements of the quadrupole moment of the Sun can be made from the solar probe, as well as in situ measurements of the solar wind in the corona.

O/E Science

Some information on the flow speed of the solar wind at the higher heliographic latitudes can be obtained from observations of interplanetary scintillations, and also from observations of ion comet tails. In this proceedings we have included a paper on scintillation observations by W. A. Coles and B. J. Rickett, and one on studies on comet tails by J. D. Brandt. It is interesting to note, however,

that the conclusions of these two papers on the behavior of the average wind speed are substantially different. These differences may be reconcilable, as Coles and Rickett suggest. However, such discrepancies in indirect observations emphasize the need for direct in situ measurements.

The remaining papers and abstracts in this proceedings discuss the impact that an O/E Mission will have on studies of the solar corona, solar x-ray and EUV emission, solar radio astronomy, the solar wind, the interplanetary magnetic field, solar and galactic cosmic rays, interplanetary dust and zodiacal light, and interstellar neutral gas. It is recognized immediately from this list that O/E science is highly multi-disciplinary, involving many areas of solar and cosmic-ray physics, and all areas of interplanetary physics. There are also many different topics in each area which will be affected by O/E measurements. It is not the purpose of this proceedings to give an exhaustive survey of all possible topics. Rather, we have simply highlighted here some of the more interesting problems in O/E science. In this same context, it should be recognized that an O/E mission is exploratory, and as such is certain to uncover new phenomena. It is one of the axioms in the space program that when we fly where we have never been before, we uncover phenomena that we cannot anticipate in advance.

The papers and manuscripts in this proceedings have been reproduced directly from the typescripts provided by the authors. In addition to considering scientific questions,

the authors in some cases have discussed the heliographic latitude that an O/E mission must obtain for best results in their particular area. NASA and ESA requested that such information be provided in the talks at the symposium.

CHAPTER I

THE MISSIONS

PRECEDING PAGE BLANK NOT FILMED

N76-24120

Experiments Out of the Solar System

Ecliptic Plane: An Introduction
to the Execliptic Mission*

J. A. Simpson

Enrico Fermi Institute and Department of Physics
University of Chicago
Chicago, Illinois 60637

February 28, 1976

I. Introduction

The dramatic step made possible by direct measurements in space with satellites and probes during the past 18 years has totally altered our concepts of the Sun, the interplanetary medium, and their influences upon Earth. This has been achieved with observations confined solely to the vicinity of the equatorial plane of the solar system. From these two-dimensional investigations we have made dubious attempts to extrapolate our knowledge to deduce what the Sun and space in the solar system is like in three-dimensions. However, the solar, interplanetary and galactic phenomena discovered in these years have raised many urgent scientific questions which can only be answered by direct observations and experiments far out of the ecliptic plane and over the solar pole to achieve a "global" concept of the Sun, the interplanetary medium, and their relationship to Earth and the boundary of the heliosphere with the interstellar medium. We have been faced for many years with this age-old problem which occurs often in science, namely, the extrapolation of physical phenomena from two-dimensions to deduce phenomena in three-dimensions. The uniqueness and importance of

* Based upon invited talk at "Symposium on the Study of the Sun and Interplanetary Medium in Three Dimensions" -- May 15-16, 1975, Goddard Space Flight Center, Greenbelt, Maryland, and "Charged Particle Astronomy in Interplanetary Space at High Solar Latitudes", J. A. Simpson, Chap. 5.3; NASA collected papers for ESRO Document MS(74) 34 (1974).

a scientific mission which can directly achieve this global study and the recognition of its potential for discovery has been clear for many years. In describing such an exploratory mission, it is not unfair to make a comparison between the importance of Man's exploration of the spherical surface of the Earth, and an ex-ecliptic mission, which is qualitatively similar in its conceptual and practical consequences for space science to the impact of the full exploration of Earth on Man's intellectual advancements.

If a mission out of the ecliptic is so vital to the advancement of science then why has it not become a reality by now since the technology for its accomplishment has been with us for several years, and Pioneers 10 and 11 have demonstrated that a Jovian gravity-assist to drive a probe out of the ecliptic is safe? Among the reasons appears to be the broad, interdisciplinary character of the most important investigations on the mission which, on the one hand, represents the greatest strength of the mission, but, on the other hand, becomes a source of weakness for marshalling the sources and the support of the scientific community, or even leadership within the federal agencies where the missions must successfully compete with other important types of space missions. Since the late 1950's an out of the ecliptic mission has been under discussion.¹ Now, hopefully, it is a mission whose time has come since it has recently elicited support from a wide segment of the scientific community on the basis of its uniqueness and importance for science and the applications of science to our understanding of the Sun and its influence upon Earth. Furthermore, as has been the case for the space program to date in the equatorial plane, out-of-the-ecliptic observations are almost certain to yield important, unanticipated discoveries. We can best describe the quality of the mission objectives as exploratory and interdisciplinary and, therefore, the investigations must be designed to encompass the unexpected.

The purpose of this note is to summarize the most likely alternatives for carrying out a mission to achieve these broad scientific goals and to illustrate with specific examples drawn

from charged particle astronomy, interplanetary and solar physics some of the experiments and observations which may be carried out. It is not within the scope of this note to describe in detail the many exciting scientific challenges opened by the mission, but the reader easily will perceive this wide range of possible investigations, many of which are discussed in the Proceedings of this Symposium² or outlined by Page.³ As a basis for discussion of the regions of the Sun and interplanetary space which may be explored by exoecliptic missions I have prepared in Figure 1 a schematic representation of the main solar latitude zones of highest interest and their possible interfaces with the interplanetary medium. In the following discussion we will summarize some of the alternative missions which reach into these regions of space and the constraints they place upon experiments. As a secondary objective we shall also describe the opportunities which some of these missions provide for unique studies of the magnetosphere of Jupiter since, for the most likely mission choices, Jupiter becomes the "gateway" to space out of the ecliptic.

II. Ten Ways to Get There

Table 1 is a summary of the most outstanding mission alternatives. There is a long history of successive proposals for these missions based primarily on available launch vehicle technology, hence some of the alternatives presented in Table 1 now are only of historical interest. Basically, the mission options are dependent on launch vehicle capabilities. Direct ballistic injection at ~ 1 a. u. (option 7 and 8) even under optimum conditions will take a spacecraft only to $\sim 37^\circ$ heliographic latitude. The addition of solar electric propulsion (SEP) makes it possible to achieve a spacecraft trajectory oscillating in latitude at 1 a. u., and synchronous with Earth thus scanning over a north-south latitude range that reaches a limit of $\pm \leq 60^\circ$ within 2.7 years, under maximum launch capabilities (option 9, for details see reference 4 and 5). The trajectory plotted in a plane at 1 a. u. is shown in Figure 2. This type

of latitude scanning spacecraft, which must be triaxially stabilized would place a strong emphasis on extending present solar observations being made at Earth to stereoscopic viewing of these solar phenomena.⁴ The rate of technical development of solar electric propulsion, however, is such that no possibility exists for considering this option in the early 1980's. Furthermore, from Figure 1 see that all of the direct injection missions discussed above do not allow observations in situ beyond the zones of solar activity and leave open all questions which could only be answered by attaining higher solar latitudes. As will be shown below, the polar cap-to-polar cap passes of Jupiter swingby missions will achieve the latitude scans of the SEP missions, although for a shorter interval of the solar cycle.

The alternative to direct injection is a gravity assist by Jupiter, i. e. by a Jupiter swingby (JSB) -- a technique first proven by Pioneer-10 to achieve a solar system escape trajectory.⁶ This technique makes it possible to achieve solar polar cap passes with maximum latitudes depending on the launch constraints (options 1 - 6). Among those options that achieve polar cap passes of $\geq \pm 80^\circ$, options 1, 2, 3 and 6, offer the greatest potential for achieving our stated prime objectives of exploration and discovery. Option 6 enables a single spacecraft to reach $\sim 79^\circ$ solar latitude with an Atlas/Centaur vehicle by requiring an Earth swingby as shown in Figure 3. However, in addition to the increased time to reach solar maximum latitude (1.7 years longer), this mission suffers further from reduced reliability because it requires an additional spacecraft propulsion subsystem to undertake two additional and critical spacecraft maneuvers as described in Figure 3. We focus on the most fruitful of all the JSB options, hopefully the most likely to be adopted, namely a dual spacecraft launch to Jupiter (options 1 or 2) which will result in spacecrafts over both solar polar caps simultaneously with trajectories as shown in Figure 4 passing from pole-to-pole in opposition. We refer to this type of mission as the tandem Jupiter swingby (TJSB).

III. The Tandem Jupiter Swingby Mission

In Figure 4 we have identified the two spacecrafts as A and B and have shown their trajectories from Jupiter swing-by until after their respective pole-to-pole passes at the Sun, all as a function of time. Although this example⁷ is for option 2 in Table 1, the trajectories for option 1 will be similar. From the point of view of scientific investigations in different disciplines, e.g. solar physics, interplanetary plasma and magnetic field, the magnetosphere of Jupiter, cosmic rays, etc., the mission is logically to be divided into five phases identified by portions of the spacecraft trajectories. These are: (I) from Earth to Jupiter, (II) through the Jovian magnetosphere, (III) out-of-the-ecliptic simultaneously in the northern and southern hemispheres over the radial range $\sim 1.5 - 5$ a.u., (IV) over the solar pole, and pole-to-pole transits of the two spacecrafts, and (V) post solar pole trajectories. In each phase there are some prime mission goals for one or more of the scientific investigations. In the following discussion we take the reader on a "guided tour" through these five phases of the TJSB missions using illustrative scientific investigations which will lead to discovery or the answer to old questions. Although it is not possible to discuss in this note all the important scientific objectives of each phase, these trajectories provide a rich source of new investigations with each phase of the mission possessing its own set of unique scientific objectives.

Phase (I): Earth to Jupiter

The two spacecraft travel near the ecliptic plane with a radial-spatial separation of order 10^6 kilometers and with simultaneous transmission of data. This separation makes it possible for us to undertake a new family of studies, since never before have spacecraft been so separated for a long period of time free from the influence of a nearby planet and never before have we had the opportunity to do correlative studies between closely spaced observation points over a large radial range. For example we may undertake:

- a) the study of charged particle-magnetic field interactions, especially for very low energy nuclear particles in the range 0.1 to 1 MeV. This spacecraft separation distance becomes comparable to the correlation length of the interplanetary magnetic field and to the scattering scale size of the particles.⁸
- b) the study of the modes of propagation and interaction with magnetic fields in interplanetary space of the electrons which have been recently found to be escaping from Jupiter.⁹⁻¹¹
- c) measurements of the interplanetary acceleration of protons¹² and electrons in the regions surrounding blast waves from the sun.¹³ It will also become possible to investigate in detail the forward-backward moving shocks which are now observed to be associated with so-called "interplanetary active regions".¹⁴ These active regions and shocks are also associated with enhanced fluxes of ~ 1 MeV protons.¹⁵

This phase of the mission corresponds to an interplanetary version of the smaller scale Mother-Daughter satellite combination devoted to magnetospheric studies in the period 1977-1980. No other interplanetary mission studies of the above type have been made, or are contemplated in the foreseeable future.

Phase (II): Jovian magnetospheric studies

Since for operational reasons the two spacecrafts in opposite hemispheres will have times of closest approach 2 to 3 days apart, we obtain a unique and valuable separation of the two spacecrafts in the Jovian magnetosphere capable of attacking problems that could not be investigated by the Pioneer 10-11 spacecraft, the Mariner-Jupiter-Saturn spacecraft, or even a single Jupiter orbiter spacecraft. In Figure 5 we display a meridional plane projection

of the trajectories of the two spacecraft A and B. Figure 6 is a projection of the two spacecraft trajectories on the ecliptic plane. For comparison the Pioneer-11 encounter trajectory to Saturn is shown. At the time of closest approach for spacecraft A (position 1), spacecraft B is at a distance of $\sim 50 R_J$, and when spacecraft B is at closest approach (position 10) spacecraft A has moved to $\sim 50 R_J$. Thus it should be possible to separate large scale spatial from temporal effects in the Jovian magnetosphere. It will also be possible to obtain measurements at four magnetic latitudes for each radial distance. Some of the key problems to be attacked are: (a) investigations of the variation of the radial position of the bow shock with time, and (b) the distortions of the magnetospheric boundary in response to fluctuations in the strength and direction of the solar wind and the rotation of the magnetosphere. An important feature of the Jovian magnetospheric observations possible with the TJSB mission is the simultaneous measurement of the solar wind outside the magnetosphere by one spacecraft while measurements within the magnetosphere are under way with the second spacecraft. (c) The nature of the "global" time dependent 10 hour variations of electron intensity and spectrum within the magnetosphere^{6, 9, 16}; how is this effect related to the rotation effects of the equatorial plasma sheet and the spatially dependent 10 hour variation? This in turn is related to the problem of the mechanism for the release of electrons from Jupiter into interplanetary space. (d) Jovian satellite interactions with the trapped radiation; special opportunities exist whereby it is possible to cross the flux tubes associated with the satellite Io and thus to investigate the nature of the control exerted by Io over decametric radio bursts.⁶

In sum, the dual spacecraft out-of-the-ecliptic mission will answer questions which would otherwise remain a puzzle for studies made with a single spacecraft.

Observations made with Pioneer 10 and 11 have established the importance of transient phenomena^{6, 16} for the magnetosphere of Jupiter, such as large scale distortions.

Observations with a single spacecraft cannot unambiguously separate the temporal and spatial dependences of such transient effects, so that a dual spacecraft mission offers our best hope for gaining a further understanding of the physics of the Jovian magnetosphere.

Phase (III): Out-of-the-ecliptic at large radial distances

Figure 4 illustrates the trajectory characteristics for spacecrafts A and B as a function of time after a Jovian swingby. In a period of ~ 2 years, the two spacecrafts traveling in the opposite hemispheres of the interplanetary medium cover a radial distance of ~ 4 a. u. while slowly traversing a solar latitude range of up to nearly 90° .

This phase of the mission offers the opportunity to take snapshots of solar active regions on the sun, (EUV, UV, x-rays, radio, etc.) for comparison with identical observations from Earth to form stereoscopic pictures of solar phenomena. It also becomes possible to investigate new aspects of the Gegenschein.²

This phase of the mission also offers the opportunity to study the behavior of magnetic sector structure at large radial distances from the Sun in the solar activity zone (Figure 1) to answer such questions as: (a) What role does the region of solar activity (10 to 35 degrees) play in determining the sector structure of magnetic fields extending from 1 to 5 a. u. ? (b) To what extent does the magnetic sector structure persist at high latitudes and at great distances from the Sun? (c) How does the Sun's differential rotation, which produces a rotation period 9 days longer at the pole than at the equator, change the structure of interplanetary magnetic fields? These and questions concerning the "global shape" of blast waves in the two hemispheres constitute major magnetic field and plasma studies for this phase of the mission. The characteristics of this region for charged particle propagation for both solar and galactic particles are entirely unknown, and their determination would be the prime goal of charged particle studies in this region.

Phase (IV): The polar observations at the Sun from ~ 1.2 - 2 a. u.

A. Solar observations from the polar viewpoint.

The evolution of coronal features above solar active regions, coronal streamers and related transient, large scale phenomena -- now observable only by solar limb studies from Earth -- may be undertaken from the A or B spacecraft by time-lapse observations obtained simultaneously at all solar longitudes. Coronagraphic studies on a spinning spacecraft are difficult, but the potential is great for understanding the origin and dynamical structure of the inner and outer corona from simultaneous, polar and equatorial observations (J. A. Simpson to G. Newkirk, private communication, 1968).

B. Solar interplanetary studies.

Somewhere in the region tentatively identified as the transition region above solar latitude $\sim 60^\circ$, characteristics of the interplanetary medium increasingly become determined by the properties of the sun and corona in the polar regions. For example, it is currently believed that the polar region may be represented by a coronal hole where a continuous emission of the solar wind at high velocities (> 700 km/sec) is expected.¹⁷ It is in this region that the rotational effects of the Sun cease to play a major role in the large-scale structure of the magnetic field carried into interplanetary space by the solar wind. The properties of this region are unknown and expected to be totally different from those so far studied in the vicinity of the equatorial plane. For studies in this region it is vital that measurements in the north and south polar regions be made simultaneously since it is well-established that both the temporal and spatial distributions of observable solar phenomena in the polar regions are frequently different at the two poles.¹⁸ In addition to the particle, magnetic field and plasma interactions which will be studied for the first time under these new physical conditions, we point out that low energy particles from the galaxy may find a relatively easy entry to this

region, as discussed below.

As shown in Figure 4, the two spacecrafts pass from pole to pole in periods the order of 260 days (or on an average of $\sim 0.7^\circ$ per day). This corresponds to an elapsed time of ~ 10 solar rotations when the two spacecrafts are at radial distances ~ 1.2 to 1.5 a.u. Clearly radially dependent effects are likely to be small compared with latitudinally dependent phenomena being studied simultaneously on the two spacecraft. The observations to be made and the scientific objectives of Phase IV of the dual spacecraft are essentially the same as those for the SEP mission (options 9 and 10). Both missions provide a scan of solar latitude at a rate of $\sim 0.4 - 0.7$ degrees per day at approximately constant radial distance from the Sun, although the dual spacecraft mission provides coverage of the polar region of the Sun, while the SEP mission does not. Among the latitude dependent phenomena to be investigated are (a) the effect of differential rotation on the magnetic field structure in interplanetary space; (b) the nature of the transition region from the polar coronal holes to the band of solar activity (Figure 1); (c) the nature of transient phenomena such as shocks and high velocity streams at high solar latitudes. Measurements relating to these questions made in Phase IV are distinguished from similar measurements in Phase III by the fact that the radial position of the spacecrafts is not an important parameter during Phase IV, thus providing a clean separation of latitudinal and radial effects.

It is likely that the combined direct solar observations, magnetic field, plasma and high energy particle studies will introduce a qualitative change in our understanding of the differential rotation of the Sun, of the ~ 22 year magnetic cycle and, thereby, in our understanding of the internal dynamics of the Sun.

C. Galactic composition of cosmic radiation.

In part B above, measurements during the pole-to-pole excursion of the

two spacecrafts were concentrated on the electrodynamics of the interplanetary medium and the role of the solar features in determining the dynamics of the medium. If conditions over the solar poles are anywhere near those predicted it would appear that cosmic ray particles of low energy from the galaxy which cannot otherwise propagate into the inner part of the solar system near the equatorial plane because of solar modulation may be able to penetrate by way of the solar polar magnetic fields to within $\sim 1 - 2$ a. u. If so, we may be able to obtain for the first time samples of the energy composition of galactic cosmic rays; that is, the relative abundances of the elements in the nuclear component of the cosmic rays and the relative isotopic abundances of hydrogen to nickel. Through such studies it may become possible to identify the low energy component of cosmic rays accelerated in our local region of the galactic arm. These studies will be of vital importance for deciding among models of nucleosynthesis of the elements in the sources of cosmic rays. Furthermore, under such circumstances, it would become possible to obtain the energy densities in interstellar space for these very low energy particles (a problem concerned with the heating of interstellar clouds).

Finally, all of these investigations over the solar pole when taken together with observations in the equatorial plane will yield a "global" model for solar modulation which takes account of the propagation of nuclear particles and electrons extending downward in energy to energies where at present their modulation is not understood. Recent observations^{19, 20} show that even at higher energies, revisions of our ideas about modulation may be required, possibly involving processes taking place off the ecliptic plane²¹, or introducing interstellar neutral particles in the heliosphere.²² The IMP satellites and Pioneer 10/11 deep space probe observations have raised a number of interesting questions regarding whether or not low energy particles could have access to the solar equatorial zone.

D. Energetic particles of solar origin.

The role of coronal transport in the propagation of solar particles from flare sites to the interplanetary medium has been much studied but is not well understood.²³⁻²⁶ Out-of-the-ecliptic missions will play a major role in deciding on the transport mechanism, on the storage time and distribution of particles at the sun, and, in turn, while using solar particles as probes of the intervening magnetic fields, will obtain information on the near-sun magnetic field structure including the distribution of irregularities in the magnetic field. It may be possible that the effects of differential rotation can be analyzed best by studying the emission of solar flare particles at high solar latitudes.

E. Models of the heliosphere.

At the present time we cannot choose conclusively among models of the heliosphere with boundaries for particle modulation which, for example, could be a) pancake-like in character, extending the order of say 20 to 50 a.u. in the equatorial region, but only a few astronomical units thick over the poles, or b) with distant boundaries over the solar poles and therefore much more spherical in character, as sketched in Figure 7.²⁷ Although these two examples represent extremes, it would appear that data obtained out-of-the-ecliptic plane could assist in deciding between them by using galactic cosmic rays as probes of the outer magnetic fields of the interplanetary medium. Predictions for the charged particle gradients, particle anisotropies and energy spectral changes as a function of solar latitude can be made; therefore a wide range of models can be tested by the dual spacecraft mission (e.g. reference 28).

Phase (V): Post solar polar observations

The above four phases of the dual mission illustrate the wide range of physical processes which can be studied during the mission. After leaving the sun the dual spacecrafts again travel outward from the Sun where they are able to repeat some of the observations which were obtained between Jupiter and the Sun in Phase III as much as a half solar cycle earlier.

These latter measurements would indeed be very interesting since they can provide further evidence on the long-term changes in the heliosphere, especially in the latitudinal structure of the interplanetary magnetic fields.

IV. Summary Remarks

We conclude from the mission alternatives that the latitude scan missions such as the SEP options 9 and 10 (Figure 2) are dedicated to more detailed observations and exploration of the solar active zones (Figure 1) with a strong emphasis on extending the stereoscopic viewing of the solar phenomena now under observation with Earth orbiting satellites. On the other hand, the solar polar cap passes further extend the exploration of new regions of the Sun and interplanetary medium, the evolution of solar coronal features seen simultaneously at all solar longitudes, and the possible access of low energy particles from interstellar space via the polar magnetic fields. Such particles can not be detected with deep space probe missions near the equatorial plane in the foreseeable future. Thus, in many aspects both types of missions are important for science, but are qualitatively different in their goals.

With regard to strategies, the TJSB missions offer the unique advantage of providing well-defined interfaces for international collaborations since one spacecraft could, for example, be the responsibility of the European Space Agency while the second spacecraft could be the responsibility of the NASA.

Some instruments should cover the same measurements simultaneously on both spacecrafts, e. g. magnetic fields, plasmas, charged particles and x-rays. However, in addition one spacecraft could carry a set of complex instruments to complement the other spacecraft, viz. a coronagraph on one spacecraft, and a complex super-thermal particle spectrometer and solar radio emission detector on the other spacecraft.

Although Table 1 suggests a wide range in costs based upon the launch vehicle, the ultimate difference between a single spacecraft JSB mission and TJSB mission is really less than indicated because the same magnitude of commitment and resources is required for scientific instrument preparation and integration, for data acquisition throughout the years of the mission and, most important, for the level of commitment of those in the scientific community motivated to undertake such a long term enterprise.

The need for simultaneous measurements at Earth during an execliptic mission must not be overlooked in order to separate spatial from temporal changes in solar interplanetary phenomena, and to relate these observations to the present day scientific knowledge derived from equatorial measurements.

Ingenious experiments and observations have been reported for many years to explore the high solar latitudes near the Sun and interplanetary space. These include the use of radio waves from distant stars to study the magnetic irregularities and electron densities near the Sun, the observation of comet tails at high latitudes and the scintillation effects of galactic cosmic rays to deduce properties of the solar wind, and the large-scale probing of the interplanetary medium by high energy cosmic rays to estimate the scale size of the heliosphere. However, they cannot substitute for direct observations in the regions of the solar system to be penetrated by an execliptic mission.

The author apologizes for not adequately covering in this note the many alternate mission options with their unique scientific objectives.

He wishes to thank Dr. Bruce McKibben and Mr. John Niehoff for assistance with the preparation of materials for this manuscript, and Mr. Dan Herman of NASA and Mr. H. F. Matthews of the NASA/Ames Research Center for providing essential background material. This work was supported in part by NASA grant NGL 14-001-006.

References

1. Simpson, J. A., B. Rossi, A. R. Hibbs, R. Jastrow, F. L. Whipple, T. Gold, E. Parker, N. Christofilos, and J. A. Van Allen, Round-Table Discussion, J. Geophys. Res. 64, 1691, 1959; Fields and Particle Astronomy, Simpson, J. A., W. A. Fowler, F. B. McDonald, N. G. Ness, E. N. Parker, A. W. Schardt, p. 202-222, Long Range Program in Space Astronomy, R. Doyle (Ed.), U. S. Government Printing Office (NASA SP-213), Washington, D. C., 1969.
2. Proceedings of the Symposium on the Study of the Sun and Interplanetary Medium in Three-Dimensions, L. A. Fisk and W. I. Axford (ed.), NASA/GSFC X-document #660-76-53, 1976.
3. Page, D. E., Exploratory Journey Out of the Ecliptic Plane, Science 190, 845, 1975.
4. Out of Ecliptic and Solar Stereoscopic Mission, ESRO Document MS(74) 34, p. 14 (1974).
5. Duxbury, J. H., Two Mission Options for an Out-of-Ecliptic Mission, Jet Propulsion Laboratory Document No. 661-2, 1975.
6. Collected papers on the Pioneer 10 Mission: Jupiter Encounter, J. Geophys. Res. 79, 3467-3674, 1974.
7. Matthews, H. F., Report on the JSB Tandem Mission, NASA Ames Research Center, 1974.
8. Jokipii, J. R. and P. J. Coleman, Jr., Cosmic Ray Diffusion Tensor and Its Variation Observed with Mariner 4, J. Geophys. Res. 73, 5495, 1968.
9. Chenette, D. L., T. F. Conlon, and J. A. Simpson, Bursts of Relativistic Electrons from Jupiter Observed in Interplanetary Space with the Time Variation of the Planetary Rotation Period, J. Geophys. Res. 79, 3551, 1974.

10. Teegarden, B. J., F. B. McDonald, J. H. Trainor, W. R. Webber, and E. C. Roelof, Interplanetary MeV Electrons of Jovian Origin, *J. Geophys. Res.* 79, 3615, 1974.
11. Smith, E. J., B. T. Tsurutani, D. L. Chenette, T. F. Conlon, and J. A. Simpson, Jovian Electron Bursts: Correlation with the Interplanetary Field and Hydromagnetic Waves, *J. Geophys. Res.* 81, 65, 1976.
12. Wibberenz, G. and K. P. Beuermann, Cosmic Plasma Physics, K. Schindler (Ed.) (New York: Plenum Press), p. 339, 1972.
13. Gloeckler, G., F. M. Ipavich, C. Y. Van, and D. Hovestadt, Post-Shock Spikes: A New Feature of Proton and Alpha Enhancements Associated with an Interplanetary Shock Wave, *Geophys. Res. Lett.* 1, 65, 1974.
14. Smith, E. J. and J. H. Wolfe, Observations of Interaction Regions and Corotating Shocks Between One and Five A. U. : Pioneers 10 and 11, *Geophys. Lett.* (in press), 1976.
15. Barnes, C. and J. A. Simpson, to be published, 1976.
16. Simpson, J. A. and B. McKibben, Dynamics of the Jovian Magnetosphere and Energetic Particle Radiation, Chap. in Jupiter (T. Gehrels, Ed.), University of Arizona Press, Tucson, 1976.
17. Skylab, to be published.
18. Bumba, V. and R. Howard, Large Scale Distribution of Solar Magnetic Fields, *Ap. J.* 141, 1502, 1965.
19. Garcia Munoz, M., G. M. Mason, and J. A. Simpson, A New Test for Solar Modulation Theory: The 1972 May-July Low-Energy Galactic Cosmic Ray Proton and Helium Spectra, *Ap. J. (Lett.)* 182, L81, 1973.

20. McDonald, F. B., B. J. Teegarden, J. H. Trainor, and W. R. Webber,
The Anomalous Abundance of Cosmic Ray Nitrogen and Oxygen Nuclei at Low
Energies, *Ap. J. (Lett.)* 187, L105, 1974.
21. Fisk, L. A., Interpretation of the Observed Cosmic Ray Modulation, *Bull. A. P. S.*
18, 664, 1973.
22. Fisk, L. A., B. Koslovsky, and R. Ramaty, An Interpretation of the Observed Oxygen
and Nitrogen Enhancements in Low Energy Cosmic Rays, *Ap. J. (Lett.)* 190, L35, 1974.
23. McKibben, R. B., Azimuthal Propagation of Low Energy Solar Flare Protons: Interpretation
of Observations, *J. Geophys. Res.* 78, 7184, 1973.
24. Reinhard, R. and G. Wibberenz, Propagation of Flare Protons in the Solar Atmosphere,
Solar Phys. 36, 473, 1974.
25. Roelof, E. C. and S. M. Krimigis, Analysis and Synthesis of Coronal and Interplanetary
Energetic Particle Plasma and Magnetic Field Observations Over Three Solar Rotations,
J. Geophys. Res. 78, 5375, 1973.
26. Simnett, G. M., The Release of Energetic Particles from the Sun, *Solar Phys.* 20,
448, 1971.
27. Wang, J. R., Dynamics of the Eleven Year Modulation of Galactic Cosmic Rays,
Ap. J. 160, 261, 1970.
28. Volk, H. J., G. Morfill, W. A. Alpers, and M. A. Lee, Spatial Dependence of the
Pitch-Angle and Associated Spatial Diffusion Coefficients for Cosmic Rays in
Interplanetary Space, *Astrophys. Sp. Sci.* 26, 403, 1974.

Table 1
SOLAR EXECLPTIC MISSION OPTIONS FOR THE EARLY 1980's

Option	Flight Mode ^f	Launch Vehicle	No. of Spacecraft	Total S/C (Science*) Mass, KG	Max. Solar Lat., Deg. [#]	Spin (SP) or Stable (ST) S/C	Launch Year(s)	Time to Max. Lat., Years	Heliographic Coverage	Cost Bracket ^d
(1)	JSB	Shuttle/IUS(3)/TE 364	2	550(60)	84	SP	1981, 83	3.9	Opposed passes, ± latitude scans	Med-Hi
(2)	JSB	Titan/Cent/-45 ^{a, b}	2	500(60)	90/90	SP	1980, 81, 83	~4	Opposed single passes ± latitude scans	Hi
(3)	JSB	Shuttle/IUS(2)/TE 364	1	300(30)	88	SP	1981, 83	3.9	Single pass to ± 88°	Lo-Med
(4)	JSB	Atlas/Cent/-45 ^b	1	250(30)	39	SP	1980	~4	Single pass	Med
			1	150(15)	77	SP	1980	~4	Single pass	Lo-Med
(5)	JSB	Delta 3914/★27 ^c	1	150(15)	~30	SP	1981, 83	~4	Single pass	Lo
(6)	ΔVEGA + JSB	Atlas/Centaur/TE 364	1	300(30)	79	SP	1982	5.6	Single pass to ± 79°	Med
(7)	DB	Titan/Cent/-45 ^{a, b}	1	250(30)	34	SP	1980-83	~0.2	Single lat. scan ~ 1 a.u.	Med-Hi
			1	150(15)	37	SP	1980-83	~0.2	Single lat. scan ~ 1 a.u.	Med
(8)	DB	Delta 3914/★27 ^c	1	150(15)	24	SP	1980-83	~0.2	Single lat. scan	Lo
(9)	DSLP (15KW)	Titan/Centaur ^a	1	250(30)	59	ST	1981, 82, 83	~2.7	Latitude scans ~ 1 a.u.	Hi
			1	150(15)	62	ST	1981, 82, 83	~2.7	Latitude scans ~ 1 a.u.	Hi
(10)	DSEP (6KW)	Atlas/Centaur ^a	1	250(30)	29	ST	1981, 82, 83	~2.2	Latitude scans ~ 1 a.u.	Med-Hi
			1	150(15)	34	ST	1981, 82, 83	~2.2	Latitude scans ~ 1 a.u.	Med

- a. This vehicle or shuttle/IUS (interim upper stage) equivalent for ≥ 1981 launches.
b. -45: TE 364-4 solid kick motor with spin table.
c. ★27: Star 27 solid kick motor
d. Cost bracket determined on basis of launch vehicles shown, not shuttle equivalents (see footnote a).

- * Science included in spacecraft masses.
Latitudes: Latitudes are heliographic. Hence when tandem spacecraft are launched to solar latitudes less than 90°, one S/C goes below the ecliptic and the other above after swingby, with ~ 14° difference in solar latitude if the swingby is at the solar node.
^f Flight Modes: JSB - Jupiter Swingby
VEGA- ΔV - Earth Gravity Assist
DB - Direct Ballistic
DSEP - Direct Solar Electric Propulsion

REPRODUCIBILITY OF THE
ORIGINAL PAGE IS POOR

Figure Captions

Figure 1 Idealized meridional plane view of the interplanetary regions associated with principal features on the sun. The shaded region represents a region $\pm 7^\circ$ in solar latitude within which all measurements to date have been made. The region of principal solar activity over a solar cycle extends from 10 to ~ 35 -40 degrees north and south latitudes and is highly variable. A region from ~ 40 to 70 degrees is a transition region between the region of solar activity and the polar region where the rotational effects on the magnetic field carried out by the solar wind begin to subside. It is believed that the polar region is mainly occupied by a coronal hole-like structure and therefore that the solar wind has a high velocity in this region.

Figure 2 The solar electric propulsion mission is one in which the spacecraft remains in a 1 A. U. orbit from the sun and is therefore synchronous with earth. The orbit inclination is increased by thrusting about the nodes. In a period of $\sim 3 \frac{1}{2}$ to 4 years a full excursion of the spacecraft is expected to be between 50 and 60 degrees. The spacecraft is normally thrusting except for ~ 100 days per year at the anti-nodes. However, the spacecraft propulsion can be turned off for a day or so during the normal operating periods to obtain scientific data.
(See references 4 and 5.)

Figure 3 The Δ VEGA flight mode (Δ -Earth Gavity Assist). In this mode the transfer event points are:

Point 1: Earth launch 4/18/82, $C_3 = 27 \text{ Km}^2\text{-sec}^{-2}$.

Point 2: Perihelion modification maneuver, $\Delta V = 900 \text{ m-sec}^{-1}$.

Point 3: Earth powered swingby, $\Delta V = 1000 \text{ m-sec}^{-1}$.

Point 4: Jupiter encounter 3.2 years after launch.

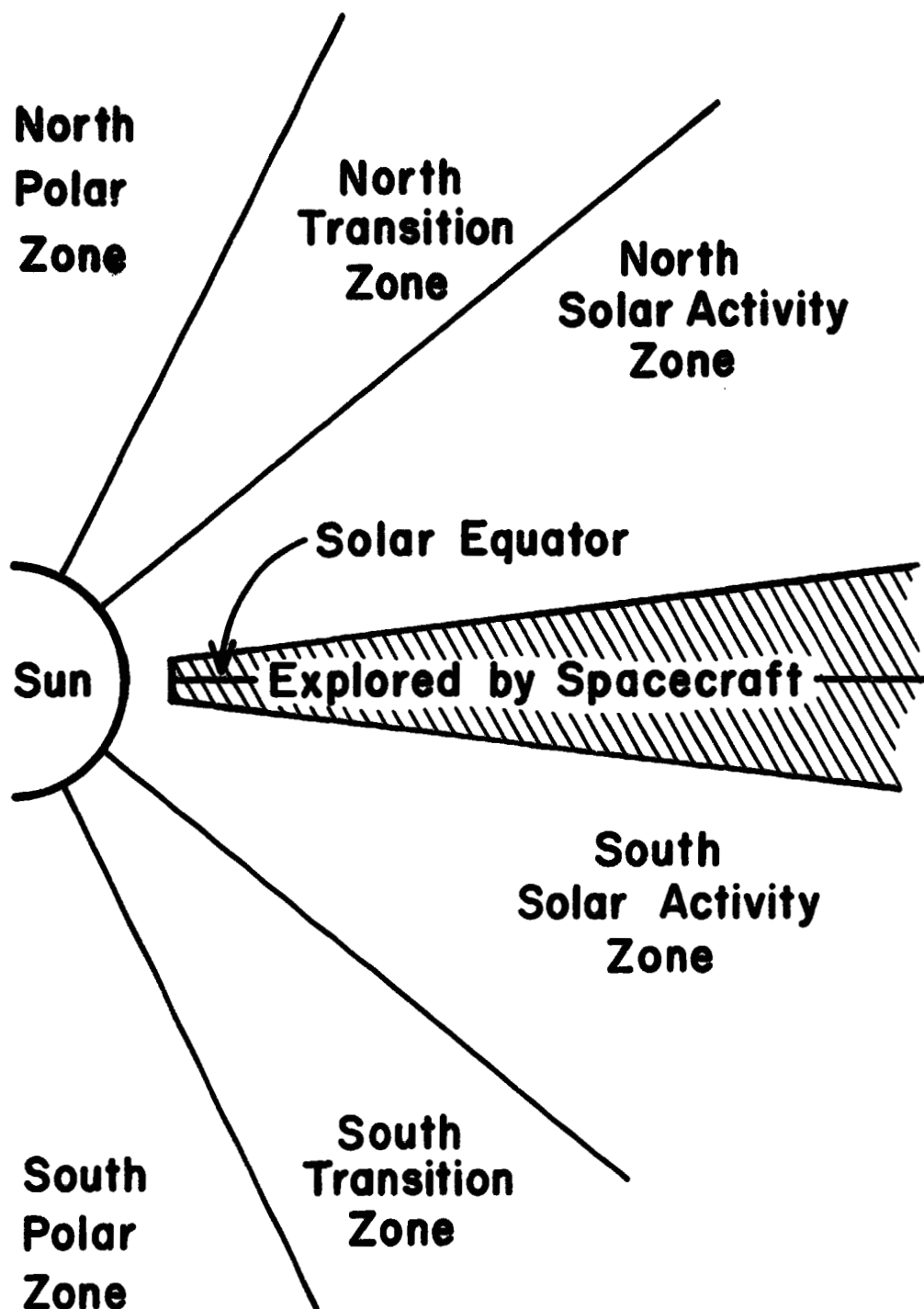
The trajectory is not to scale.

Figure 4 The out-of-the-ecliptic trajectory for the dual mission after Jupiter swingby, showing the radial distance of the spacecrafts from the sun and the heliographic latitude of each spacecraft as a function of time. (Adapted from reference 7.)

Figure 5 The dual spacecrafts A and B enter the Jovian magnetosphere approximately 2 or 3 days apart. The figure is a meridional projection of the spacecraft trajectory with Jupiter at the center of the coordinate system. The fiducial marks on trajectory A represent 6 hour intervals which correspond in numbers to the 6 hour intervals along trajectory B. Thus it is seen that one spacecraft is near closest approach when the other spacecraft is at 50 Jovian radii. The trajectory of Pioneer 11 is shown for comparison.

Figure 6 Projection on the ecliptic plane of the trajectories of spacecraft A and spacecraft B. For comparison the trajectory of Pioneer 11 is shown.

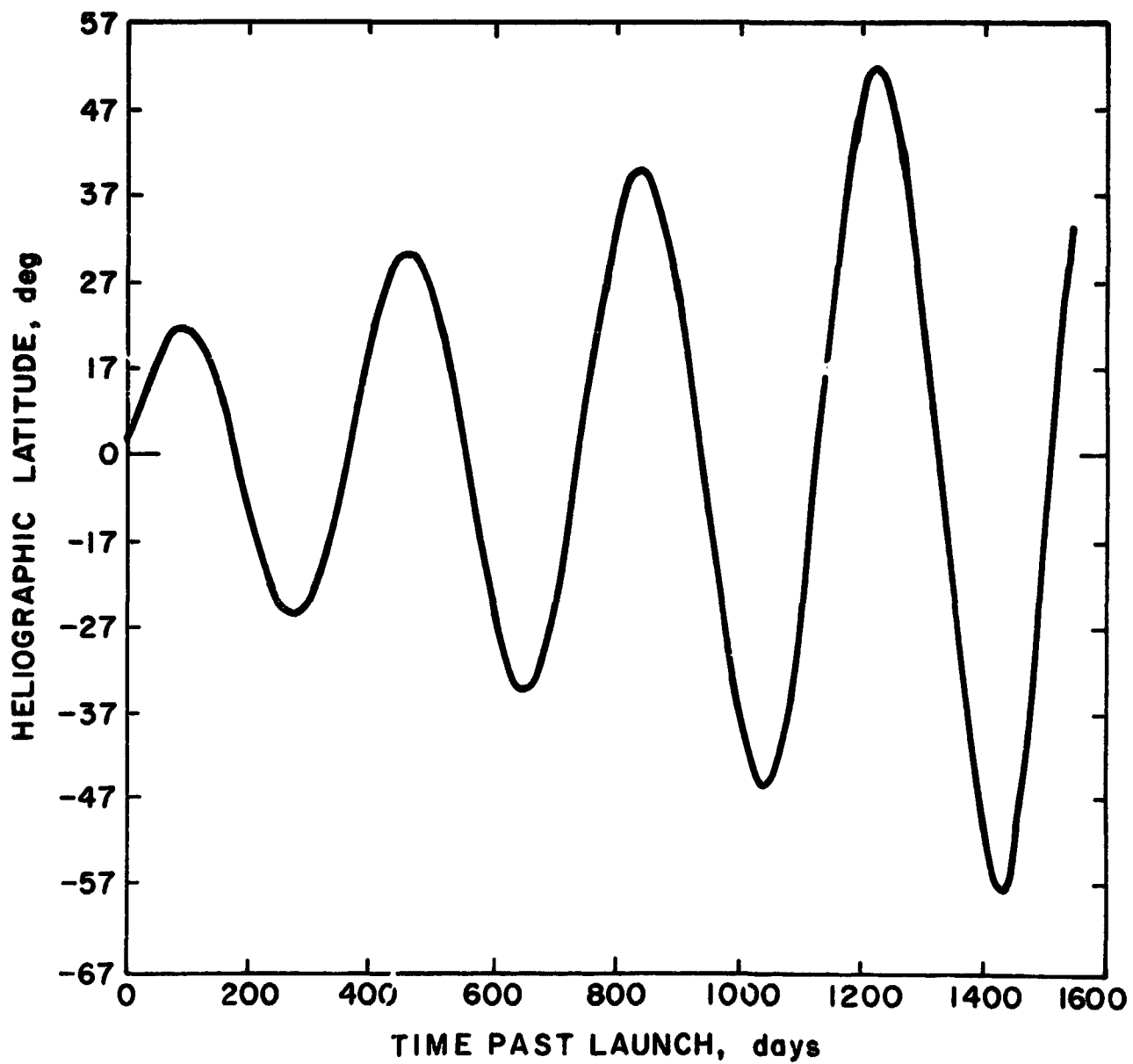
Figure 7 Two alternate models for the shape of the heliosphere. (See reference 27.)



Idealized Meridional Diagram of Solar Regions Connecting with the Interplanetary Medium

Figure 1

HELIOGRAPHIC LATITUDE PROFILE



(From J.P.L. Report by J.H. Duxbury, 9/26/74)

Figure 2

REPRODUCIBILITY OF THE
PAGE IS POOR

www.ck12.org

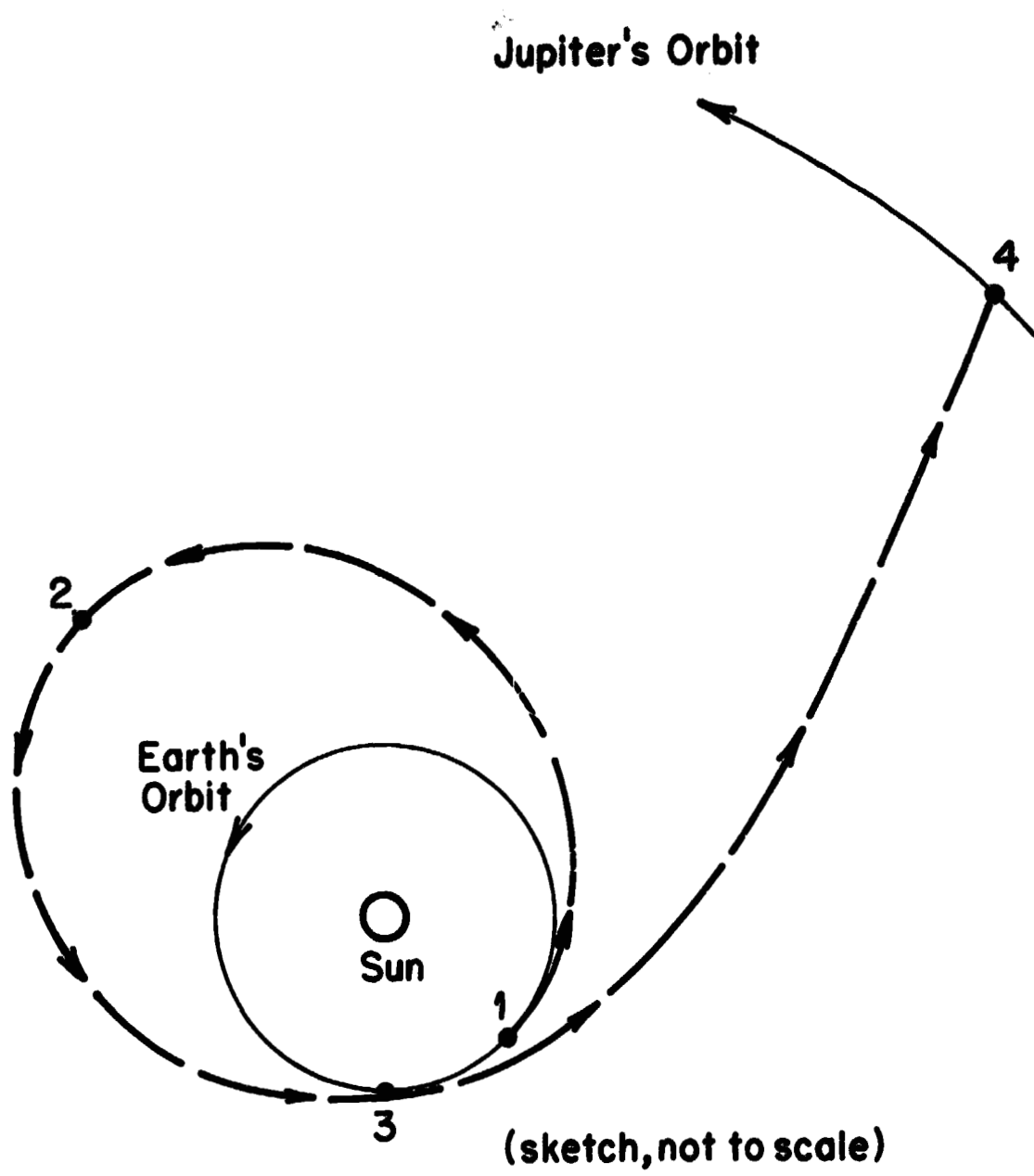
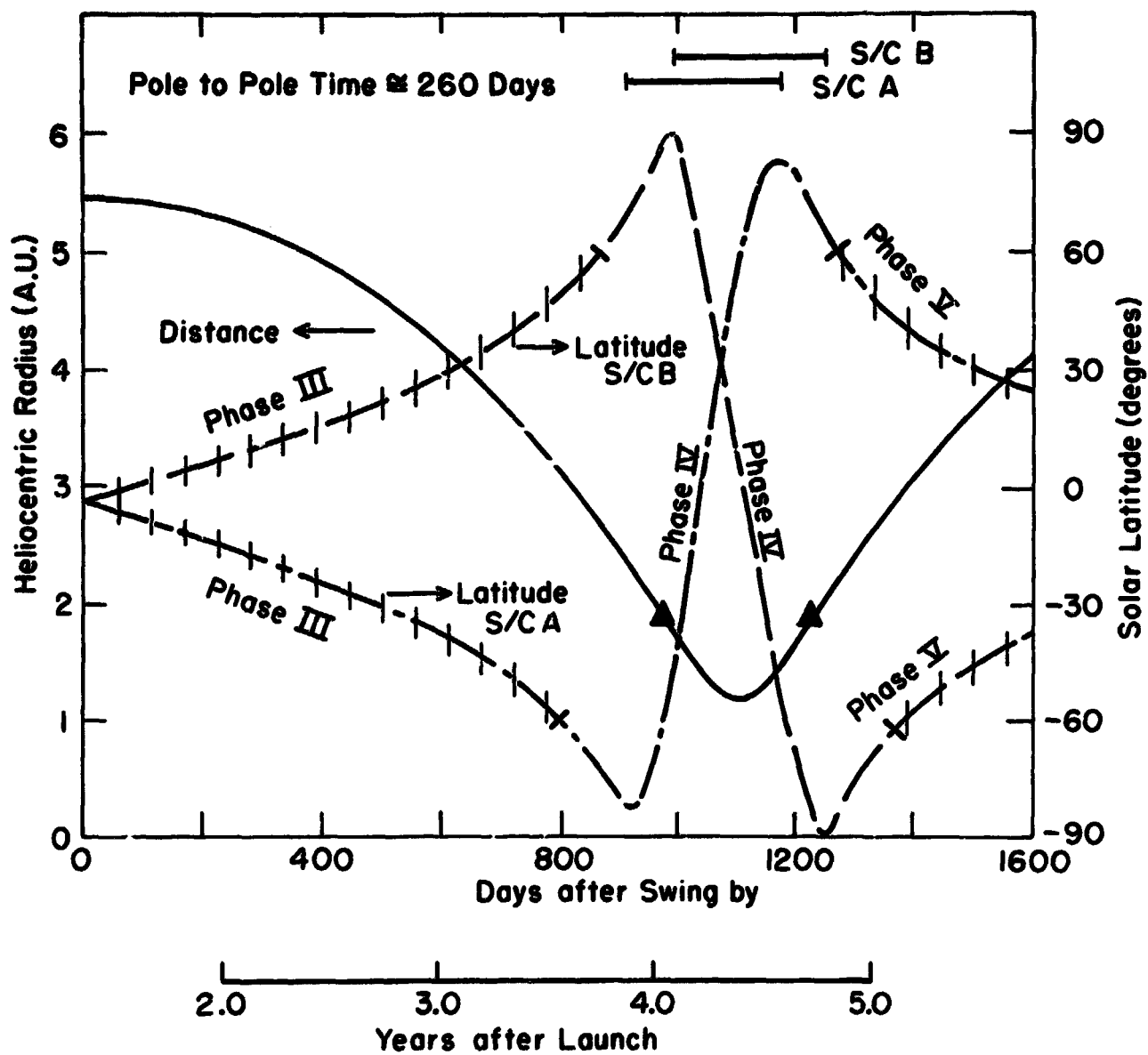


Figure 3

**Out of Ecliptic Trajectory, Heliographic Distance and Latitude
Dual Pioneer Spacecraft, Single Titan 3E/Centaur/TE 364-4**



(adapted from Figure by H.F. Matthews, NASA/ARC)

Figure 4

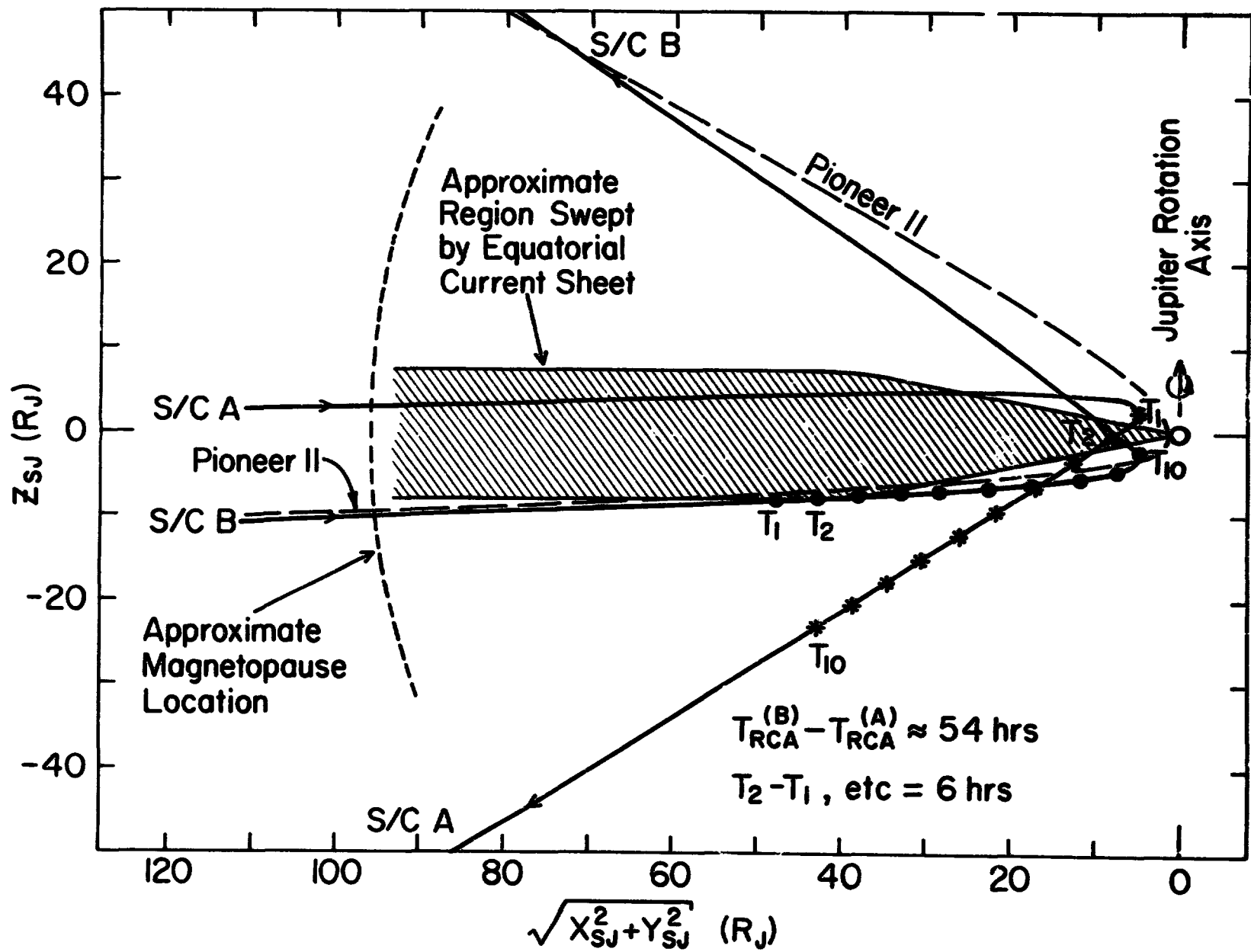


Figure 5

REPRODUCIBILITY OF THE ORIGINAL PAGE IS POOR

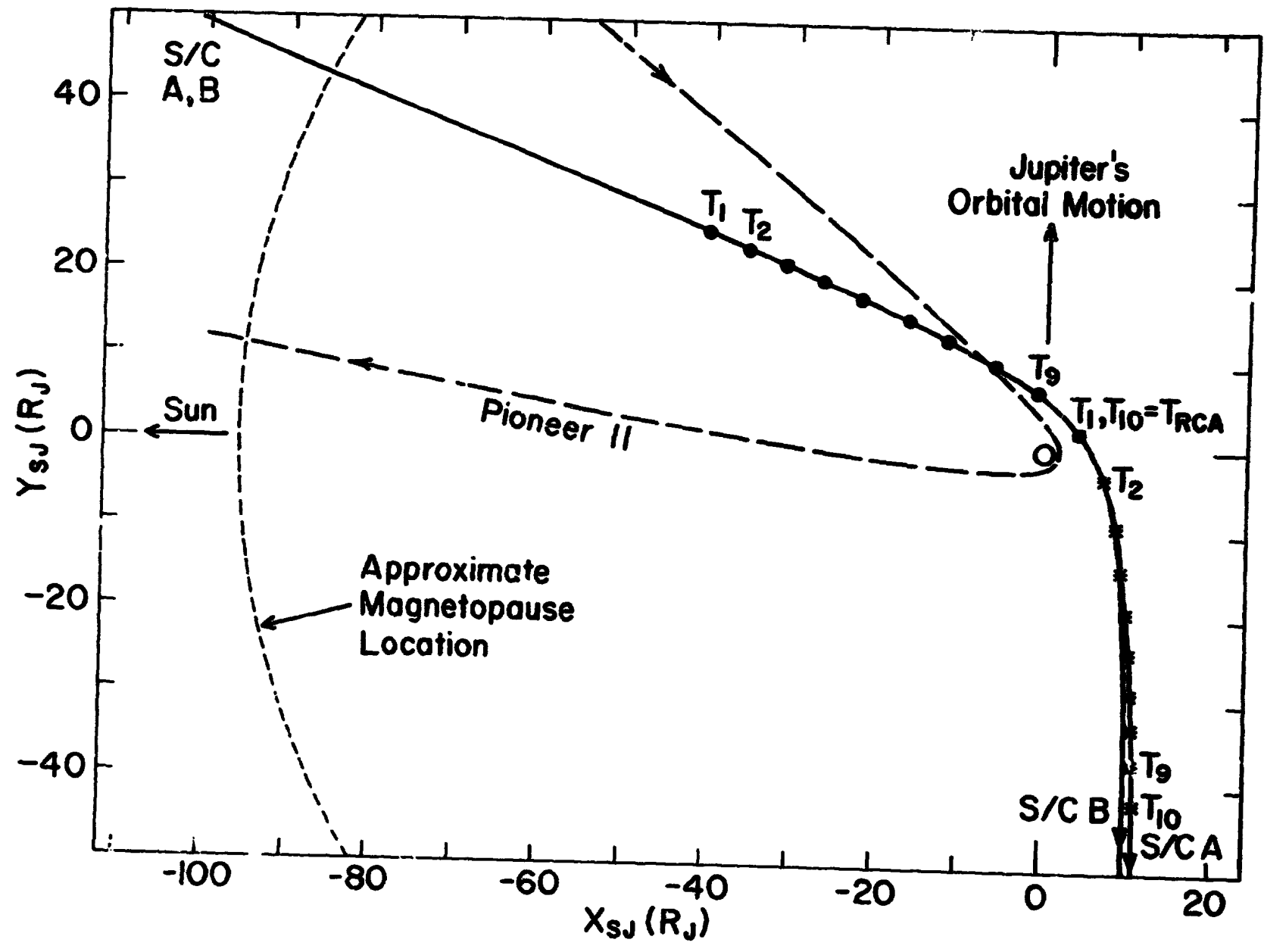


Figure 6

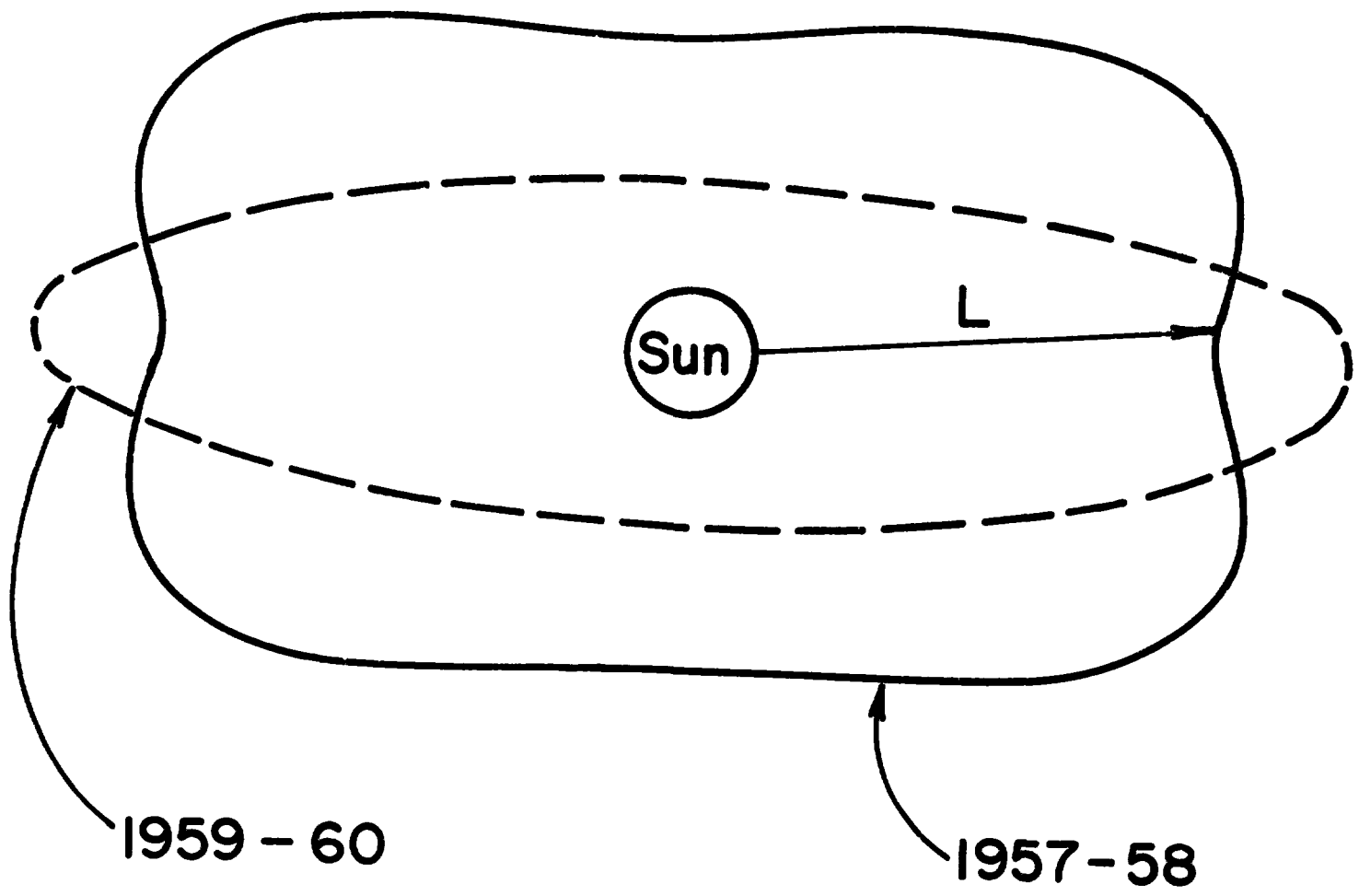


Figure 7

N76-24121

**AN ALTERNATIVE OPTION TO THE DUAL-PROBE OUT-OF-ECLIPTIC MISSION
VIA JUPITER SWINGBY**

**G. Colombo
and
D. A. Lautman
Center for Astrophysics
Harvard College Observatory and Smithsonian Astrophysical Observatory
Cambridge, Massachusetts 02138
and
G. Pettengill
Massachusetts Institute of Technology
Department of Earth and Planetary Sciences
Cambridge, Massachusetts 02140**

We have recently conducted a preliminary study on the possibility of combining the out-of-ecliptic (OOE) mission with a solar-probe mission. In particular, we have been looking at the possibility of having a high-inclination OOE probe complemented by a second probe going from Jupiter to the sun along a rectilinear path (at least for the segment from 0.3 a.u. inward to the sun).

The scientific interest in approaching close to the sun is obvious since it enhances observation of particles, fields, and gravitational harmonics. Our particular choice of path results from the associated simplicity of the spacecraft configuration needed to provide, for example, good thermal control, a drag-free system, and good communications with the earth.

A preliminary error analysis conducted by J. D. Anderson of the Jet Propulsion Laboratory leads to very interesting conclusions for an elliptical orbit with a perihelion distance of $16R_{\odot}$. Assuming that the nongravitational forces are compensated by a drag-free system (with three degrees of freedom) and that the spacecraft is tracked down to perihelion, the quadrupole moment of the sun can be determined with an accuracy of 3 parts in 10^7 . Since the estimated value of J_2 ranges from 3×10^{-5} (applying Dicke's theory) to 1×10^{-7} (assuming rigid rotation of the interior with the observed surface), the interest in determining this moment with an accuracy of at least 1 part in 10^7 is clear. We remember that J_2 gives a fundamental constraint to the moment of inertia (or the ratio C/MR^2) and, therefore, on the internal density distribution of the sun.

As mentioned above, the result obtained by Anderson implies a three-axis drag-free system with an accuracy of 10^{-8} cm/sec². A drag-free system having this accuracy has recently been flown in the TRIAD satellite. If, however, we choose a solar-impact trajectory, then by using a spinning spacecraft, a one-axis drag-free system can be implemented that requires much less complexity. In fact, a spacecraft spinning about an axis aligned with the rectilinear path would allow 1) gyro-stabilization (from 0.3 a.u. to the sun), 2) an easier design for thermal shielding, and 3) a one-degree-of-freedom drag-free system. In particular, a sphere with an electrostatic

suspension is free to move along the spin axis with no exchange of forces along the path. The displacement of the sphere along the spin axis will be sensed, causing the thruster (oriented along the spin axis) to compensate the nongravitational forces along the path to the desired accuracy. The spacecraft will be forced to follow the proof mass and, therefore, to follow a purely gravitational path. Transverse forces should be 4 orders of magnitude smaller and need not be compensated. The drag-free system can be calibrated when the probe is far from the sun (5 a.u.) in order to find the equilibrium position along the spin axis of the proof mass in the gravity field of the spacecraft.

During the 3.5 days that the spacecraft will spend in going from 0.25 a.u. to 0.01 a.u. and closer, the earth-sun-probe geometry will permit the earth to be in the beam of the 0.2-m-diameter antenna pointing parallel to the spacecraft spin axis. The Jupiter-swingby technique has enough flexibility to enable the mission to be timed so that the earth-spacecraft line remains within a few degrees of the direction of the spacecraft track. A 20-cm dish mounted on the spacecraft operating in the X band has a beamwidth of 8° and a gain of 27 db. By using a 64-m dish on the earth, this will allow a transmission data rate from 50 to 100 bits/sec, even with the noise of the sun in the background. Doppler tracking using two frequencies in the X band (8 and 12 GHz) should yield a relative-velocity measurement accuracy of the order of 10^{-2} cm/sec (1σ) with 60-sec integration time.

From Jupiter inward to 0.5 a.u., the spacecraft will operate in the Pioneer mode, performing selected experiments related to the solar stereoscopic and OOE missions. The two-frequency radio-science experiment will allow the integrated electron content to be determined at each instant, and perhaps a weighted component of the integrated magnetic field (from Faraday rotation).

From 0.5 a.u. inward, however, the mission will become more sun-oriented. The spacecraft spin axis will be directed sunward at this time, and the drag-free servo system will be activated. Some relevant probe parameters inside 0.5 a.u. are given in Table 1.

Table 1. Probe parameters.

Solar Distance (a.u.)	R_{\odot}	Time to $4R_{\odot}$ (days)	Velocity (km/sec)	Equilibrium Temperature (°K)
0.5	100	10.5	54	215
0.4	80	7.4	60	235
0.3	60	4.8	70	275
0.2	40	2.6	85	335
0.1	20	0.9	121	470
0.05	10	0.25	171	680
0.02	4	0	270	1060

The temperatures shown in the table are surface temperatures related to a properly designed reflective heat shield that covers the "front" side of the spacecraft; the internal temperatures of the spacecraft will not necessarily be so high. Furthermore, the last few solar radii are traversed in less than an hour, during which time, thermal equilibrium will not be established. It is entirely possible that the system will survive to $2 R_{\odot}$. If it does, a straightforward calculation shows that tracking to a doppler accuracy of 10^{-2} cm/sec over the half-hour interval required for the spacecraft to fall from 3 to $2 R_{\odot}$ would permit J_2 to be determined to an accuracy of 10^{-8} . Since a realistic estimate of the magnitude of J_2 is about 10^{-7} , as is shown in the Appendix, an extremely valuable result would be guaranteed.

Obviously, many details of engineering design and scientific applicability remain to be worked out for this mission. But the preliminary effort so far expended appears more than sufficient to warrant this further pursuit.

APPENDIX

J₂ OF THE SUN

The value of J₂ can be inferred for a rotating axially symmetric body by means of the first-order formula (Jeffries, 1970)

$$\frac{3}{2} J_2 = f - \frac{1}{2} m \quad , \quad (1)$$

where f is the flattening and $m = \omega^2 R_e / g_e$ is the ratio of centrifugal force at the equator to gravity at the equator. The assumptions made are that the gravitational potential is given by its first two terms only,

$$V_g = \frac{\mu}{r} \left[1 - J_2 \left(\frac{R_E}{r} \right)^2 P_2(\sin \phi) \right] \quad , \quad (2)$$

and that the surface is rotating uniformly so that the centrifugal force can be derived from the potential

$$V_c = \frac{1}{2} \omega^2 r^2 \cos^2 \phi \quad (3)$$

Then the actual surface will be a level surface of the potential

$$V = V_g + V_c.$$

if the surface is not rotating uniformly, we can modify equation (1) by assuming that, at any latitude, the surface will be perpendicular to the resultant of the gravity force given by the gradient of equation (2) and the centrifugal force equal to $\omega^2(\phi)r \cos \phi$ and directed away from the axis of rotation. Assuming that the shape of the surface is given by $r = R_E (1-Y)$, we find, to first order,

$$\frac{dY}{d\phi} = (3J_2 + \frac{R_E^3 \omega^2(\phi)}{\mu}) \sin \phi \cos \phi \quad , \quad (4)$$

We assume that the angular velocity of the sun's surface can be approximated by $\omega(\phi) = \omega_0 - \omega_2 \sin^2 \phi$ and obtain

$$\frac{3}{2} J_2 = f - \frac{1}{2} m_0 \left[1 - \frac{\omega_2}{\omega_0} + \frac{1}{3} \left(\frac{\omega_2}{\omega_0} \right)^2 \right] \quad , \quad (5)$$

where $m_0 = \omega_0^2 R_e^2 / g_e$. For the sun, we have $m = 2.14 \times 10^{-5}$, $\omega_0 = 14.4^\circ/\text{day}$, and $\omega_2 \cong 4.5^\circ/\text{day}$, so the second term in equation (5) lies between 7.7×10^{-6} and 10.7×10^{-6} , depending on whether the differential rotation is included or not. The best determination of the flattening of the sun (Hill, 1974) is $f = (9.6 \pm 6.5) \times 10^{-6}$. It is clear that J_2 cannot be derived with any accuracy from equation (5), since it is the difference between two not very well-known quantities of nearly equal magnitude.

If the sun is rotating uniformly and if the density distribution is known, J_2 can be directly calculated. Following an analysis by Sterne (1939a), we define the "apsidal motion coefficient,"

$$k = \frac{3 - \eta_s}{4 + 2\eta_s} \quad ,$$

where η_s is the value at the surface of the variable η , which is zero at $r = 0$ and which satisfies Radeau's equation:

$$r \frac{d\eta}{dr} + \eta^2 - \eta - 6 + \frac{6\rho}{\rho_m} (\eta + 1) = 0 \quad . \quad (6)$$

In equation (6), ρ is the density at r and ρ_m is the mean density interior to r . Then,

$$J_2 = \frac{2}{3} km \quad , \quad (7)$$

where m has been previously defined. The coefficient k depends solely on the distribution of mass within the star, ranging from zero for a completely concentrated star to $3/4$ for a homogeneous star. Values of k have been calculated (Motz, 1952) for solar models by Schwarzschild (1946) and by Epstein (1951). Motz obtained $k = 0.00585$ and 0.00599 , which leads to $J_2 = 8.3 \times 10^{-8}$ and 8.5×10^{-8} , respectively. Calculating J_2 for three later solar models, we found $J_2 = 1.56 \times 10^{-7}$ for a zero-age sun (Schwarzschild, 1958) and $J_2 = 1.41 \times 10^{-7}$ and 1.20×10^{-7} for two models of the present sun (Weymann, 1957, and Sears, 1964). Although we do not at present have detailed calculations of later solar models, we note that a recent one (Hoyle, 1975), proposed to explain the low neutrino emission from the sun, has the unusually low central density of 75 g/cm^3 . The ratio of central to mean density is then 53.2, which is quite close to 54.2, the ratio of central to mean density of the "standard model," a polytrope of index 3. Russell (1928) found $k = 0.0144$ for a polytrope of index 3, so we consider 2×10^{-7} to be a reasonable upper limit to the value of J_2 for a uniformly rotating sun.

It is of interest to consider a lower bound to k and, hence, to J_2 . The most concentrated star with a given central density is the generalized Roche model, which consists of a homogeneous core, with a density equal to the central density containing all the star's mass, and an envelope with infinitesimal

density. Radeau's equation can then be solved analytically (Sterne, 1939b) to obtain

$$J_2 = \frac{1}{2} m \left(\frac{\rho_c}{\bar{\rho}} \right)^{-5/3} \quad (8)$$

With current estimates of the central density of the sun ranging from about 75 to about 150 g/cm³, we find the lower limit of J_2 to be between 1.4×10^{-8} and 4.5×10^{-9} .

References

- Epstein, I. 1951, Ap.J., 114, 4380.
- Hill, H.A., et al. 1974, Phys. Rev. Letters, 33, 25, 1497.
- Hoyle, F., 1975, Ap.J. (Letters), 197, L127.
- Jeffries, H., 1970, The Earth, Fifth ed., Cambridge, p. 171.
- Motz, L., 1952, Ap.J., 115, 562.
- Russell, H. N., 1928, M.N., 88, 641.
- Schwarzschild, M., 1946, Ap.J., 104, 203.
- Schwarzschild, M., 1958, Structure and Evolution of the Stars,
Princeton.
- Sears, R.L., 1964, Ap.J., 140, 477.
- Sterne, T.E., 1939a, M.N., 99, 451.
- Sterne, T.E., 1939b, M.N., 99, 670.
- Weymann, R., 1957, Ap.J., 126, 208.

CHAPTER II

SOLAR PHYSICS

N76-24122

OUT-OF-ECLIPTIC
STUDIES OF CORONAL HOLES AND THEIR RELATION TO THE
SOLAR WIND

R. W. Noyes

Center for Astrophysics
Harvard College Observatory and
Smithsonian Astrophysical Observatory
Cambridge, Massachusetts 02138

Recently solar physicists have gained the ability to view the solar corona from a new perspective, by means of space observations at x-ray and extreme ultraviolet (EUV) wavelengths, which permits us to observe the forms of the hot, but very tenuous, corona against the relatively cool solar disk (Figure 1). Ground-based observations of the corona, except for relatively low-resolution radio data, require natural (via eclipse) or artificial occultation of the bright disk, limiting coronal observations to "side views" through the atmosphere extending beyond the occulting disk. The direct face-on view provided by EUV and x-ray space observations, combined with detailed information on density and temperature of the emitting regions conveyed by the spectral character of the ultraviolet and x-ray data, has given us the first detailed information on the complex structures of the corona and their interrelations.

The possibility of looking down on the sun from a spacecraft high above the ecliptic plane opens up yet another perspective on the sun, one that is certain to help us understand the nature of coronal holes at high latitudes, and their relationship to the expansion of the three-dimensional solar wind.

The large dark area on the x-ray image of Figure 1 is a coronal hole - a phenomenon whose properties are just now becoming understood, largely through EUV and x-ray observations. Although the existence of large regions of low coronal density had earlier been inferred from coronagraph "side views", we are now obtaining detailed knowledge of their size, shape, density, temperature, magnetic field, and evolution from spacecraft observations at EUV and x-ray wavelengths.

Briefly, coronal holes are large regions of the corona whose density is some 3-10 times less than that of the "average" quiet corona. The temperature, at least at the level where measurable x-ray and EUV radiation is emitted, is also less, having a value of about 1×10^6 °K instead of about 1.8×10^6 °K, as in the average corona. Analysis of low-resolution OSO data (Munro and Withbroe, 1972) suggested that the temperature gradient between the 10^4 °K chromosphere and 10^6 °K corona is about an order of magnitude less in coronal holes than in the average sun. As a result, the energy loss to the corona by thermal conduction back to the chromosphere, which is a very important energy sink for the average corona, may be much less significant for coronal holes. Due to the low density in holes the radiative losses are also less (which is of course why they appear dark in the x-ray image of Figure 1). Since energy losses by radiation and conduction are both drastically decreased in holes, we may conclude that either the heating of the corona is less in holes or some additional mechanism of energy loss is present in holes that is not found in other regions of the quiet sun.

Coronal holes are assuming great importance today because of their apparent association with high-speed streams of the solar wind. The association, first suggested by Krieger et al (1973) on the basis of rocket x-ray data, has been put on a much firmer footing from detailed correlative studies of OSO-7 and Skylab data during the period 1973 to 1974. Nolte et al (1976) found that every large near-equatorial hole observed during the Skylab mission was associated with a high-speed stream at 1 a. u. Furthermore, there was a clear positive correlation between the velocity of the observed solar wind stream and the area of the associated coronal hole as measured from Skylab x-ray photographs. Finally, a very high correlation was found between the polarity of the interplanetary magnetic field associated with the high-speed streams and the magnetic field underlying the associated coronal holes.

During the Skylab mission coordinated ground-based and space data revealed that the location of coronal holes can also be detected through ground-based observations of subtle properties of certain Fraunhofer absorption lines, notably He I, λ 10830 (Harvey et al, 1975). This discovery has permitted the mapping of coronal hole

boundaries during the two years after the termination of the Skylab mission. These two years were a time of large and persistently recurring high-speed solar wind streams, and significantly, a pattern of long-lived coronal holes was detected from the He I 10830 observations. Harvey et al (1976) have shown that, as before, there is a good correlation between central meridian passage of holes that cross the equator and high-speed streams during that time. In addition, when the data also include high latitude holes that also extend down to $\pm 40^\circ$ latitude, the correlation becomes even better. Thus there appears little question that the high-speed streams are related to coronal holes, and in addition there is evidence that some of the streams observed in the ecliptic plane are associated with holes at latitudes at least as high as 40° .

To establish that the holes are the origin of the high-speed solar wind streams, however, it is necessary to identify a physical mechanism in addition to finding a high correlation between the two phenomena. In a search for a physical mechanism, we first note that coronal holes occur over areas of unipolar photospheric magnetic fields. Although magnetic fields are measurable only in the photosphere, they may be mapped upwards into the corona, using potential theory along with the assumption that above about 1.6 to 2.5 solar radii they are stretched out radially by the expanding solar wind (Newkirk, 1972). Such calculations show the magnetic fields underlying holes to reach the source surface and thus to open out into the interplanetary medium, while fields underlying other regions in the corona generally close back on themselves (Altshuler et al, 1976). Thus holes seem an easy pathway for the escape of coronal plasma into the solar wind.

We have already noted that the density and temperature structure of holes in the low corona suggest that either the coronal heating rate is less in holes or excess energy may be available to accelerate the solar wind outward in holes. It is interesting that coronal holes are almost impossible to detect in the chromosphere or below, suggesting that at those levels the atmospheric structure does not depend on whether or not a hole exists in overlying corona. This suggests (although it does not prove) that the amount of mechanical heating that passes upward through the photosphere is independent of

the existence of coronal holes. Under that assumption Pneuman (1973) and Noci (1973) showed that the solar wind, expanding outward in regions of open field lines, would carry off energy through acceleration of the solar wind and through outward thermal conduction, sufficient to compensate for the decreased energy losses from holes by radiation and inward thermal conduction. The exact mechanism by which originally closed field lines break open to allow the expansion of the solar wind and the creation of a hole is not yet clear, but arguments based on energy flow support the reality of the process.

If radial outflow really occurs over coronal holes, it should give rise to observable doppler shifts of XUV emission lines. Preliminary reports (Cushman and Rense, 1976) indicate the detection of outward velocities of the order of 16 km/sec, which may in fact be the beginnings of the solar wind expansion. However, the data are scanty and further verification is needed.

What does all of this have to do with the out-of-ecliptic mission? The significance lies in the fact that coronal holes have been found to occur very frequently at the solar poles. The polar holes appear to be very similar to equatorial holes in their physical properties, with a major difference that they are much larger. A plausible hypothesis is that they too give rise to high-speed solar wind streams. These streams may emanate from the poles but spread out to lower latitudes, even reaching the ecliptic plane if the polar hole extends to low enough latitudes.

Unfortunately observations of polar holes from the orbit of earth still suffer partly from the projection problem described at the beginning of this paper. Because polar holes always occur near the limb (as opposed to near-equatorial holes, which are carried past disk center by rotation), we always observe them from the side. This of course leads to loss of spatial resolution due to foreshortening. In addition, observations from the side are particularly troublesome for observations of coronal holes, which are by their nature only very weakly emitting, and therefore are very easily obscured by foreground and background emission from the neighboring "normal" corona.

It is also extremely difficult to get accurate measurements of magnetic fields associated with polar holes. Firstly, projection effects lead to loss of resolution. Secondly, the sensitivity of a magnetograph is proportional to the line-of-sight component of the field direction; for vertical fields near the limb this becomes very small.

Finally, of course, velocities of radial outflow above a coronal hole at the polar limb would not give rise to a line-of-sight doppler shift when observed from the orbit of earth.

What might one hope to observe from a spacecraft situated over the pole? Figure 2 shows a reconstruction of the appearance of the south polar hole as it would have been observed from such a vantage point during nine months of the Skylab mission. The images of Figure 2 were rectified using Skylab data from the Naval Research Laboratory XUV monitor instrument (Sheeley, 1975, personal communication). The large size of the hole compared to typical equatorial holes (cf. Figure 1), and its extended lifetime, are immediately apparent.

A spacecraft able to observe the sun from higher latitudes (say greater than 60°) for several months at a time, and properly instrumented, should be able to accomplish many significant observations of coronal holes. Large and sophisticated instruments such as have been flown on Skylab are by no means necessary, and are probably out of the question for the foreseeable future. The following are examples of important observational objectives, that could be met by realistic instrumentation aboard an out-of-ecliptic mission.

- 1) Continuous mapping of the location of polar holes, and study of their evolution. A simple imager at any of a number of XUV or x-ray wavelengths, chosen such that the emission within the band pass largely originates at temperature in excess of about 1.5×10^6 °K, would be adequate. Spatial resolution of about 30 arcsec would be sufficient. For a small instrument, count rates would be quite low, but time resolution need be only of the order of many hours, so long integration times are

possible. Images could be built up by scanning a point detector (perhaps using the rotation of the spacecraft for scanning). Data on the location of the hole and its boundaries would be correlated with measurements from the same spacecraft of local plasma parameters (density, velocity, magnetic field, composition, temperature), and as the spacecraft traverses directly above different parts of the hole or its boundaries, some idea of the three-dimensional flow field could be obtained. In addition, from the absolute intensities recorded, some useful limits on the density and temperature of the emitting plasma inside the hole could be obtained.

2) With imagery at two or more XUV or x-ray wavelengths, one can obtain much better information on the physical conditions in the coronal hole itself. Approximate values of density and temperature can be determined independently, and combined with modeling techniques, the data can give information on the variation of the parameters with height. Since both the density and temperature distribution in the low corona strongly determine the plasma flow properties at one a. u., correlation with these properties measured at the spacecraft itself will be very important.

3) XUV spectroscopy at high spectral resolution ($\lambda/\Delta\lambda \approx 3 \times 10^4$) would be very useful to measure the outflow velocity of material in the polar hole, in the manner already reported by Cushman and Rense (1976) for equatorial holes. Unfortunately the weakness of XUV emission lines in coronal holes, combined with the requirement for high spectral resolution, implies either a rather large instrument or extremely long integration times. This experiment, while very important, may therefore not be a suitable candidate for a very early exploratory out-of-the-ecliptic mission.

4) Measurement of the polar magnetic field from an out-of-ecliptic spacecraft appears to be a natural and important objective. As mentioned above, there are considerable advantages in observing polar magnetic fields from more nearly above the poles. Spatial resolution of 30 arcsec would be adequate to determine the gross structure of the fields and to follow their evolution. A small magnetograph operating with a solid etalon fabry-perot filter in visual wavelengths might well be feasible for inclusion on an exploratory out-of-ecliptic mission.

All of the above objectives would be considerably furthered by simultaneous measures from the ecliptic plane, in order to obtain stereoscopic information. In the case of magnetic fields, for instance, observations from the earth would record those fields not recorded from the out-of-ecliptic spacecraft, and vice versa. Comparison of relative signal strengths from such paired observations could help determine the vector field in the photosphere, thus putting potential mapping of high-latitude magnetic fields on a more secure footing. Similarly observations from an earth-orbiting satellite of the XUV or x-ray structures in coordination with simultaneous out-of-ecliptic observations of the same structures would yield the 3-dimensional structure unambiguously.

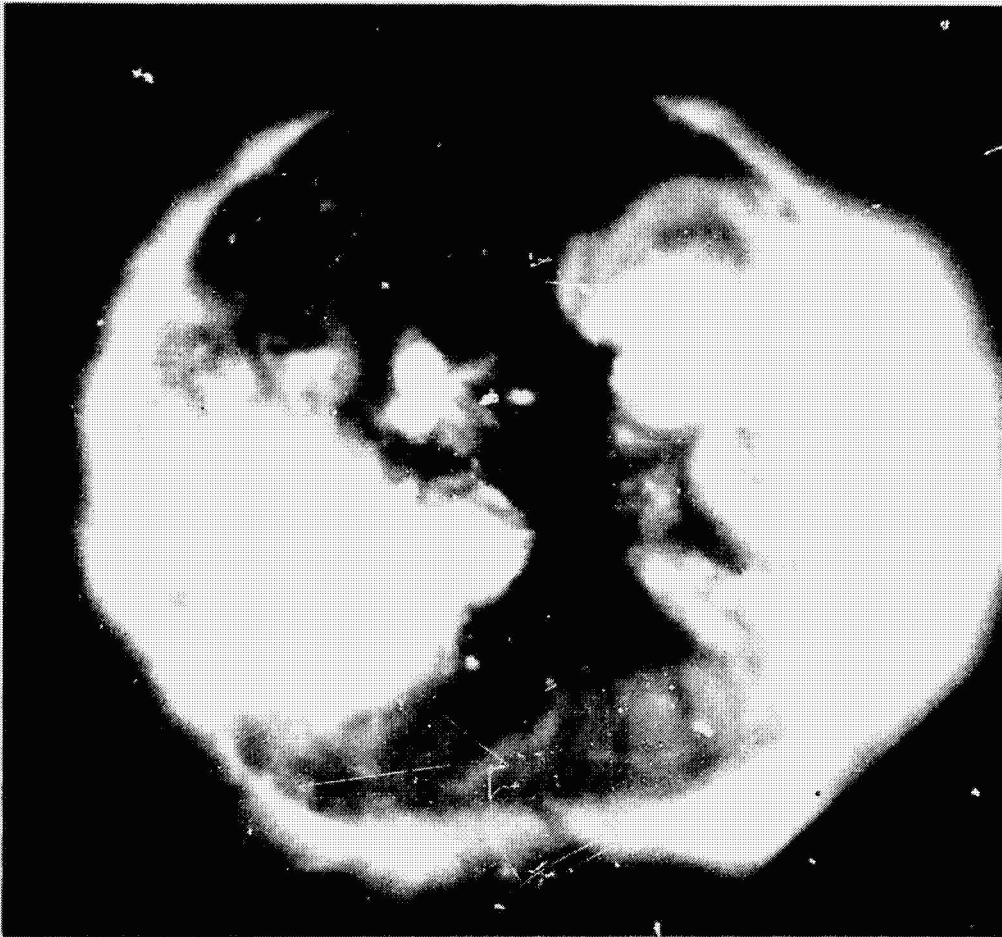
We should note that the success of a program to study polar holes from out-of-ecliptic may depend strongly on the phase of the cycle during which the program is carried out. It appears that polar holes may shrink and even disappear near sunspot maximum, doubtless reflecting the shrinkage and disappearance of the unipolar magnetic field cap associated with reversal of the general dipole field of the sun, which occurs about that time. At about sunspot minimum, unipolar magnetic fields at the poles and polar coronal holes appear to reach their greatest extent. From the point of view of studying polar holes and their relation to the solar wind, then, it may be useful to time the passage of an out-of-ecliptic satellite over the solar poles, or at least over high latitudes, to occur with a few years either side of sunspot minimum.

References

- Altshuler, M.D., Levine, R.H., Harvey, J.W., and Stix, M. 1976, "High-resolution mapping of the magnetic fields of the solar corona," submitted to Solar Physics.
- Cushman, G.W. and Rense, W.A. 1976, Astrophys. Journ. Letters, submitted.
- Harvey, J.W., Krieger, A.S., Timothy, A.F., and Vaiana, G.S. 1975, Bull. A.A.S. 7, 358.
- Harvey, J.W., Sheeley, N.R., Feldman, W.C. 1976, presented at NASA Coronal Holes Workshop, February, 1976; to be submitted.
- Krieger, A.S., Timothy, A.F., and Roelof, E.C. 1973, "A coronal hole and its identification as a source of a high-velocity solar wind stream," Solar Physics 29, 505-525.
- Munro, R.H. and Withbroe, G.L. 1972, "Properties of a coronal hole derived from EUV observations," Astrophys. Journ. 176, 511-520.
- Newkirk, G., Jr., 1972, "Coronal magnetic fields and the solar wind," in Solar Wind, ed. C.P. Sonett, P.J. Coleman, Jr., and J.M. Wilcox, NASA SP-308, Washington, D.C.
- Noci, G. 1973, "Energy budget in coronal holes," Solar Physics 28, 403-407.
- Nolte, J.T., Krieger, A.S., Timothy, A.F., Gold, R.E., Roelof, E.C., Vaiana, G.S., Lazarus, A.J., Sullivan, J.D., and McIntosh, P.S. 1976, "Coronal holes as sources of solar wind," submitted to Solar Physics.
- Pneuman, G.W. 1973. "The solar wind and the temperature-density structure of the solar corona," Solar Physics 28, 247-262.
- Vaiana, G.S.. 1976. "The x-ray corona from Skylab," presented at discussion meeting on "The Physics of the Solar Atmosphere" of the Royal Society, London, 14-15 Jan. 1975. Proc. Roy. Soc. London, in press

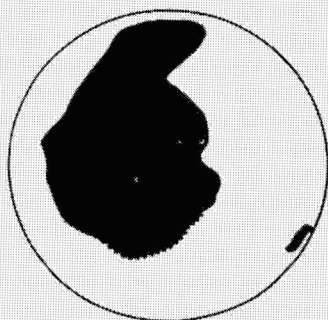
Figures

- Figure 1.** Skylab soft x-ray image of the sun, June 1, 1973. Filter bandpass 2-32A and 44-54A. See Vaiana (1976) for details. Photo courtesy American Science and Engineering, Inc., and Harvard College Observatory.
- Figure 2.** Diagram of the evolution of a coronal hole as it would have been seen from above the south pole. Data are rectified from ATM Skylab observations, May 1973 to February 1974, made with the Naval Research Laboratory XUV monitor instrument. Data courtesy N. R. Sheeley, Naval Research Laboratory.

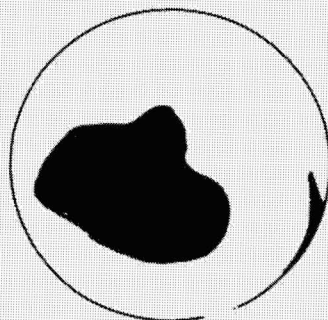


... OF THE
... POOR

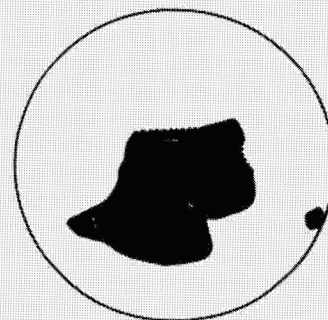
SOUTH POLAR HOLE, 1973-1974,
RECTIFIED FROM
NRL XUV MONITOR DATA



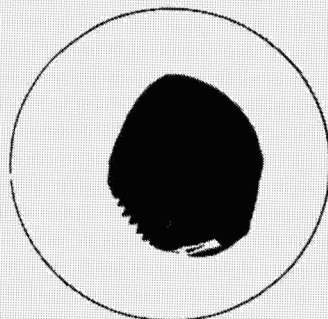
MAY 29 - JUNE 19



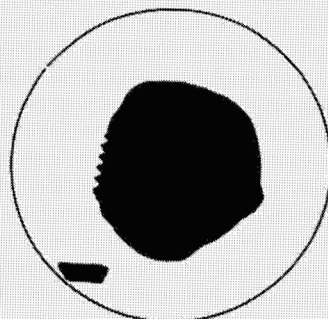
AUG 7 - SEPT 2



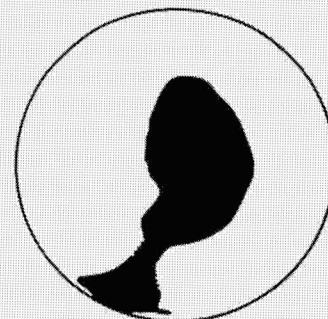
SEPT 3 - SEPT 19



NOV 26 - DEC 22



DEC 24 - JAN 19



JAN 20 - FEB 7

N76-24123

Out-of-Ecliptic Mission
Seminar

Solar Magnetic Fields
and the
Corona

Gordon Newkirk, Jr.
High Altitude Observatory
National Center for Atmospheric Research*

*The National Center for Atmospheric Research is sponsored by the
National Science Foundation.

The state of the solar atmosphere, which is considered to include the solar wind, is largely determined by magnetic fields. Both the magnitude and the configuration of fields at photospheric level appear to determine the flux of non-radiative energy, mass, and momentum into the base of the corona. Likewise the interaction between coronal field and plasma modulates the flow and produces the density distribution we see in the corona as well as the state of the interplanetary medium. Rapid annihilations of the field in the lower atmosphere associated with flares and slower readjustments of the field associated with eruptive prominences both lead to disruptions in the structure of the overlying corona and solar wind.

Although a definitive test of the relation between coronal morphology and magnetic fields is still lacking, several characteristic coronal structures are associated with distinct topologies of the field:

- . The tightly closed coronal loops and arches above active regions with similar configurations in the field.
- . Coronal holes at low latitude or over the poles with magnetic fields which open directly into the solar wind. Such regions appear to be the origin of fast streams in interplanetary space.
- . Coronal streamers with large arcades in the magnetic field below 2 to $2.5R_{\odot}$ and a current sheet above that height. Such features are detected as the "sector" boundary between large scale, oppositely directed fields in interplanetary space.
- . Hot, dense knots of plasma in the very low corona and visible as "bright points" in X-ray images with minute bipolar regions

distributed more or less uniformly over the surface. In the upper corona and interplanetary space such regions are hypothesized to give rise to minute current sheets which play a role in determining the electrical and thermal conductivity, the propagation of radio waves and energetic particles, and, possibly, coronal heating.

The characteristics of the photospheric field in magnitude, spacial extent, and lifetime suggest that the corona and interplanetary medium can be divided into 3 regions having relatively distinct properties as shown in the table. We note that although interplanetary measurements have sampled both the plasma originating in the latitude zone $\leq 10^\circ$ and shocks originating at higher latitudes, the influence of the $10^\circ - 50^\circ$ zone, which contains active regions, on the interplanetary medium is still uncertain.

A real understanding of the structure and evolution of the corona and interplanetary medium can be claimed only after we have constructed a self consistent 3-D model of the entire region and have tested it with concomitant observations in the lower solar atmosphere, in the corona, and in interplanetary space. The Out-of-the-Ecliptic Mission will provide not only the critical tests of such models but will also afford insight into the fundamental mechanisms governing this entire region through the sampling of zones where different field topologies, magnitudes, and evolutionary timescales (and presumably different mechanisms of mass, energy and momentum transport) dominate. Several specific questions may be considered:

- . Are the polar regions identical to the coronal holes at low latitude?
- . If this is so, how do we account for the fact that polar regions with apparently identical magnetic configuration display a vastly different appearance in the corona?
- . Does the coronal and interplanetary microstructure change with latitude? What influence does this have upon the heating, electrical and thermal conductivity, wave content, and energetic particle propagation of the medium?
- . How is the corona "mapped" into interplanetary space?
- . How does the solar-interplanetary field couple to the interstellar field?
- . What role does the continuous occurrence of coronal transients, which originate at $\lambda \leq 60^\circ$, play in determining the state of the interplanetary medium and energetic particle propagation?
- . What mechanisms control coronal and interplanetary abundances?

These are but a few of the questions concerning the role of solar magnetic fields in determining the structure of the corona and interplanetary medium which will be explored by an Out-of-Ecliptic Mission.

Concerning the mission options two points should be kept in mind:

- 1) Although the appearance of the corona suggests that a mission restricted to $\lambda < 40^\circ$ might be successful in reaching the polar zone, only a polar mission can guarantee that a truly new region of the interplanetary medium is to be explored.

2) The corona and interplanetary medium are continually evolving.

To assure success the Out-of-Ecliptic Mission must encompass a coordinated program of solar and interplanetary measurements so that a coherent attack can be made upon the important problems which beckon.

This presentation was made possible through the generosity of colleagues at Kitt Peak National Observatory, High Altitude Observatory, Smithsonian Astrophysical Observatory, and American Science and Engineering who kindly allowed the use of illustrative material.

	PHOTOSPHERE		CORONAL	INTERPLANETARY
Latitude	Field Pattern*	Lifetime	Counterpart	Counterpart
<10°	Large	Months	Open Field-Hole	Fast Streamer
	Scale Weak	to Years	Large Closed Field-Streamer	Sector Boundary
10° to 50°	Active Region	Minutes- Hours	Transient	Shocks + ?
		Month	Open B - ? Closed B - Arches	? None
	Large Scale	S A M E	A S "	< 10°
> 50°	Large Scale	Years	Open B - Hole	?

*Very Small Scale Patterns With Lifetime ~ Hours Exist at All Latitudes With Only a Weak Decrease Towards the Poles

N 76-24124

3-D Solar Radioastronomy and the Structure of the Corona and the Solar Wind

J.L. Steinberg and C. Caroubalos
Observatoire de Paris, Meudon, 92190, France.

Solar radio bursts are intense radio emissions from localized regions in the corona and interplanetary medium. Their brightness temperature is so much higher than the electron temperature of the ambient plasma that the mechanism which produces them is certainly non-thermal ; the necessary energy is brought into the source region by energetic electrons which can give rise to different types of transient radiation. One of them is the type III radioburst produced by energetic electrons travelling along open magnetic lines of force. Another quite usual form is the type I burst, typical of the meter wave lengths range.

We do not fully understand yet how the non-thermal energy is converted into electromagnetic energy ; but we know that, to be efficient enough, the conversion must take place at frequencies close to the resonant frequencies of the medium. At these frequencies, the refractive index for radio waves takes extreme values : close to 0 for the plasma resonance, much larger than 1 for the gyro-resonances. As electromagnetic waves travel away from their source, those resonance conditions are no longer fulfilled because of the non-uniformity of the electron density or magnetic field ; the refractive index comes back quickly to unity ; such a variation of the refractive index is favourable to beaming effects. The radiation mechanism itself which can involve some amplification may also produce a directive primary emission. In both cases, the beam will be oriented along or at definite angles to the principal directions of the medium : the electron density gradient or the magnetic field.

Using results from the STEREO-1 experiment, it is shown that stereoscopic observations in the deci to decameter λ range can provide information on

- the burst emission mechanisms
- the local electron density gradient and magnetic field vector at the source
- the macrostructure of the corona and the solar wind
- the characteristics of small scale electron density inhomogeneities.

Radio bursts of type III can also be used to map solar magnetic field lines of force throughout the interplanetary medium up to the earth orbit and beyond.

Future experiments of these kinds should be carried out between an out-of-the-ecliptic probe and the earth or an earth satellite.

Beaming of the radiation of type I and type III bursts was predicted long ago, but not observed until recently. Rather than giving up the basic mechanisms which seemed capable of explaining many observed properties but implied beaming effects, radio astronomers suggested that random inhomogeneities of the refractive index scattered the radiation. (Roberts, 1959). This suggestion received strong support when scintillations from radio stars seen through the upper corona were discovered. Fokker (1965), Steinberg et al (1971), and Riddle (1972) carried out Monte Carlo numerical computations of the scattering of the radiation from a source embedded in the inhomogeneous medium. These authors used models which were extrapolated to low coronal altitudes from measurements of radio scintillations made for paths which did not cross the corona lower than 5 solar radii or so. However, these studies were successful in accounting for several observations which could hardly be explained in any other way. They showed that the inhomogeneous medium produces a scattered image broader than the source and appreciably displaced from it ; at the same time, the random propagation tends to suppress any beaming of the radio waves and smoothes the radiation pattern of the source.

Measurements of the angular distribution of the intensity of a source of radio bursts can therefore yield information on :

- the orientation of the principal directions of the medium : $\text{grad } N_e$ or \vec{B} , the radiation mechanism and beaming processes.
- the characteristics of small scale inhomogeneities which cannot be obtained in any other way.

To measure directivity, observations from the ground only are inadequate. For many years, authors tried to reach at least a statistical view of the directivity of radio bursts ; for instance, from their E.W. probability of occurrence ; but, if the orientation of the radiation pattern of individual bursts relative to the local vertical through the source is not constant, no information on the directivity can be obtained from a single observing site. Simultaneous observations should be made in at least two widely different directions (Steinberg and Caroubalos, 1970).

We have seen that the suprathermal electrons which produce type III bursts are guided along open magnetic lines of force. These lines are carried away by the solar wind into interplanetary space so that type III are observed from low in the corona to the earth orbit and beyond. If we were able to map the successive positions of the type III source, we could also draw 3-D maps of some solar magnetic lines of force.

Stereoscopic observations of radio bursts are powerful tools to study the corona and solar wind. This may be illustrated by some recent results obtained with the STEREO-1 experiment carried out in 1971-1972 at 169 MHz in cooperation between France and the Soviet Union. (Caroubalos and Steinberg, 1974; Caroubalos, Poquerusse and Steinberg, 1974 ; Steinberg, Caroubalos and Bougeret, 1974). At 169 MHz, radio bursts of types I and III occur at altitudes in the range 0.3 - 0.5 solar radius.

STEREO RADIOASTRONOMY OF TYPE I BURSTS

Let θ be the stereo angle between the two observing directions. When θ increases, the correlation between the two intensity- VS time -

records taken simultaneously (in the source time scale) decreases in general. Even with $\theta \approx 15^\circ$, this is clearly visible, but when $\theta \approx 35^\circ$, the correlation coefficient is less than 0.1. This means that the beamwidth of type I radiation is sometimes smaller than about 25° . However, on some consecutive days, the same intensity may be received at both observing sites and then the beam pattern looks nearly isotropic. Such an apparent contradiction can be resolved if we note that the STEREO-1 observations were carried out in the ecliptic ; so that we are actually analyzing only a plane section of a 3-D beam pattern and we do not know the configuration of the beam pattern out of that plane ; we cannot, for instance, know if the 3-D beam pattern is solid, multilobed or even hollow. It is easy to conceive beam shapes whose cross sections by different planes can be either narrow or broad.

The ratio R of the burst intensity measured in Space I_S to that measured at the earth I_E varies widely from event to event ; so that the beam has to be randomly oriented if its shape is assumed almost constant ; the rms deviation of the orientation is about 0.25 of the beamwidth and this is a rather clear indication that the source does not contain a large number of inhomogeneities.

This is, in turn, connected to an old problem : type I burst intensity can vary by a large factor in 0.1 second ; but the observed source size is about 3 arc min or 0.3 light-second ; so that it was suggested long ago (Högbom, 1960 ; Fokker, 1960) that what we see is actually the scattered image of a deeper and smaller source. In a scattering corona, the assumed small scale inhomogeneities do produce a broad scattered image of a point source but at the same time they

broaden the angular distribution of the radiation from that point source. Both effects are intimately connected together via the scattering power distribution along the path. The total rms random angular deviation of the radio rays over their trip from the source to us cannot be larger than half the observed beamwidth ; STEREO observations yield directly a measure of the beamwidth and, thus, an upper limit to the rms angular deviation along the path. This limit is too small for the existing models to account for more than a small part of the image size. Therefore either there is less scattering than generally assumed to account for most of the source apparent size or the inhomogeneities built in the models are inadequate.

In any case it has been demonstrated that very interesting information on the beam orientation and shape can be obtained from stereoscopic observations. To learn more, it is necessary to go out of the ecliptic plane for the following reasons :

- to compare the beam orientation to that of the density gradient we must know the latter and therefore the 3-D electron density distribution in the source region. This can be obtained from coronagraphic measurements on the limb where the electron density distribution as a function of latitude will always be better known than the longitudinal one. It is therefore much more effective to measure the beam orientation in a plane perpendicular to the ecliptic than in the ecliptic.

- operating a stereoscopic experiment between an out-of-the-ecliptic probe and the earth will also provide a larger variety of cross sections of the beam pattern using solar rotation (fig.1); in the ecliptic, solar rotation moves the same cross section of the beam across our lines of sight. Using an out-of-the-ecliptic set-up

one should be able to get much closer to a complete description of the 3-D beam pattern of the bursts.

If the out-of-the-ecliptic probe is on a 1 AU orbit, in a plane tilted to the ecliptic, the stereo angle will also vary quite rapidly and this is again favourable to a detailed description of this beam pattern.

STEREO RADIOASTRONOMY OF TYPE III BURSTS

The spectrum of a type III in a frequency-time domain (dynamic spectrum) shows a band of noise drifting from high to low frequencies. This band is sometimes split in two components which, at a given time, are centered on harmonic frequencies. Some type III's are therefore made of two components which are believed to be produced, one (the "fundamental") at the local plasma frequency f_p , the other at twice that frequency. When observed with a single frequency receiver, the first component is recorded first and the second some seconds later, making up a "pair" of type III's.

This interpretation of pairs as fundamental-harmonic pairs has been questioned in recent times but not in a convincing way ; and to settle that question, directivity measurements are important : indeed, the conversion mechanism and the propagation conditions are different for the fundamental and the harmonic ; for instance, the fundamental is generated at about the local plasma frequency so that it should be beamed into a narrow cone ; and if the corona is assumed quasi spherical this cone should be about radially oriented so that few fundamental components should be seen in high longitude events ; this is not the case :

fundamental components are seen nearly all over the disc.

Stereoscopic observations showed that the first (fundamental) component of a pair is systematically more directive than the second (harmonic) and this is a strong argument for the fundamental-harmonic interpretation of pairs (fig.2).

The time profile of a type III at a fixed frequency is also rich in information as it is the convolution of an exciter function by the transient response of the corona which includes the effects of multipath propagation. At 169 MHz, it was found independent from the direction of observation ; therefore propagation conditions do not play an important role in the formation of the time profile.

While the time profile is independent of the direction of observation the intensity ratio $R = I_S / I_E$ can take values very different from unity ; the rate of change of the intensity with the observing directions can reach ± 10 dB and more over 30° . This proves, again, that coronal scattering is less effective than previously thought ; even less effective than necessary to account for some other observations ; for instance, scattering has been invoked to explain that, at a given observing frequency f , the fundamental component (local plasma frequency $f_p = f$) and the harmonic component ($2f_p = f$) are observed at the same position although the first should take place at the f critical level and the second at the $f/2$ critical level, higher up in the corona. This observation is indeed explainable in a scattering corona (Riddle, 1972 ; Leblanc, 1973) but the scattering power has to be larger than the one deduced from directivity measurements.

Another result from STEREO observations is that the directivity ratios of various type III's can be very different. This can be

interpreted if the observed directivity is produced by coronal macro-structures mostly in the form of streamers. On Nov. 14, 1971, for instance type III have been observed through a streamer ; the overdense streamer material reflects, absorbs and scatters the type III radiation, away from its source and produces the observed directivity. If this interpretation is correct, the streamers or "lames coronales" detected by Axisa et al (1971) do control the type III image size and shape as a piece of ground glass or a light shade. Observations of these images with radioheliographs together with Stereoscopic observations can be used to study the streamer structure which is hard to resolve optically because of line of sight integration effects. We still do not know where are the type III sources located as compared to streamers ; to settle that question 2-D position measurements at radio frequencies are necessary but at the present time, they are no more accurate than 1 arc min or so. Occultation effects are only detectable with Stereoscopic observations but they are very sensitive to the position of the source relative to the occulting structure. They open up new ways to localize the path of the type III electrons relative to streamers and the site where these electrons are accelerated in the active region. Here again the stereoscopic observations should be carried out on an out-of-the-ecliptic probe because the macro-structure of the corona is better known from optical observations as a function of latitude than of longitude.

One of the most useful properties of type III's is that they are produced over trajectories which span the interplanetary medium. At each altitude the 10-100 keV electrons induce plasma waves which are scattered into electromagnetic waves at the local plasma frequency f_p or at twice that the frequency. Therefore from the measurement of the position of type III's at several frequencies, a map of the electron density along the trajectory and a map of that trajectory itself can be drawn.

As the energetic electrons travel most probably along magnetic lines of force, we have a way of plotting such sun-rooted lines of force up to the earth orbit and beyond even out of the ecliptic.

Such an experiment should be carried out at frequencies lower than 10 MHz if we are interested in the coronal and solar wind structure higher than $10 R_{\odot}$; this means that observations should be made from space as radiation of these frequencies do not reach the earth. As a matter of fact IMP-6 has just done that (Fainberg and Stone, 1974). IMP-6 was spin stabilized around an axis perpendicular to the ecliptic and carried a dipole perpendicular to that axis. Using the nulls in the receiving pattern of a short electric dipole it is quite possible to measure the direction of a source as projected on the ecliptic plane. An experiment jointly designed and built by Paris Observatory and Goddard Space Flight Center teams will measure the direction of the type III source at 24 frequencies on ISEE-C. Using a spin plane and a spin axis dipole, the experiment will measure a complete direction (two angles) at each frequency and will produce 3-D maps of some magnetic lines of force from $10 R_{\odot}$ altitude to the earth orbit and beyond. It will, however, be necessary to assume that these lines of force rotate with the sun as a solid body. The use of a second remote satellite equipped in much the same way as ISEE-C could eliminate this restriction.(fig.3).

There are some indications from the radioastronomy experiments on IMP-6 and other experiments that few type III have been detected far out from the ecliptic. This might very well be due to some directivity of the radiation, but this difficulty can be overcome by going out of the ecliptic.

One of the main purposes of any out-of-the-ecliptic mission will certainly be to explore the 3-D topology of the interplanetary magnetic field and more specifically its latitude variation ; the role of solar active regions in the determination of this topology will be studied. Equipments designed to measure the local magnetic field vector will be flown to achieve this goal but it will be very hard to reconstruct the magnetic configuration in the whole heliosphere from local measurements only. Type III tracking at several frequencies can provide the overall description of this field topology which will be essential to the interpretation of most local measurements made on the O/E probe : for instance the modulation of cosmic rays by the interplanetary magnetic field cannot be understood without a description of this magnetic field in the whole heliosphere.

CONCLUSION

Stereoscopic observations of solar radio bursts are not needed only to improve our knowledge of the physics of these transient radio emissions. In the deci- to decameter- λ range, they can be used to probe the macro and microstructure of the corona. In the hm to km- λ range, type III's are natural tracers of sun-rooted magnetic lines of force ; tracking them as a function of frequency will give a 3-D map of some lines of force from low in the corona to the earth orbit and provide an overall picture of the interplanetary medium which is essential to the interpretation of local measurements.

The choice between the two wavelength ranges depends upon the scientific objectives of the mission ; but it has been shown that, in both cases, observations should be carried out from an out-of-ecliptic probe.

ACKNOWLEDGMENTS

Most of this work has been sponsored by Centre National d'Etudes Spatiales (CNES). The STEREO-1 mission was part of a cooperative program between the USSR (Intercosmos) and France (CNES).

- Axisa, F., Y. Avignon, M.J. Martres, M. Pick, and P. Simon,
Solar coronal streamers observed at 169 MHz with the Nançay
East-West radioheliograph, *Solar Phys.*, 19, 110-127, 1971.
- Caroubalos, C. and J.L. Steinberg, Evidence of solar bursts
directivity at 169 MHz from simultaneous ground based and
deep-space observations (Stereo-1 preliminary results),
Astron. and Astrophys., 32, 245-253, 1974.
- Caroubalos, C., M. Poquerusse, J.L. Steinberg, The directivity
of type III bursts, *Astron. and Astrophys.*, 32, 255-267, 1974.
- Fainberg, J. and R.G. Stone, Satellite observations of type III
solar radio bursts at low frequencies, *Space Science Reviews*,
16, 145-188, 1974.
- Fokker, A.D. Studies of enhanced solar radio emission at frequencies
near 200 MHz, Doctoral thesis, University of Leiden, 1960.
- Fokker, A.D., Coronal scattering of radiation from solar radio
sources, *Bull. Astr. Inst. Netherlands*, 18, 111-124, 1965.
- Högbon, J.A., The structure and magnetic field of the solar
corona, *Mon. Notices Roy. Astron. Soc.*, 120, 530, 1960.
- Leblanc, Y., Scattering effects on the relative positions
and intensities of fundamental and harmonic emission of solar
radio bursts, *Astrophysical Letters*, 14, 41-45, 1973.
- Riddle, A.C., The effect of scattering on solar radio sources at
80 MHz, *Proc. Astron. Soc. Austral.*, 2, 98-100, 1972.
- Roberts, J.A., Solar radio bursts of spectral type II, *Australian
J. Phys.*, 12, 327-356, 1959.
- Steinberg, J.L., M. Aubier-Giraud, Y. Leblanc and A. Boischot,
Coronal scattering, absorption and refraction of solar radiobursts,
Astron. and Astrophys., 10, 362-376, 1971.
- Steinberg, J.L. and C. Caroubalos, Space radioastronomy of solar
bursts at all frequencies : the Stereo-project, *Astron. and
Astrophys.*, 9, 329-338, 1970.
- Steinberg, J.L., C. Caroubalos and J.L. Bougeret, Stereo-1
measurements of the beam pattern of 169 MHz type I bursts on
November 18, 1971, *Astron. and Astrophys.*, 37, 109-115, 1974.

Steinberg - Caroubalos

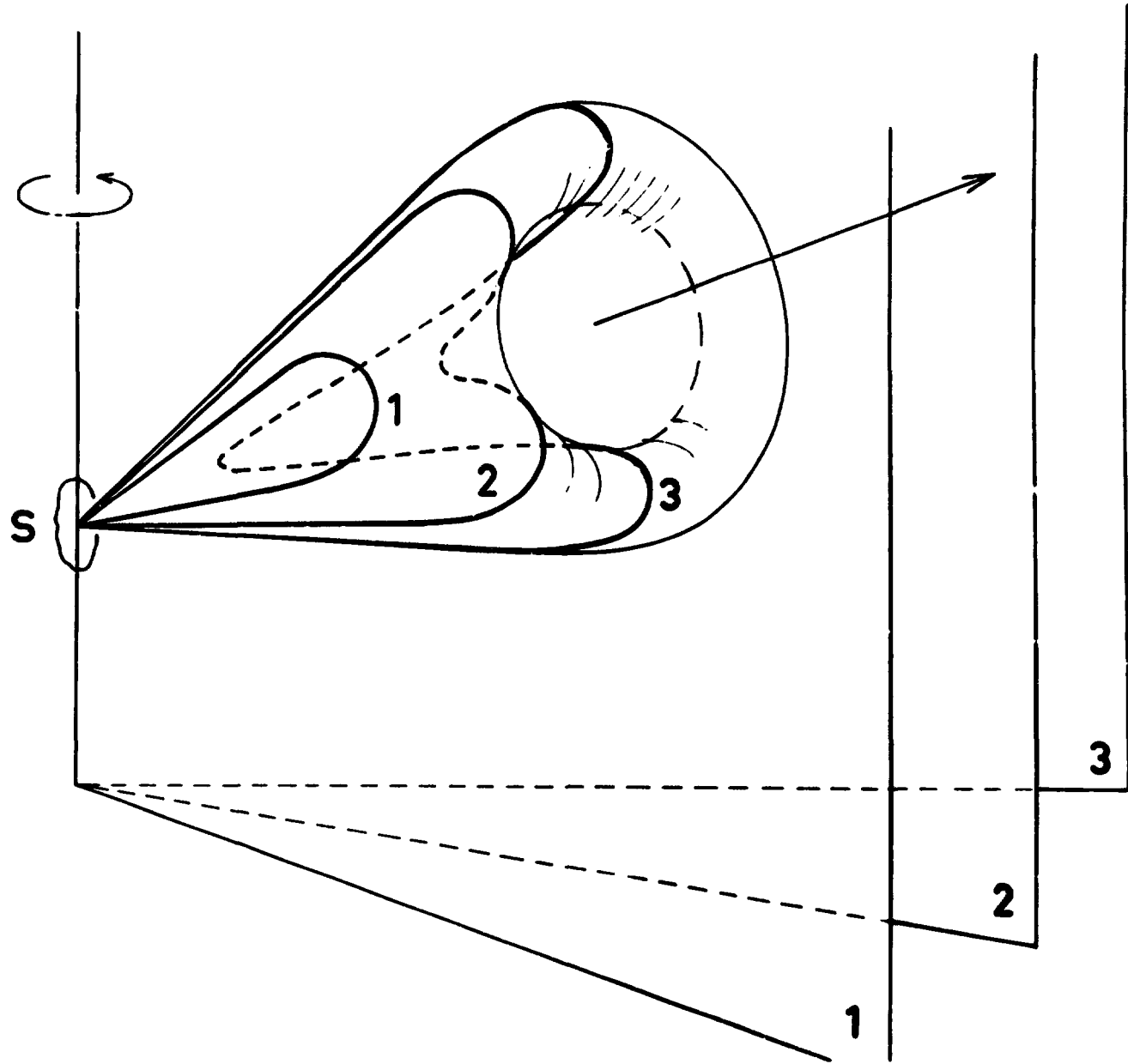
3-D Solar radioastronomy

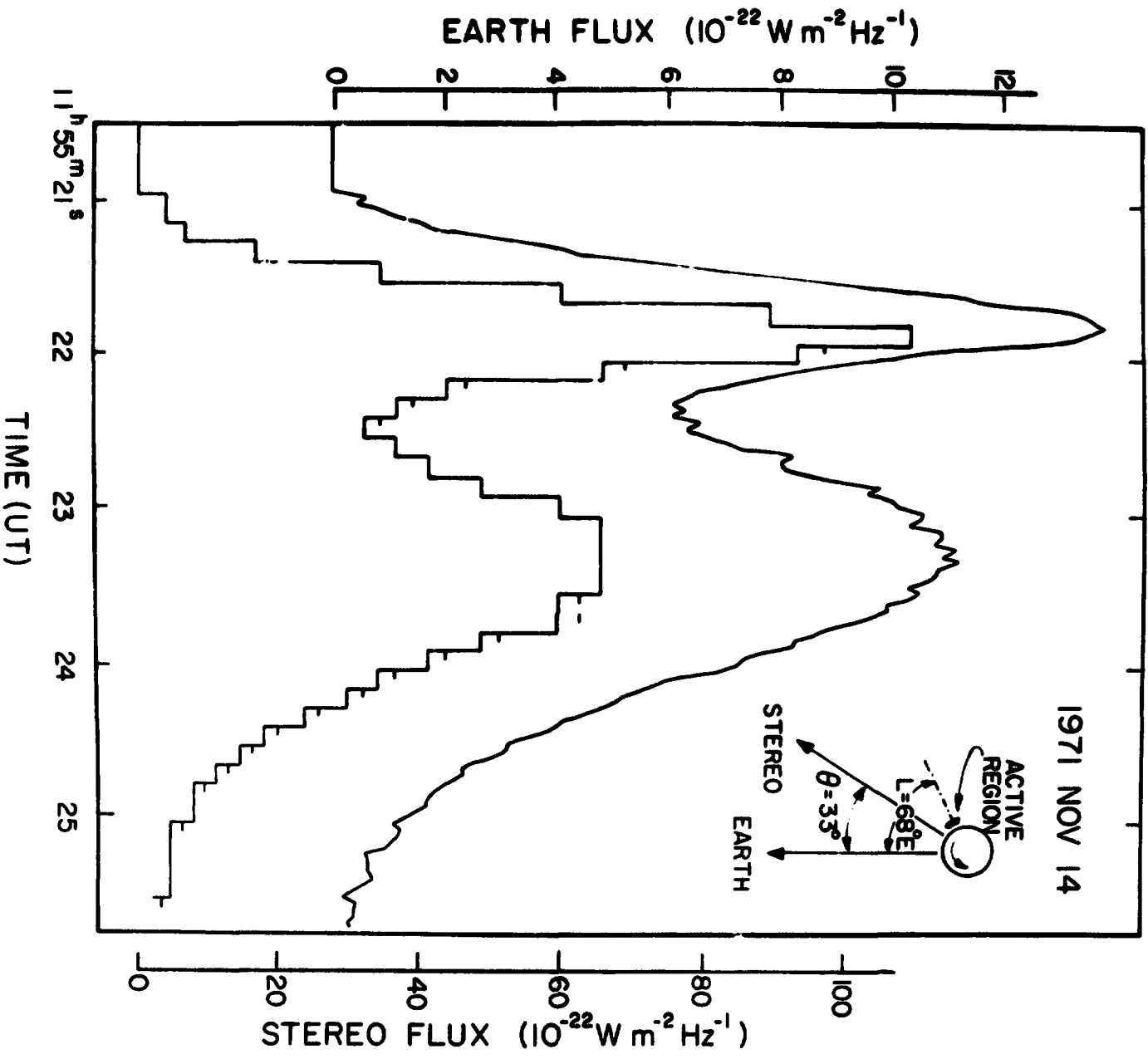
Figure Captions.

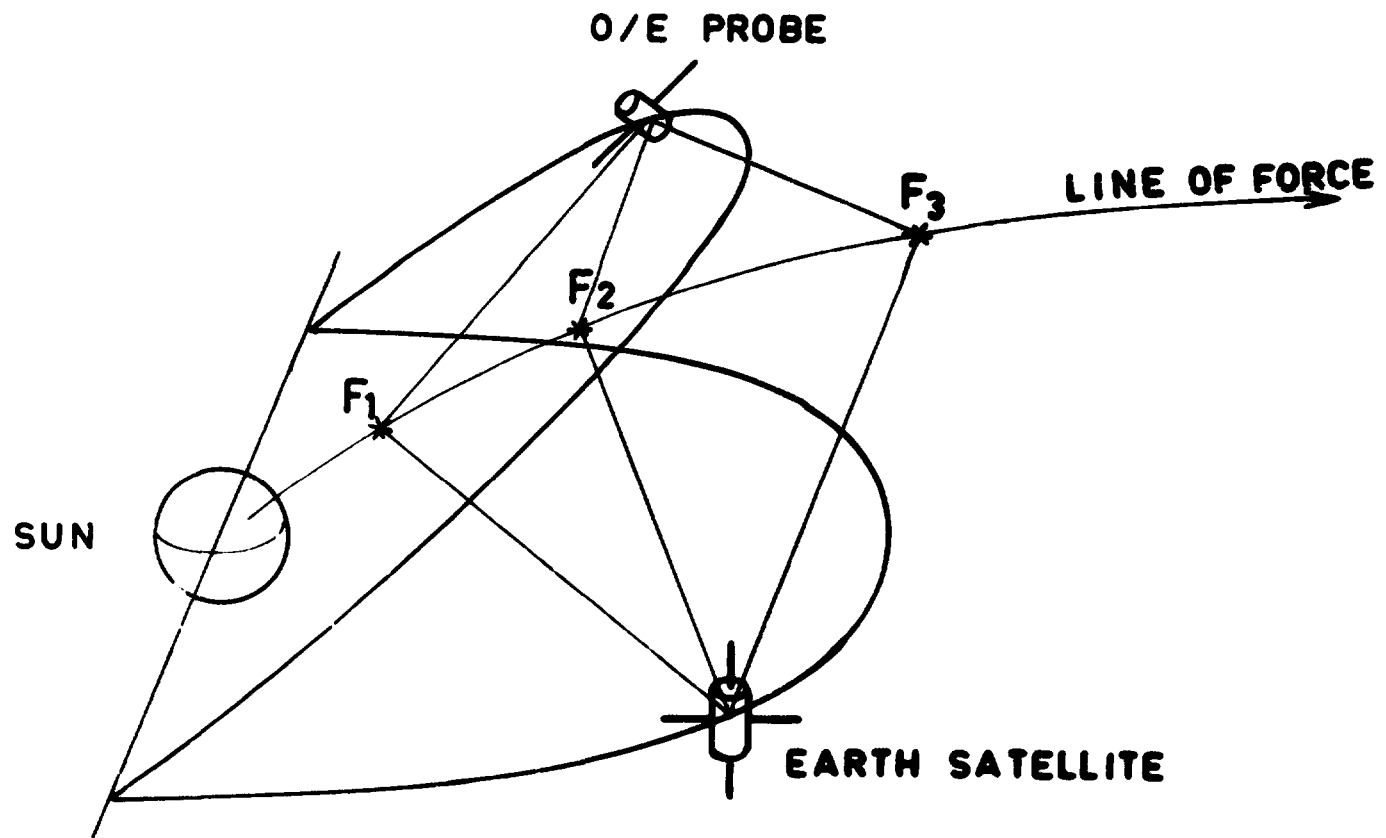
Fig.1 Exploration by stereoscopy in a plane perpendicular to the ecliptic of the radiation pattern of a radio burst using solar rotation. The plane sections 1 to 3 are analyzed at different times. If the exploration was carried out in the ecliptic, only one plane section would be studied.

Fig.2 A typical pair of type III bursts at 169 MHz as recorded from the earth (top) and from the Mars-3 Soviet space probe on Nov.14, 1971. The intensity ratio $I_{\text{Space}}/I_{\text{Earth}}$ first component (fundamental) is always greater than that of the second component (harmonic).

Fig.3 3-D mapping of a solar magnetic line of force using a type III burst as a tracer.







CHAPTER III

SOLAR WIND

PRECEDING PAGE BLANK NOT FILMED

N76-24125

**IPS OBSERVATIONS OF THE SOLAR WIND SPEED OUT
OF THE ECLIPTIC**

by
W. A. Coles
and
B. J. Rickett

**APPLIED PHYSICS & INFORMATION SCIENCE DEPARTMENT
UNIVERSITY OF CALIFORNIA, SAN DIEGO
LA JOLLA, CALIFORNIA 92093**

[Invited paper presented at the NASA/ESRO Symposium "The Sun and Interplanetary Medium in Three Dimensions" G.S.F.C., May 1975].

September, 1975

Abstract

Interplanetary scintillation (IPS) observations from 1971-1975 show that the average solar wind speed increases away from the solar equator, with a mean gradient of 2.1 km/s per degree. These results are compared with spacecraft observations over the $\pm 7^\circ$ attainable in the ecliptic and with those deduced from comet tails. The role of temporal variations, especially those caused by latitude dependent solar wind streams, is emphasized. This points to the need for extensive ecliptic and ground-based observations during an out-of-the-ecliptic spacecraft mission.

Introduction

The solar wind both in and out of the ecliptic can be studied from the earth by the method of Interplanetary Scintillations (IPS). The method was pioneered by Hewish and his colleagues, who deduced the solar wind speed from multiple station observations. In 1966 Dennison and Hewish (1967) found an increased speed out of the ecliptic, while in 1967 Hewish and Symonds (1969) found no such increase. Their multiple station observations then ceased. In this paper we report solar wind speeds deduced from 74 MHz IPS observations made at UC San Diego from May 1971 through to April 1975. The observing system was described by Armstrong and Coles (1972) and by Coles et al (1974). Results from 1972 were reported by Coles and Maagoe (1972). We will also mention briefly the relevance of IPS observations simultaneous with an out-of-the-ecliptic spaceprobe mission.

IPS Method

The scintillation signal is the sum of waves scattered along the line of sight from a given radio source. Most of the scattering occurs where the line of sight is closest to the sun, because of the steep decrease with solar distance in the strength of the electron density microstructure which causes IPS. For a spherically symmetric solar wind a weighting function can be defined and the IPS "mid-point" speed (Coles and Maagoe 1972) can be shown to be a spatial average of the solar wind speed centered on the point of closest approach. However, in the presence of solar wind streams spherical symmetry does not apply.

The effect of the spatial average through such streams has been investigated by comparing the IPS observation with those expected by mapping point observations made on the IMP-7 spacecraft out along the line of sight in question.

Harmon (1975) and Coles et al. (1975) demonstrated a close agreement between IPS "mid-point" speed and the IMP-7 data mapped to the point where the line of sight is closest to the sun. More detailed comparisons are in progress, investigating the precise form of the spatial weighting caused by streams. However, for the present purposes the comparison demonstrates that each IPS observation is representative of the solar wind speed at the point of closest approach.

Results

This effective observing point changes in solar latitude, longitude and radial distance as the sun rotates and the earth orbits the sun. Thus for radiosources not in the ecliptic, about two months of high solar latitude data can be obtained each year. The geometry, however, is such that the high latitudes occur together with small solar distances. The distance dependence can be separated out by studying the four ecliptic radio-sources, for which the latitude remains within 10° of the equator; Figure 1 shows the solar wind speeds averaged into intervals of 0.1 AU in radial distance during 1971-1975. We conclude that there is no significant variation of average solar wind speed with radial distance between 0.4 AU. and 1.1 AU. Figure 2 shows a similar plot for all sources versus latitude and, because there is no radial distance dependence, it can be interpreted as showing the solar wind speed as a function of latitude. The vertical bars are ± 2 standard deviations in the average solar wind speed over latitude intervals indicated by the horizontal bars. The r.m.s. variation in a single speed observation is remarkably constant at about 120 km/s, showing no significant change with latitude. The vertical error bars are larger at high latitudes because there are fewer data points at high latitudes. (In a

typical year, 300 observations from 0-10⁰N decreasing to 25 observations from 50⁰-70⁰N). The major conclusion is that there is a systematic increase of solar wind speed with latitudes both north and south of the solar equator. This is evident in each year from 1971 through 1975 as well as in the grand average of all data. The average gradient is close to 2.1 km/s per degree of latitude. However, the curves are not quite symmetrical but centered near 10⁰N, giving an apparently steeper gradient in the south than in the north. This asymmetry is only marginally significant and we are still checking for second order systematic errors which could cause this.

Discussion

Our observed latitude gradient must be compared with other data. As already mentioned, the Cambridge IPS observations detected a latitude gradient in 1966 but not in 1967. Whereas this could conceivably be influenced by solar cycle effects, it is more likely that the small number of observations at high latitudes is responsible. Their measurements included only about 30 days each year which corresponded to latitudes above 20⁰; the long term average behavior could well be masked by the day-to-day and month-to-month variability found in the solar wind speed.

Spacecraft observations have been analyzed to look for effects due to the $\pm 7^{\circ}$ latitude range available in the ecliptic (e.g. Hundhausen et al. 1971). Smith and Rhodes (1974) and Rhodes and Smith (1975) deduced large apparent gradients (10-15 km/s per degree) by comparing solar wind speeds observed near Earth (Explorer 33,34,35) and at Mariner 5. They analyzed data from nearly six solar rotations over latitude differences from 0⁰ to 6⁰. We suggest that a possible explanation of their large gradient over a few degrees of latitude comes from solar wind streams. From our IPS data it is clear that solar wind streams often exist for several solar rotations with steep latitude gradients near the equator (see for example the wide southerly stream in

Figure 13 of Coles et al. 1974). It is likely that such features contribute strongly to a six month average. Figure 2 shows that in 1972 the apparent gradient between $\pm 5^\circ$ was + 4 km/s per degree, while in 1973 the apparent gradient reversed to - 3 km/s per degree. The influence of steep latitude gradients from specific recurrent streams was probably the cause for such large values.

More difficult to reconcile are the results from comet tail observations. Brandt et al. (1975) have analyzed 678 comet observations spread over 75 years and conclude that the latitude gradient is $- 0.9 \pm 0.7$ km/s per degree north or south; that is not significantly different from zero. Their observations are concentrated in the range 0° to 50° N (as are the IPS observations) and are scattered fairly well through the phases of the solar cycle. It would be of interest to see if the high latitude data were uniformly distributed over the phases of the solar cycle. Except for solar cycle effects we cannot suggest any simple explanation for the discrepancy; though long term systematic or random temporal variations could be responsible.

Conclusions

We have presented strong evidence that during 1971 through 1975 the average solar wind speed increased out of the equatorial plane giving an average gradient of 2.1 km/s per degree of latitude either north or south. Our observations show that stream and also slower variations can obscure the average latitude behaviour in the solar wind (as they do also for average properties in the ecliptic). In planning out-of-the-ecliptic spacecraft missions such changes must be expected. Jupiter "swing-by" missions would give 12-18 months at more than 30° from the equator. During this time it will be important to maintain regular observations in the ecliptic in order to

disentangle temporal and latitude effects. A continued program of IPS observations throughout the period would cover a range of longitudes and latitudes and further help build a picture of the spatial and temporal structure in the solar wind. In addition to the average latitude behaviour such joint observations would allow the latitude structure of individual streams to be explored.

Acknowledgements

We are very grateful to all the people who have helped make the IPS observations at UCSD since 1971. In particular we thank John Armstrong, John Harmon, Jay Kaufman, Steffen Maagoe, Steve Scott and David Sime. This research is supported by the Atmospheric Sciences Division of the N.S.F. under grant DES 75-13451.

References

- Armstrong, J. W. and W. A. Coles, Analysis of Three-Station Interplanetary Scintillation, J. Geophys. Res., 77, 4602, 1972.
- Brandt, J. C., R. S. Harrington, and R. G. Rosen, Interplanetary Gas. XX. Does the Radial Solar Wind Speed Increase with Latitude?, Astrophys. J., 196, 877, 1975.
- Coles, W. A., B. J. Rickett, and V. H. Rumsey, Interplanetary Scintillations, Solar Wind Three (Edited by C. T. Russell), published by IGPP, UCLA, 1974.
- Coles, W. A. and S. Maagoe, Solar Wind Velocity from IPS Observations, J. Geophys. Res., 77, 5622, 1972.
- Coles, W. A., J. K. Harmon, A. J. Lazarus, and J. D. Sullivan, Comparison of 74 MHz IPS and IMP 7 Observations of the Solar Wind during 1973, Trans. A.G.U., EOS, 56, 440, 1975.
- Dennison, P. A. and A. Hewish, The Solar Wind Outside the Plane of the Ecliptic, Nature, 213, 343, 1967.
- Harmon, J. K., Scintillation studies of density microstructure in the solar wind plasma, Ph.D. Thesis, UC San Diego, 1975.
- Hewish, A. and M. D. Symonds, Radio Investigation of the Solar Plasma, Planet. Space Sci., 17, 313, 1969.
- Hundhausen, A. J., S. J. Bame, and M. D. Montgomery, Variations of Solar Wind Properties: Vela Observations of a possible heliographic latitude dependence, J. Geophys. Res., 76, 5145, 1971
- Rhodes, E. J., Jr., and E. J. Smith, Multispacecraft study of the solar wind velocity at Interplanetary Sector boundaries, J. Geophys. Res., 80, 917, 1975.
- Smith, E. J. and E. J. Rhodes, Jr., Evidence of a Velocity Gradient in the Solar Wind, Solar Wind Three (Edited by C. T. Russell), published by IGPP, UCLA, 1974.

Figure Captions

Figure 1. Solar wind speeds from 1971-1975 measured within 10° of the solar equator, averaged into 0.1 AU intervals of radial distance. The vertical error bars are \pm twice the standard deviation in the mean.

Figure 2. Solar wind speeds from 1971 through 1975 averaged into latitude intervals shown by the horizontal bars. Vertical bars are \pm twice the standard deviation in the mean. The lower right graph is the overall average from the other five graphs.

Figure 1.

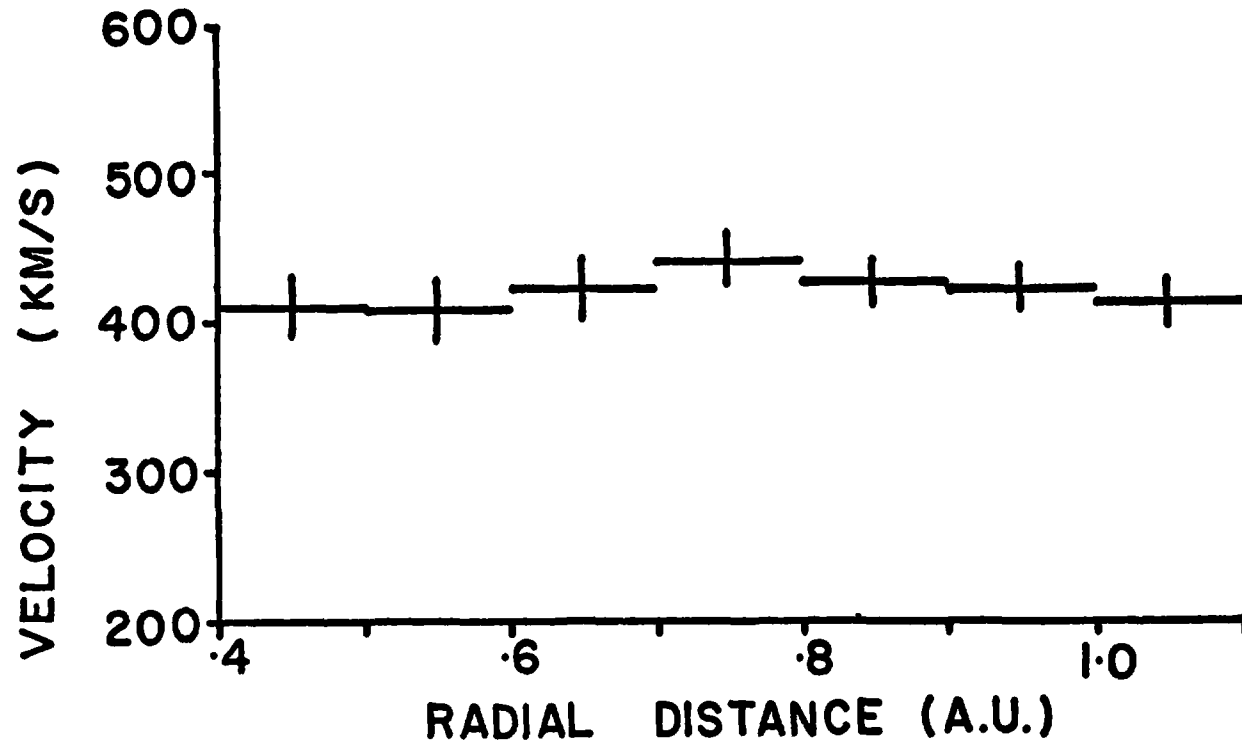
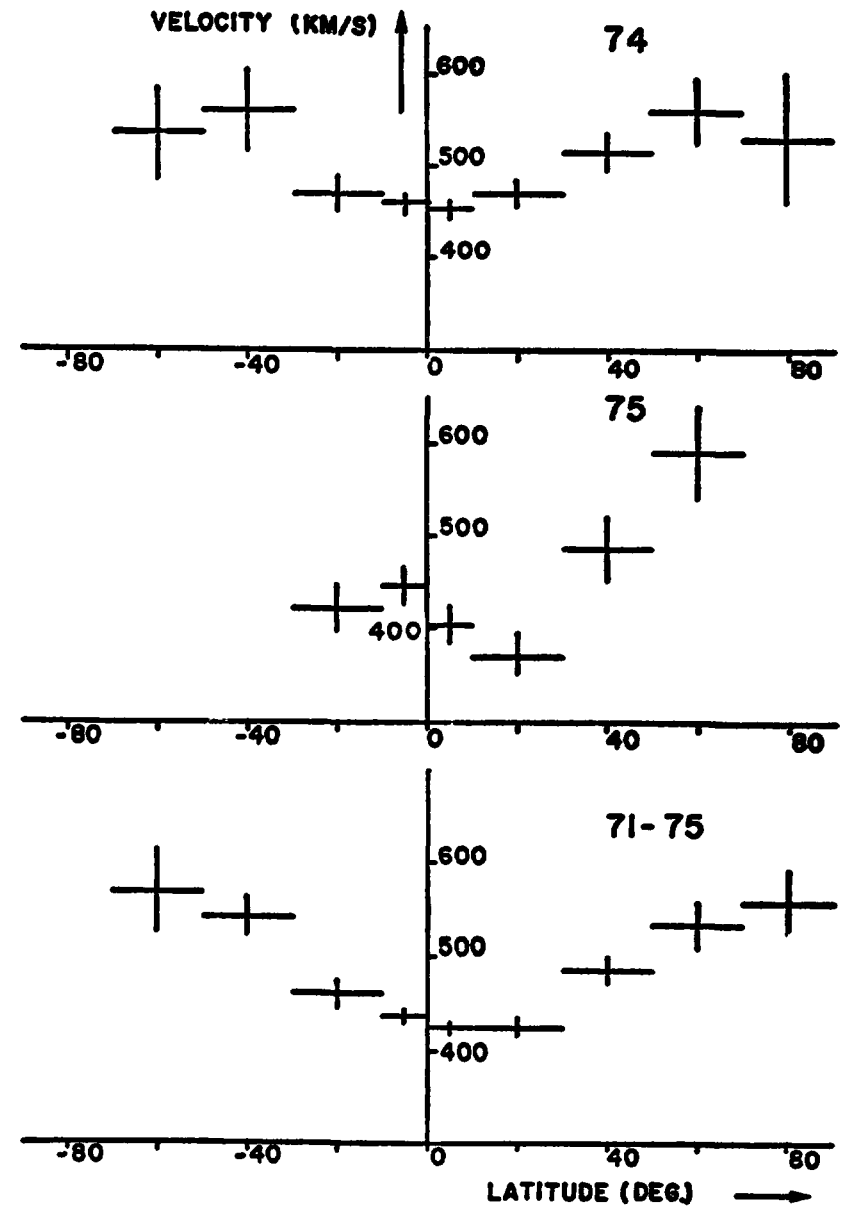
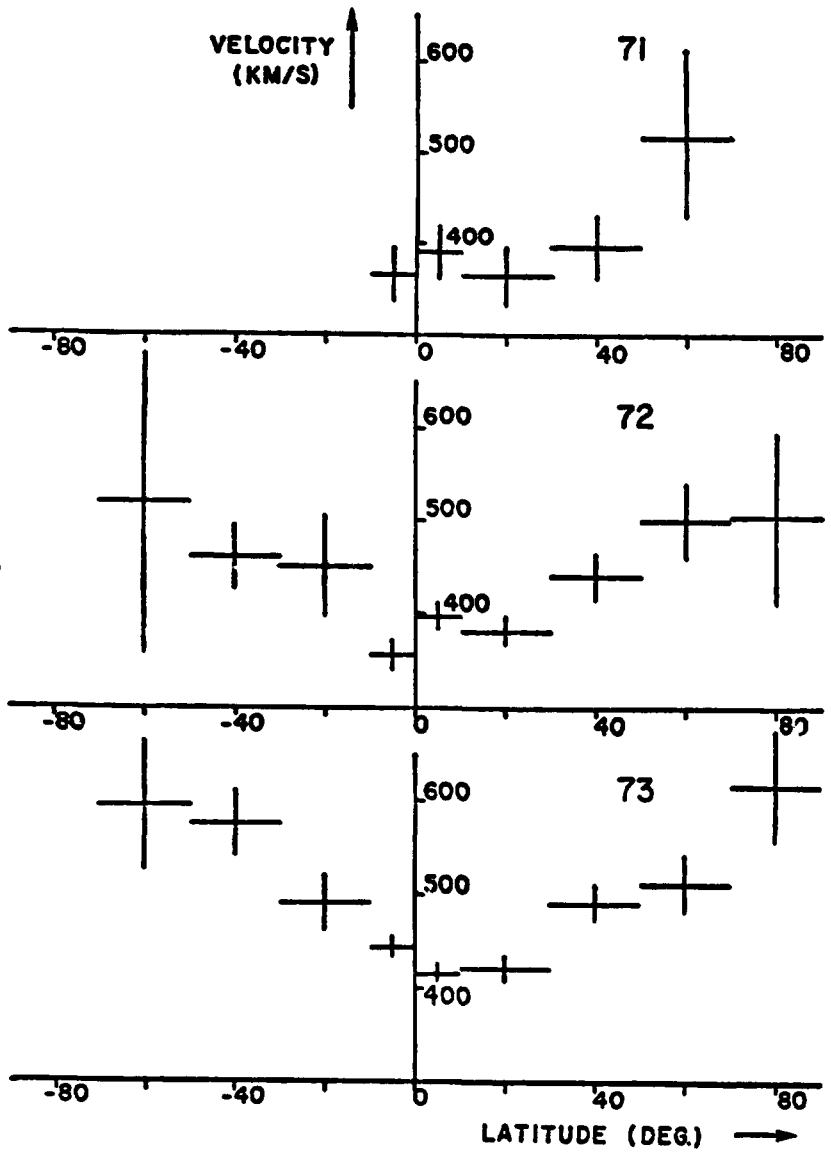


Figure 2.



' N76-24126

LATITUDINAL PROPERTIES OF THE SOLAR WIND
FROM STUDIES OF IONIC COMET TAILS

John C. Brandt
Laboratory for Solar Physics and Astrophysics
NASA-Goddard Space Flight Center
Greenbelt, Maryland 20771

Abstract - Analysis of the orientations of ionic comet tails gives no support for the suggestion that the radial solar wind speed is higher near the solar poles than near the equator. These results refer to a long-term, global flow pattern and do not refer to short-term variations.

Evidence from comets concerning the latitudinal variation of solar wind parameters has been discussed previously by Pflug (1966), Brandt (1967), and by Bertaux, Blamont and Festou (1973). In this short report, I summarize the evidence based on ionic comet-tail orientations as recently analyzed by Brandt, Harrington, and Roosen (1975), and show the distribution of the sample in latitude, time, and phase of the solar cycle.

The basic observation is the position angle of the tail axis on the plane of the sky (Belton and Brandt 1966). The position angle Θ is interpreted in terms of a tail vector \underline{T} whose direction in space is determined by dynamical aberration, viz.,

$$\underline{T} = \underline{w} - \underline{V} \quad (1)$$

where \underline{w} is the solar wind velocity vector and \underline{V} is the vector velocity of the comet. The astrometric technique developed by Brandt, Roosen, and Harrington (1972) does not assume that the comet tail lies in the plane of the comet's orbit. Each observation determines essentially a half plane in velocity space. A preferred solar wind velocity vector (w_r, w_θ, w_ϕ) is determined as the one which minimizes the sum of the squares of the residuals between the computed and observed position angles.

At present, a sample of 678 observations are available and these are spread over approximately 75 years in time and between roughly 0.5 to 1.5 a.u. in heliocentric distance. The basic results are a radial velocity, $\langle w_r \rangle \approx 400$ km/sec, an azimuthal velocity $\langle w_\phi \rangle \approx 6-7$ km/sec (varying with solar latitude b and distance r as $\cos^{2.315} |b|/r$), and a

RMS dispersion of 3.7° . An additional result from comet tail orientations, but not from the astrometric technique, is that $w_r \geq 225$ km/sec (Brandt and Heise 1970). These values are in good agreement with results from spacecraft and provide confirmation of the basic approach.

This technique has been previously used to search for a meridional flow pattern in the solar wind. A value $w_m \approx 2.5$ km/sec (at $\theta = 45^\circ$, varying as $\sin 2\theta$) has been found in the sense of a flow diverging from the plane of the solar equator by Brandt, Harrington, and Roosen (1973). This result implies a radial variation in the equatorial density of the solar wind of $N \propto r^{-2.013}$. If this law held from the sun to earth, the density would be 7% smaller than on spherically symmetric models.

The basic technique can be used to search for a latitudinal variation of the radial solar wind speed by assuming that it varies as

$$w_r = w_0 + \frac{dw_r}{d|b|} |b| \quad (2)$$

where w_0 and $dw_r/d|b|$ are constants to be determined. The results are given in Table 1.

Table 1.

Solar-Wind Speeds With and Without a Latitudinal Variation in Radial Speed				
w_r or w_o (km sec ⁻¹)	$dw_r/d b $ (km sec ⁻¹ deg ⁻¹)	w_m (km sec ⁻¹)	w_ϕ (km sec ⁻¹)	RMS Dispersion in ($\Theta - \Theta_c$)
402.5±11.9	≡0	+2.6±1.2	7.0±1.8	3 ^o .749
418.5±27.3	-(0.9±0.7)	+2.9±1.3	5.3±2.2	3 ^o .750

The latitudinal variation found in our sample, if any, is in the sense of decreasing radial speed with increasing latitude. However, the error in $[dw_r/d|b|]$ is almost as large as the value of $-0.9 \text{ km sec}^{-1} \text{ deg}^{-1}$ found, and there is clearly no trend. In addition, the best solution as judged by RMS dispersion is still the solution with $[dw_r/d|b|] = 0$. When an additional significant parameter is included in the model, the dispersion must decrease even if only marginally. The lack of a decrease is a definite flag that the additional parameter has no significance. The slight increase in RMS dispersion is simply due to round-off error. The errors in the components of the solar wind speed increase with a latitudinal variation included because then all components are functions of heliographic latitude and can be correlated. Possible correlations between components are calculated and are used to assign the probable errors. This is the explanation for the increase in errors while the RMS residuals remained essentially constant.

The negative result for significant latitudinal variation in w_r refers only to a long-term, global situation. It does not rule out shorter term results such as the one presented by Rickett (1975; preceding paper). It does appear to imply that such short-term variations average out over the long term.

The sample is concentrated in the range $0 \leq |b| \leq 50^\circ$ as shown in Figure 1a where the solid line represents the present sample of 678 observations and the dashed line represents the same number distributed at random; only 60 observations lie in the range $50^\circ \leq |b| \leq 90^\circ$. If we plot the distribution against latitude instead of the absolute value of latitude as shown in Figure 1b, we find a strong concentration of observations in the northern hemisphere. There is no obvious reason to expect an adverse effect from this observational bias. The sample by year of observation is shown in Figure 1c which reflects the irregular nature of cometary apparitions and the reduction of observations. Figure 1d shows the distribution of the sample with phase in the solar cycle; the observations are concentrated toward solar maximum.

Because the astrometric technique can be applied only to fairly large groups of observations, results on short-term variations in the solar wind speed cannot be obtained directly. Work on an indirect technique is currently in progress.

Nevertheless, there is ample direct evidence for large, short-term variations in solar wind properties. The time required to establish a meaningful measurement of an average property at a

particular latitude is probably at least one solar rotation. This was found to be the case for spacecraft observations of w_{ϕ} as reported by Lazarus and Goldstein (1971). Hence, direct out-of-the-ecliptic observations of the solar wind should utilize an orbit with a slowly changing latitude. Several passes through all solar latitudes and possibly several spacecraft will be required to map out the basic structure of the solar wind in three dimensions.

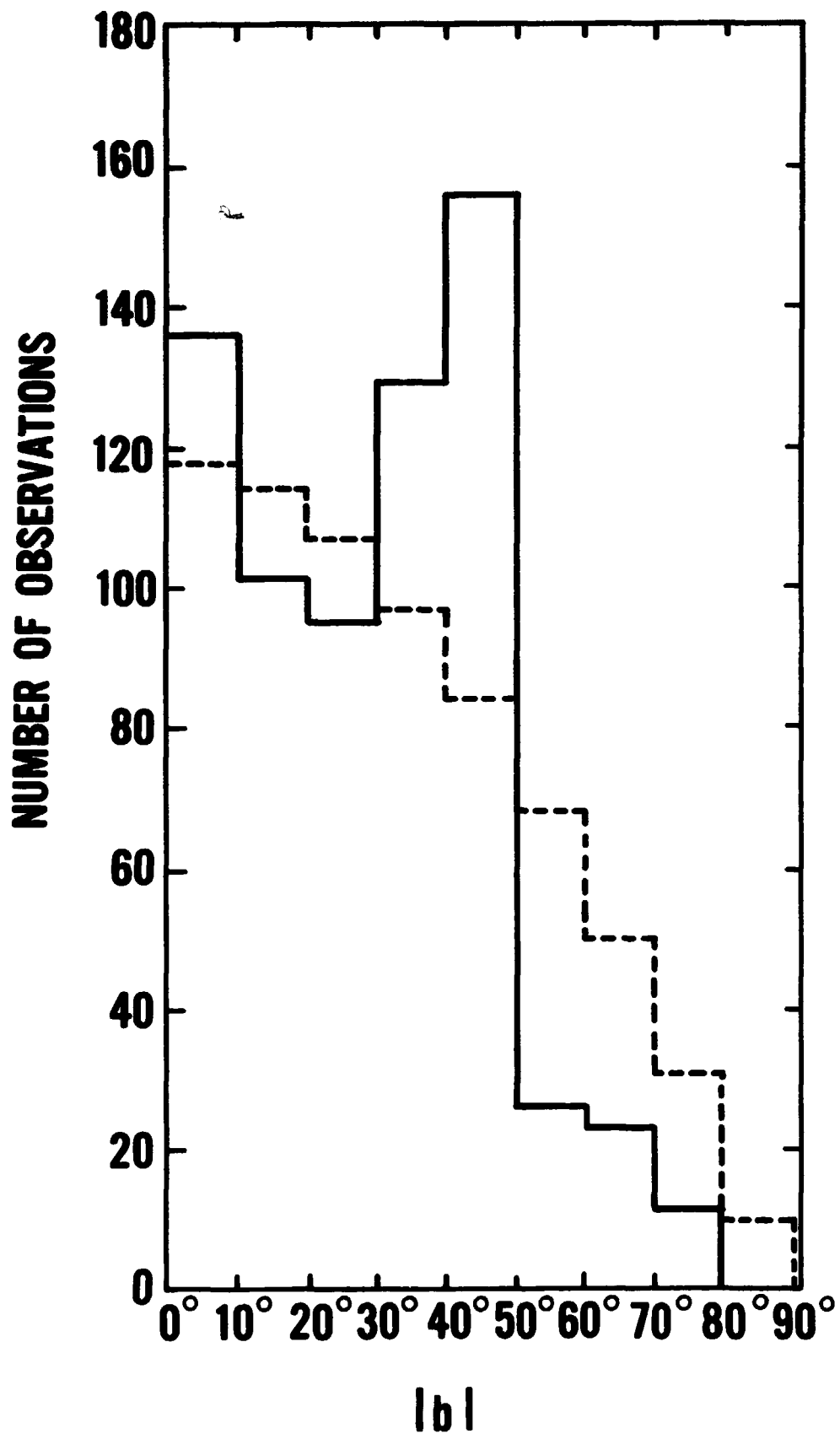
REFERENCES

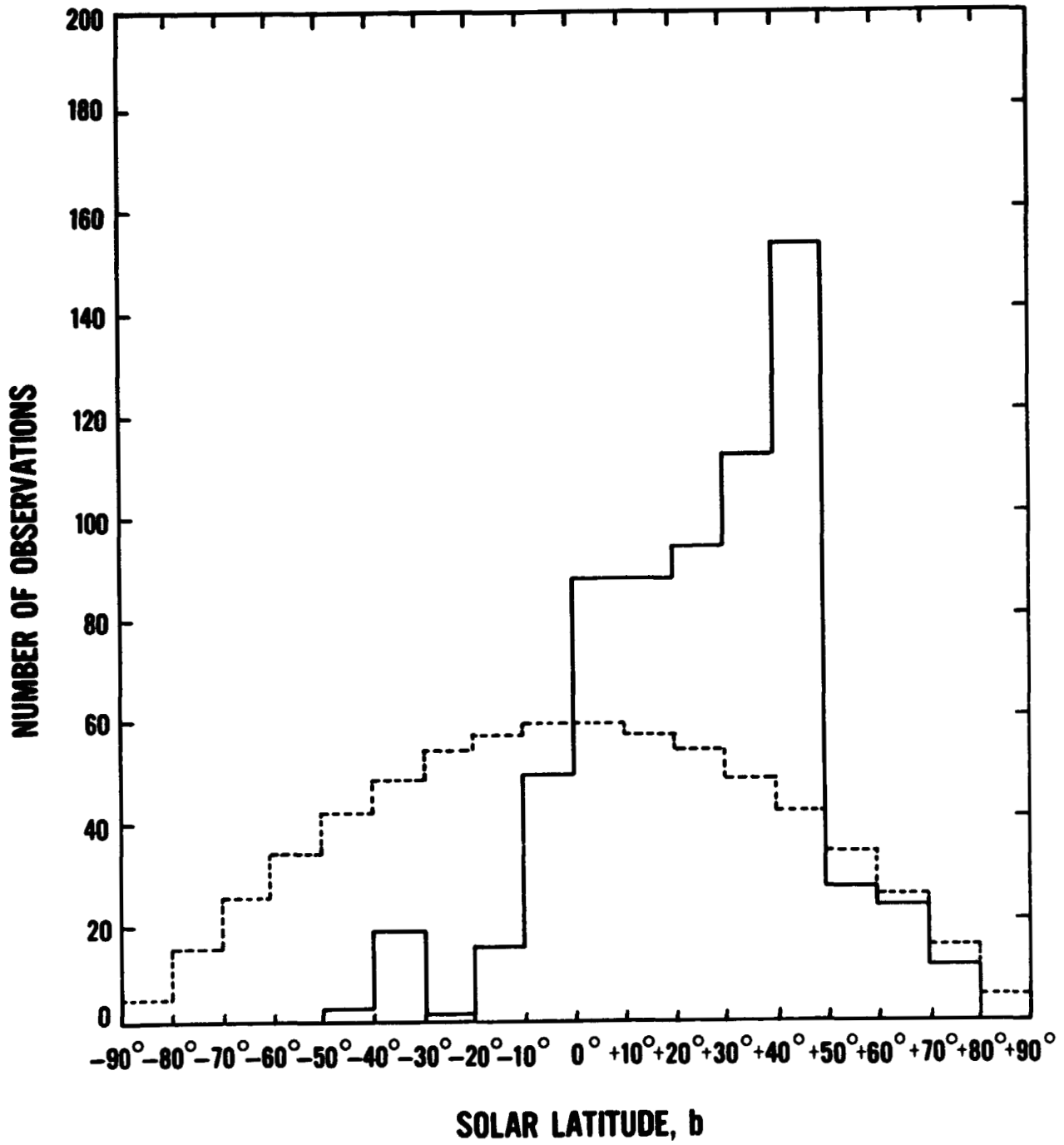
- Belton, M. J. S., and J. C. Brandt, Interplanetary Gas. XII. A catalog of comet-tail orientations, Ap. J. Suppl., 13, 125 (No. 117), 1966.
- Bertaux, J. L., J. E. Blamont, and M. Festou, Interpretation of hydrogen Lyman-alpha observations of Comets Bennett and Encke, Astr. and Ap., 25, 415, 1973.
- Brandt, J. C., Interplanetary Gas. XIII. Gross plasma velocities from the orientations of ionic comet tails, Ap. J., 147, 201, 1967.
- Brandt, J. C., R. S. Harrington, and R. G. Roosen, Interplanetary Gas. XIX. Observational evidence for a meridional solar-wind flow diverging from the plane of the solar equator, Ap. J., 184, 27, 1973.
- Brandt, J. C., R. S. Harrington, and R. G. Roosen, Interplanetary Gas. XX. Does the radial solar wind speed increase with latitude?, Ap. J., 196, 877, 1975.
- Brandt, J. C., and J. Heise, Interplanetary Gas. XV. Nonradial plasma motions from the orientations of ionic comet tails, Ap. J., 159, 1057, 1970.
- Brandt, J. C., R. G. Roosen, and R. S. Harrington, Interplanetary Gas. XVII. An astrometric determination of solar-wind velocities from orientations of ionic comet tails, Ap. J., 177, 277, 1972.
- Lazarus, A. J., and B. E. Goldstein, Observation of the angular-momentum flux carried by the solar wind, Ap. J., 168, 571, 1971.
- Pflug, K., Die bestimmung der ausbreitungsgeschwindigkeit und anderer eigenschaften des interplanetaren plasmas aus der richtung der gasschweife der kometen, Pub. Ap. Obs. Potsdam, No. 106, 1966.

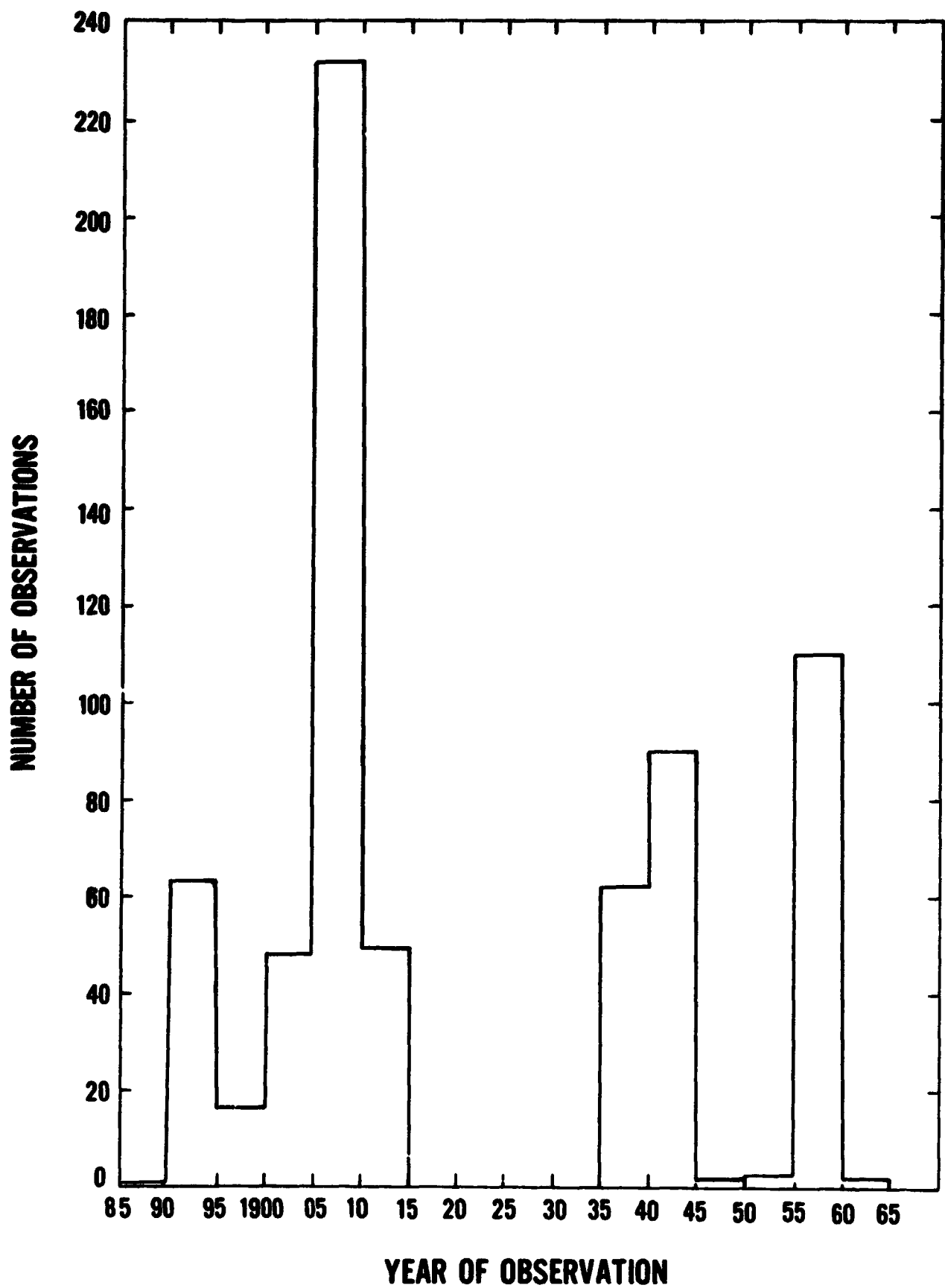
**Rickett, B. J. The solar wind velocity in 1972-1974 as
measured by radio scintillations, preceding paper, 1975.**

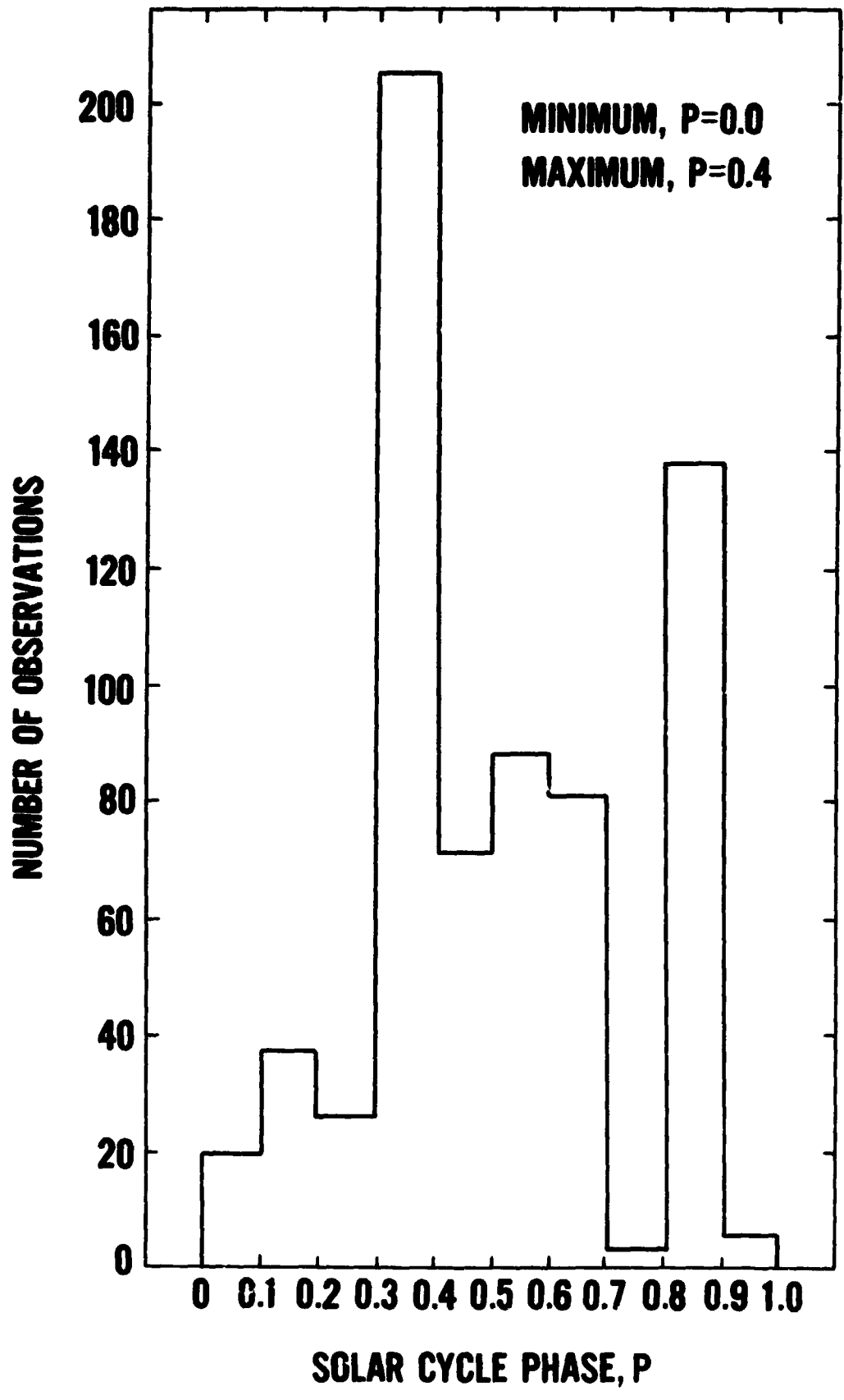
FIGURE CAPTION

Figure 1. The distribution of the sample of comet observations:
(a) in absolute value of solar latitude; (b) in solar latitude;
(c) in date of observation; and (d) in solar cycle phase. See text
for discussion.









N76-24127

**Implications of Saito's Coronal Density Model on the Polar Solar Wind Flow
and Heavy Ion Abundances**

William C. Feldman

University of California, Los Alamos Scientific Laboratory

Los Alamos, New Mexico 87545

ABSTRACT

A comparison of polar solar wind proton flux upper limits derived using Saito's coronal density model, with Ly α measurements of the length of the neutral H tail of comet Bennet at high latitudes, shows that either extended heating beyond $2 R_{\odot}$ is necessary some of the time or that Saito's polar densities are too low. Whichever possibility is the case, the fact that the solar wind particle flux does not appear to decrease with increasing latitude, indicates that the heavy element content of the high latitude wind may be similar to that observed in the ecliptic. It is then shown that solar wind heavy ion observations at high latitudes allow a determination of the electron temperature at heights which bracket the nominal location of the coronal temperature maximum thus providing information concerning the magnitude and extent of mechanical dissipation in the intermediate corona.

1. Introduction

There is, at present, a lack of information on the physical conditions in the polar regions of the solar corona and solar wind. This lack results in a corresponding uncertainty in the global characteristics and extent of that plasma of solar origin which fills interplanetary space and thereby controls the near solar environment. For example, only little is known about the variation with heliographic latitude of so fundamental a flow parameter as the solar wind mass flux. Similarly, hardly anything is known about latitude variations of the solar wind energy and momentum fluxes. Yet, these parameters may be very important in determining the physical state of the polar corona and the size of the solar dominated cavity over the poles which separates the sun from the local interstellar medium. In addition, the existence of heavy elements in the polar solar wind may depend (Allouche, 1967, 1970; Geiss et al., 1970) on whether or not the proton particle flux exceeds a temperature dependent lower limit.

It is therefore useful to consider hypothetical variations of solar wind particle and energy fluxes with heliographic latitude. This task is approached in section 2 of this paper by calculating upper limit values of the polar solar wind particle flux implied by the most comprehensive coronal density model developed to date (Saito, 1970). This model was determined from an average K corona brightness distribution constructed using 15 solar eclipse observations as well as K-coronameter measurements all made at the minimum phases of the solar activity cycle. As a necessary result of the method employed, the model densities (and hence

the upper limit values of the solar wind particle flux derived below) determined for the polar regions are uncertain because it is not possible to uniquely invert the convolution integral which relates the coronal brightness distribution to the average line of sight electron density. Nevertheless, it is shown that if the polar coronal densities are as low as calculated using Saito's model, then without extended heating, the emitted polar particle flux should be substantially less than that observed in the ecliptic plane at 1 AU and less than that necessary to drag coronal heavy elements away from the sun. However, limited evidence based on Ly α measurements of the neutral hydrogen tail of comet Bennet (Bertaux et al., 1973; Keller, 1973), is consistent with a polar solar wind flux at least as large as that observed in the ecliptic at 1 AU. These observations therefore require either an extended coronal heat source distinct from electron heat conduction or that Saito's polar densities are too low. In any event since the particle flux in the polar wind may be comparable to that observed in the equatorial wind, it is possible that coronal heavy ions at polar latitudes do indeed expand with the protons into interplanetary space.

Since it is reasonable to expect that heavy elements will be observable in the polar solar wind, the range of ionization state "freezing in" distances is estimated in section 3 for selected heavy ion species at polar latitudes. It is found that the polar coronal density may be sufficiently low that the ionization states "freeze in" below the nominal location of the temperature maximum. Hence high latitude heavy ion observations may allow a determination of the thermal state of the intermediate and low corona and provide an estimate of the magnitude and

extent of mechanical dissipation. Section 4 summarizes the main conclusions.

2. Latitude Variations of the Solar Wind Particle Flux

It is currently thought that the solar wind evolves from open field regions in the corona (see Hundhausen, 1972 for a review). Such regions are generally distinct from regions of activity and are generally characterized by low density. For these regions, the electron density, N , as a function of solar distance, r , and heliographic latitude, θ , has been modeled by Saito (1970) with the relation

$$N = \frac{3.09 \times 10^8 (1 - 0.5 \sin\theta)}{R^{16}} + \frac{1.58 \times 10^8 (1 - 0.95 \sin\theta)}{R^6} + \frac{0.0251 \times 10^8 (1 - \sin^{1/2}\theta)}{R^{2.5}} \text{ cm}^{-3} \quad (1)$$

where $R = r/R_{\odot}$ and R_{\odot} is the solar radius.

Upper limit values for the polar solar wind particle flux can be derived using relation 1 if various subsets of several reasonable assumptions concerning the state of the intermediate corona are adopted. These assumptions are 1) the coronal gas consists of H, He and electrons only, 2) there is no extended heating other than that due to electron heat conduction much beyond the coronal temperature maximum, 3) the energy equation may be closed with the standard relation $\bar{Q} = -\kappa_{\odot} T^{5/2} \nabla T$ (Chapman, 1954; Spitzer, 1956) which assumes that binary coulomb interactions limit the mean scattering length of a thermal electron, 4) coronal electron and proton velocity distributions are very

nearly Maxwellian, 5) wave-particle interactions and macroscopic wave pressure effects are negligible above the heating region, and 6) the magnetic field is open but not necessarily radial.

The purpose of this section is to show that if the coronal density over the pole drops off as quickly as implied by Saito's analysis then some of the above assumptions may be tested by in situ solar wind observations. We begin with a standard single fluid formulation of the coronal expansion using equation 1 in place of an energy equation and derive upper limits for the particle flux at 1 AU. A separate treatment based on various possible forms of the energy equation is considered next to provide independent estimates of the 1 AU flux upper limit. The results of this analysis are in agreement with those obtained by Durney and Hundhausen (1974). As will be shown in section 3 these upper limits are substantially lower than that observed in the ecliptic at 1 AU and are sufficiently low, that if all of the above assumptions are correct, He⁺⁺ and many of the heavier ions should not expand with the protons away from the sun at polar latitudes.

(i) Mass Flux, Momentum Flux and Density Equations

The mass and momentum conservation equations are respectively;

$$NVA(R) = F \quad (2)$$

$$m_p MNV \frac{dV}{dR} = - \frac{d}{dR} (NkT) - \frac{NGM_\odot m_p M}{R^2 R_\odot} \quad (3)$$

Here A(R) is the area of a flux tube which varies as R² if the expansion is radial, G is the gravitational constant, M_⊙ is the mass of the sun, m_p is the proton mass, M is the mean molecular weight = (1 + 4α)/(2 + 5α) where α is the He

abundance by number, k is Boltzmann's constant, N is the proton density, V is the bulk convection speed and T is the one fluid temperature. Concentrating on the region in the intermediate corona between $R = r/R_0 = 2$ and 4, equation 1 for $\theta = 90^\circ$ can be simplified to the form:

$$N(R) \cong \frac{7.9 \times 10^6}{R^6} \text{ cm}^{-3} \quad (4)$$

If it is assumed that $A(R)$ varies as R^S then equations 2, 3, and 4 can be integrated analytically to obtain $T(R)$

$$\frac{T(R)}{T_0} = \left(\frac{R}{R_0}\right)^6 \left\{ 1 - \left(\frac{GM_{\odot} m_p M}{7kR_0 R_{\odot} T_0}\right) \left[1 - \left(\frac{R_0}{R}\right)^7 \right] - \left(\frac{m_p M (NV)_0^2}{N_0^2 k T_0}\right) \left(\frac{6-S}{6-2S}\right) \left[\left(\frac{R}{R_0}\right)^{(6-2S)} - 1 \right] \right\} \quad (5)$$

Here the subscript 0 refers to parameters evaluated at the base radius R_0 .

In the following R_0 is chosen equal to 2.

Equation 5 can be rewritten in simplified form as follows:

$$T(R) = \left(\frac{R}{R_0}\right)^6 \{ T_0 - C_1 \left[1 - \left(\frac{R_0}{R}\right)^7 \right] - C_2 (NV)_0^2 \left[\left(\frac{R}{R_0}\right)^{6-2S} - 1 \right] \} \quad (6)$$

Here C_1 and C_2 are constants which are readily evaluated by comparing equations 6 and 5. Inspection of equation 6 shows that $T(R)$ depends parametrically on two variables, T_0 and $(NV)_0$. Following the analysis of Brandt et al. (1965) it is possible to show that two physically reasonable assumptions imply stringent constraints on the range of realizable values of T_0 and $(NV)_0$. These two assumptions are: 1) the derived temperature, $T(R)$, must remain positive throughout the range of validity of equation 1; according to Saito (1970), $R \leq 4$, 2) there is not sufficient external heating beyond $R = 2$ to produce a second peak in $T(R)$.

It is seen from the third term on the right hand side of equation 5 that for a constant T_0 , increasing $(NV)_0$ eventually drives $T(R)$ negative. The radius at which this happens can be increased beyond $R = 4$ by increasing T_0 . However if T_0 is too large, the $(R/R_0)^6$ term in front on the right hand side produces a second peak in $T(R)$ beyond $R = 2$. Therefore acceptable ranges of T_0 and $(NV)_0$ can be determined as follows. The minimum value of T_0 , T_L , is calculated for $(NV)_0 = 0$ under the assumption that $T(R) \leq 0$ for $R \geq R_X$ where R_X is the limiting distance of validity of equation 1. This gives

$$T_L = \left(\frac{GM_p M}{7kR_0 R_0} \right) \left[1 - \left(\frac{R_0}{R_X} \right)^7 \right] \quad (7)$$

Given $R_0 = 2$, $M = 0.547$ (corresponding to a 4% He abundance by number) and assuming $R_X = 3$ and 3.5 then $T_L = 0.85 \times 10^6 K$ and $0.89 \times 10^6 K$ respectively.

Upper limits for T_0 and $(NV)_0$ are determined from equation 5 by finding the largest value of T_0 and $(NV)_0$ such that $T(R) \geq 0$ and $dT/dR \leq 0$ for R in the range $R_0 \leq R \leq R_X$. Thus for each R the following two relations must be satisfied;

$$T_0 \geq \left(\frac{GM_p M}{7kR_0 R_0} \right) \left[1 - \left(\frac{R_0}{R_X} \right)^7 \right] + \left(\frac{m M (NV)_0^2}{N_0^2 k} \right) \left(\frac{6 - S}{6 - 2S} \right) \left[\left(\frac{R}{R_0} \right)^{6-2S} - 1 \right] \quad (8)$$

and

$$T_o \leq \left(\frac{GM_e m_p}{7kR_o R_e} \right) \left[1 + \frac{1}{6} \left(\frac{R_o}{R} \right)^7 \right] + \left(\frac{m_p M (NV)_o^2}{N_o^2 k} \right) \left(\frac{6-s}{6-2s} \right) \left[\left[\frac{6-s}{3} \right] \left(\frac{R}{R_o} \right)^{6-2s} - 1 \right] \quad (9)$$

Inspection of equations 8 and 9 shows that for $(NV)_o = 0$ both conditions can be satisfied simultaneously. However for each R both conditions cannot be satisfied if $(NV)_o$ is larger than some maximum value. This maximum is obtained by equating the right hand sides of equations 8 and 9.

$$(NV)_o \leq \frac{N_o \left(\frac{GM_e}{7R_o R_e} \right)^{1/2} \left[\frac{1}{6} \left(\frac{R_o}{R} \right)^7 + \left(\frac{R_o}{R_x} \right)^7 \right]^{1/2}}{\left\{ \left(\frac{6-s}{6-2s} \right) \left[\left(\frac{R_x}{R_o} \right)^{6-2s} - \left(\frac{6-s}{3} \right) \left(\frac{R}{R_o} \right)^{6-2s} \right] \right\}^{1/2}} \quad 2 \leq s < 6 \quad (10)$$

Setting $s = 2$ (radial flow) and $(NV)_e = (NV)_o (R_o/R_e)^2$ (the subscript e refers to parameters evaluated at the orbit of the earth), equation 10 is plotted in Figure 1 for $R_x = 3$ and 3.5. The minimum value of the right

REPRODUCIBILITY OF THE ORIGINAL PAGE IS POOR

hand side of equation 10 for R in the range $R_0 \leq R \leq R_X$ is the maximum flux at 1 AU consistent with the assumptions $dT/dR \leq 0$ for $R \geq 2$ and $T \geq 0$ for $R \leq R_X$. Thus for $R_X = 3.0$, $(NV)_e \leq 0.4 \times 10^8 \text{ cm}^{-2} \text{ sec}^{-1}$ with $0.85 \times 10^6 \text{ K} \leq T(R=2) \leq 1.1 \times 10^6 \text{ K}$ and for $R = 3.5$, $(NV)_e \leq 0.2 \times 10^8 \text{ cm}^{-2} \text{ sec}^{-1}$ with $0.89 \times 10^6 \text{ K} \leq T(2) \leq 0.98 \times 10^6 \text{ K}$. The curves for $T(R)$, corresponding to values of $(NV)_e$ and $T(2)$ determined from equations 9 and 10 evaluated near the minimum of the curves in Figure 1, are drawn in Figure 2. Drawn also for comparison are the polar scale height temperature, $T_H(R) = (GM_\odot m_p M)/(kr^2 d\ln i/dr)$ and the curve $T \propto R^{-2/7}$.

Since it is likely that the flow is more divergent than R^{-2} inside of some radius, R_D , it is necessary to consider how this possibility affects the upper limit of $(NV)_e$. This may be accomplished by assuming the area of a flux tube increases as R^S out to R_D and then as R^2 from there to 1 AU, R_e . Using this model, $(NV)_D = (NV)_0 (R_0/R_D)^S = (NV)_e (R_e/R_D)^2$ and hence $(NV)_e$ can be determined from equation 9 using the relation

$$(NV)_e = (NV)_0 \left(\frac{R_0}{R_e}\right)^2 \left(\frac{R_0}{R_D}\right)^{S-2} \quad R_0 \leq R \leq R_X \leq R_D \quad (11)$$

Investigations of equations 10 and 11 for S in the range $2 \leq S \leq 4$, $(R_D/R_0) = 2$, $(R_X/R_0) = 1.75$ and $R_0 \leq R \leq R_X$ show that the maximum flux at 1 AU consistent with a single temperature maximum below R_0 is not significantly changed from its value for $S = 2$ ($(NV)_e \leq 0.2 \times 10^8 \text{ cm}^{-2} \text{ sec}^{-1}$). However, if S is sufficiently large and/or (R_D/R_0) is sufficiently small, this upper limit is raised. For example choosing $S = 5$ with $(R_D/R_0) = 2$ (which is equivalent to expansion from a polar region defined by $60^\circ \leq \theta \leq 90^\circ$ at

R_0 to the full hemisphere at R_D), $(NV)_e \leq 0.28 \times 10^8 \text{ cm}^{-2} \text{ sec}^{-1}$. It should be noted though that for all cases of nonradial expansion $(NV)_0$ is significantly raised over that obtained for $S = 2$.

ii) Energy Flux Supply to the Polar Wind

An alternative approach to the polar particle flux problem is possible by considering the energy equation. Here, a limit on $(NV)_e$ may be established if the velocity at 1 AU is known and if the usual assumptions about the state of the intermediate corona are made. Using a one-fluid, steady-state, spherically symmetric model, the energy equation

$$\frac{1}{A(R)} \frac{d}{dR} (A(R)Q) = -kTV \frac{dN}{dR} + \frac{3}{2} NkV \frac{dT}{dR} \quad (12)$$

may be combined with equations 2 and 3 and integrated to yield

$$A(R)Q + F \left[\frac{1}{2} m_p MV^2 + \frac{5}{2} kT - \frac{GM_{\odot} m_p M}{R R_{\odot}} \right] = \epsilon_0 = \text{constant}. \quad (13)$$

If a supersonic solar wind exists at 1 AU but not at F_0 then the dominant term at 1 AU is $F \left[\frac{1}{2} m_p MV_e^2 \right]$ while at R_0 , the dominant terms are $A(R_0)Q + F \left[\frac{5}{2} kT_0 - \frac{GM_{\odot} m_p M}{R_0 R_{\odot}} \right]$. Therefore

$$\frac{1}{2} m_p MV_e^2 \cong \frac{Q_0}{(NV)_0} + \frac{5}{2} kT_0 - \frac{GM_{\odot} m_p M}{R_0 R_{\odot}} \quad (14)$$

Further progress is not possible without an additional closure relation which gives Q_0 in terms of the lower velocity moments. Usually the Spitzer conductivity is assumed valid so that

$$\bar{Q} = -\kappa_0 T^{5/2} \bar{\nabla} T \quad (15)$$

with $\kappa_0 = 7.7 \times 10^{-7} \text{ erg cm}^{-1} \text{ sec}^{-1} \text{ K}^{-7/2}$ (Chapman, 1954; Spitzer, 1956).

However, it is also possible that the density is sufficiently low over the poles that equation 15 is not obeyed. In particular, it is possible that the polar density is so low that the dimensionless third moment, $q = Q/[1.5 NkT(kT/m_e)^{1/2}]$, becomes impossibly large at a low altitude (Parker, 1964). For example if $N_0 = 1.23 \times 10^5 \text{ cm}^{-3}$ (Saito, 1970), $T_0 = 0.98 \times 10^6 \text{ K}$ (see section (i) above) and $T \propto R^{-2/7}$ then $q = (0.15)(R/R_0)^{(31/7)}$ or $q \geq 1$ when $R \geq 1.5 R_0$. It is therefore probable that below this altitude instabilities develop (Forslund, 1970) which will limit Q to a value less than the Spitzer upper limit. In other words, the heat flux will be limited within $1.5 R_0$ thus effectively producing an isothermal region at lower altitudes and a region of steeper than $R^{-2/7}$ temperature decrease at higher altitudes.

It is thus not clear how to estimate the value of Q_0 in equation 14. For the sake of concreteness two alternate approaches are adopted below. The first assumes equation 15 to be valid with $T \propto R^{-2/7}$ and the second adopts an exospheric approach. In both cases the solar wind He abundance is assumed to be a free parameter since its value is observed to be highly variable in the ecliptic at 1 AU and is not known at high polar latitudes. Such an assumption is necessary since, in contrast to the analysis presented in section (i) where upper limits for $(NV)_0$ were independent of M (see e.g. equation 10), the magnitude of the He abundance may be significant here. This fact results because most of the energy needed to drive the solar wind expansion goes into gravitational potential and kinetic energy which are both mass dependent. However this effect is more than compensated for by the fact that maximum values of

T_o derived from the analysis in section (i) scale linearly with M (see e.g. equation 9).

Assuming first that equation 15 is valid, $T \propto R^{-2/7}$ and $T_o = (0.98 \times 10^6)(M/0.547)$ K (see Figures 1 and 2) then upper limit values for $(NV)_e$ can be calculated from equation 14 for chosen values of M and V_e . The results are summarized in Table 1 under the label $(NV)_e$ (Spitzer) for $V_e = 320, 450$ and 750 km/sec and M values corresponding to a He abundance of 0, 0.04 and 0.08 by number.

In the appendix, an analysis is presented which shows that it is not clear whether or not electrons are collisionless below $R = R_X$. If indeed coronal electrons are collisionless near to but outside of $2 R_\odot$ then Q must be calculated using exospheric theory (Jockers, 1970; Lemaire and

QUALITY OF THE
PAGE IS POOR

Scherer, 1971a,b; Schulz and Eviatar, 1972; Hollweg, 1974; Eviatar and Schulz, 1975). In this approach, only those electrons above the electric potential barrier, $|e\Delta\phi|$ with velocities directed away from the sun can carry heat. The three fluid energy equations may be combined and integrated to yield

$$|e\Delta\phi| = M \Delta \left[\left(\frac{1}{2} m_p v^2 \right) - \left(\frac{GM_\odot m_p}{R R_\odot} \right) \right] \quad (16)$$

where the Δ symbol signifies a difference between any two radial distances and e is the electronic charge. Choosing R_\odot and $R_e = 1 \text{ AU}$ as the two reference distances then

$$|e\Delta\phi| \cong M \left[\frac{1}{2} m_p v_e^2 + \frac{GM_\odot m_p}{R_\odot R_\odot} \right] \quad (17)$$

If both v_e and the shape of the electron distribution at R_\odot , $f(v)$, are known then Q_\odot is readily evaluated using the relation

$$Q_\odot = \int_{v_B}^{\infty} \int_{-\pi/2}^{\pi/2} \int_{-\pi/2}^{\pi/2} \left(\frac{1}{2} m_e v^3 \cos\theta \cos\phi \right) f(v) v^2 dv \cos\theta d\theta d\phi \quad (18)$$

where $\frac{1}{2} m_e v_B^2 = |e\Delta\phi|$. Assuming a Maxwellian shape for $f(v)$ then

$$Q_\odot = \frac{N_\odot kT_\odot}{\sqrt{2\pi}} \left(\frac{kT_\odot}{m_e} \right)^{1/2} e^{-\left(\frac{|e\Delta\phi|}{kT_\odot} \right)} \left[\left(\frac{|e\Delta\phi|}{kT_\odot} \right)^2 + 2 \left(\frac{|e\Delta\phi|}{kT_\odot} \right) + 2 \right] \quad (19)$$

Equations 14, 17, and 19 can be combined to give a self-consistency condition for $\beta = Q_0 / [(NV)_0 kT_0]$ and hence an upper limit for $(NV)_0$ if the bulk convection speed at 1 AU is to be greater than or equal to V_e .

$$(NV)_0 \leq N_0 \left(\frac{kT_0}{2m_e} \right)^{1/2} e^{-(\beta+2.5)} \left[\beta + 7 + \frac{13.25}{\beta} \right] \quad (20)$$

where

$$\beta = \frac{1}{2} \frac{M_m V_e^2}{kT_0} + \frac{GM_0 M_m}{R_0 R_0 kT_0} - \frac{5}{2} \quad \text{and } V_e \geq 0 \quad (21)$$

Using equations 20 and 21 along with the assumptions that $R_0 = 2$, $N_0 = 1.23 \times 10^5 \text{ cm}^{-3}$ (Saito, 1970) and $T_0 = 0.98 \times 10^6 (M/0.547) \text{ K}$ (see e.g. Figures 1 and 2), upper limit values for $(NV)_e$ have been calculated for various values of M and V_e and are also listed in Table 1.

A comparison of the exospheric upper limits with the Spitzer upper limits for $(NV)_e$ shows that if both the wave-particle collision frequency and the coronal electron density are low enough over the solar pole so that an exospheric formalism is appropriate, very severe upper limits can be placed on the solar wind flux at 1 AU whether or not the He particles expand with the plasma. These upper limits fall well below that calculated from the mass and momentum equations alone. However, since it is likely that the corona is sufficiently turbulent that an exospheric formalism is not appropriate, the true upper limits for $(NV)_e$ may be less than but closer to that calculated using the Spitzer conductivity.

A comparison of the upper limit values for $(NV)_e$ derived using the form of the energy equation which incorporates the Spitzer conductivity, with that

derived using the mass and momentum equations, requires a knowledge of M and V_e . Reasonable choices for values of these quantities are made as follows. First, inspection of Table 1 shows that by choosing the solar wind He abundance to be 4% by number, the error made in estimating $(NV)_e$ is probably less than 20%. Therefore, for the purposes of this comparison, M is chosen to be 0.547. Concerning the speed of the polar solar wind at 1 AU several pieces of evidence have recently indicated that V_e over the pole is higher than that observed in the ecliptic (Cole, 1974) and may be close to 750 km/sec (Gosling et al., 1976; Feldman et al., 1976). If this is the case then from Table 1, energy considerations require that $(NV)_e$ be less than approximately $0.4 \times 10^8 \text{ cm}^{-2} \text{ sec}^{-1}$.* This value compares favorably with that derived using the mass and momentum equations ($(NV)_e \lesssim (0.2 \text{ to } 0.4) \times 10^8 \text{ cm}^{-2} \text{ sec}^{-1}$). It is therefore concluded that if heat conduction is the dominant mode of energy transport at about $2 R_\odot$, and if Saito's polar density model is correct then the particle flux of the polar solar wind should be less than about $0.5 \times 10^8 \text{ cm}^{-2} \text{ sec}^{-1}$. This upper limit is about a factor of 7 times less than the solar wind particle flux observed in the ecliptic at 1 AU (Feldman et al., 1976).

3. Latitude Variations of Heavy Ion "Freezing In" Distances

Allouche (1967) derived an approximate criterion necessary for a heavy ion of mass $A m_p$ and charge Z to diffuse upward in an expanding corona.

*It should be noted that this value is an upper limit. If the heat flux, Q , is regulated below $1.5 R_\odot$ as suggested earlier, then the region below $1.5 R_\odot$ becomes more nearly isothermal thereby reducing ∇T , Q , and hence the upper limit value derived for $(NV)_e$.

His result is:

$$(NV)_o > \frac{3kT_o \left(\frac{GM_o m_p}{R_o^2 R_\odot^2} \right) \left[\frac{kT_o}{m_p} \right]^{1/2}}{8\sqrt{\pi} e^4 \ln\lambda (Z^2/A)} \quad (22)$$

where the symbols are as previously defined and $\ln\lambda$ is the coulomb logarithm. Choosing $N_o = 1.23 \times 10^5 \text{ cm}^{-3}$, $T_o = 0.98 \times 10^6 \text{ K}$ and expressing 22 in terms of $(NV)_e$ we get:

$$(NV)_e > \frac{2.0 \times 10^8}{(Z^2/A)} \left(\frac{R_o}{R_D} \right)^{S-2} \text{ cm}^{-2} \text{ sec}^{-1} \quad (23)$$

Since for a radial expansion ($S = 2$) this limit is approximately a factor of 4 to 10 times greater than the upper limit for $(NV)_e$ derived above, it is reasonable to conclude that if Saito's model is correct and if the polar corona is not externally heated above $r = 2R_\odot$, He may not expand with the solar wind. This conclusion remains valid for $S \leq 4$ and $(R_D/R_o) = 2$ as well.

However, observation of the length of the neutral hydrogen tail of Comet Bennet (Bertaux et al., 1973; Keller, 1973) as a function of heliographic latitude indicates that the polar solar wind flux is at least as large as $2 \times 10^8 \text{ cm}^{-2} \text{ sec}^{-1}$ at 1 AU. This value is in disagreement with the upper limits deduced in section 2. It is therefore concluded that at least one of the assumptions made in the above analysis is not correct and that it should indeed be possible to observe solar wind heavy ions at polar latitudes at 1 AU. If true then measurements of the population densities of individual heavy ion ionization states will yield information concerning the temperature

structure of that region in the polar solar corona where the various ionization states "freeze in."

It is possible to determine the "freezing in" distances of the various heavy ion species as a function of heliographic latitude using equation 1 if the following assumptions are made: 1) the flow is radial; 2) the velocity distribution is Maxwellian; and 3) the electron temperature, T , depends on the radius, r , as $T = T_{\odot} (r/R_{\odot})^{-\gamma}$. Following previous work (Hundhausen et al., 1968a, b; Bamert et al., 1974) these distances are defined as those for which the expansion rate, $\tau_e^{-1} = (V d \ln N / dr)$ becomes larger than the ionization state changing rate, $\tau_{ri}^{-1} + \tau_{ci}^{-1} = N(R_i + C_i)$. Here T_{\odot} is the electron temperature at the base of the corona, V is the solar wind speed, R_i is the rate of recombination from state i to state $i-1$ and C_i is the rate of collisional ionization from state i to state $i+1$.*

Changes in the "freezing in" distances with latitude of a sample of the most abundant ions are shown schematically in Figure 3 superimposed on scale height temperatures calculated using equation 1 for $\theta = 0^\circ$ and 90° . For purposes of illustration an isothermal corona with $T_F = 1.0 \times 10^6$ K and a 1 AU particle flux of $2.5 \times 10^8 \text{ cm}^{-2} \text{ sec}^{-1}$ were assumed for evaluating $\tau_{ri}^{-1} + \tau_{ci}^{-1}$. The scale height temperature for a static corona is given by $T_H = (GM_{\odot} m_p) / (kr^2 d \ln N / dr)$. Inspection of Figure 3 shows that the region in the corona for which temperature values can be determined from solar wind heavy ion data moves inward from above to below the temperature maximum as θ varies between 0° and 90° . Thus at some intermediate latitude, coronal temperatures bracketing the maximum can be sampled allowing the magnitude and extent of mechanical dissipation in the intermediate corona to be estimated (see e.g. the analysis of Brandt et al., 1965).

*Collisional ionization and radiative recombination (including dielectronic recombination) coefficients for O, Si, and Fe were kindly supplied by Dr. A. Dupree.

4. Summary and Conclusions

In this paper two related aspects of the physical state of the interplanetary plasma at high solar latitudes were explored. In the first part upper limits for the polar solar wind particle flux were derived using a set of reasonable assumptions concerning the base coronal conditions along with Saito's (1970) coronal density model. In the second part, it was determined whether this flux was sufficient to drag the heavier ions away from the sun into interplanetary space.

From the analysis in the first part it was concluded that if Saito's model is correct, the polar electron density is sufficiently low that in the absence of extended heating the solar wind flux at high latitudes should be at least a factor of from 4 to 10 times less than that observed in the ecliptic at 1 AU. Such a low particle flux was shown in the second part to be small enough that most heavy ions would not be expected to expand with the protons into interplanetary space.

However, indirect and limited evidence available at present is consistent with a polar solar wind that has at least as large a velocity (Coles et al., 1974; Brandt et al., 1974) and as large a particle flux (Bertaux et al., 1973; Keller, 1973) as that observed in the ecliptic at 1 AU. From the analysis presented in section 2, these observations then require either that extended heating distinct from that provided by electron heat conduction is necessary some of the time above $2R_{\odot}$ or that Saito's polar densities are too low. Whichever is the case, the fact that the solar wind particle flux does not appear to decrease with increasing heliographic latitude (Bertaux et al., 1973; Keller, 1973) indicates that coronal heavy ions may be expected to expand with the protons away from the sun. If true

then measurements of the population densities of individual heavy element ionization states in the polar wind will provide information at 1 AU concerning the thermal state of that region in the intermediate corona where the respective ionization states freeze in. It turns out that the latitude variation of these freezing in distances calculated using Saito's model is such that the region in the corona for which temperature values can be determined moves inward from above to below the nominal location of the temperature maximum as θ varies between 0° and 90° . Therefore, measurements of heavy ions at high solar latitudes may provide valuable information concerning the magnitude and extent of mechanical dissipation in the intermediate polar corona.

Acknowledgments

I wish to thank Drs. L. Biermann, J. Gosling, A. Hundhausen and M. Montgomery for many useful discussions.

This work was performed under the auspices of the U.S. Energy Research and Development Administration.

References

- Alloucherie, Y. J., Heavy Ions in the Solar Corona, Ph.D. Thesis, The University of Maryland, 1967.
- Alloucherie, Y. J., Diffusion of Heavy Ions in the Solar Corona, J. Geophys. Res., 75, 6899, 1970.
- Bame, S. J., J. R. Asbridge, W. C. Feldman and P. D. Kearney, The quiet corona: temperature and temperature gradient, Solar Phys., 35, 137, 1974.
- Bame, S. J., J. R. Asbridge, W. C. Feldman, M. D. Montgomery, and P. D. Kearney, Solar wind heavy ion abundances, to be published in Solar Phys., 1975.
- Bame, S. J., Spacecraft observations of the solar wind composition, in Solar Wind, C. P. Sonett, P. J. Coleman, Jr., and J. M. Wilcox, ed., NASA SP 308, p. 535, 1972.
- Bertaux, J. L., J. E. Blamont, and M. Festou, Interpretation of hydrogen Lyman-alpha observations of comets Bennett and Encke, Astron. and Astrophys. 25, 415, 1973.
- Brandt, J. C., R. W. Michie, and J. P. Cassinelli, Interplanetary gas X. Coronal temperature, energy deposition and the solar wind, Icarus, 4, 19, 1965.
- Brandt, J. C., R. S. Harrington, and R. G. Roosen, Interplanetary gas XX. does the radial solar wind speed increase with latitude?, Astrophys. J., 196, 877, 1975.
- Chapman, S., The viscosity and thermal conductivity of a completely ionized gas, Astrophys. J. 120, 151, 1954.

Coles, W. A., B. J. Rickett, and V. E. Rumsey, Interplanetary Scintillations, in Solar Wind Three, C. T. Russell, ed., Inst. of Geophys. and Planet. Phys., U.C.L.A., Publ., p. 351, 1974.

Durney, B. R. and A. J. Hundhauser, The expansion of a low-density solar corona: a one-fluid model with magnetically modified thermal conductivity, J. Geophys. Res., 79, 3711, 1974.

Eviatar, A. and M. Schulz, Quasi-exospheric heat flux of solar wind electrons, Report SAMSO-TR-75-139, 1975.

Feldman, W. C., J. R. Asbridge, S. J. Bame, and J. T. Gosling, High speed solar wind flow parameters at 1 AU, submitted to J. Geophys. Res., 1976.

Forslund, D. W., Instabilities associated with heat conduction in the solar wind and their consequences, J. Geophys. Res., 75, 17, 1970.

Geiss, J., P. Hirt, and H. Leutwyler, On acceleration and motion of ions in corona and solar wind, Solar Phys., 12, 458, 1970.

Gosling, J. T., J. R. Asbridge, S. J. Bame and W. C. Feldman, A study of solar wind speed variations: 1962-1974, submitted to J. Geophys. Res., 1976.

Hirayama, T., The abundance of helium in prominences and in the chromosphere, Solar Phys., 19, 38¹, 1971.

Hollweg, J. V., On electron heat conduction in the solar wind, J. Geophys. Res., 79, 3845, 1974.

Hundhausen, A. J., Coronal Expansion and solar Wind, Springer-Verlag, Berlin-Heidelberg, 1972.

Hundhausen, A. J., H. E. Gilbert, and S. J. Bame, The state of ionization of Oxygen in the solar wind, Astrophys. J., 152, L3, 1968a.

Hundhausen, A. J., H. E. Gilbert, and S. J. Bame, Ionization state of the interplanetary plasma, J. Geophys. Res., 73, 5485, 1968b.

- Jockers, K., Solar wind models based on exospheric theories, *Astron. and Astrophys.*, 6, 219, 1970.
- Keller, H. U., Hydrogen production rates of comet Bennett (1969i) in the first half of April, 1970, *Astron. and Astrophys.*, 27, 51, 1973.
- Lemaire, J. and M. Scherer, Simple model for an ion-exosphere in an open magnetic field, *Phys. of Fluids*, 14, 1683, 1971a.
- Lemaire, J. and M. Scherer, Kinetic models of the solar wind, *J. Geophys. Res.*, 76, 7479, 1971b.
- Nakada, M. P., A study of the composition of the solar corona and solar wind, *Solar Phys.* 14, 457, 1970.
- Parker, E. N., Dynamical properties of stellar coronas and stellar winds, 2, integration of the heat flow equation, *Astrophys. J.*, 139, 93, 1964.
- Saito, K., A non-spherical axisymmetric model of the solar K corona of the minimum type, *Annals Tokyo Astron. Observ.*, 12, 53, 1970.
- Schulz, M. and A. Eviatar, Electron-temperature asymmetry and the structure of the solar wind, *Cosmic Electrodyn.*, 2, 402, 1972.
- Spitzer, L., Jr., *The Physics of Fully Ionized Gases*, Interscience, N. Y., 1956.
- Yeh, T., A three-fluid model of solar winds, *Planet. Space Sci.*, 18, 199, 1970.

Table 1

Upper Limit Values of $(NV)_e$
Consistent With the Energy Equation

km/sec	%	$\text{cm}^{-2} \text{sec}^{-1}$	$\text{cm}^{-2} \text{sec}^{-1}$
V_e	He/H	$(NV)_e$ (Spitzer)	$(NV)_e$ Exospheric
320	0	1.02×10^8	1.24×10^6
450	0	0.70×10^8	4.96×10^4
750	0	0.33×10^8	0.41
320	4	1.28×10^8	1.3×10^6
450	4	0.88×10^8	5.2×10^4
750	4	0.41×10^8	0.4
320	8	1.54×10^8	1.40×10^6
450	8	1.06×10^8	5.59×10^4
750	8	0.49×10^8	0.46

Appendix

Comparison of Expected Electron-Electron Collision Lengths

with Scale Lengths in the Polar Corona

The magnitude of the electron conductivity in the polar corona depends critically on the electron-electron collision length, λ_c . If λ_c is small enough then the Spitzer conductivity is applicable but if it is too large, then an exospheric approach is needed to evaluate the polar electron heat flux. It turns out that, according to Saito, N_0 is sufficiently low over the pole that it is not clear whether or not thermal electrons are collisionless above $R = 2R_0$. For example the self scattering time for a thermal electron at $2R_0$ is $\tau_c = (1.1 \times 10^{-2}) T_0^{3/2} / N_0 = 87$ sec (Spitzer, 1956) whereas at that distance the expansion time (assuming a radial magnetic field) is $\tau_e = [(kT_0/m_e)^{1/2} d \ln N / dR]^{-1} = 60.5$ sec. Furthermore the coulomb scattering length, λ_c , defined by

$$l = \frac{R_0}{(kT_0/m_e)^{1/2}} \int_{R_0}^{R_0 + \lambda_c} \frac{dR}{\tau_c} \quad (A1)$$

may be either larger than or smaller than the temperature scale length, $\lambda_T = [-d \ln T / dR]^{-1} = 3.5 R_0$, depending on the value of the maximum altitude at which Saito's density model is valid, R_X . This is readily shown by assuming a density model consistent with Saito's results (1970):

$$N = N_0 \left(\frac{R}{R_0} \right)^{-6} \quad 2 \leq R \leq R_X$$

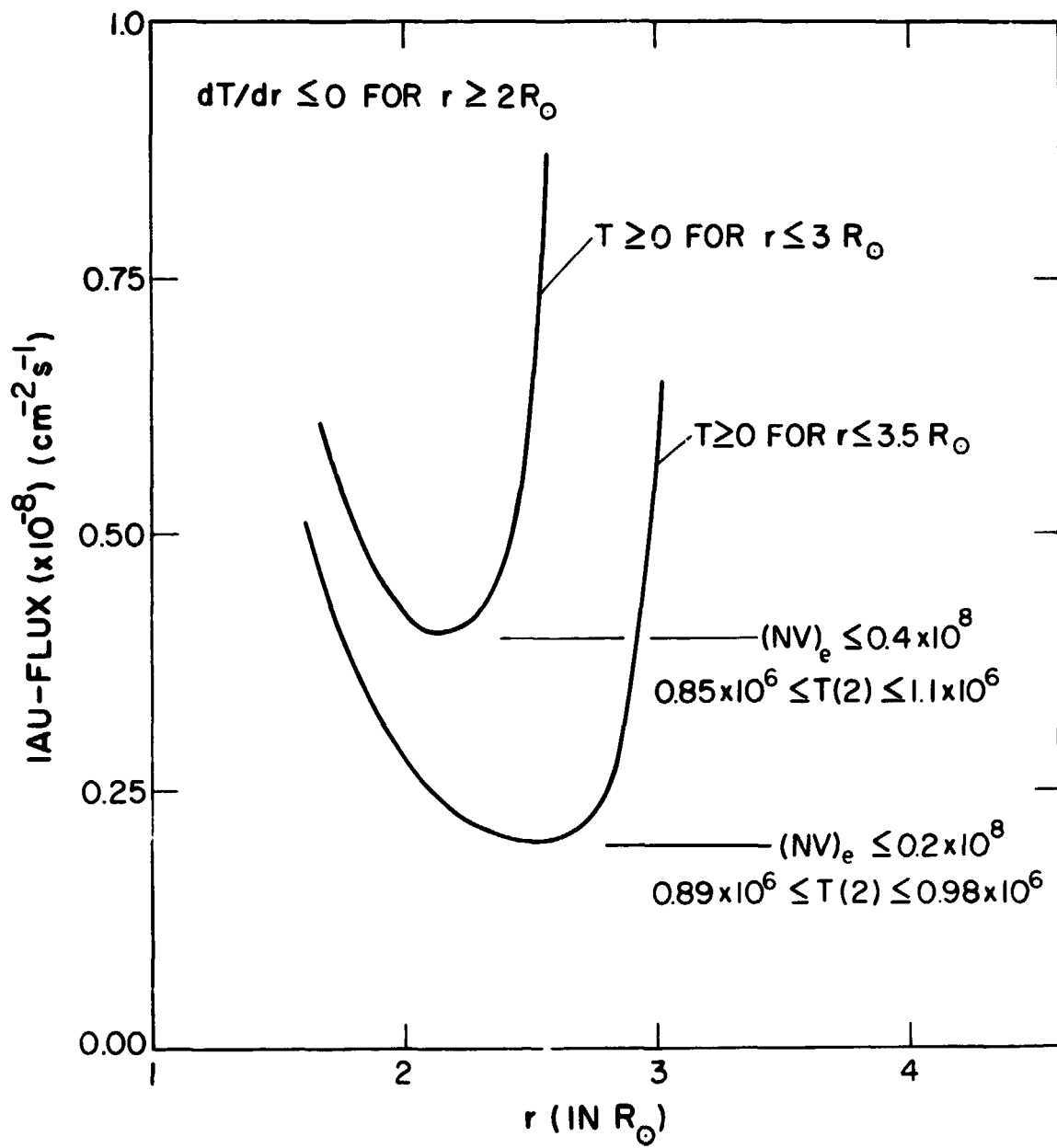
$$N = N_0 \left(\frac{R_X}{R_0} \right)^{-6} \left(\frac{R}{R_X} \right)^{-2.5} \quad R_X < R \quad (A2)$$

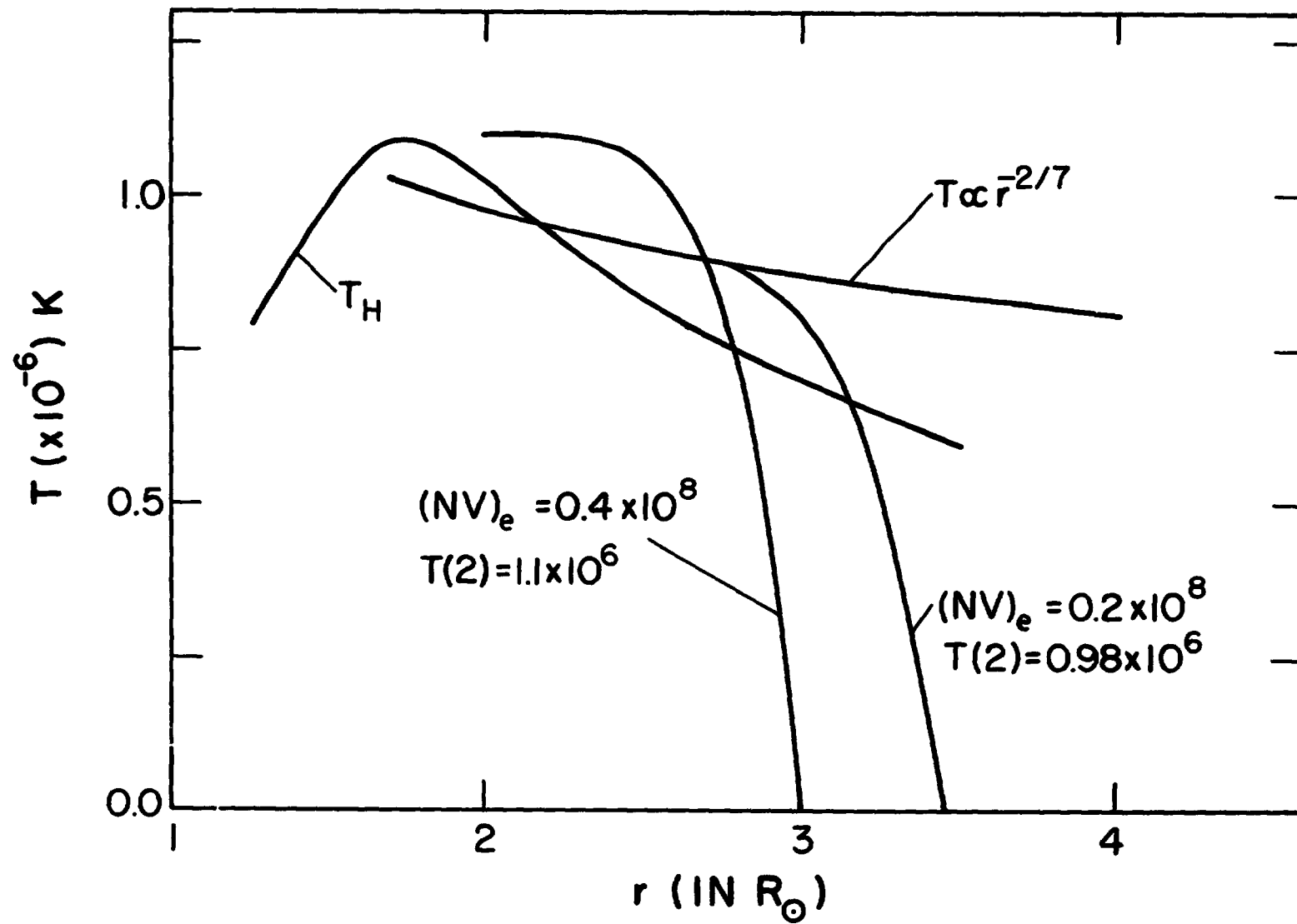
with $R_X \leq 4$. Combining A1 and A2 and using $R_0 = 2$ with N_0 from equation 1 evaluated at $\theta = 90^\circ$ it is found that $l_c/R_0 = 1.33, 2.48$ and 6.69 for $R_X = 3.0, 3.5$ and 4.0 respectively.

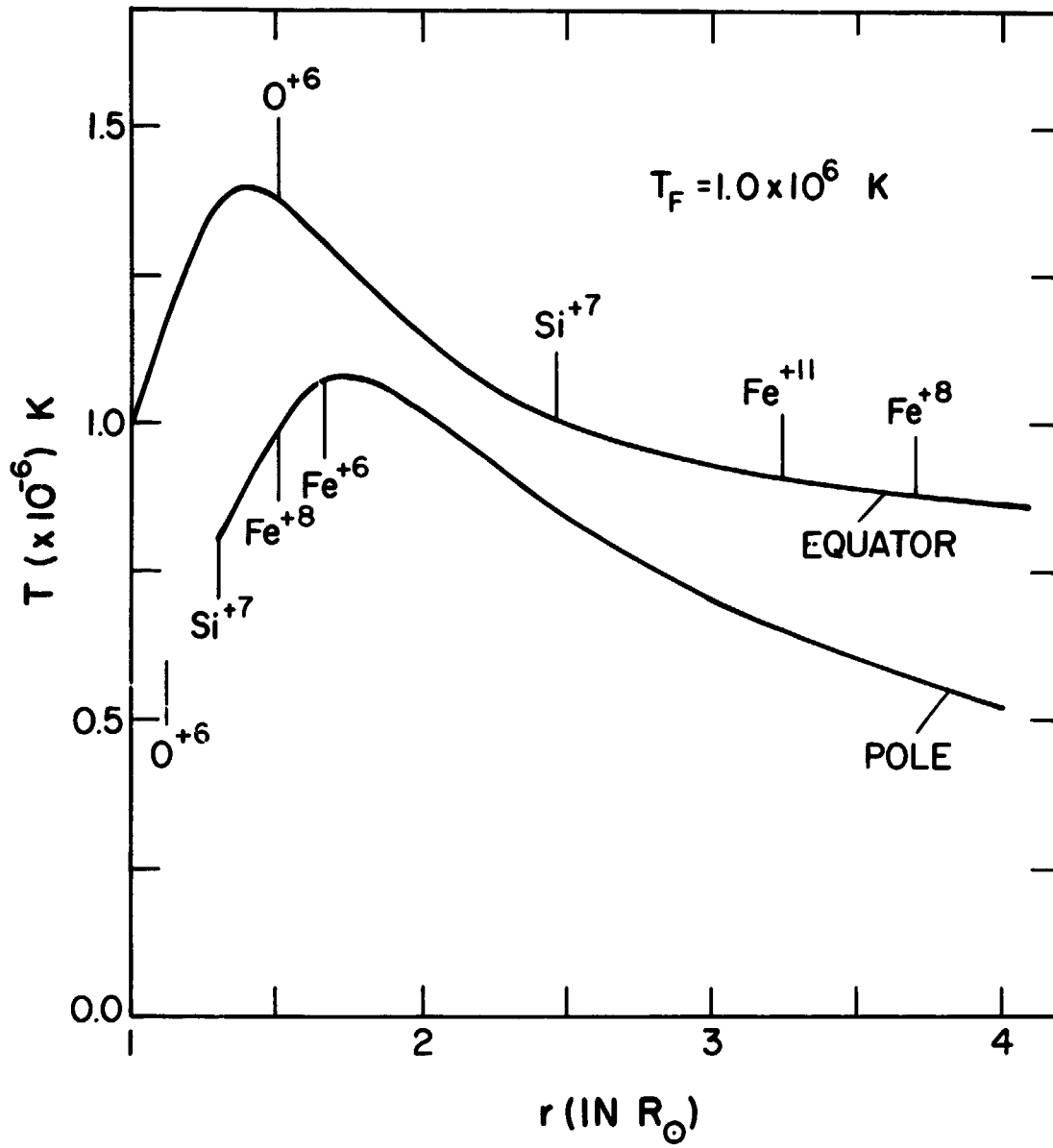
Since the actual value of l_c may be either less than or greater than l_T depending on the value of R_X , it is not known whether the Spitzer conductivity or a conductivity calculated using exospheric theory is most valid in the polar solar corona. However, the fact that l_c is of the same order of magnitude as l_T suggests that neither of the above is correct and that to obtain an accurate determination of the true conductivity a kinetic approach may be necessary.

Figure Captions

- Figure 1. Plots of equation 9 for $R_L = 3$ and 3.5. Radial flow is assumed and hence $(NV)_e = (NV)_o (R_o/R_e)^2$. The minimum value of each curve corresponds to the maximum flux at 1 AU consistent with the assumptions $dT/dR \leq 0$ for $R \geq 2$ and $T \geq 0$ for $R \leq R_X$.
- Figure 2. Coronal temperatures, $T(R)$ for values of $(NV)_e$ and $T(2)$ determined from equations 9 and 10 evaluated at the minima of the curves in figure 2. Drawn also for comparison are the polar scale height temperature, $T_H(R)$ and the curve $T \propto R^{-(2/7)}$.
- Figure 3. Variations with latitude of the "freezing in" distances of a sample of the most abundant heavy ions. Scale height temperatures are calculated using equation 1 for $\theta = 0^\circ$ and 90° and a constant "freezing in" temperature of $T_F = 1 \times 10^6$ K is assumed.







CHAPTER IV

INTERPLANETARY MAGNETIC FIELDS

PREPARED BY S. HANKS AND ~~WILSON~~

THE LARGE-SCALE MAGNETIC FIELD
IN THE SOLAR WIND

by

L. F. Burlaga
and
N. F. Ness

THE LARGE-SCALE MAGNETIC FIELD

IN THE SOLAR WIND

N76-24128

by

L.F. Burlaga

and

N.F. Ness

Laboratory for Extraterrestrial Physics
Goddard Space Flight Center
Greenbelt, Maryland

ABSTRACT

The large-scale, three dimensional magnetic field in the interplanetary medium is expected to show the classical spiral pattern to zeroth order. However, systematic and random deviations can be expected, although their nature and magnitude cannot be predicted. The sector structure should be evident at high latitudes, but the actual extent is unknown and the shape of the sector boundaries is controversial. Interplanetary streams will probably determine the patterns of magnetic field intensity but the actual patterns cannot be calculated at present because of our limited knowledge of speed profiles and the source conditions. The large-scale spiral field can induce a meridional flow which might alter the field geometry somewhat. The non-uniformities caused by streams will probably significantly influence the motion of solar and galactic particles. Unambiguous and detailed knowledge of the 3-dimensional field and its dynamical effects can only be obtained by in situ measurements by a probe which goes over the sun's poles.

I. INTRODUCTION

One cannot be certain of what will be observed on an out-of-the-ecliptic mission. It is basically exploratory. One can try to predict what will be seen, using current theories and the available interplanetary observations, and this paper attempts to do so for the interplanetary magnetic field. However, extrapolations to as little as 10^0 above the ecliptic are highly uncertain. Only in situ measurements can provide us the unambiguous and detailed knowledge that we seek.

Many of the properties of the magnetic field observed in the ecliptic plane follow from a simple relation which is valid when the magnetic stresses are not so large as to appreciably alter the motion, viz.

$$\underline{B}(r) = [\rho(r)/\rho_0] \underline{B}_0 - \nabla_0 \underline{X} \quad (1)$$

where $\underline{B}(r)$ is the field in a radially moving volume element with constant speed, ρ is the density, \underline{B}_0 and ρ_0 are the field and density at some surface near the sun, and $\nabla_0 \underline{X}$ is the gradient of the displacement vector which is determined if the speed is known on the source surface. Thus, if \underline{B}_0 , ρ_0 and V_0 are known at some inner boundary (say 0.1 or 0.2 AU), and if $\rho(r)$ is known, then to good approximation one can project or map the field anywhere within 1 AU by (1), if the magnetic stresses can be neglected. This approach to the interplanetary magnetic field is discussed in Schatten (1972), Nolte and Roelof (1973), and more generally in Burlaga and Barouch (1975) and Barouch and Burlaga (1975a). It is valid for both time-dependent flows and steady flows.

Very little is known about the latitudinal variations of V near the sun ($V_0(\theta)$) so one must be content to explore several reasonable alternatives in order to study the effects of $\nabla_0 \underline{X}$ on the three dimensional field. Of

course, the simplest assumption is $V=\text{constant}$, which gives the spiral field, as discussed below.

The values of $B_0(r_0, \theta, t)$ can be estimated by projecting photospheric magnetic field measurements upward through the solar envelope to the Alfvén point and beyond. Several techniques for doing this are available in the literature, although none is completely satisfactory. The problem is illustrated in Figure 1 from Schatten (1971), which shows a sketch of an eclipse in which the lines presumably represent magnetic field lines. One sees a variety of structures. Near the sun, the field is complex with many closed loops visible at low latitudes. Farther from the sun, the field lines generally tend to diverge and to become nearly radial. This is represented formally by assuming potential fields near the sun and supposing that only the lowest order harmonics contribute to the interplanetary field. The transition to radial fields is generally made artificially at some distance, and structures such as helmet streamers can be modeled by postulating that currents are present only in thin sheets. Such methods are sufficient for us to make estimates of the field out of the ecliptic, but it must be emphasized that these are only approximations based on models rather than firm theoretical predictions. There is no substitute for in situ measurements of \underline{B} out of the ecliptic.

II. MAGNETIC FIELD DIRECTION

Parker (1958) presented a model for the zeroth order configuration of the magnetic field lines, assuming constant V_0 , B_0 , and ρ_0 , and steady corotation. In this case, (1) gives the well-known Archimedean spiral. A good illustration of this pattern may be found in Hirose et al. (1970). Measurements have shown that Parker's model given an acceptable zeroth

order approximation for the field in the ecliptic plane between 0.3 AU and 5 AU (see the review by Behannon, 1975, and the paper by Mariani et al. (1975)). There is appreciable scatter of the observed points about the theoretical curve, which might be due in part to variations in B_0 and ρ_0 (Burlaga and Barouch, 1975), and one can expect to observe similar scatter away from the ecliptic. One might also see systematic effects in the direction of \underline{B} due to systematic variations in B_0 associated with structures such as helmet streamers and polar plumes.

Stenflo (1971) attempted to compute realistic interplanetary magnetic field configurations by introducing a reasonable model for $V(r)$ near the sun, projecting measured photospheric fields to a source surface at $2.6r_\odot$ using the potential field mapping technique, and mapping fields from the source surface to 1 AU by a technique equivalent to Eq.(1). An important result is that although there are complex loop-configurations close to the sun, farther from the sun the field becomes more radial and only the lowest harmonics are significant for the solar wind flow. In particular, the large-scale (≈ 1 AU), 3-dimensional field which he computed for the period Feb. 17 to March 10, 1970 was found to have the spiral form predicted by Parker's model (see Figure 2).

The pattern that we have been discussing is altered by the presence of streams. The magnetic field lines will be more radial when the speed is high than when it is low. This effect is small, however, being just a few degrees in the ecliptic plane (e.g., see Burlaga and Barouch, 1975) and probably even smaller at higher latitudes.

III. MAGNETIC FIELD SENSE (SECTORS)

Wilcox and Ness (1965) showed that the interplanetary magnetic field is structured such that it tends to point away from the sun for several consecutive days, then abruptly changes direction by 180° and points toward the sun for several days, etc.. In other words, the "sense" of the field is sectorized on the mesoscale. In 1964, four sectors were observed by IMP 1 (Wilcox and Ness, 1967). Several papers, beginning with that of Wilcox and Ness (1965), show that the interplanetary sector structure is related to the polarity of the photospheric magnetic field. In a recent study of this sort, Nolte (1974) (see Ruclof, 1974) computed the cross-correlation (calculated over nine solar rotations) between the interplanetary polarities which were mapped to their connection longitudes on the sun using the solar wind speed and an empirical technique and the H_{α} chromospheric polarities. He found that the cross-correlation peaks at latitudes $+30^{\circ}$ and -20° , suggesting that the base of the field lines is generally not in the solar equator; however, the correlation was low, ≈ 0.3 . When he computed the cross-correlation coefficient for magnetic field data corresponding to speeds >400 km/sec, he found a peak of ~ 0.5 at a latitude very near to the solar equator, suggesting that the streams which are observed originate near the solar equator.

Ness and Wilcox (1967) showed that the sector structure changes with time. Two sectors were observed in 1962, four in 1964, and the structure was complex in 1965. Similar plots for 1970-1972 are given in Fairfield and Ness (1974) together with references to other papers on time variations. Generally, the pattern of 2 or 4 sectors is the dominant one.

Wilcox and Svaalgard (1974) considered an interesting pattern in 1969, when 2 sectors were predominant for several solar rotations. Comparison with the solar fields, as determined by the "hairy-ball" (potential field mapping) model, showed that the sector boundary, projected from 1 AU to the sun, corresponded to an "arcade" of closed loops running approximately N-S. Thus, one expects that the sector boundary extends to rather high latitudes in this case.

Altschuler et al. (1974) computed the large-scale photospheric magnetic field in terms of surface harmonics ($P_n^m(\theta) \cos m\phi$ and $P_n^m(\theta) \sin m\phi$) for the years 1959 through 1972. For the year 1969 they found that the dominant pattern was a dipole whose axis was in the solar equatorial plane; in other words, they found a two-sector pattern, the sector boundaries running N-S, consistent with the results of Wilcox and Svaalgard described above.

Altschuler et al. (1974) found that the solar field pattern changed with time in a way consistent with spacecraft observations of the interplanetary magnetic field polarity. For example, in 1962 the dominant pattern was again a dipole in the equatorial plane, in agreement with the Mariner 2 observations. In 1963 they found that $m=1$ and $m=2$ were equally frequent, corresponding to 2 sectors and four sectors, respectively, consistent with the IN2 observations. Thus, it appears that the lowest harmonics of the solar field determine the sector structure and can be used to predict the sector structure at all latitudes.

Altschuler et al. (1974) found that 2 sectors, with the sense of a

dipole whose axis is in the equatorial plane, is the dominant pattern. They also found that four sectors occur frequently and that a N-S dipole predominates only occasionally. Thus, one expects that generally there will be two sectors whose boundaries extend N-S, sometimes four sectors will be present, and occasionally the polar regions will tend to be unipolar with a "sector boundary" in the solar equatorial plane. The time variations can be very important for a S/C mission lasting more than a year. It will be important to correlate measurements of the solar field, out-of-ecliptic measurements, and measurements made near the ecliptic, to separate the space-time variations

Svalgaard et al. (1974) proposed a model to describe the more complex configurations in which both a N-S dipole and a dipole whose axis is in the equatorial plane contribute to the interplanetary magnetic field. This is illustrated in Figure 3 (bottom), which shows that the polar fields and the equatorial fields might combine to give sector boundaries that are tilted with respect to the solar equator, the direction of tilt depending on the polarity of the fields. The figure also illustrates the magnetic arcades and the associated helmet streamers that are presumed to be associated with sector boundaries. Svalgaard et al. (1974) presented evidence that strongly supports this picture for the period that they studies. An alternative model (see Figure 3) was presented by Hansen et al. (1972) based on data obtained in 1972, when 4 sectors were observed at 1 AU and coronal streamers were observed by OSO-1. Hansen et al. postulate a coronal bridge corresponding to the low-latitude arcades of Svalgaard et al., but they differ in postulating independent

streamers at high latitudes. The relative merits of these two models has not been established. Out-of-ecliptic measurements could be decisive.

Rosenberg and Coleman (1969) showed that the number of days with negative polarity varied sinusoidally with a period of 1 year between 1964 and 1967, randomly in 1968-1969, and sinusoidally with a 180° phase shift in 1970-1973. This pattern showed the expected change in 1974-1975 (Fairfield and Ness, 1974). Following a suggestion of Rosenberg and Coleman (1969), Schulz (1973) suggested that this is a consequence of "warping" of the equatorial plane (minimum B surface) of a dominantly N-S solar dipole with significant quadrupole contributions. This conflicts with the results of Altschuler et al. (1974) which show that the N-S dipole is not frequently observed at the sun. It also implies that the sector boundaries should trace a "sinusoidal" line with small amplitude about the solar equator, in contradiction with the results of Svalgaard et al. which suggested that sector boundaries are not tilted so much. This difference has not been resolved, but could be settled by an out-of-ecliptic mission.

IV. MAGNETIC FIELD INTENSITY

Parker's model, based on the assumption of constant and uniform V and B_0 , provides the zeroth order approximation of the interplanetary magnetic field intensity. It predicts the measured value of $\approx 5\gamma$ in the ecliptic plane at 1 AU for reasonable values of B_0 near the sun, and it predicts somewhat smaller fields near the poles. A somewhat more complicated model, assuming constant V and a N-S dipole giving \underline{B}_0 , was discussed by Parker (1958) and considered in more detail by Stern (1964).

In view of the results of Altschuler et al. (1974), which showed that a N-S dipole rarely dominates, this model is generally not appropriate.

Superimposed on the large-scale variations in magnetic field intensity are non-uniformities due to streams. These are the result of $\nabla_{\phi} X \neq 0$ in Eq. (1). Faster plasma overtakes slower plasma, causing a compression of the plasma and (because the field is "frozen" to the plasma) an enhancement in B. Shears in V can also cause a change in the magnetic field intensity, and this too is implicit in (1) (see Burlaga and Barouch, 1975). Enhancements in B are generally observed at the leading edge of streams at 1 AU, often as large as four times the ambient value. Similar enhancements might be observed out of the ecliptic, depending on the velocity profiles. They might be the most important magnetic field intensity variations at high latitudes. Illustrative spatial configurations of the magnetic field intensity on a spherical shell with radius 1 AU, relative to the unperturbed equatorial field at 1 AU, are shown in Figure 4 from Barouch and Burlaga (1975a). At the top, is the result for $V = V_0 (1+A \cos 4\phi) \cos \theta$; at the bottom is the result for $V = V_0 (1+A \cos 4\phi) \exp[-(\theta-\theta_0)/\theta_0]^2$. In the first case, one expects that the field intensity might be approximately twice the unperturbed intensity in some regions out of the ecliptic, if the streams extend to high latitudes. In the second case, in which streams are confined near the ecliptic, B(θ) is strongly perturbed only near the ecliptic.

Billings and Roberts (1955) suggested that streams come from regions of open and diverging magnetic field lines near the sun and that slow plasma is associated with closed loops. This is consistent with the

observation that the solar wind speed is generally small near sector boundaries, which according to Svalgaard et al. (1974) are associated with "arcades" of closed loops near the sun. It is also consistent with mappings of streams back toward the sun (Roelof, 1974). Pneuman (1973) and Pneuman and Kopp (1970, 1971) modeled this situation with a dipole in the solar equatorial plane. The basic idea is that when the field lines diverge, heat is readily conducted to the critical point where it can effectively accelerate the solar wind, whereas when the field lines are closed heat cannot be conducted radially because of the low perpendicular conductivity and energy is not available for acceleration. Of course, other models are also possible. The point that we wish to emphasize is that stream profiles might be related to the magnetic field near the sun. Calculations which explore the consequences of variable $B_0(\theta, \phi)$ are given in Barouch and Burlaga (1975a). The result is that there might be a latitudinal variation of the stream induced perturbations in B which results from the latitudinal dependence of B_0 .

We conclude that streams induce significant distortions in the magnetic field intensity which must be considered in measuring a "zeroth" order field. They are also interesting in themselves and may help to understand the source of streams. Finally, they have important effects on solar particles, galactic particles, and possibly solar wind flow perturbations, as discussed in the next section.

V. EFFECTS OF $B(\theta, \phi)$ ON COSMIC RAYS AND PLASMA

Several authors (e.g. see the review of Montgomery, 1975) suggested that particles should have easier access and shorter paths if they enter

the solar system over the radially diverging polar field, then if they enter the tightly wound spiral in the ecliptic. The actual effect is not known, since it depends on the fluctuations of B away from the ecliptic as well as on the large scale topology. Direct measurements would be decisive.

It has also been suggested that mesoscale configurations associated with shock waves (Gold, 1959; Parker, 1963) can appreciably perturb cosmic rays and cause "Forbush decreases" in their intensity, and there is some evidence in support of this view (e.g. Barnden, 1973). Obviously, latitudinal variations in such configurations would have corresponding effects on the cosmic rays, but direct measurements are needed to determine the nature of these variations and the size of the effects.

The presence of stream-induced gradients in B can also significantly affect cosmic rays. Barouch and Burlaga (1975b) showed that Forbush decreases and similar galactic cosmic ray intensity variations are strongly correlated with magnetic field enhancements associated with streams. They proposed that these are the results of perpendicular gradient drifts, and Barouch and Burlaga (1975a) showed that the drift speeds are appreciably higher than the speeds in streams, as required. If streams extend to high latitudes, one expects to observe Forbush decreases there. If streams do not extend to high latitudes, there will be small drifts due to the spiral field configuration (Winge and Coleman, 1968), but there may be no observable effects.

Streams cause field lines to diverge less rapidly and eventually converge in the compression regions in front of streams. Thus, solar particles moving in such mesoscale configurations will be collimated less

strongly than in the large-scale spiral field, and some will mirror (Barouch and Burlaga 1975a), giving stream related intensity and anisotropy profiles. One expects systematic differences in these profiles with increasing latitude, depending on the variations of the streams.

Low energy (thermal) particles are also influenced by the magnetic field, although not as strongly as the high energy particles whose energy density is much less than $B^2/(8\pi)$. In fact, Parker's model, which assumes constant V and gives a spiral field, is not exactly self-consistent for this reason (Gussenhoven and Carovillano, 1973; Alekseyev et al. 1971). In particular, the spiral field gives a $\underline{J} \times \underline{B} = (\nabla \times \underline{B}) \times \underline{B}$ force that causes a meridional flow away from the ecliptic. This flow has been studied by Winge and Coleman (1974) and by Suess (1974). Its magnitude might be as much as ≈ 1 km/sec in the ecliptic at 1 AU. Rosenberg and Coleman (1973) invoked this flow and the frozen field condition to explain his observations that the magnetic field direction diverges away from the ecliptic plane. These effects are small and have not been confirmed. They vary with latitude in the spiral field configuration, and they might be strongly modified by streams.

VI. SUMMARY

One expects the large-scale, three-dimensional magnetic field lines of the solar wind to have the form of spirals wrapped on cones, as described by the solutions of Parker. Solar wind streams and solar magnetic field configurations probably will not alter this very much, although small, systematic effects due to the variation of the orientation of B near the sun might be observable.

REPRODUCIBILITY OF THE
ORIGINAL PAGE IS POOR

The sector pattern possibly extends to high latitudes and can change appreciably during a year. The pattern and extent of sector boundaries is a matter of controversy. Extrapolations of the solar field and mapping of the interplanetary field to the sun suggest that the boundaries extend nearly north-south, although tilted somewhat depending on the polar and sector field directions. On the other hand, the "Rosenberg-Coleman dominant polarity effect" and some calculations suggest that sector boundary surfaces are confined closer to the equator. Two distinctly different models of sector boundaries have been proposed by Svalgaard et al. and Hansen et al., but one cannot choose one or the other at the moment.

The interplanetary magnetic field intensity will vary with latitude depending on the photospheric field configuration. For a solar monopole, the polar field near 1 AU is ≈ 2 smaller than the equatorial field. The intensity might vary more than this on a smaller scale, ≤ 1 AU, due to the presence of streams. The actual configuration depends on both the stream profiles and the magnetic field intensity profiles near the sun, but these are not known at present.

The gradients in magnetic field intensity produced by streams cause energetic particles to drift away from the ecliptic, and they might be responsible for Forbush decreases. If so, these decreases should disappear at high latitudes if the speeds are confined near to the ecliptic. Stream induced magnetic field enhancements might also mirror solar particles and reduce their collimation, causing stream-related changes in intensity and anisotropy. The effect varies with latitude in a systematic way, so that one can test these ideas with an out-of-the-ecliptic mission.

The large-scale spiral field causes a small meridional flow as a consequence of the $\mathbf{J} \times \mathbf{B}$ force. The magnitude of this flow might be altered by streams and vary with latitude for this reason.

In conclusion, an out-of-the-ecliptic mission will allow us to test present models of the interplanetary magnetic field, resolve some controversies, provide information needed to understand energetic particle and plasma motions, and it will probably give new results that we cannot anticipate.

References

- Aleksejev, I.I., V.P. Shebansky, and A.R. Shister, Spherically symmetric outflow of plasma from the sun, Geomag. and Aeron., 11, 651, 1971.
- Altschuler, M.D., D.E. Trotter, G. Newkirk, Jr., and R. Howard, The Large-scale solar magnetic field, Solar Physics, 39, 3, 1974.
- Barnden, L.R., The large-scale magnetic field configuration associated with Forbush decreases, Proc. Int. Conf. Cosmic Rays 13th, 2, 1277.
- Barouch, E., and L.F. Burlaga, Three-dimensional interplanetary stream magnetism and energetic particle motion, submitted to J. Geophys. Res., 1975a.
- Barouch, E., and L.F. Burlaga, Causes of Forbush decreases and other cosmic ray variations, J. Geophys. Res., 80, 449, 1975b.
- Behannon, K.W., Variation of the interplanetary magnetic field with heliocentric distance, NASA/GSFC X-692-75-143, 1975.
- Billings, D.E., and W.O. Roberts, Solar corpuscles responsible for geomagnetic disturbances, J. Geophys. Res., 60, 33, 1955.
- Burlaga, L.F., and E. Barouch, Interplanetary stream magnetism: kinematic effects, Astrophys. J., in press, 1975.
- Fairfield, D.H., and N.F. Ness, Interplanetary sector structure: 1970-1972, J. Geophys. Res., 79, 5089, 1974.
- Gold, T., Plasma and magnetic fields in the solar system, J. Geophys. Res., 64, 1665, 1959.
- Gussenhoven, M.S., and R.L. Carovillano, Restrictions on radial magnetic field and flow solutions for the solar wind, Solar Physics, 29, 233, 1973.

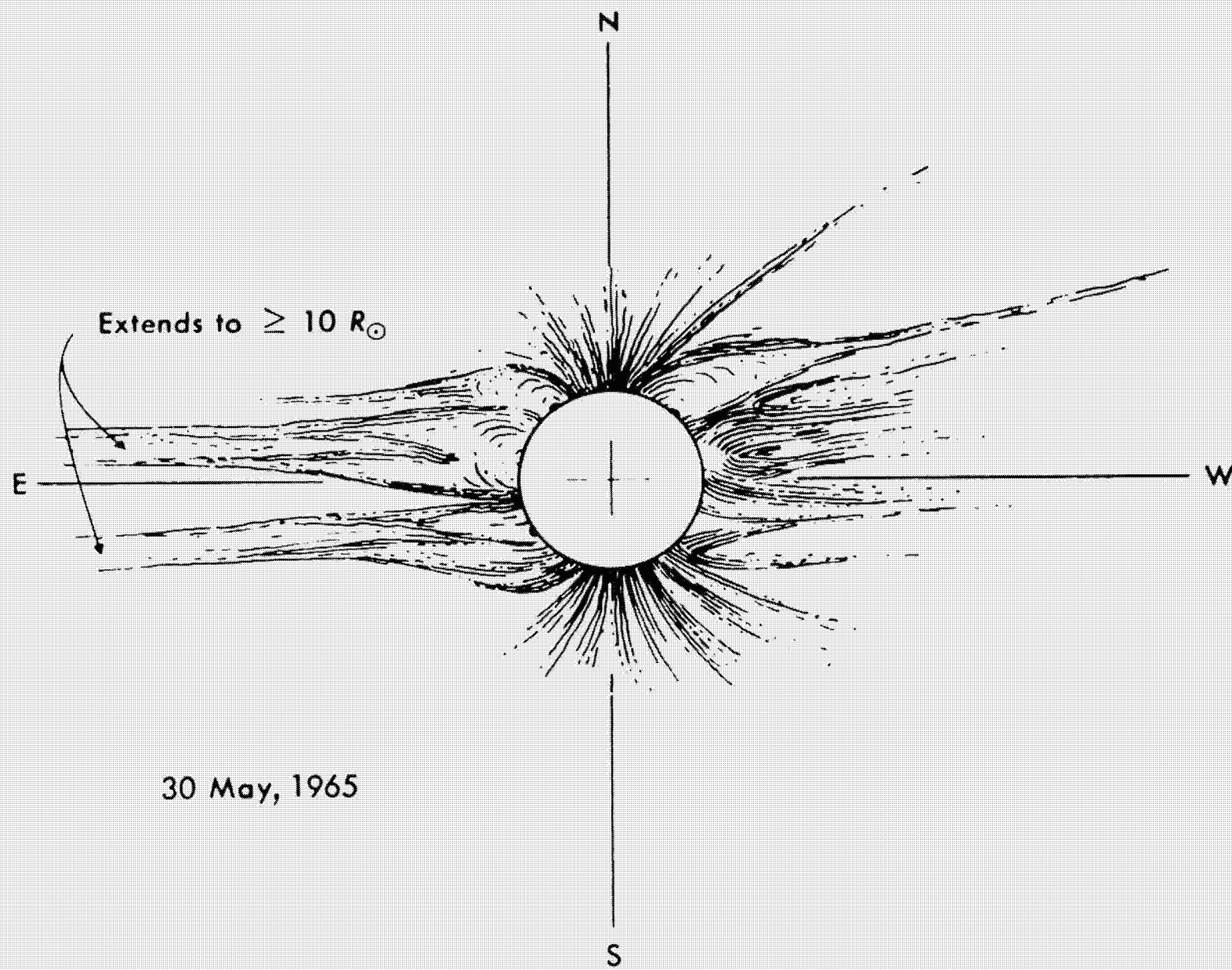
- Hansen, S., R.T. Hansen, and C.J. Garcia, Evolution of coronal helmets during the ascending phase of solar cycle 20, Solar Division, 25, 202, 1972.
- Hirose, T., M. Fujimoto and K. Kawabata, Magnetohydrodynamical processes of the sector structure of the solar wind, Pub. Astron. Soc. Japan, 22, 495, 1970.
- Mariani, F., N.F. Ness, L.F. Burlaga, S. Cantarano, B. Bavassano and U. Villante, Radial and time variations of the interplanetary magnetic field between 1 AU and 0.3 AU, Technical Report - LPS-75-1975.
- Nolte, J.T., Inter-relationship of energetic particles, plasma and magnetic fields in the inner heliosphere, Ph.D. Dissertation, University of New Hampshire, 1974.
- Nolte, J.T., and E.C. Roelof, Large-scale structure of the interplanetary medium, Solar Phys., 33, 483, 1973.
- Parker, E.N., Dynamics of the interplanetary gas and magnetic fields, Astrophys. J., 128, 664, 1958.
- Parker, E.N., Interplanetary Dynamical Processes, p. 177, Interscience, New York, 1963.
- Pneuman, G.W., The solar wind and the temperature-density structure of the solar corona, Solar Physics, 28, 247, 1973.
- Pneuman, G.W., and R.A. Kopp, Coronal streamers: III. Energy transport in streamer and interstreamer regions, Solar Physics, 13, 176, 1970.
- Pneuman, G.W., and R.A. Kopp, Gas-magnetic field interactions in the solar corona, Solar Physics, 18, 258, 1971.

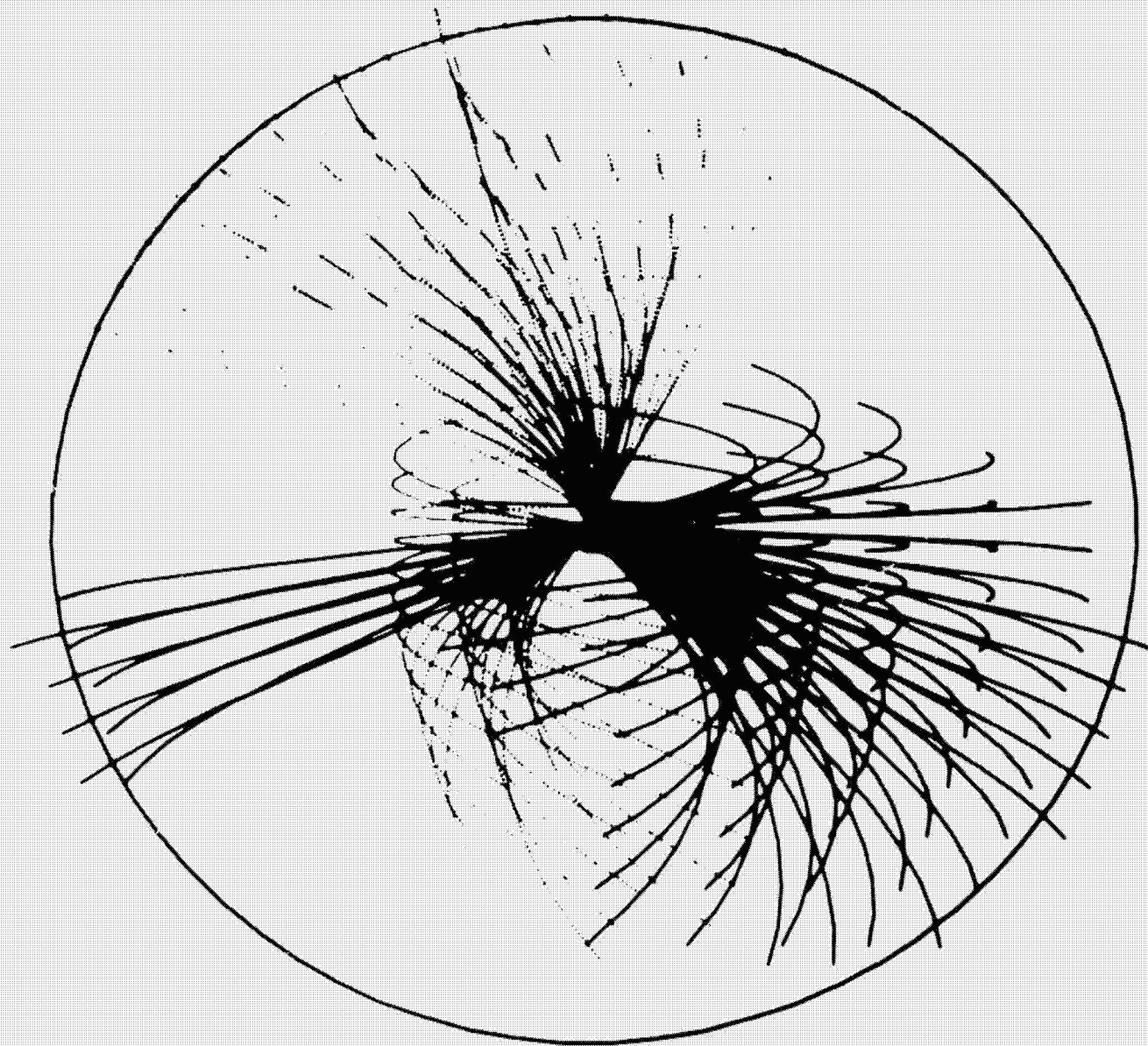
- Roclof, E.C., Coronal structure and solar wind, in Solar Wind Three, p. 98, ed. C.T. Russell, Institute of Geophysics and Planetary Physics, University of California, Los Angeles, 1974.
- Rosenberg, R.L., and P.J. Coleman, Jr., Latitude dependence of the dominant polarity of the interplanetary magnetic field, J. Geophys. Res., 74, 5611, 1969.
- Rosenberg, R.L., and P.J. Coleman, Jr., Further study of the θ component of the interplanetary magnetic field, J. Geophys. Res., 78, 51, 1973.
- Schatten, K.H., Current sheet model for the solar corona, Cosmic Electrodynamics, 2, 232, 1971.
- Schatten, Large-scale properties of the interplanetary magnetic field, in Solar Wind, ed. C.P. Sonett, P.J. Coleman, Jr., and J.M. Wilcox, p. 65, NASA SP-308, 1972.
- Schulz, M., Interplanetary sector structure and the heliomagnetic equator, Astrophys. and Space Science, 24, 371, 1973.
- Stenflo, J.O. The coronal and interplanetary magnetic fields at the time of the solar eclipse of 7 March 1970, Solar Physics, 21, 263, 1971.
- Stern, D., A simple model of the interplanetary magnetic field, Planet. Space Sci., 12, 961, 1964.
- Suess, S., Three dimensional modeling, in Solar Wind Three, p. 311, ed. C.T. Russell, Institute of Geophysics and Planetary Physics, University of California, Los Angeles, 1974.
- Svalgaard, L., J.M. Wilcox and T.L. Duvall, A model combining the polar and sector-structured solar magnetic fields, Solar Physics, 37, 157, 1974.

- Wilcox, J.M. and N.F. Ness, Quasi-stationary corotating structure in the interplanetary medium, J. Geophys. Res., 70, 5793, 1965.
- Wilcox, J.M. and N.F. Ness, Solar source of the interplanetary sector structure, Solar Phys., 1, 437, 1967.
- Wilcox, J.M., and L. Svalgaard, Coronal magnetic structure at a solar sector boundary, Solar Physics, 34, 461, 1974.
- Winge, C.R., and P.J. Coleman, Jr., The motion of charged particles in a spiral field, J. Geophys. Res., 73, 165, 1968.
- Winge, C.R., Jr., and P.J. Coleman, Jr., Theoretical predictions of latitude dependencies in the solar wind, in Solar Wind Three, p. 318, ed. C.T. Russell, Institute of Geophysics and Planetary Physics, University of California, Los Angeles, 1974.

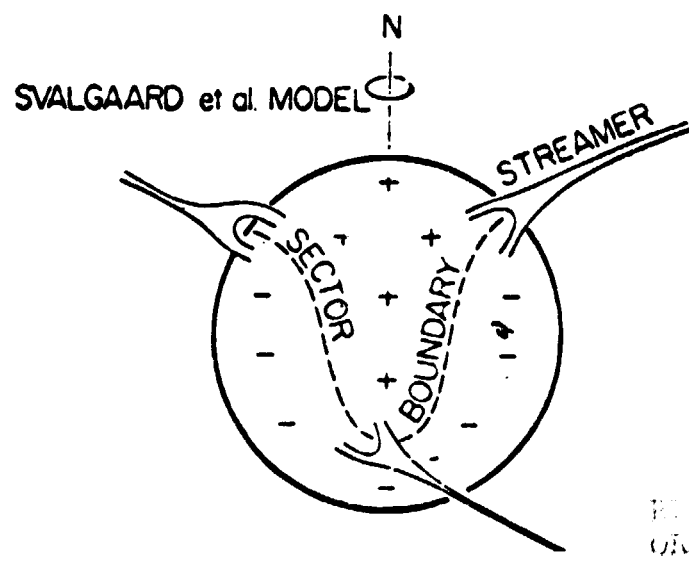
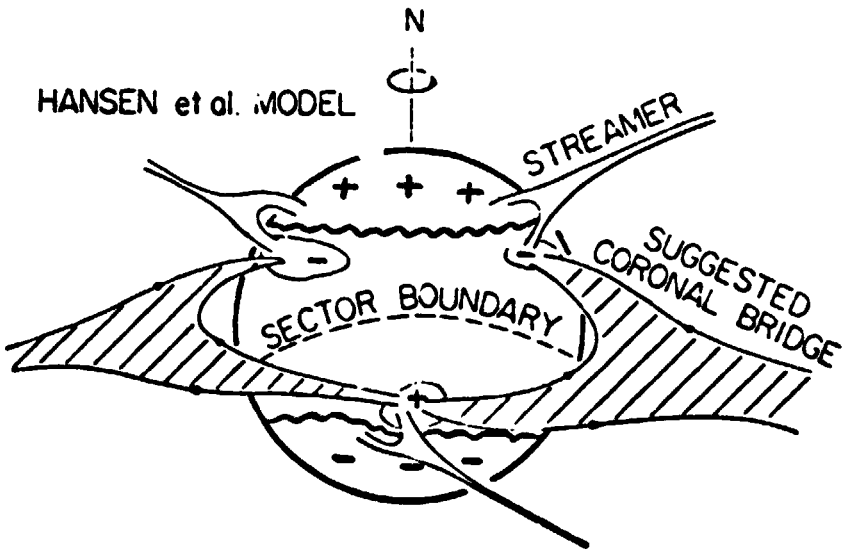
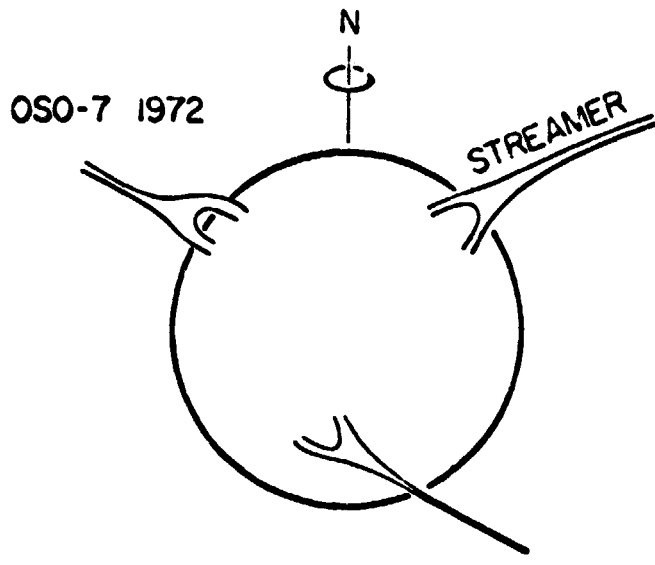
FIGURE CAPTIONS

- Figure 1 Sketch of a solar eclipse on 30 May 1965. The contours are believed to indicate the direction of the magnetic field
- Figure 2 Interplanetary magnetic field lines on a scale of 1 AU, seen by an observer in the ecliptic plane. They were computed by Stenflo using photospheric magnetic field measurements.
- Figure 3 Sector boundaries. This illustrates two conceptual models of sector boundaries and their relation to coronal streamers.
- Figure 4 Magnetic field intensity contours relative to the unperturbed intensity in the ecliptic plane at 1 AU, on a surface with radius 1 AU. The top figure shows the pattern caused by a stream which varies with latitude as $\cos \theta$, and the bottom figure describes the result of a stream which is confined near the ecliptic.

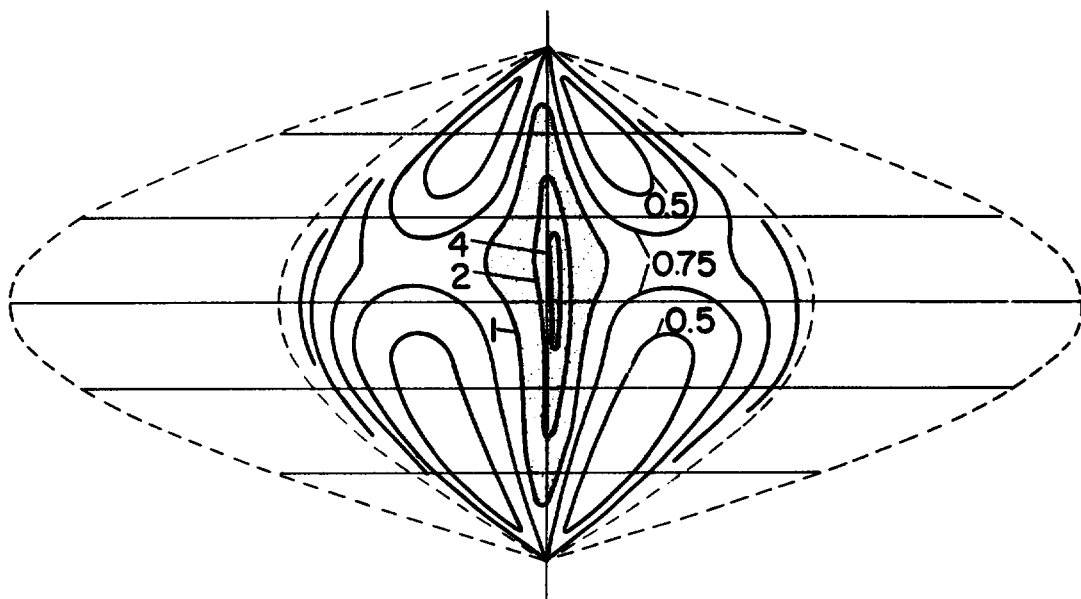
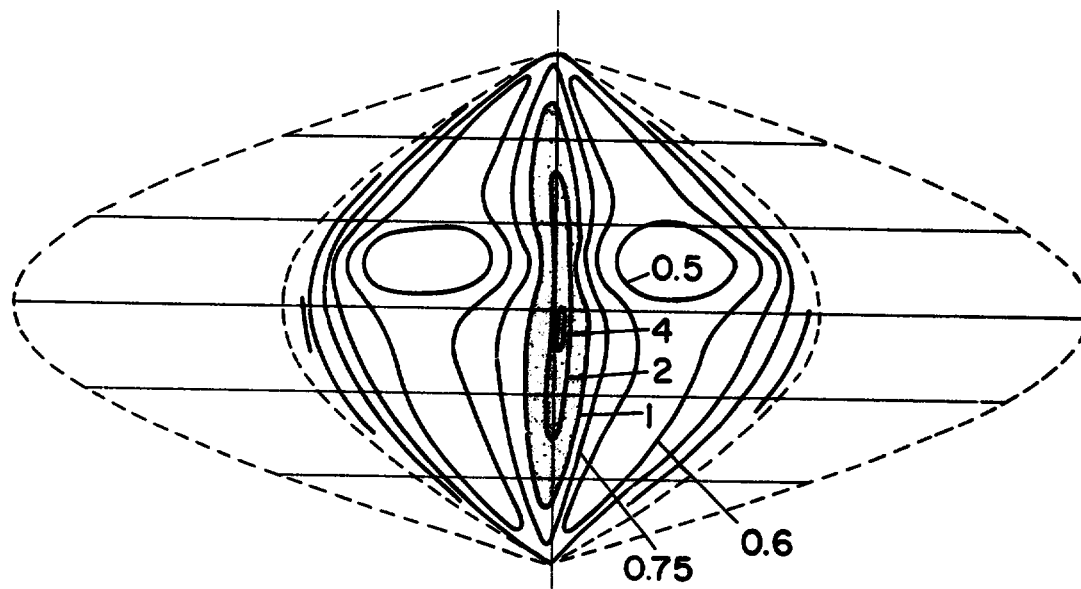




LONGITUDE OF DISK CENTER = 0 DEGREES



REPRODUCED FROM THE ORIGINAL PAGE IS POOR



N 76 - 24129

Three Dimensional Aspects of Interplanetary Shock Waves

G. L. Siscoe

**Department of Meteorology
University of California, Los Angeles, Ca. 90024**

September 1975

Abstract

Initially spherical blast waves are systematically distorted due to persistent latitudinal solar wind structure. This is to be distinguished from the non-systematic (random) distortion due to varying structure in longitude which introduces an $\approx 30^\circ$ average deflection of shock normals from radial. The systematic latitudinal effect should be at least 25° at mid-latitudes, and observable in the 30° noise level with 14 or more shocks for statistics. The observed occurrence rate of shocks during solar maximum is sufficient to detect the effect. Corotating shocks should become detectable between 1 and 5 AU. Identification could be a problem because of the 30° noise level becoming greater beyond 1 AU. However, the three-dimensional geometry of corotating shocks show a strong latitudinal structure which can be used in an out-of-the-ecliptic mission for a statistical identification based on shock occurrence rates.

Introduction

Most of the interplanetary shock waves observed with 1 AU of the sun originate from some short lived solar event, such as a solar flare, and then propagate out as a more-or-less spherical shock wave until they leave the solar system. Beyond 1 AU another class of interplanetary shock wave becomes common-- the cortating shock pair formed by the interaction of long lived solar wind streams. We discuss here the three dimensional geometry of these two classes of interplanetary shocks and how these geometries can be studied with an out-of-the-ecliptic mission.

Out-of-the-Ecliptic Distortion of Solar Blast Waves

Lack of spherical symmetry in the solar wind distorts the surface of a shock wave as it propagates away from its solar origin into interplanetary space. This phenomenon is observed near the solar equatorial plane at 1 AU, where the inhomogeneities associated with solar wind streams produce typically a 30° deflection of the shock wave normal away from the radial direction (Heinemann and Siscoe, 1974; Hirshberg et al., 1974). The distortion results from differential advection of the shock front due to solar wind speed variations and from differential propagation speed of the shock in the solar wind due to density variations--the shock propagates more slowly in high density regions. In spite of the large distortion of individual shocks, the averaged shock normal direction near the equatorial plane at 1 AU is radial from the sun (Chao and Lepping, 1974; Heinemann and Siscoe, 1974).

A systematic variation in latitude of the solar wind speed and density produces a systematic distortion in latitude of the surfaces of solar produced shock waves. That is, the averaged shock normal direction (\bar{n}_s) in general will not be radial from the sun. The angle between \bar{n}_s and the radial direction will depend on latitude in a manner which reflects the average latitudinal dependence of the solar wind speed and density.

A lower limit on the deviation of \bar{n}_s from radial is shown in Figure 1. Here a shock wave that was spherical at 20 solar radii becomes distorted into a quasi-ellipse

at 1 AU by the action of a differential advection of 400 km sec^{-1} at the equator increasing smoothly to 600 km sec^{-1} at the poles. This latitudinal gradient of solar wind speed, approximately $2 \text{ km sec}^{-1} \text{ deg}^{-1}$, is at the lower end of the range of gradients suggested in the literature (see reviews by Gosling, 1975, Hundhausen, 1975, Dobrowolny and Moreno, 1975). The figure probably also underestimates the distortion for the assumed gradient since it neglects the possible latitudinal gradient in density--decreasing toward the poles (Hundhausen et al., 1971)--causing the shock to propagate faster in the solar wind at higher latitudes.

The maximum deviation of \bar{n}_s from radial ($\Delta\theta_{\text{max}}$) occurs at mid-latitude and is about 25° at 1 AU. In order to observe this effect, enough solar generated shock waves must be measured while a spacecraft is in the mid-latitude region to obtain a value for the polar angle ($\bar{\theta}_s$) of \bar{n}_s with a statistical error considerably less than $\Delta\theta_{\text{max}}$. For the sake of having a numerical example, we take the requirement that the expected standard deviation of $\bar{\theta}_s$ be less than or equal to 1/3 of the conservative value obtained above for $\Delta\theta_{\text{max}}$, i.e. S. D. ($\bar{\theta}_s$) $\leq 8^\circ$.

Near the equatorial plane the distortions produced by solar wind streams cause approximately a 30° standard deviation in the angle between individual shocks and their average, radial direction. The standard deviation of the average angle of N shocks is $30^\circ/\sqrt{N}$. For $N = 14$, this is $\sim 8^\circ$. Thus in a 30° background noise level in the angle of individual shocks due to stream structure, it takes 14 shocks to obtain a value of $\bar{\theta}_s$ with an expected standard deviation of 8° from the true value. It is likely that the noise level at mid-latitudes is less than 30° since the effect of streams

in producing solar wind inhomogeneities as measured by enhanced radio scintillations is apparently confined to within 40° of the equator (Houminer, 1973). Thus the requirement of 14 shocks is probably more than necessary.

To estimate the time needed to observe 14 solar generated shocks, we use the 100 years of SSC statistics compiled by Mayaud (1975). The validity of this procedure is based on the study of Chao and Lepping (1974) showing that at least 87% of SSC's can be associated with solar activity such as solar flares and type 2 and type 4 radio bursts. There are on average about 10 SSC's per year during solar minimum and about 35 SSC's per year during solar maximum. Thus about 17 months are required in the first case and 5 months in the second of mid-latitude observations to observe 14 shock waves originating from a solar surface source. We conclude that an out-of-the-ecliptic mission scheduled for solar maximum would have high probability of observing systematic shock wave distortion even if the worst-case example discussed above should apply.

The importance of measuring the systematic distortion of the shock shape lies in its use in determining the systematic latitudinal dependence of solar wind parameters. This method is independent of all other methods. It does not involve unravelling separate space and time variations. In the case of an out-of-the-ecliptic mission via Jupiter, the space dependence involves both radial distance and latitude angle which can give independent contributions to any variation observed in in situ measurements. Knowledge of the three dimensional shape of blast waves is important also for determining the flow of flare energy into interplanetary space. A non-spherical shock shape implies that energy is not distributed uniformly but converges in some places--relative to

a purely radial flow--and diverges in others. In the case considered, energy would diverge away from the equator causing the shock strength to decrease faster in the equatorial plane than would be expected on the basis of spherical symmetry.

Three Dimensional Structure of Corotating Shocks

Near the equatorial plane the border between contiguous solar wind streams is a spiral (Sarabhai, 1963; Dessler, 1967). If the trailing stream--in the sense determined by the direction of the solar rotation--is faster, a pair of shock waves will form at some distance from the sun (Hundhausen, 1973 a,b). Such shock wave pairs have apparently been observed between 1 and 5 AU by the Pioneers 10 and 11 spacecraft (Hundhausen and Gosling, 1975; Smith and Wolfe, 1975). In a steady state situation, the streams, their spiral border, and the shock pair all corotate with the sun. In this section we estimate the heliocentric distance of shock formation in the equatorial plane as a function of the speed differential between the streams and give a qualitative description of the three dimensional shape of the shock surfaces. For the latter we assume that the stream border is perpendicular to the equatorial plane. This example illustrates the essential aspects of the geometry and possibly represents the typical case as indicated by radio scintillation observations (Houminer, 1973) and the north-south alignment of coronal holes which might be the sources of fast streams (Krieger et al., 1973; Noyes, 1975).

Figure 2 shows the relevant geometry in the equatorial plane. The figure also illustrates one argument for expecting the existence of shock pairs which at the same time suggests a simple calculation for the approximate heliocentric distance to their point of formation. The spiral labeled stream interface is the border between

the streams. Sample flow streamlines--labeled fast and slow--are shown in the corotating reference frame in which all geometrical features are time independent. With the fast stream trailing, the pitches of the spiral streamlines in both streams are such that they would intersect the spiral interface unless prevented from doing so by forces that act to deflect the flows away. The build up of pressure at the interface resulting from the convergence of the flow there produces such a force (Siscoe, 1972). Relative to the flows in the two streams, the interface looks, like a curving wall and the flows are forced to follow the curve because of the increased pressure. The compressive deflection of a supersonic flow by a curving wall is known to produce a detached shock wave in the flow (Landau and Lifschitz, 1959, p. 429). Streamlines intersecting the shock waves are deflected parallel to the interface spiral, bringing to an end the compressive interaction between the streams.

The approximate location of the origin of the shock waves can be found by considering the characteristics of the flow emanating from a point, A, on the interface close enough to the sun that the streamlines are essentially radial but far enough from the sun to be in the supersonic region. The characteristics are generated by following the progress of a sound wave starting at A and subsequently expanding and being convected with the flow, as illustrated in the figure. However, before the shocks are formed, the flow converges on the interface; thus the sound speed must be greater than the speed characterizing the convergence in order for the sound wave to expand. As the wave moves out from point A, the sound speed decreases because the solar wind cools as it expands, and the speed of convergence increases because of the relative

pitches of the spirals. A distance is reached when convergence exceeds the speed of sound and the wave begins to shrink.

From the point of view of an observer moving with the flow along a streamline, and looking at the wall represented by the interface, he sees the wall approach him—that is, convergence in his frame of reference. If we think of the wall as a piston moving into the flow, at the point where the sound wave begins to shrink, the piston is moving faster than the local speed of sound, and a shock wave will form upstream from the piston. Thus, the origins of the shock waves will be approximately at points B in the slow stream and C in the fast stream marking where the sound wave stops expanding away from the interface.

To find the approximate locations of these points and their dependence on the speed difference between the streams, we consider an idealized case in which the slow stream has constant speed V_s , the fast stream has constant speed V_f , the speed at the interface is $V_o = (V_s + V_f)/2$, and the Mach number, M , is constant throughout. Using the procedure given in Heinemann and Siscoe (1974), we find the equations of the characteristics to be

$$\begin{aligned}\eta_s &= \frac{1}{M} (1 + \Omega r/r_s - r/r_s) \\ \eta_f &= \frac{1}{M} (1 - \Omega r/r_f - r/r_f)\end{aligned}\tag{1}$$

where η is the azimuthal angle in the corotating reference frame, r is the heliocentric distance, and $r_s = V_s/M\Omega$, $r_f = V_f/M\Omega$. Without the Ω terms, these are the equations

of Parker's solar wind spirals (Parker, 1963, p. 138). The θ_n terms represent the movement of the sound wave away from the spiral. The equation of the interface is

$$\eta_0 = \frac{1}{M} (1 - r/r_0) \quad (2)$$

with $r_0 = V_0/M\Omega$. To estimate where the shocks form we determine where the radial separation between the characteristics and the interface begins to decrease, i.e. set $d\Delta r/d\eta = 0$. The result is shown in Table 1 for different speed differentials, $V_f - V_s$ with $V_0 = 400 \text{ km sec}^{-1}$ and $M = 4$.

As expected, the bigger the differential, the nearer the sun the shocks form. In the biggest case considered 160 km sec^{-1} , they form near the orbit of Mars. Any differential bigger than approximately 50 km sec^{-1} produces shocks inside the orbit of Jupiter. Although this example is idealized, it gives a fair test of the argument based on characteristics to predict qualitatively the essential geometrical aspects of the formation of corotating shocks. The prediction that typical solar wind streams, which have differentials bigger than 50 km sec^{-1} , should form shocks between the orbits of Earth and Jupiter is apparently confirmed by the Pioneer 10 and 11 observations. This justifies applying the argument to determine the out-of-the-ecliptic shape of corotating shock waves.

The application is straightforward, and the result is immediate if we consider the situation at the poles. Here the border between the streams is a radial line--the polar axis. The pitches of the streams lines are essentially zero and, hence, so is the speed of convergence of the streams. A sound wave starting here will expand forever,

although it will slow down because of the radial decrease in sound speed. Thus corotating shocks will not form over the poles. At intermediate latitudes, the pitches of the streamlines and the border are not zero, but they are less than at the equator. A sound wave must travel further before the convergence speed overtakes the sound speed and shocks form. Thus, the distance to the formation of the shocks increases with latitude.

The three dimensional geometry of the stream interface and the shock pair is sketched in Figure 3. The interface is generated by an expanding meridian circle that rotates about the polar axis as it expands so that its intersection with the equatorial plane moves along the border spiral. The leading points of the shocks are in the equatorial plane and the leading edges spiral outward as they move away from the equator, maintaining a proximity to the interface. A sketch on an expanded scale of a single corotating shock surface is shown in Figure 4. The motion of this surface is analogous to that of a tapered paper banner attached to a stick that is being twirled around the polar axis. The length of the banner is determined by the lifetime of the solar wind stream.

To study these structures an out-of-the-ecliptic mission is needed that covers the radial range between Earth and Jupiter. Knowledge of the three dimensional nature of these shock waves is essential for the interpretation of cosmic ray data and for applications to other astrophysical situations. The distortion of solar shock waves as described earlier and the highly structured geometry of corotating shocked waves

illustrate the complexity of the problems faced by galactic cosmic rays as they try to enter the inner solar system. Three dimensional probing of the interplanetary medium is required to obtain a complete picture of the extended stellar envelope of a representative from a major population of main sequence stars. The interaction of such stars with the interstellar medium in various galactic situations can they be treated with a fuller understanding of the stellar parameters. Comprehension of the three dimensional aspects of structures generated because a star rotates has application to contemporary astrophysical problems such as the interaction of the Crab pulsar with the Crab nebula.

Acknowledgments

This article is based on material prepared for a talk at the Symposium on the Study of the Sun and Interplanetary Medium in Three Dimensions held at the Goddard Space Flight Center, May 15-16, 1975. The material was prepared while the author was at the Center for Space Research, Massachusetts Institute of Technology. This research was supported in part by NASA under grants NGL 22-009-015 and NGL 22-009-372 (M.I.T.) and by NSF under grant GA 13842 (UCLA).

$V_f - V_s$	$d\Delta r/d\eta = 0$
16 (km/sec)	12.5 (AU)
32	6.2
48	4.2
64	3.1
80	2.5
96	2.1
112	1.8
128	1.6
144	1.4
160	1.3

Table 1. Approximate heliocentric distances in the equatorial plane to the formation of shock pairs due to interacting streams with various speed differentials. In this example the average speed is 400 km sec^{-1} and the Mach number is 4 throughout.

References

- Chao, J. K., and R. P. Lepping, A correlative study of SSC's interplanetary shocks and solar activity. J. Geophys. Res., **79**, 1799, 1974.
- Dessler, A. J., Solar wind and interplanetary magnetic field. Rev. Geophys. Space Phys., **5**, 1, 1967.
- Dobrowolny, M., and G. Moreno, Latitudinal structure of the solar wind and interplanetary magnetic field. Space Sci., Rev., in press, 1975.
- Gosling, J. T., Large-scale inhomogeneities in the solar wind of solar origin. Rev. Geophys. Space Phys., **13**, 1053, 1975.
- Heinemann, M. A., and G. L. Siscoe, Shapes of strong shock fronts in an inhomogeneous solar wind. J. Geophys. Res., **79**, 1349, 1974.
- Hirshberg, J., Y. Nakagawa, and R. E. Welck, Propagation of sudden disturbances through a nonhomogeneous solar wind. J. Geophys. Res., **79**, 3726, 1974.
- Houminer, Z., Enhanced scintillation sectors outside the plane of the ecliptic. Planet. Space Sci., **21**, 1617, 1973.
- Hundhausen, A. J., S. J. Bame, and M. D. Montgomery, Variations of solar wind properties: Vela observations of a possible heliographic latitude dependence. J. Geophys. Res., **76**, 5145, 1971.
- Hundhausen, A. J., Nonlinear model of high-speed solar wind streams. J. Geophys. Res., **78**, 1528, 1973a.
- Hundhausen, A. J., Evolution of large scale solar wind structure beyond 1 AU. J. Geophys. Res., **78**, 2035, 1973b.
- Hundhausen, A. J., Solar wind dynamics. J. Geophys. Res., this issue, 1975.
- Hundhausen, A. J., and J. T. Gosling, Solar wind structure at large heliocentric distances: an interpretation of Pioneer 10 observations. Submitted to J. Geophys. Res., 1975.
- Krieger, A. S., A. F. Timothy, and E. C. Roelof, A coronal hole and its identification as the source of a high velocity solar wind stream. Solar Phys., **29**, 505, 1973.

- Landau, L. D., and E. M. Lifschitz, Fluid Mechanics, Addison-Wesley Publishing Company, Reading, Massachusetts, 1959.
- Mayaud, P. N., Analysis of storm sudden commencements for the years 1868-1967. J. Geophys. Res., 80, 111, 1975.
- Noyes, R. W., Solar EUV/X-ray studies. J. Geophys. Res., this issue, 1975.
- Parker, E. N., Interplanetary Dynamical Processes. Interscience Publishers, New York, 1963.
- Sarabhai, V., Some consequences of nonuniformity of solar wind velocity. J. Geophys. Res., 68, 1555, 1963.
- Siscoe, G. L., Structure and orientations of solar-wind interaction fronts: Pioneer 6, J. Geophys. Res., 77, 27, 1972.
- Smith, E. J., and J. H. Wolfe, Observations of interaction regions and corotating shocks between one and five AU: Pioneers 10 and 11. Submitted to J. Geophys. Res., 1975.

Figure Captions

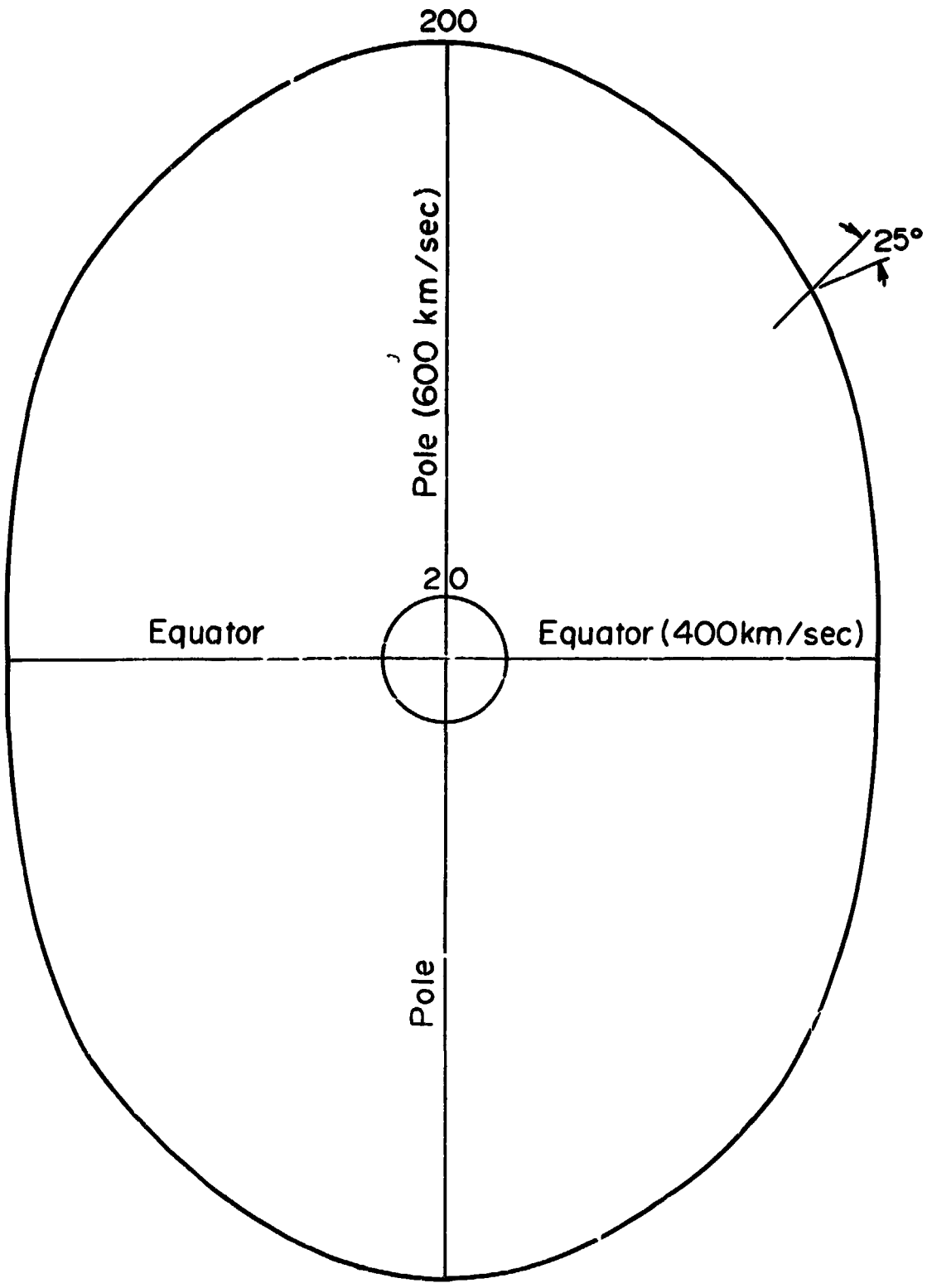
Figure 1. A meridian plane cross section through a solar origin shock surface assumed to be circular at 20 solar radii and distorted into a quasi-ellipse at 200 solar radii by the action of equator to pole solar wind speed differential of 200 km sec⁻¹.

Figure 2. A sketch of geometrical features of the flow in the equatorial plane and in the corotating reference frame. The stream interface separates a slow stream (leading) and a fast stream (trailing). Sample streamlines and corotating shocks in both streams are shown. The shocks deflect the streamlines parallel to the stream interface--with no deflection they would intersect the interface. The circles are sequential snapshots of a sound wave starting at A and expanding while being convected with the flow (distortion due to the flow speed differential is neglected). Shocks form where the sound wave begins to shrink which happens when the speed of convergence of the streams toward the interface (due to the differences in the pitches of the various spirals) becomes bigger than the local sound speed.

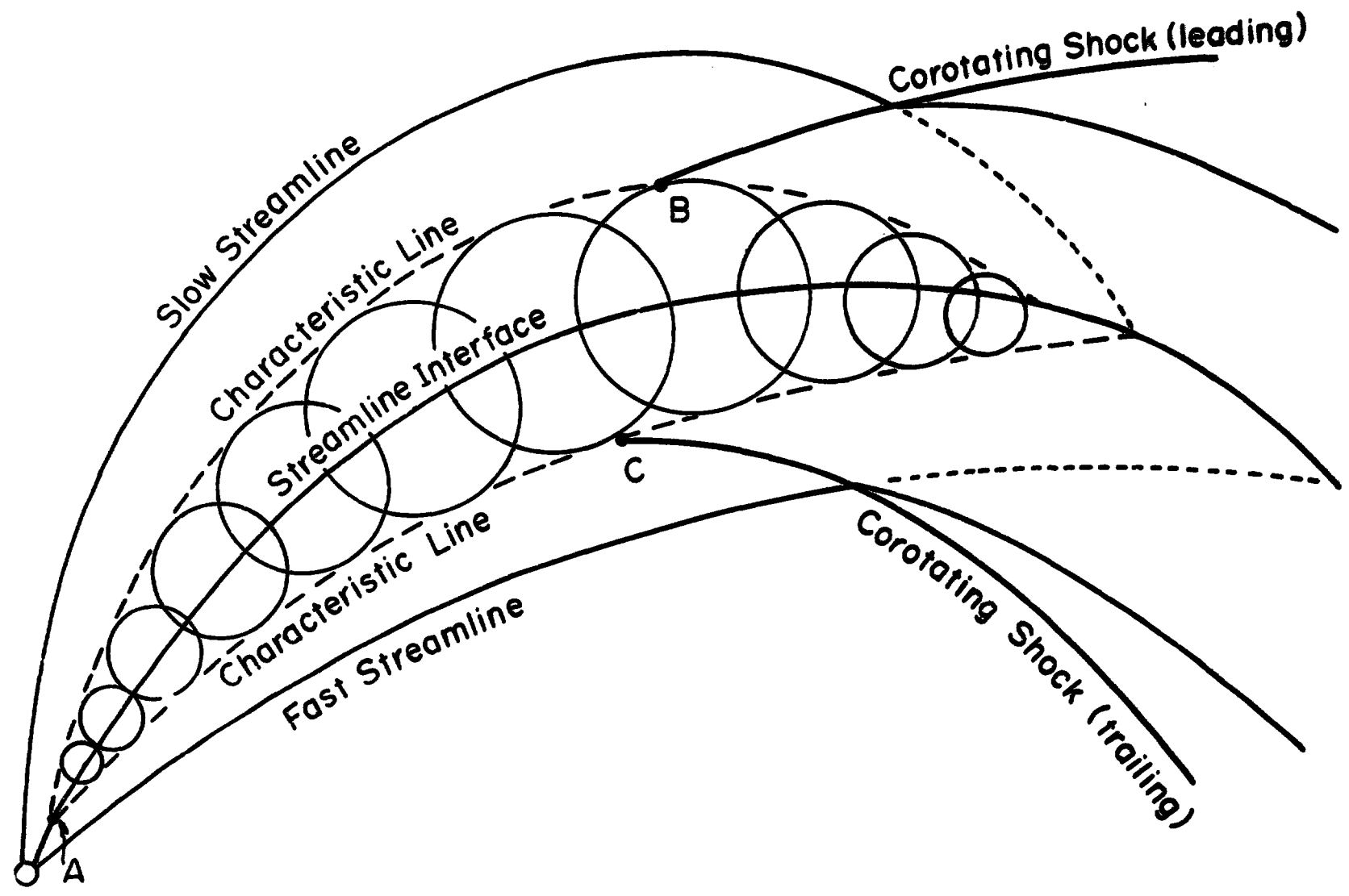
Figure 3. A sketch of the three dimensional geometry in the northern hemisphere of the stream interface and associated shock pair. The interface is generated by an expanding meridian circle that rotates about the polar axis as it expands so that its intersection with the equatorial plane follows the interface spiral, like

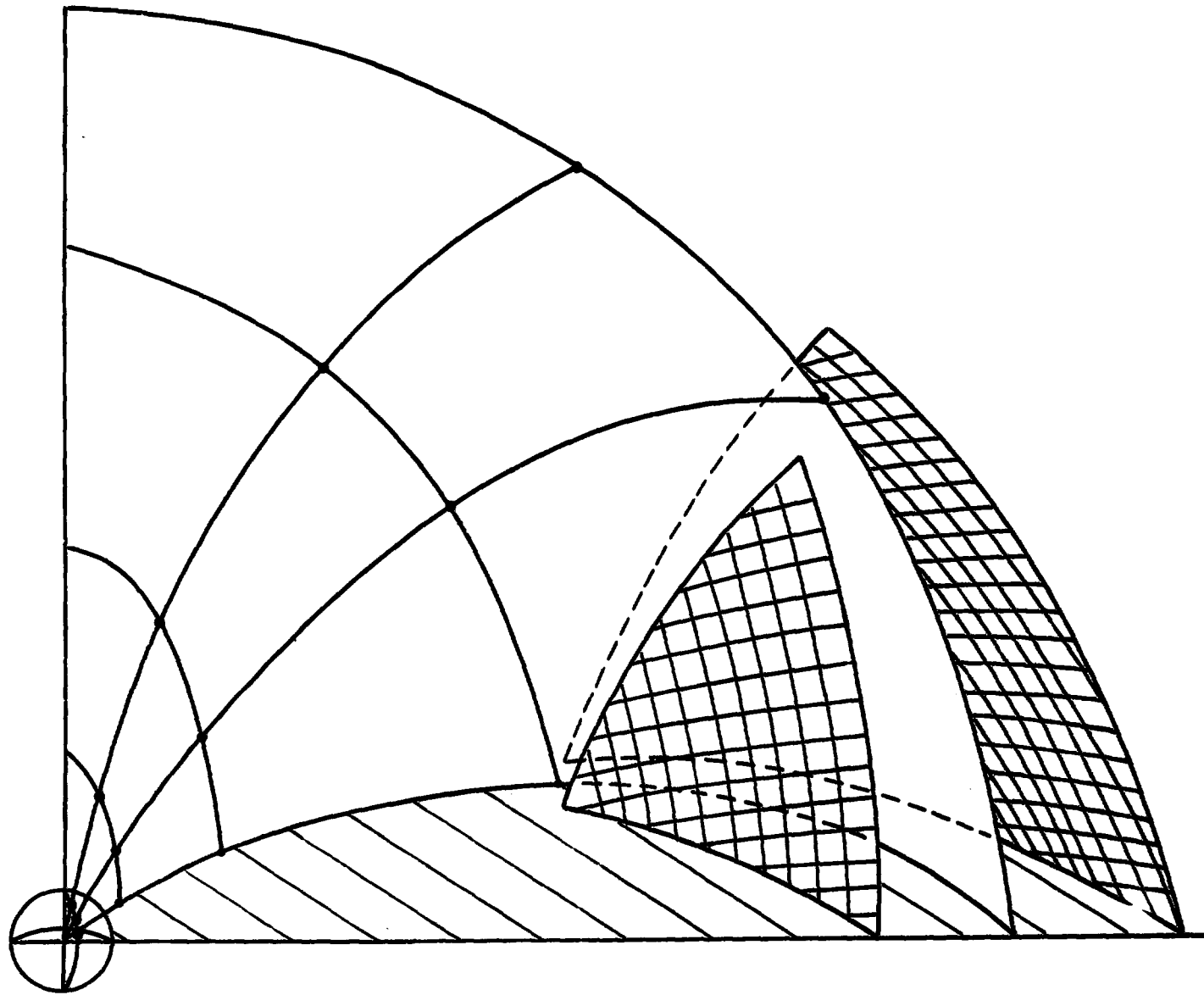
a needle in the groove of a record. The interface separates the shock pair. Their leading point is in the equatorial plane and their leading edges spiral away from the sun as they move away from the equatorial plane, maintaining a proximity to the interface.

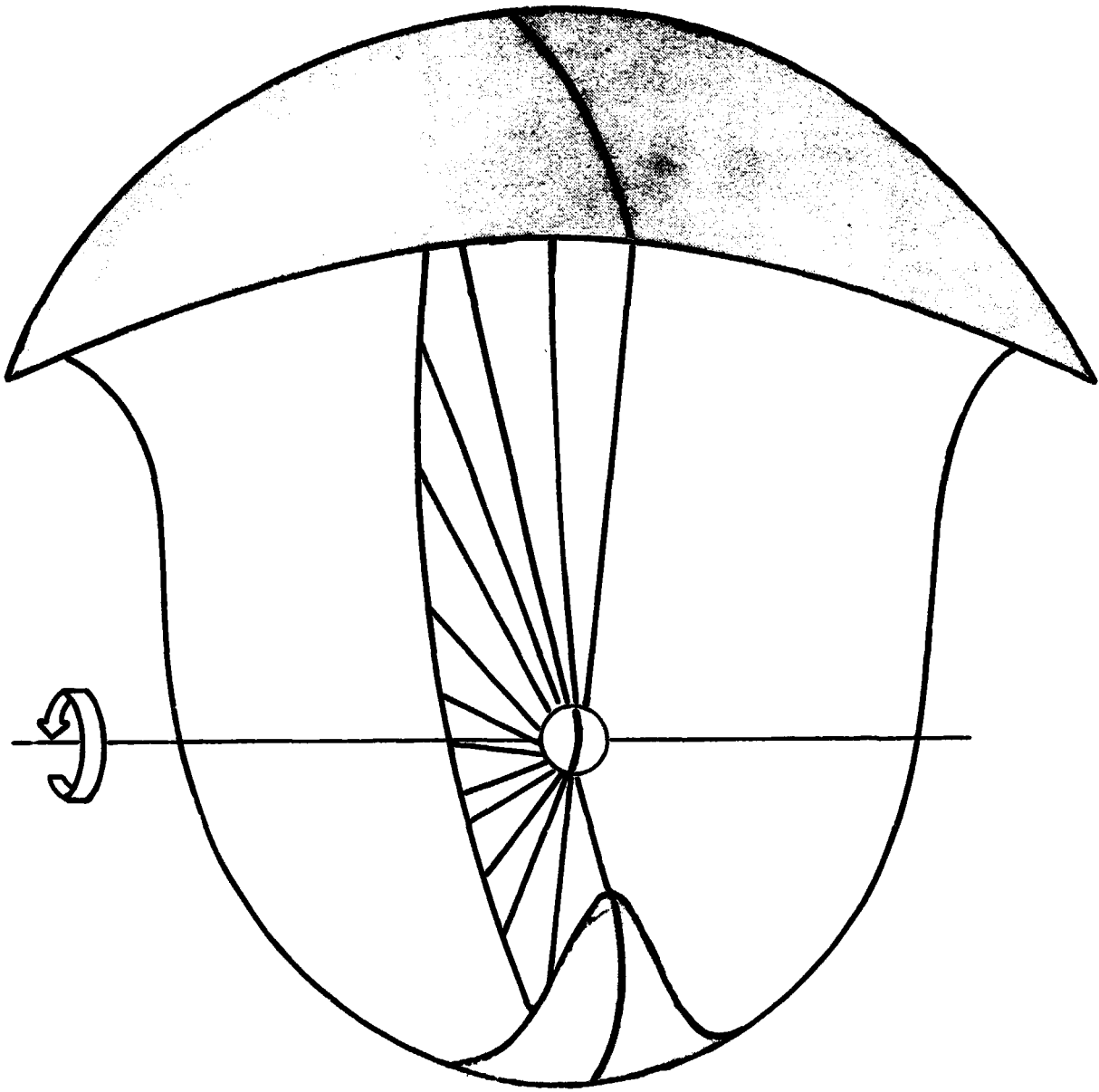
Figure 4. A sketch on an expanded scale of a single shock surface. The location of the equatorial plane is indicated by lines radiating from the sun. The motion of the surface is similar to that of a tapered paper banner attached at its point to a stick that is being twirled around the polar axis. The length of the banner is determined by the lifetime of the streams.



R₃







CHAPTER V

SOLAR AND GALACTIC COSMIC RAYS

* N76-24130

Cosmic-Ray Transport Theory and Out-of-the-Ecliptic Exploration

J. R. Jokipii

**Department of Planetary Sciences and Department of Astronomy
University of Arizona**

Abstract

The reasons for studying cosmic-ray transport theory are summarized and the fundamentally three-dimensional nature of the process is pointed out. Observations in the ecliptic plane cannot unambiguously test transport theories since the solutions to the transport equations depend critically on boundary conditions and variation of parameters such as diffusion tensor out of the ecliptic. Sample calculations are shown which illustrate the problem. It is concluded that out-of-the-ecliptic observations are essential to further test transport theory.

I. Introduction

The study of cosmic-ray transport theory has an old and venerable history, for it is clear that in order to understand anything in cosmic-ray astrophysics we must first understand transport. The observed near-isotropy of cosmic rays was early recognized to imply that the orbits of the particles have been severely distorted in their motion through space. Since the work of Fermi (1949) it has been understood that the motion must be treated statistically, since the plasmas and magnetic fields through which the cosmic rays move are irregular and turbulent. This basic fact leads to the view that the spatial motion of cosmic rays is to a very good first approximation a random walk in three dimensions.

The solar wind provides an excellent local laboratory for testing our ideas of cosmic-ray transport by comparing in situ observations with theory. A comprehensive theory has been developed which has had reasonable success in explaining the various cosmic-ray phenomena in the solar wind (see reviews by Jokipii, 1971 and Völk, 1975). Before going on to discuss this theory in detail, it is useful to emphasize that irrespective of the detailed theory, cosmic-ray transport theory is fundamentally three-dimensional and that this problem is much more severe than for some other aspects of the physics of the interplanetary medium. The general picture is illustrated in figure 1 for particles originating in the galaxy or at the sun. It

is evident that, for example, there is no viewing direction in which one sees cosmic rays which have sampled only the ecliptic plane. This conclusion depends only on the turbulent nature of the interplanetary plasma and the consequent stochastic motion of the cosmic-ray particles.

One can, of course, dream up experiments which could be used to study cosmic-ray transport locally. For example, a useful experiment would be to inject a small beam of "tagged" cosmic rays at one point and measure them a distance ~ 0.1 a.u. away. But such experiments are clearly not possible in the near future. We must be content with what nature provides, and work with the full three-dimensional problem.

The preceding discussion has intentionally been as general as possible in order to emphasize the fundamental nature of the conclusions. In the next section, the current detailed theory of cosmic-ray transport is discussed, then some quantitative calculations are presented which illustrate the effects of uncertainties in parameter outside of the ecliptic.

II. Current Transport Theory

The current theory of cosmic-ray transport has been comprehensively discussed in an earlier review by the author (Jokipii, 1971). The theory works at two levels, which could be termed the "macroscopic" and the "microscopic". This is illustrated schematically in figure 2 which shows the particle being scattered randomly by the magnetic fluctuations. Hence the particle pitch angle θ undergoes a random walk. The details of this scattering process and its relation to the detailed microstructure of the magnetic fluctuations are studied in the microscopic theory, whereas the resulting spatial diffusion is considered in macroscopic theory. Thus, for example, in the simplest form of quasilinear theory, where only planar magnetic fluctuations with wave vector parallel to the average field are considered, the pitch-angle scattering is characterized by the Fokker-Planck coefficient

$$\frac{\langle \Delta\theta^2 \rangle}{\Delta t} = \frac{\omega_0^2}{|\mu| w B_0^2} P_{\perp} \left(k = \frac{1}{\mu r_c} \right), \quad (1)$$

where $\omega_0 = qB_0/mc$ is the particle cyclotron frequency in the average field B_0 , $\mu = \cos\theta$, w = particle speed, $r_c = w/\omega_0$, and $P_{\perp}(k)$ is the spatial power spectrum of the magnetic fluctuations as a function of wavenumber k (see, e.g., Jokipii 1966, 1971). Other more complex expressions result if other magnetic fluctuation configurations are assumed. Similar expressions result for the other Fokker-Planck coefficients such as $\langle \Delta x^2 \rangle / \Delta t$, etc. Hence, if x is a direction

normal to B_0 , we have

$$\frac{\langle \Delta x^2 \rangle}{\Delta t} = \frac{|\mu|w}{B_0^2} P_{\perp}(k=0) . \quad (2)$$

The above expressions are examples of microscopic transport theory.

However, in most situations the cosmic-ray angular distribution is driven essentially isotropic by the scattering, so that the transport must be described by the diffusion approximation. If $U(\underline{r}, t, T)$ is the particle density averaged over pitch angle as a function of position \underline{r} , time t and energy T , then the diffusion equation reads in the rest frame (Parker 1965, Gleeson and Axford 1967, Jokipii and Parker 1970)

$$\frac{\partial U}{\partial t} = \frac{\partial}{\partial x_i} \left[\kappa_{ij} \frac{\partial U}{\partial x_j} - v_{w,i} U \right] + \frac{1}{3} \frac{\partial v_{w,i}}{\partial x_i} \frac{\partial}{\partial T} (\alpha T U) \quad (3a)$$

with an associated flux of particles in the rest frame

$$F_i = -\kappa_{ij} \frac{\partial U}{\partial x_j} + v_{w,i} U - \frac{v_{w,i}}{3} \frac{\partial}{\partial T} (\alpha T U), \quad (3b)$$

where κ_{ij} is the cosmic-ray diffusion tensor, v_w is the solar wind velocity and $\alpha(T) = (2mc^2 + T)/(mc^2 + T)$. The associated anisotropy is $|\delta| = 3|F_i|/wU$. In a coordinate system with the z -direction oriented along the average magnetic field B_0 , κ_{ij} may be written

$$\kappa_{ij} = \begin{bmatrix} \kappa_{\perp} & \kappa_A & 0 \\ -\kappa_A & \kappa_{\perp} & 0 \\ 0 & 0 & \kappa_{\parallel} \end{bmatrix} \quad (4)$$

where the parallel diffusion coefficient κ_{\parallel} , the perpendicular diffusion coefficient κ_{\perp} and the antisymmetric diffusion coefficient κ_A can be written

$$\kappa_{\parallel} = w^2 \int_{-1}^1 d\mu' \left[\mu' \int^{\mu'} \frac{d\mu}{\langle \Delta \theta^2 \rangle / \Delta t} \right] \quad (5)$$

$$\kappa_{\perp} = \frac{1}{2} \int_0^1 \frac{\langle \Delta x^2 \rangle}{\Delta t} d\mu \quad (6)$$

$$\kappa_A = \frac{1}{3} r_c w \cdot \quad (7)$$

The diffusion equation (3) embodies the macroscopic theory which is connected to the microscopic theory by equations (5) - (7). At present, comparison of transport theory with observation must be done through the use of macroscopic theory and then working back to the microscopic theory. We are unable to measure $\langle \Delta \theta^2 \rangle / \Delta t$, etc. directly.

With regard to the problem of out-of-the-ecliptic exploration, it is clear that the solution to equation (3) depends on a knowledge

of κ_{ij} and V_w throughout the modulating region and on the value of U on the boundary. There appear to be no purely locally measurable properties of the solution which can be used in checking transport theory.

III. Illustrative Calculations

To illustrate the rather large uncertainties introduced by lack of knowledge of parameters out of the ecliptic, I present in this section a summary of some analytical calculations published elsewhere (Owens and Jokipii, 1971). This problem has also been considered by Sarabhai and Subramanian (1966) and Lietti and Quenby (1968). Consider the 11-year solar cycle modulation of galactic cosmic rays by a solar wind which is not spherically symmetric. The 11-year solar cycle variations are usually regarded as slow enough that the time derivative in equation (3) can be neglected in solving for U . In this calculation the various parameters in the transport equation are allowed to vary with heliographic latitude and the effects of the variation on the density U and the flux F in the solar equatorial plane are considered.

The following forms for the various parameters were assumed: The various components of the diffusion tensor are independent of energy T and are proportional to heliocentric radius r out to some boundary $r = D$ where $\kappa_{ij} \rightarrow \infty$. The cosmic-ray density $U(r, T)$ is assumed to take on a given interstellar value $U_{\infty}(T) = AT^{-2.5}$ at $r = D$.

Finally, we follow the usual practice of circumventing the problem of proper boundary conditions at the Sun by requiring the solution for U to be finite at the origin. This will be shown to lead to negligible error in the present case. See Jokipii (1971) for a more complete discussion of this problem.

Equation (3a) for $U(r, \theta, \phi, T)$ becomes, in spherical polar coordinates

$$\begin{aligned} \frac{1}{r^2} \frac{\partial}{\partial r} \left[r^2 (v_w u - \kappa_{\parallel} \frac{\partial U}{\partial r}) \right] - \frac{1}{r \sin \theta} \frac{\partial}{\partial \theta} \left[\sin \theta \left(\frac{\kappa_{\perp}}{r} \frac{\partial U}{\partial \theta} - \frac{\kappa_A}{r \sin \theta} \frac{\partial U}{\partial \phi} \right) \right] \\ - \frac{1}{r \sin \theta} \frac{\partial}{\partial \phi} \left(\frac{\kappa_{\perp}}{r \sin \theta} \frac{\partial U}{\partial \phi} + \frac{\kappa_A}{r} \frac{\partial U}{\partial \theta} \right) - \frac{2v_w}{3r} \frac{\partial}{\partial T} (TU\alpha) = 0. \end{aligned} \quad (8)$$

In what follows, we consider only models which are axisymmetric (independent of ϕ). If $\theta = 0$ is the axis of solar rotation, this corresponds to a latitude-dependent solar wind. Effects of magnetic sectors could be represented by taking $\theta = 0$ along a sector. The two terms containing κ_A cancel from the density equation (8) if $\partial \kappa_A / \partial \theta = \partial \kappa_A / \partial \phi = 0$, as in our axisymmetric model. Thus the terms in κ_A do not contribute, and equation (8) becomes

$$\frac{1}{r^2} \frac{\partial}{\partial r} \left[r^2 (v_w u - \kappa_{\parallel} \frac{\partial U}{\partial r}) \right] - \frac{1}{r^2 \sin \theta} \frac{\partial}{\partial \theta} (\kappa_{\perp} \sin \theta \frac{\partial U}{\partial \theta}) - \frac{2v_w}{3r} \frac{\partial}{\partial T} (TU\alpha) = 0. \quad (9)$$

Since κ_{\parallel} and κ_{\perp} are taken to be independent of energy, equation (9) separates, and one writes

$$U(r, \theta, T) = S(r, \theta) \psi(T). \quad (10)$$

REPRODUCIBILITY OF THE
ORIGINAL PAGE IS POOR

Upon neglecting the small energy dependence of $\alpha(T)$, one finds immediately that S must satisfy

$$\frac{1}{r^2} \frac{\partial}{\partial r} \left[r^2 (V_w S - \kappa_{\parallel} \frac{\partial S}{\partial r}) \right] - \frac{1}{r^2 \sin \theta} \frac{\partial}{\partial \theta} \left[\kappa_{\perp} \sin \theta \frac{\partial S}{\partial \theta} \right] = \frac{q V_w S}{r}, \quad (11)$$

with

$$\phi(T) = T^{(3q/2\alpha)-1}. \quad (12)$$

The separation constant q must be chosen to agree with $U_{\infty}(T) \propto T^{-2.5}$, in which case we choose $q \approx -1$.

A number of different forms for the variation of the parameters V_w , κ_{\parallel} and κ_{\perp} were chosen. Define

$$V_w(\theta, r) = V_0 [1 + \delta(\theta)], \quad \kappa_{\parallel}(\theta, r) = \kappa_0 [1 + \epsilon(\theta)] r$$

$$\text{and } \kappa_{\perp} = \mu \kappa_{\parallel}. \quad (13)$$

The problem may be solved in terms of a series of Legendre polynomials and the general solution is given by Owens and Jokipii (1971). An illustrative velocity variation is given by $V = V_0 [1 + .30 P_2(\cos \theta)]$ where V_0 is the average velocity and P_2 is the Legendre polynomial of order 2. This velocity variation is illustrated in figure 3. Some typical results of the calculations

are illustrated in figures 4, 5, and 6. It is clear that many of the parameters observed in the solar equatorial plane can be substantially changed by varying the solar-wind parameters out of the solar ecliptic plane. Of particular note is the fact that the radial anisotropy observed in the equatorial plane is extremely sensitive to parameters outside the equatorial plane. As shown in figure 6, even the sign of the anisotropy can be changed by relatively small velocity variations.

IV. Conclusions

One may conclude from the above discussion that fundamental ambiguities in testing cosmic-ray transport can be removed by carrying out measurements out of the ecliptic. The out-of-the-ecliptic measurements most necessary to study cosmic-ray propagation are:

- a) Measurements of the flux of cosmic rays as a function of solid angle and energy with as much resolution as possible. The anisotropy measurements are easier to carry out on a spinning spacecraft.
- b) Simultaneous measurements on board the same spacecraft of the plasma and magnetic field. These measurements should be spaced in time so that good time-series analyses (power spectra, etc.) can be obtained.
- c) The spacecraft should go as far out of the ecliptic as possible to insure that any variations with heliographic latitude will be seen.
- d) Good base-line measurements at Earth or in the ecliptic plane should be obtained simultaneously.

It is not crucial that these measurements be carried out at constant heliocentric radius, although this might aid interpretation. It appears that measuring protons and possibly electrons will be adequate and it is better to optimize measurements for one species rather than compromise these in order to study composition.

Acknowledgment

This work was supported, in part, by the National Aeronautics and Space Administration under Grant NSG-7101.

References

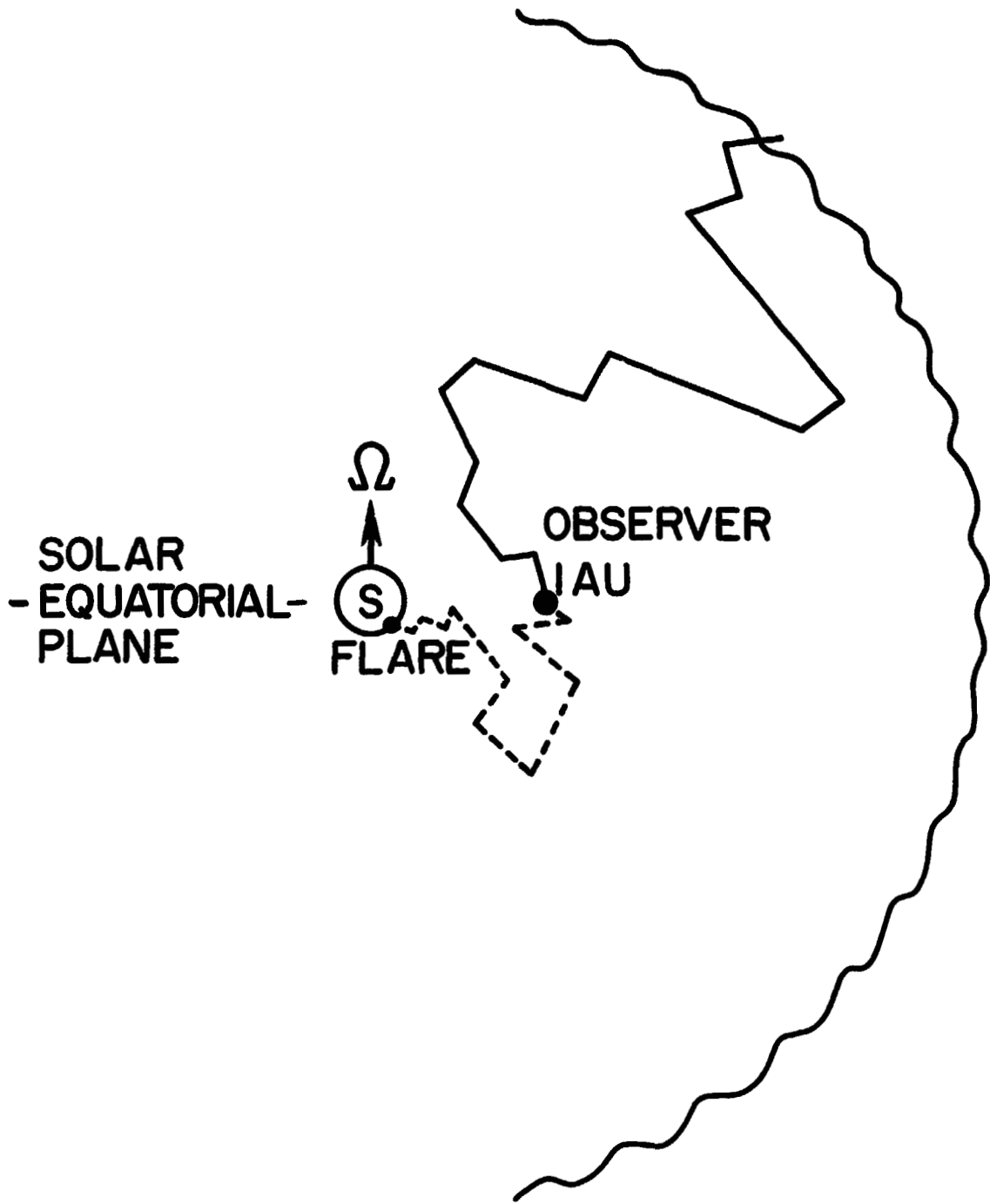
- Fermi, Enrico, On the origin of cosmic radiation, Phys. Rev. 75, 1169, 1949.
- Gleeson, L., and W. I. Axford, Cosmic rays in the interplanetary medium, Astrophys. J. 149, L115, 1967.
- Jokipii, J. R., Cosmic-ray propagation, 1, Charged particles in a random magnetic field, Astrophys. J. 146, 480, 1966.
- Jokipii, J. R., Propagation of cosmic rays in the solar wind, Rev. Geophys. and Sp. Phys. 9, 27, 1971.
- Jokipii, J. R., and E. N. Parker, On the convection, diffusion, and adiabatic deceleration of cosmic rays in the solar wind, Astrophys. J. 160, 735, 1970.
- Lietti, B., and J. J. Quenby, The daily-variation second harmonic and a cosmic-ray intensity gradient perpendicular to the ecliptic, Can. J. Phys. 46, S942, 1968.
- Owens, A. J., and J. R. Jokipii, Cosmic-ray modulation by an angle-dependent solar wind, Astrophys. J. 167, 169.
- Parker, E. N., The passage of energetic charged particles through interplanetary space, Planet. Space Sci. 13, 9, 1965.
- Sarabhai, V., and G. Subramanian, Galactic cosmic rays in the solar system, Astrophys. J. 145, 206, 1966.
- Völk, Heinrich J., Cosmic ray propagation in interplanetary space, Rev. Geophys. and Sp. Phys., to be published, 1975.

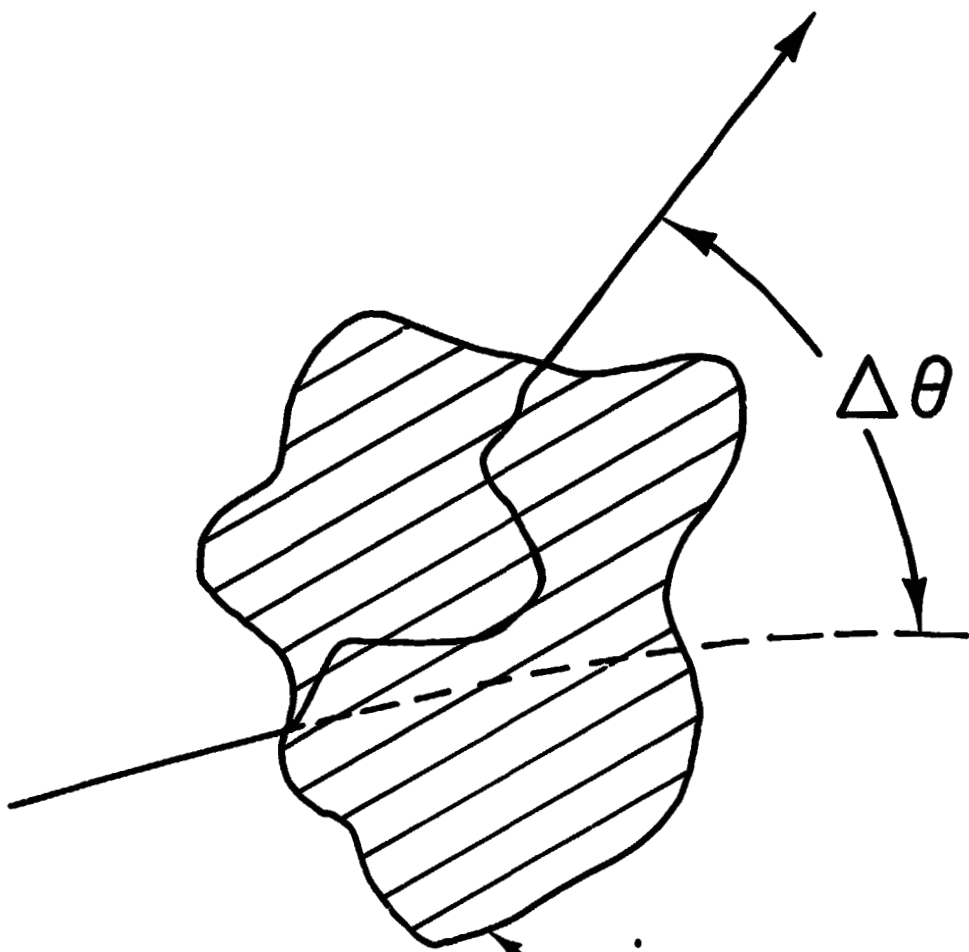
Figure Captions

- Fig. 1. Schematic illustration in a meridian plane of typical trajectories of solar cosmic-rays (dashed line) and galactic cosmic rays (solid line) which reach a detector at 1 a.u. The fundamentally 3-dimensional character of the motion is apparent.
- Fig. 2. Illustration of the "scattering" of a cosmic-ray particle by a magnetic irregularity. If the region over which $\Delta\theta$ is correlated is small, a Fokker-Planck equation results.
- Fig. 3. Illustration of the velocity profile used in some of the calculations. θ is the angle relative to the z-axis.
- Fig. 4. Comparison of linearized and exact solutions for the case $V = V_0 [1 + 0.30 P_2(\cos \theta)]$, $\kappa_{\parallel} = \kappa_0 r$, $\mu = \frac{1}{2}$. The density $U(r, \theta)$ is given for both solutions as a function of angle θ $r = 0.2 D$ in terms of $U_{\infty} = U(r = D, \theta)$. Straight line shows the corresponding result for an isotropic wind $V = V_0$. The linearized calculation keeps terms only to first order in δ as defined in equation (4). From Owens and Jokipii (1971).
- Fig. 5. Total cosmic-ray flux as a function of r, θ , and with F_{ϕ} suppressed. The pattern is azimuthally symmetric and even about the equator. (a) The parameters $V(\theta) = V_0 [1 + 0.30 P_2(\cos \theta)]$, $\kappa_{\parallel}(r, \theta) = \kappa_0 r$ and $\mu = \frac{1}{2}$ were used. The position of Earth for $D = 5$ a.u. is indicated. Of particular interest is the

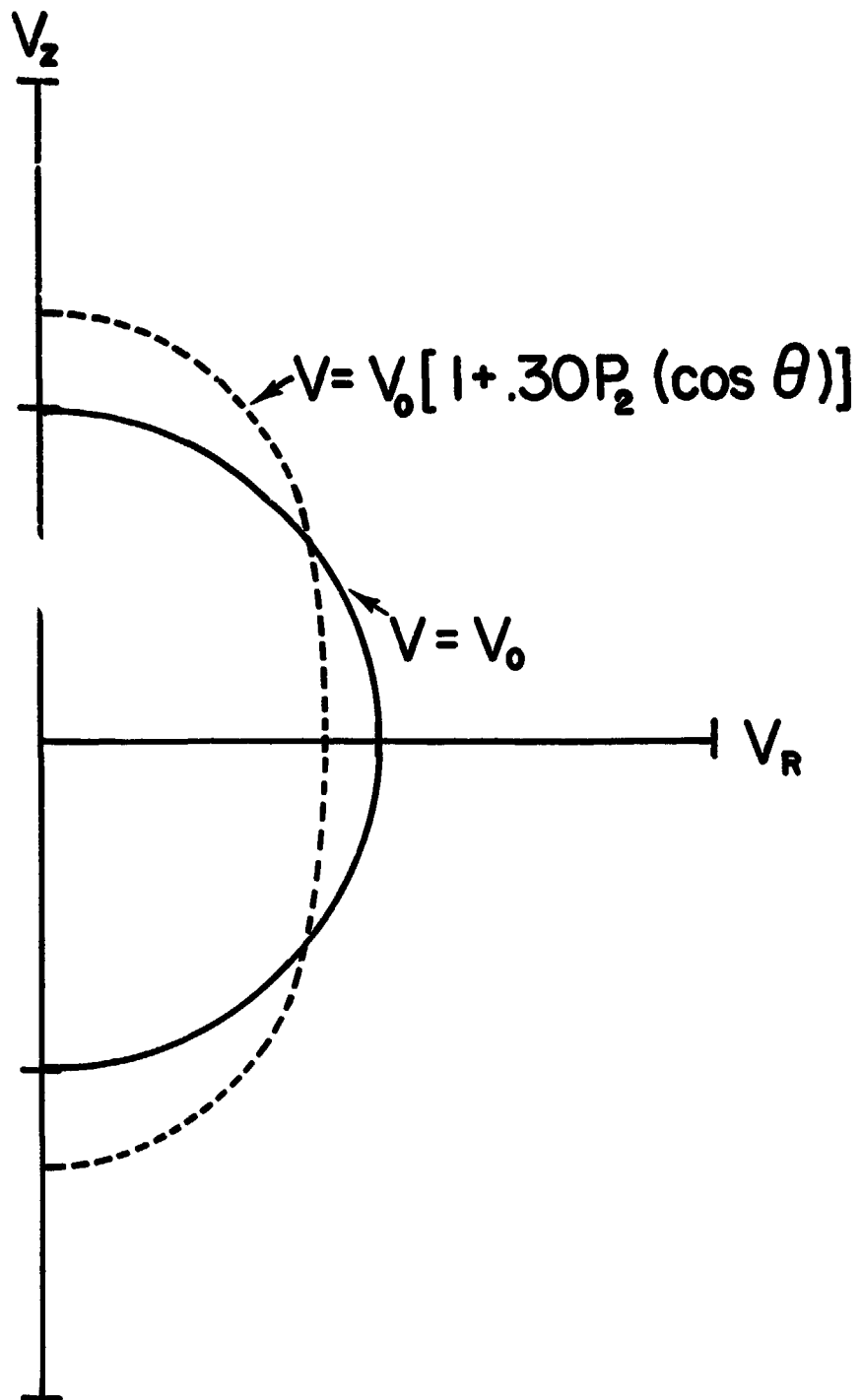
virtual source of particles in the equatorial plane at
 $r = 0.5 D$. (b) Same as (a) except that $V(\theta) = V_0 [1 + 0.46 P_2(\cos \theta)]$.
Note that the flux is much larger and virtual source has
moved out to $r \sim 0.9 D$. From Owens and Jokipii (1971).

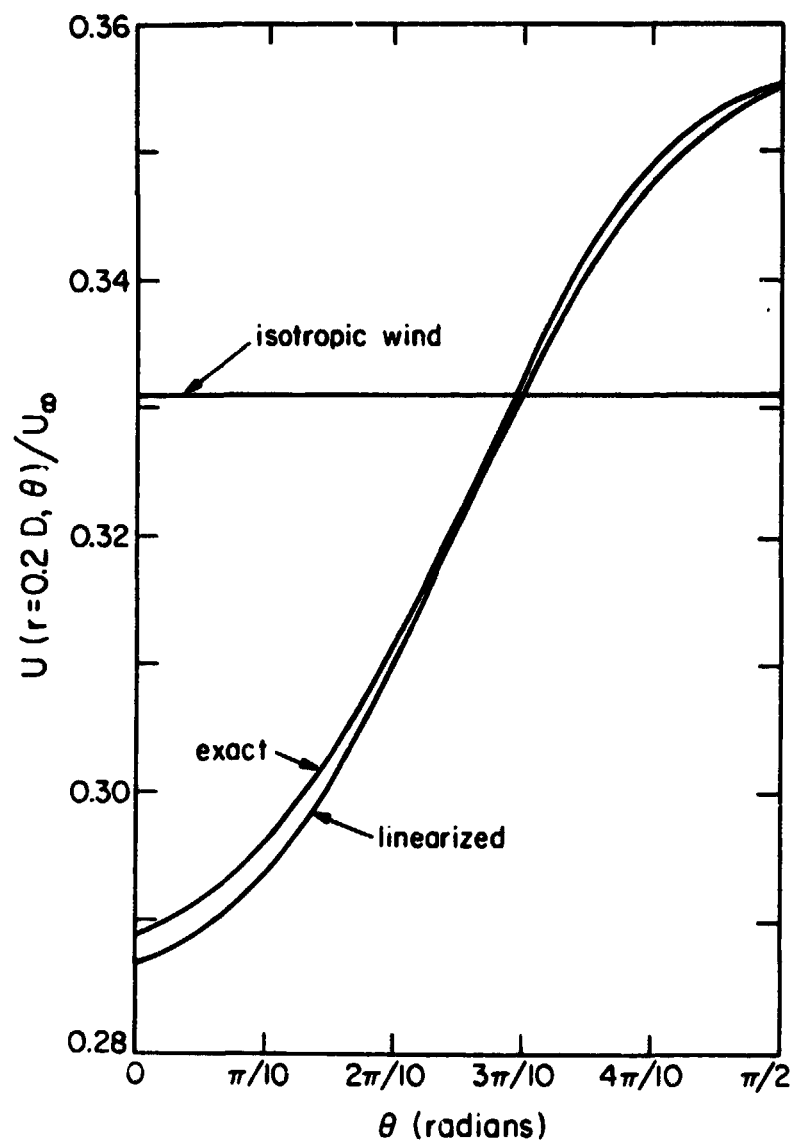
Fig. 6. Anisotropy in the equatorial plane at $r = 0.2 D$ for
 $V(\theta) = V_0 + V_2 P_2(\cos \theta)$, as a function of V_2/V_0 .
Note that in our model the anisotropy is radial. From
Owens and Jokipii (1971).

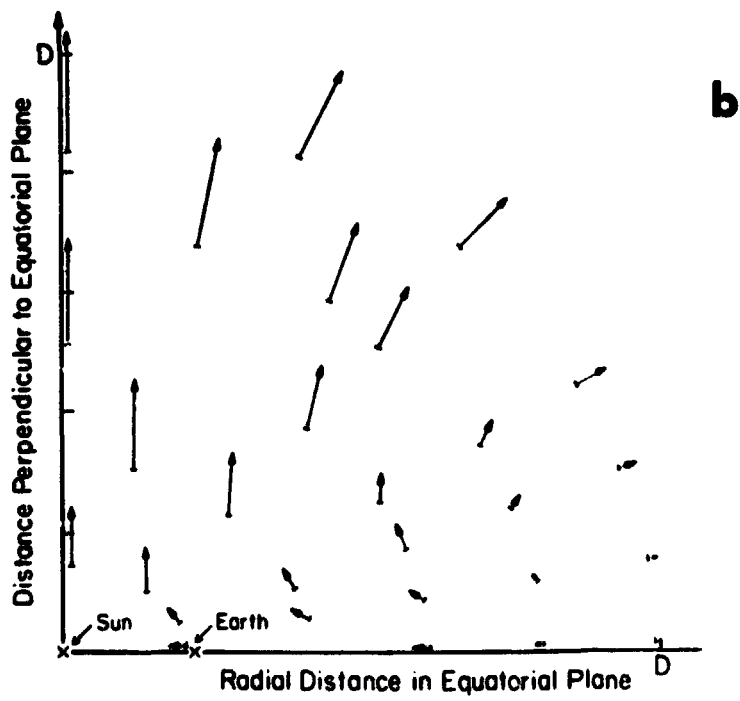
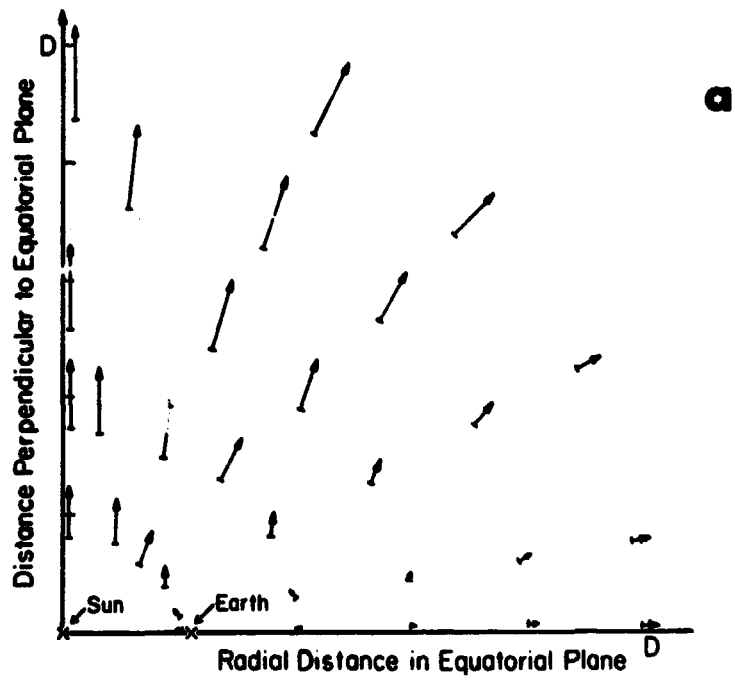


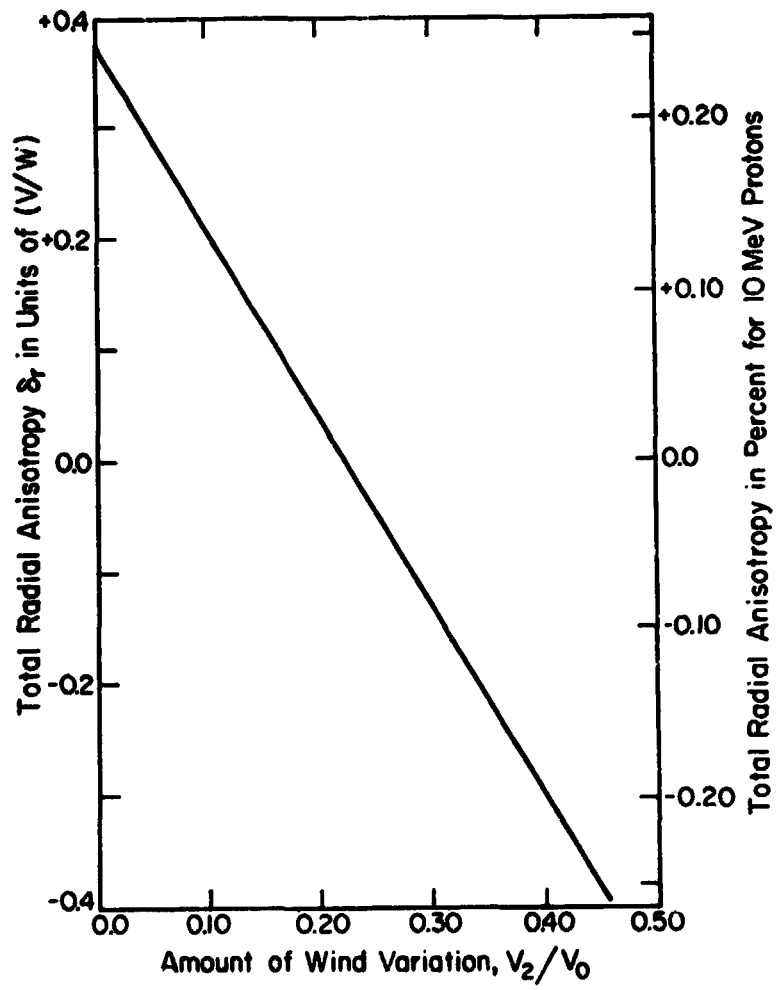


region over which
 $\Delta\theta$ is correlated









COSMIC RAY MODULATION IN THREE DIMENSIONS

N76-24131

J. J. Quenby

Physics Department, Imperial College, London SW7 2BZ

Abstract. A brief critique of spherically symmetric conventional modulation theory is supplied. Estimates are made of the cosmic ray intensity at high solar latitudes. Direct evidence for significant off-ecliptic cosmic ray gradients is reviewed in support of the requirement for an off-ecliptic spacecraft mission. The possibility of measuring the galactic spectrum is discussed.

1. Spherically symmetric modulation theory and its problems.

Cosmic ray modulation arises because motion of the energetic particles along the spiral interplanetary magnetic field lines is controlled by scattering due to magnetic irregularities which are being convected outwards by the solar wind. Inward diffusion is balanced both by outward convection and energy loss of the particles as they suffer adiabatic deceleration in the expanding wind. A Fokker-Planck equation expressing these effects in a spherically symmetric, steady-state situation is (Parker 1965, Gleeson and Axford 1967)

$$\frac{1}{r^2} \frac{\delta}{\delta r} (r^2 V U - r^2 K_r \frac{\delta U}{\delta r}) = \frac{2}{3} \frac{V}{r} \frac{\delta}{\delta T} (\alpha T U) \quad (1)$$

Here U is the differential particle number density at position r and kinetic energy $T, \alpha = \frac{T + 2T_0}{T + T_0}$ with T_0 as rest mass energy, V is the solar wind velocity and K_r , the effective radial diffusion coefficient, is given by $K_r = K_{||} \cos^2 \psi + K_{\perp} \sin^2 \psi$ for $K_{||}$ and K_{\perp} respectively the parallel and perpendicular diffusion coefficients with $\psi = \cos^{-1} (\underline{B} \cdot \underline{r} / |\underline{B}| |\underline{r}|)$.

Particle streaming \underline{S} is due to diffusion in the wind frame plus an additional term involving a Lorentz transformation to the rest frame via the Compton-Getting factor C such that

$$\underline{S} = C\underline{V}U - \tilde{K} \cdot \text{grad } U \quad (2)$$

with $C = 1 - \frac{1}{3U} \frac{\delta}{\delta T} (\alpha T U)$ and \tilde{K} as the tensor diffusion coefficient.

At magnetic rigidities exceeding about 1 GV, radial streaming is usually negligible and under these circumstances the Fokker-Planck (1) can be integrated to give a relation between the Galactic density $U(r_g, T_g)$ and the observed density $U(r, T)$,

$$U(r, T) = U(r_g, T_g) \exp \left(- \int_r^{r_g} \frac{CV}{K_r} dr \right) \quad (3)$$

for spherical symmetry with r_g determined by the effective outer bound to the interplanetary scattering process.

It is important for Astrophysics to know the energy spectra of various nuclear species of cosmic rays in the galaxy and a common method for achieving this "demodulation" is as follows:

- (a) Estimate the Galactic electron spectrum from radio synchrotron data.
- (b) Compare the near-earth electron spectrum with the Galactic spectrum to find the magnitude and rigidity dependence of $\int_r^{r_g} \frac{CV}{K_r} dr$.
- (c) Use the results of (b) to correct the near-earth proton and heavy nuclei spectra for modulation.

Various objections can be raised to this scheme. First, the average Galactic electron spectrum derived from radio data may not represent the local spectrum and in any case one must be sure of the model enabling the effects of local, cold, absorbing interstellar clouds (Goldstein et al. 1970a) to be taken into account. Second, there is no adequate theoretical explanation as yet for the magnitude, rigidity dependence and radial dependence of K_r , as witnessed by investigations of solar proton diffusion (e.g. Webb et al. 1973) and the measurement of cosmic ray radial gradients ($<10\%/AU$) which are much less than those expected on the basis of theoretical K_r values (e.g. Webber and Lezniak, 1973). It is important to know the r dependence of the integrand in (3) since adiabatic deceleration is inversely proportional to r . This importance becomes apparent in our third point, based on the work of Goldstein et al. (1970b) and Gleeson and

Urch (1971) who, for certain choices of r dependence and reasonable magnitudes of K_r , find that adiabatic deceleration may completely exclude all $\lesssim 100$ MeV/nucleon particles from the inner solar system. Thus no certain knowledge of the lowest energy Galactic primaries is possible. Fourth, the cause of time variations in the modulation is unknown, with not enough solar cycle variation in the solar wind parameters being observed near earth to account for the known changes in the cosmic ray flux (e.g. Hedgecock et al. 1972). For example, the power spectrum of magnetic irregularities at 10^{-4} Hz should change by a factor >2 in order to account for the observed modulation of 1 GV particles between 1965 and 1969 according to resonant, wave/particle interaction theory while in practice the change is $<10\%$ (Hedgecock 1975). Off-ecliptic control of modulation via the effects far beyond 1 AU of solar streams emerging from the zones of maximum solar activity may be the only way to explain the cosmic ray 11-year cycle. Hence careful study by off-ecliptic spacecraft is required.

2. The off-ecliptic route to the boundary.

It has been thought that a direct determination of the Galactic cosmic ray charge and energy spectrum can be achieved employing ecliptic plane spacecraft trajectories to the outer planets. In this way the problems of section 1 are all by-passed. However, the boundary to modulation could be as far as 100 AU and the low, measured cosmic ray density gradients seen by Pioneer 10 render this approach uncertain. Alternatively, we note that cosmic rays have an easier inward motion over the solar poles where the geometric path length along the interplanetary field lines is much shorter than in the tightly wound spiral regime of the equatorial plane (Lietti and Quenby 1968). An appropriate Fokker-Planck equation for the steady state which relinquishes the requirement of spherical symmetry and takes into account the spiral geometry is then

$$\frac{1}{A} \frac{\delta}{\delta s} \left(AK_{\perp} \frac{\delta U}{\delta s} \right) = \frac{1}{r^2} \frac{\delta}{\delta r} (r^2 CVU) \quad (4)$$

if $K_{\perp} = 0$ for path length s along a magnetic flux tube of area A .

Allowing $K_{\perp} = K_e r \sin^q \theta$ where θ is solar latitude yields

$$U/U_g = (r/r_g)^{CVr/K_e} \exp - \left\{ \frac{CVr^2 \sin^2 - q \theta}{2K_e r} \right\} \quad (5)$$

and if $q = 0$ and $U/U_g = 1/e$ at 1 GV, we obtain the following table for the percentage residual modulation at 1AU:

	$\theta = 90^\circ$	$\theta = 30^\circ$	$\theta = 0^\circ$
U/U_g (at 1 GV)	63%	22%	9%

Thus on a simple model for scattering, a spacecraft passing over the poles at 1 AU may see ~90% of the unmodulated intensity and therefore get a better measurement of galactic conditions than is available at Jovian distances.

3. Direct evidence for off-ecliptic gradients

Observations confined to the ecliptic plane can only reveal the existence of off-ecliptic effects by noting modifications to cosmic ray streaming from the expectations of the spherically symmetric model case. Equation (2) in a more general form is

$$\underline{S} = CUV - K_{||} \left(\frac{\delta U}{\delta r} \right)_{||} - \frac{v^2}{3\omega} \left(\frac{\delta U}{\delta r} \right) \times \underline{B} \quad (6)$$

where v is energetic particle velocity and ω is cyclotron frequency. It has been assumed that direct slippage of particles across field lines makes only a small streaming contribution ($K_{\perp}/K_{||} \sim \frac{1}{\omega^2 \tau^2} \ll 1$, τ being time to travel one parallel mean free path). Furthermore, we assume the short-circuiting by scattering of that perpendicular gradient which would cancel out the anisotropy due to $(\underline{E} \times \underline{B})_{\perp}$ drift in the non-scattering limit when Liouville's theorem applies to the particle intensity. At high rigidities, some few to a hundred GV, the radial streaming is negligible over long periods with the third term on the right of (6) cancelling out on average. Then the first two terms combine to give the streaming from the east or 1800 hr LT anisotropy. When, however, the anisotropy is studied in practice as a function of sign of the interplanetary field sector structure, two effects of the third term become apparent. A north-south anisotropy arises due to $\left(\frac{\delta U}{\delta r} \right)_{\text{radial}} \times \underline{B}$, or the effect of the radial gradient and an ecliptic plane anisotropy arises due to $\left(\frac{\delta U}{\delta r} \right)_z \times \underline{B}$, or the effect of off-

ecliptic gradient. Hashim and Bercovitch (1972) find $G_2 = 5.5 R^{-0.6}\%/AU$ directed north \rightarrow south in 1967/68 for the latter effect, possibly physically resulting from the excess northern hemisphere solar activity suggested at that time by coronal green line 5303A emission.

The previous discussion refers to the first derivative of density, but studies of the second harmonic of the cosmic ray intensity can reveal the presence of a rising or falling, symmetric, off-ecliptic gradient via a dependence on the second derivative. Lietti and Quenby (1968) essentially use a version of (5) for the rising gradient case to predict a second harmonic with direction of maximum perpendicular to \underline{B} and amplitude $a_2 = \frac{1}{2} \frac{\rho^2}{r^2} \frac{\delta^2 U}{\delta \theta^2} \sim 0.005P\%$ at rigidity P , cyclotron radius ρ . This expression is in reasonable accord with observations although Nagashima et al. (1972) claim that a cylindrical pitch angle particle distribution about \underline{B} with a different physical cause better fits cosmic ray anisotropy data.

With finite K_{\perp} , the symmetrical gradient will either feed particles into the equatorial plane or draw them off to higher latitudes, thus setting up radial streaming. A correction to the Fokker-Planck (1) is employed by adding

$$\text{div} \left[- \frac{K_{\perp}}{\omega^2 \epsilon^2} \left(\frac{\delta U}{\delta r} \right) \right]$$
 to the right hand side. Dyer et al. (1974) in particular evoke this streaming for a falling gradient to explain a sunward flow at ~ 1 GV seen by a satellite detector which is too large to be explained by any energy loss effects in a spherically symmetric model. These authors require maximum modulation over the sunspot zones with meridional flow patterns set up to draw particles down from $\theta = 0^\circ$ and up from $\theta = 90^\circ$. Cecchini et al. (1975) have developed a computational model to confirm the above model. Chief features are:

$$K = K_0 \beta P f(\theta) \begin{cases} \exp r/r_0 / \exp(1) & r < 1 \text{ AU} \\ r/r_0 & r > 1 \text{ AU} \end{cases}$$

$$K = \epsilon K_0 \beta P_0 f(\theta) \begin{cases} (r/r_0)^3 & r < 1 \text{ AU} \\ (r/r_0) & r > 1 \text{ AU} \end{cases}$$

$$f(\theta) = 1 + \cos \theta (-3 + 5 \cos^2 \theta) ;$$

$$K_0 = 2.2 \cdot 10^{19} \text{ cm}^2 / \text{sec Mev at 1AU} ;$$

$$\epsilon = 0.5, 1\text{AU}; V_w = \text{const.}; P_0 = 100 \text{ MV}; U_g \propto (T + T_0)^{-2.75}$$

Thus $K_{\perp}/K_{\parallel} = 0.05$ at 1 GV. The results of employing an alternating gradient technique to solve the corrected Fokker-Planck, with finite K_{\perp} , is to predict an inward streaming $\sim 0.3\%$ in amplitude between 2 and 10^{-1} GeV, a radial gradient $\sim 10\%/AU$ at 1.1 GeV between 1 and 10 AU and a ratio $U(\theta)/U(\theta = \frac{\pi}{2})$ at 1 AU varying from 2.5 at $\theta = 0$ to 0.7 at $\theta = 60^\circ$ for 1.1 GeV protons. Hence it is possible to explain the radial streaming with reasonable gradients and K_{\perp}/K_{\parallel} ratios.

4. Conclusions.

We have shown that study of cosmic ray modulation by integrating the transport equation outwards in the ecliptic plane, assuming spherical symmetry, encounters various problems. The transport processes and boundary conditions are insufficiently well understood, modulation may be controlled by off-ecliptic gradients and assymetries can have noticeable effects on solar equatorial plane observations. Three-dimensional study of the solar cavity cosmic ray distribution is required to:

- (a) Measure off-ecliptic gradients and streaming.
- (b) Enhance understanding of the solar control of intensity time variations.
- (c) Gain better knowledge of boundary conditions, especially the possibility of measuring a near-Galactic energy spectrum over the solar poles.

Objectives (a) and (c) are satisfied by a Jovian swing-by mission but (b) requires a direct injection at 1 AU spacecraft for detailed time variation studies on solar wind and solar parameters.

References

- Cecchini, S. and Quenby, J.J. Three dimensional models of galactic cosmic ray modulation, Paper MG 2-6, Munich Cosmic Ray Conf., 1975.
- Dyer, C.S., Engel, A.R., Quenby, J.J. and Webb, S. Observation and explanation of a 0.3% sunward radial streaming of 1 to 5 GV cosmic radiation, Solar Phys. 39, 243, 1974.
- Gleeson, L.J. and Axford, W.I. Cosmic rays in the interplanetary medium, Astrophys.J.(Lett.) 149, L 115, 1967.
- Gleeson, L.J. and Urch, I.H. Energy losses and modulation of galactic cosmic rays, Astrophys. and Space Sci. 11, 288, 1971.
- Goldstein, M.L., Ramaty, R. and Fisk, L.A. Interstellar cosmic ray spectra from the non-thermal radio background from 0.4 to 400 MHz, Phys.Rev. Lett. 24, 1193, 1970a.
- Goldstein, M.L., Fisk, L.A. and Ramaty, R. Energy loss of cosmic rays in the interplanetary medium, Phys.Rev.Lett. 25, 832, 1970b.
- Hashim, A. and Bercovitch, M. A cosmic ray density gradient perpendicular to the ecliptic plane, Planet.and Space Sci. 20, 791, 1972.
- Hedgecock, P.C., Quenby, J.J. and Webb, S. Off-ecliptic control of cosmic ray modulation, Nature Phys.Sci. 240, 173, 1972.
- Hedgecock, P.C. Measurements of the interplanetary magnetic field in relation to the modulation of cosmic rays, to be publ. 1975.
- Lietti, B. and Quenby, J.J. The daily variation second harmonic and a cosmic ray intensity gradient perpendicular to the ecliptic, Canad.J.Phys. 46, S942, 1969.
- Nagashima, K., Ueno, H., Fujimoto, K., Fujii, Z. and Kondo, I. Three-dimensional cosmic ray anisotropy in interplanetary space, Rep.Ion. Space Res. Jap. 26, 1, 1972.
- Parker, E.N. The passage of charged particles through interplanetary space, Planet.and Space Sci. 13, 9, 1965.
- Webb, S., Balogh, A., Quenby, J.J. and Sear, J.F. A comparison of theoretical and experimental estimates of the solar proton diffusion coefficient during three flare events, Solar Phys. 29, 477, 1973.
- Webber, W.R. and Lezniak, J.A. Interplanetary radial gradients of galactic cosmic ray protons and helium nuclei: Pioneer 8 and 9 measurements from 0.75 to 1.10 AU, J.of Geophys.Res. 73, 1979, 1973.

COSMIC RAY ACCESS AT POLAR HELIOGRAPHIC LATITUDES

by

Heinrich J. Völk

Max-Planck-Institut für Kernphysik

Heidelberg, FRG

Abstract

Based on a modified WKB analysis of the interplanetary irregularity spectra, a discussion of the radial dependence of the radial cosmic-ray diffusion coefficient at polar heliographic latitudes is presented. At 1 AU radial distance the parameters are taken to equal those observed in the ecliptic. In the sense of a present best estimate it is argued that relativistic nuclei should have significantly easier access to 1 AU at the pole than in the ecliptic. The reverse may very well be true for the direct access of very low rigidity particles.

REPRODUCIBILITY OF THE
PAGE IS POOR

1. Introduction

The access of galactic cosmic rays to the inner solar system is regulated by the cumulative effect of the irregular fields which scatter the particles on their way in. To determine the degree of this access at heliographic latitudes that are significantly different from the solar equatorial plane, one has to rely on theoretical estimates. These conventionally assume a diffusive propagation scheme. Of primary importance is then the spatial diffusion coefficient or, more generally, the diffusion tensor, and in particular its spatial variation in the solar system.

In the earlier work of Völk et al. (1974) the irregular fields were assumed to be Alfvén waves of solar origin, convected outwards by the solar wind.

In a (on the average) stationary interplanetary medium with axial symmetry around the solar rotation axis, this led to a radial direction for almost all wave normals beyond about 1 AU. Assuming the effective average magnetic field to be in the ideal spiral field direction and the wave amplitudes to vary according to the (WKB) approximation of geometrical optics, a radial dependence of the coefficient for diffusion along the average field was calculated. As a sensitive function of the angle between wave normals and average field, the value of this diffusion coefficient, or equivalently, of the mean free path, varies from a minimum at 0 degrees to infinity at 90 degrees. Since in the solar equatorial plane the angle between the radial and the spiral field direction is large already at 1 AU, and increases with radial distance, deviations of the wave normals from the radial direction have been discussed by Richter (1974) in the context of the solar wind stream structure; see also Hollweg (1975).

We do not intend to evaluate here the effects of deviations from the simple picture of Völk et al. (1974) at low latitudes and refer to a future publication (Morfill et al., in preparation). We shall rather concentrate on the situation at polar heliographic latitudes. There the assumption of all wave vectors \underline{k} being radial and parallel to the average field \underline{B} leads to the minimum value of the radial diffusion coefficient \mathcal{K} as far as its dependence on the angle between \underline{k} and \underline{B} is concerned. Thus, within the WKB approximation for the radial development of the scattering centers, this provides a lower limit for \mathcal{K} . Such a lower limit is of interest, if it can be argued, or at least be speculated in a reasonable way that even in this case there is essentially unimpeded access to about 1 AU for a significantly larger part of the galactic energy spectrum than in the solar equatorial plane.

We shall give a short discussion here, motivated by three considerations. The first one is that in two earlier publications this author was associated with (Völk et al., 1974; Völk, 1975), a rather different result was believed to hold true. Another reason is given by the present discussion of an ex-ecliptical probe to explore the sun and the interplanetary medium. The final reason is that via easy access at the poles much larger regions of interplanetary space might possibly be populated by particles of galactic origin.

In the next section we shall present the general behavior of \mathcal{K} in a modified WKB analysis, using simple approximations to two rather different measured interplanetary power spectra. In the last section the relation to the expected actual situation at the heliographic pole is discussed.

2. WKB Analysis

Consider the simplest, axisymmetric, interplanetary medium, where all quantities depend on heliocentric distance r and where only the ideal spiral field \underline{B} with components

$$(1) \quad B_r = B_{r_0} \left(\frac{r_0}{r} \right)^2; \quad B_\theta = 0; \quad B_\phi = B_{r_0} \cdot \frac{r_0}{r} \cdot \frac{r_0 \cdot \Omega_s \cdot \sin \theta}{V}$$

and the power spectrum $P(f, r, \theta)$ may in addition depend on heliographic latitude θ . Here r_0 is a radial reference level, B_{r_0} is independent of θ ; ϕ denotes heliographic longitude, $\Omega_s \approx 2.65 \times 10^{-6}$ cps is the angular frequency of the sun's rotation, V is the solar wind speed (assumed to be radial and constant), and f is the wave frequency seen by an observer at rest relative to the sun's center. Then it is simple to show (Völk et al., 1974) that for $\theta \rightarrow \frac{\pi}{2}$ the radial diffusion coefficient is given by

$$(2) \quad K = \beta R^2 \frac{2c}{(V + |v_A|)} \frac{|\delta B_\phi(r, \theta)|^2}{|\delta B_r(r, \theta)|^2} \int_0^1 d\mu \cdot \mu \cdot (1 - \mu^2) \left\{ P \left(\phi = \frac{1}{2\pi} \left| \frac{B(V + |v_A|)}{R \cdot \mu} \right|, \theta = \frac{\pi}{2}, r_1 \right) \right\}^{-1}$$

In equation (2) we have $\beta = \frac{w}{c}$, the ratio of particle velocity w to the velocity of light c ; R denotes particle rigidity; $v_A = \underline{B} \cdot (4\pi \rho)^{-1}$ is the (vectorial) Alfvén - speed, where ρ is the average solar wind mass density; $\mu = w_{\parallel} / w$ is the cosine of the particle's pitch angle, where w_{\parallel} is the velocity component parallel to \underline{B} ; $r_1 = 1$ AU. The amplification factor

for the Alfvén wave amplitudes δB_k

$$(3) \frac{|\delta B_k(r)|^2}{|\delta B_k(r_1)|^2} = \left(\frac{V + v_{Ar}(r)}{V + v_{Ar}(r_1)} \right)^2 \cdot \frac{v_{Ar}(r)}{v_{Ar}(r_1)} \left(\frac{r_1}{r} \right)^2 \approx \left(\frac{r_1}{r} \right)^3$$

is independent of wavevector k and Θ . If both r_1 and r are large compared to the Alfvénic critical radius ($\approx 20 R_\odot$ in the equatorial plane), then the approximation on the far r.h.s. of equation (3) holds in this lowest order WKB approximation. However, following equations (1) and (3) we have (at $\Theta = 90^\circ$): $\langle \delta B^2(r, \Theta) \rangle / B^2(r, \Theta) \sim r$, where $\langle \delta B^2 \rangle$ is the total power in the fluctuations. Thus, the possibility arises that $\langle \delta B^2 \rangle / B^2 > 1$ beyond some radial distance in which case we expect wave propagation to be rather drastically altered by nonlinear effects that ultimately should lead to dissipation of wave energy. To take this possible effect into account, we modify equation (3) so that for all r

$$(3a) \quad \langle \delta B^2(r) \rangle \leq B^2(r)$$

A similar device has been used by Hollweg (1973) and appears as a simple if crude way to take the inadequacy of the linearised WKB approximation into account.

It is clear physically that equations (1), (2), (3) and (3a) also hold if, at given r_0, B_{r0}, v and \mathfrak{g} are different from their values at $\Theta \approx 0$, as long as their dependence on Θ is weak enough, such that for example $\frac{1}{v} \frac{dv}{d\Theta} \ll 1$.

For the rest of this section, however, we will consider $B_r(r_1), v, \mathfrak{g}(r_1)$ and $P(f, \Theta, r_1)$ as given by their values in the equatorial plane.

Observed power spectra at $\theta \approx 0$ and $r \approx r_1$ (e.g. Jokipii and Coleman, 1968; Bercovitch, 1971), generally approximate rather well a power law for $P(f, r_1)$ at high frequencies, while flattening at low frequencies. Qualitatively, an analytical form

$$(4) \quad P(f, r_1) = C_f \cdot \frac{f_0^q}{1 + (f/f_0)^q}$$

with parameters C_f , f_0 , and $q < 0$, is not an unreasonable representation. With equation (4) the general character of $K(r)$ can be inferred. For small enough rigidity R , so that $|\underline{B}| \cdot V/R > 2\pi f_0$ we have $K \sim r^{3+2q}$ whereas $K \sim r^3$ for $|\underline{B}| \cdot V/R \ll 2\pi f_0$. The exponent of r is additively increased by unity whenever the supplementary restriction (3a) comes into force. For our present discussion we choose $q = -3/2$. Thus, $K \approx \text{const}$ (or $\sim r$) for small $R \cdot r^2$, whereas $K \sim r^3$ (or $\sim r^4$) for large $R \cdot r^2$. At sufficiently large r , K will be $\sim r^3$ (or $\sim r^4$) for any R . At fixed values of q and R , the transition of K to the r^3 (or r^4) dependence increases with decreasing f , cf. equation (2). As an aside we should mention that for this value of q and for the present case of $\underline{k} \parallel \underline{B}$ the quasilinear expression for K used in writing in equation (2) is numerically quite satisfactory and the modifications in the region around $\mu = 0$ (e.g. Jones et al., 1973) therefore not essential.

Numerical results are shown in Figures 1 and 2. Figure 1 is calculated using the spectrum of Jokipii and Coleman (1968) where, in reference to equation (4), $C_f \approx 16 \times 10^{-3} \cdot \gamma^2 \cdot (\text{Hz})^{-1-q}$; $f_0 \approx 7 \times 10^{-5} \cdot \text{Hz}$; $q \approx -3/2$, and Alfvén wave propagation was started at $r_0 = 20 R_\odot$ (solar radii). Figure 2 uses the spectrum published by Bercovitch (1971) which we roughly approximate by $C_f \approx 6 \times 10^{-3} \cdot \gamma^2 \cdot (\text{Hz})^{-1-q}$; $f_0 \approx 7 \times 10^{-6} \cdot \text{Hz}$; $q \approx -3/2$. Although the results are not very much

different for both cases near $r = 1$ AU, the very different f_0 -values lead to strong differences in the onset distance of the r^3 (or rather r^4) law. We should mention here that we used here the component of the magnetic spectral tensor perpendicular to the ecliptic to represent the total power per frequency interval. For true axisymmetry of the spectrum all K values in Figures 1 and 2 should be multiplied by a factor 1/2. This is an unavoidable uncertainty

The interesting aspect of these results is that they imply little modulation for relativistic nuclei, where adiabatic deceleration is small, considering the value of f_0 in Figure 2 as a rather extreme lower limit to the actual situation. For 1 GeV protons, for example, a 10-20 percent modulation is estimated in the diffusion convection approximation.

3. Discussion

The above results were obtained by fitting, at 1 AU, the average solar wind parameters as well as power spectra by the corresponding quantities observed at 1 AU in the ecliptic; the spatial dependence of the spectra assumed a modified WKB approximation for the irregularities. In reality, the polar region of the corona may well be a large, stationary coronal hole, resulting in a somewhat (perhaps fifty percent) larger flow speed and, possibly, somewhat more power in the frequency region $f \gg f_0$. All this would lead to a moderately increased modulation.

On the other hand, it may very well be that the power in frequencies $f \lesssim f_0$ is much smaller at $\theta = \pi/2$ than near $\theta = 0$. We have taken these fluctuations also to be Alfvénic which leads to the amplitude variation given in equation (3). In reality, the part in the spectrum with $f \lesssim f_0$ may well be due to the solar wind stream structure (Goldstein and Siscoe, 1972). If the latter is assumed to be absent at $\theta = 90^\circ$, also the power at $f \lesssim f_0$ would be absent with a corresponding decrease in modulation. In this light, also

the possibility of increased scattering at larger distances due to local production of waves - a situation that is quite likely at $\theta \approx 0$ - appears rather weak. Irregularities produced by enhanced (compared to the ecliptic) turbulence due to radially increasing departures from thermal equilibrium at the poles should be assumed to have small scales, irrelevant for cosmic rays even in the case of the Firehose instability. It should be added that in contrast to a popular feeling this result for \mathcal{K} and the consequent argument for modulation has little to do with the shorter geometrical path along \underline{B} of a galactic particle to, say, 1 AU, but rather to the strong decrease with r of the magnetic field at the poles.

Thus, barring unknown new effects, the present best estimate is that cosmic ray access at the poles should be significantly better than at $\theta \approx 90^\circ$ for relativistic nuclei. For very low-rigidity particles on the other hand, the sharp increase of \mathcal{K} with r occurs only at such a large radial distance that their direct access may be at least as strongly prohibited as in the equatorial plane. However, for this last kind of statement, the present estimate is not well suited.

Acknowledgment:

The author would like to thank Dr. G. Morfill for discussions and the numerical calculation of the results.

REPRODUCIBILITY OF THE
ORIGINAL PAGE IS POOR

References

- Bercovitch, M., "The heliocentric radial density gradient of relativistic cosmic rays in 1967-68",
Proc. 12 th Int. Conf. Cosmic Rays, Hobart. 2, MOD-12, 579 (1971)
- Goldstein, B. and G.L. Siscoe, "Spectra and cross spectra of solar wind parameters from Mariner 5", in "Solar Wind", NASA SP - 308, p. 506
(1972)
- Hollweg, J.V., "Alfvén waves in a two-fluid model of the solar wind",
Astrophys. J. 181, 547 (1973)
- Hollweg, J.V., "Alfvén wave refraction in high-speed solar wind streams",
J. Geophys. Res. 80, 908 (1975)
- Jokipii, J.R., and Coleman, P.J., Jr., "Cosmic-ray diffusion tensor and its variation observed with Mariner 4", J. Geophys. Res. 73, 5495
(1968)
- Jones, F.C., Kaiser, T.B., and T.J. Birmingham, "New approach to cosmic-ray diffusion theory", Phys. Rev. Lett. 31, 485 (1973)
- Morfill, G., Völk, H.J., and M.A. Lee, "The effect of stochastic averaging of the background magnetic field on the cosmic ray diffusion coefficient", to be submitted to J. Geophys. Res. (1975)
- Richter, A.K., "Wave-trains in the solar wind, 3, Alfvén waves in the azimuthally dependent interplanetary medium", to appear in Astrophys. Space Sci. (1975)
- Völk, H.J., Morfill, G., Alpers, W., and M.A. Lee, "Spatial dependence of the pitch-angle and associated spatial diffusion coefficients for cosmic rays in interplanetary space", Astrophys. Space Sci. 26, 403 (1974)

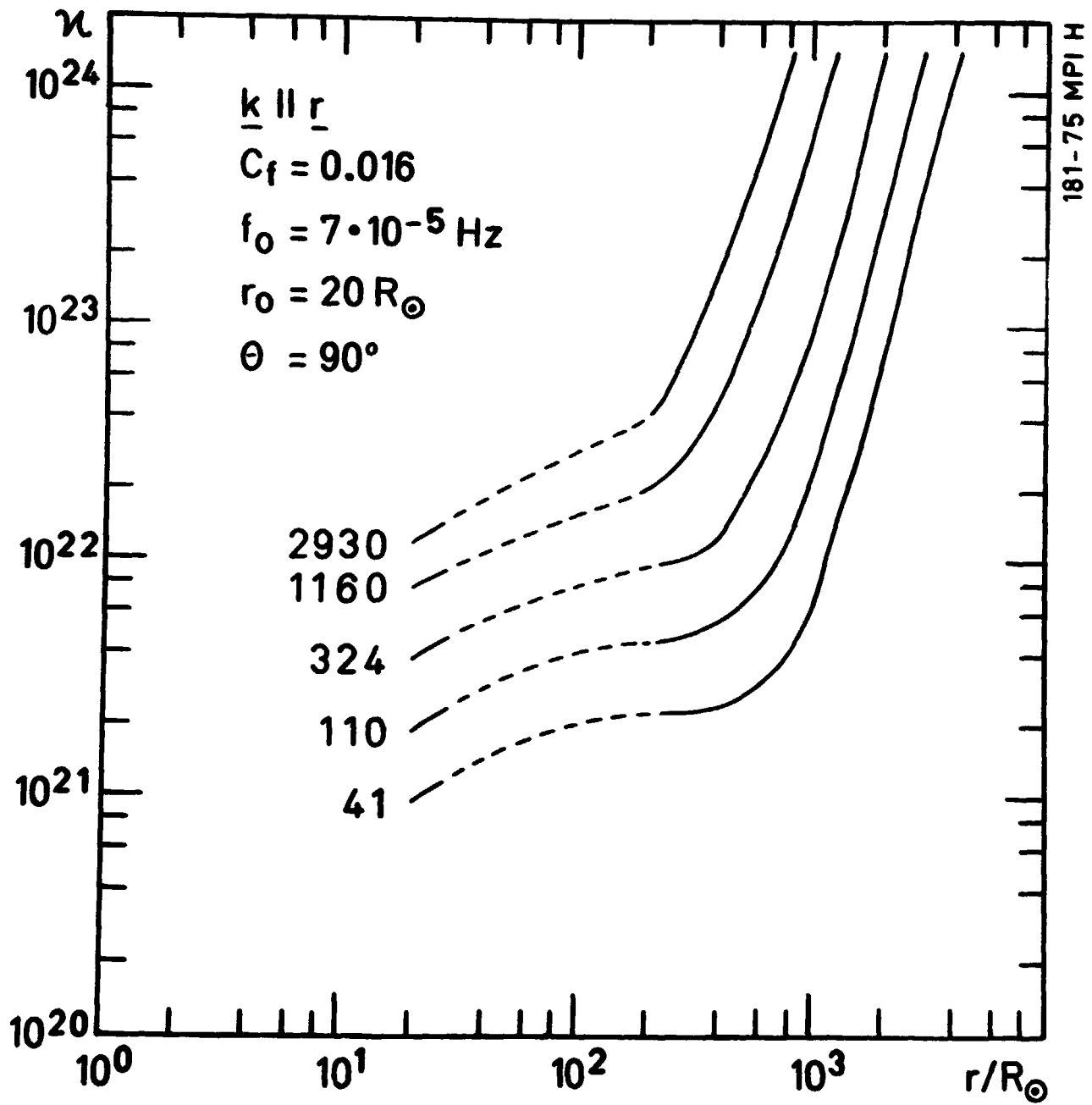
References cont'd

**Völk, H.J., "Cosmic ray propagation in interplanetary space", Rev. Geophys.
and Space Phys., (1975) ,to be published**

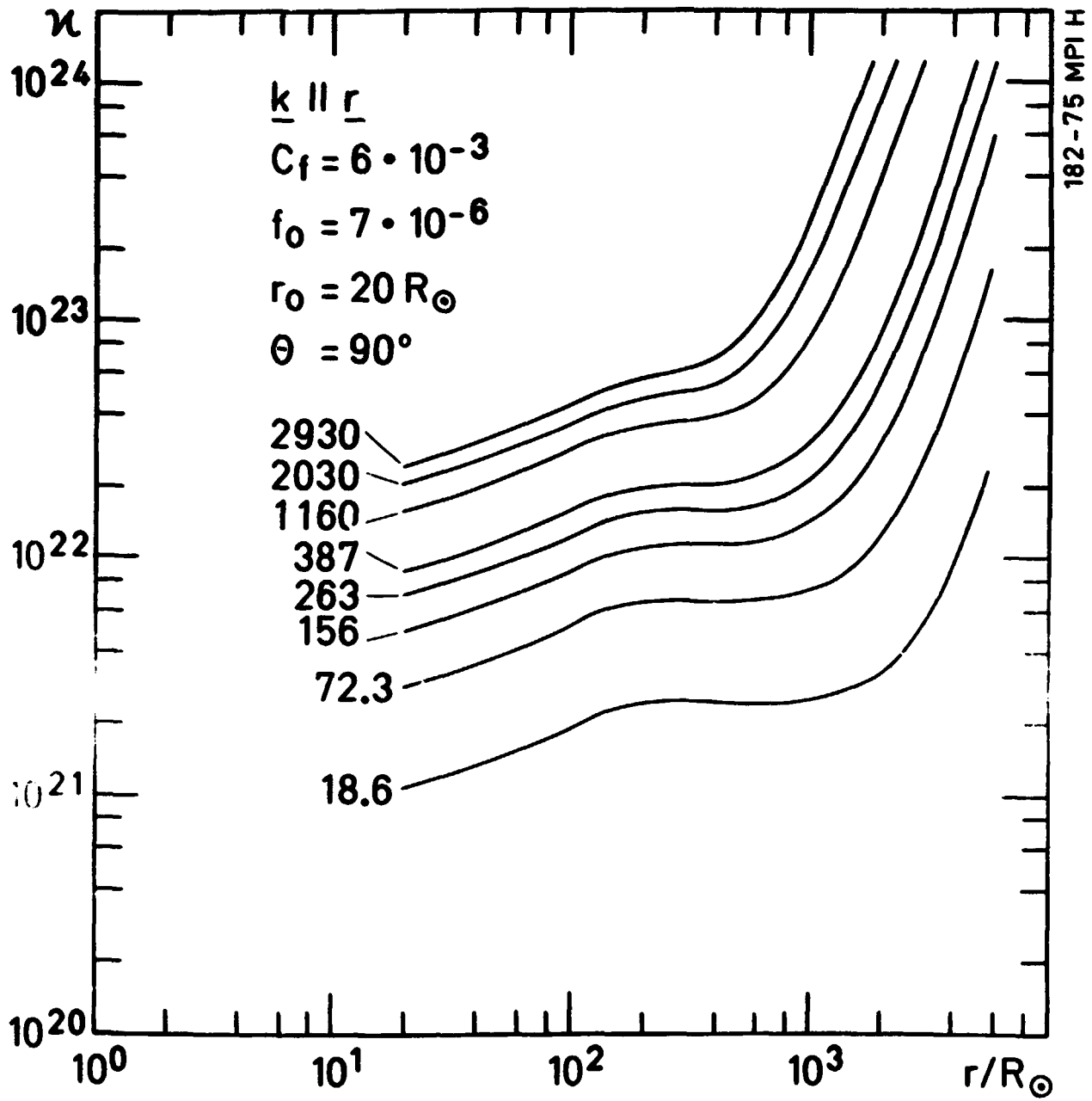
Figure Captions

Figure 1: The radial diffusion coefficient κ at heliographic latitude $\theta = 90^\circ$ as a function of radial distance r in solar radii R_\odot for various proton energies. The power spectrum $P(f) = C_f \cdot f^q$ with the values $C_f = 16 \times 10^{-3} \gamma^2 (\text{Hz})^{-1-q}$, $f_0 = 7 \times 10^{-5} \text{ Hz}$ (Jokipii and Coleman, 1968). Wave normals k are assumed to be radial. The calculation was started at $r_0 = 20 R_\odot$.

Figure 2: The same as Figure 1 with values of C_f and f_0 adapted to the spectra of Bercovitch (1971).



THE QUALITY OF THE
 THIS IS POOR



N 76-24132

Solar Cosmic Ray Measurements at

High Heliocentric Latitudes

Kinsey A. Anderson

**Physics Department and Space Sciences Laboratory
University of California
Berkeley, California 94720**

Introduction

Observation of solar cosmic ray fluxes at high heliocentric latitudes would provide several new dimensions in specifying important physical processes in the solar atmosphere and interplanetary space. Valuable new approaches would be available for such problems as the steady state acceleration in the solar atmosphere, propagation of fast charged particles in the solar coronal magnetic fields and in interplanetary space, the true interplanetary particle spectra free of transient solar influence, and acceleration in interplanetary space by shock waves. For this brief review of what might result from a program of solar cosmic ray observations on "out-of-the-ecliptic" spacecraft the following outline will be used:

- A. The magnetic fields of the Sun at high latitudes
- B. Propagation of fast charged particles in the solar corona and in interplanetary space at high latitudes
- C. Origin of interplanetary particle populations
- D. Other particle phenomena in interplanetary space (e.g., acceleration of shock waves)
- E. Effect of spacecraft mission characteristics on solar cosmic ray studies at high latitudes

A. Solar Coronal Magnetic Fields

It is now well known that the magnetic fields close to the Sun control the intensities of charged particles that appear in interplanetary space. They do so in a variety of ways and to varying degrees. For example, particles from flares near the East limb are detected at central meridian and more westerly longitudes only several hours after the flare (Van Hollenbeke et al., 1975). The measured low cross field diffusivity of the particles in interplanetary space requires that the diffusion occurs in the corona. This is a reasonable requirement since hydromagnetic wave activity should be more intense in the solar corona and the wavelength of such waves can be of the size needed to effectively scatter solar flare particles.

Energetic solar particles stream from the solar corona in high intensities for many days, even weeks, following large solar flares. In general terms, this basic observation means that there is a sequence in which the particles are first accelerated, then stored for some time in the solar corona, then released into interplanetary space. The quantitative behavior of each of these steps is not well known and in fact is at the center of much controversy. For example, the acceleration may be essentially steady state and the storage transient. On the other hand there is the possibility that the acceleration is impulsive and the storage long term. Such a situation requires very low collisional energy losses, something that might be achieved in a "cosmic ray plasma" where all particles are

energetic, approaching a Maxwellian distribution (Anderson, 1972). In either case the magnetic fields of the sun play a major role in each step of the three step sequence. All our experience with these processes has been in the magnetic fields of the solar activity zones. It seems unlikely that the full sequence of acceleration, storage and release takes place in the high latitude coronal fields. However, there are two inversely related questions of basic importance:

1. Do solar particles, accelerated in the activity zones, propagate into the high latitude solar regions?
2. Can we use the solar particles, if they do indeed move into the high latitude regions, as probes of the solar magnetic fields there?

With these two questions as the basic motivation for solar cosmic ray studies at high heliographic latitudes, we next summarize some of the information now available on high latitude solar magnetic fields. Figure 1 is a photograph of the solar corona that shows the polar plumes. This old photograph is of interest because it shows an intermediate corona, the kind expected in the 1983 to 1985 period. The polar plumes have generally been considered to outline the magnetic fields over the Sun's polar cap and their appearance suggests that the field lines in these high latitude regions are open. Notice that the polar plumes appear only above latitudes of 50 to 60°. Because these field lines are so different from the activity zone and transition zone field lines, a strong impetus

is given to going to the highest possible solar latitudes in order to encounter a qualitatively different phenomenology.

Magnetograph observations suggest that the Sun's polar magnetic fields are not uniform bundles of lines. Figure 2 shows measurements by Stenflo (1971) that lead to the following conclusions about the high altitude fields:

1. They are patchy with large regions (channels) of weak (less than 10 Gauss) fields. These channels extend from the poles down to latitudes less than 50° .
2. The strengths in the strong field patches range from 10 to 20 Gauss.

Polarization methods of magnetic field determination (Charvin, 1971) indicate that the polar fields may not consist entirely of open field lines. Figure 3 shows the polar field topology based on the optical technique. On the other hand the Skylab coronagraph shows the polar regions as large coronal holes which are evidently stable at least over the duration of the Skylab mission (Newkirk, 1975). This observation implies that most of the field lines over the poles are open.

B. Solar Cosmic Ray Propagation at High Solar Latitudes

A recent statistical study of solar flare cosmic ray events by Van Hollenbeke et al. (1975) has revealed that:

1. The onset time of 20-80 MeV proton fluxes at Earth systematically decreases with heliolongitude away from a minimum point at $50^\circ \pm 30^\circ$ W of central meridian (Figure 4).

2. The intensity of solar cosmic rays at Earth is strongly dependent on the distance in longitude from the flare site. The preferred connection region is 20° W to 80° W longitude with some of the spread being due to the variable solar wind velocity.
3. Flare sources on the back side can sometimes be identified by very large X-ray and radio emission regions which extend above the limb. Particles from flares located away from the preferred longitude region as much as 150° are sometimes detected at Earth in this way.
4. The energy spectra of the protons from individual flare events located in the preferred connection region (20 to 80° W) are remarkably similar: most of these spectra are fit by power law exponents between -2 and -3.1 (Figure 5).
5. The energy spectra of flare particles measured near Earth changes systematically with distance from the preferred-connection longitude. At 40° E the range of power law exponents is -3.7 to -5.0 (Figure 5).

The authors have eliminated interplanetary diffusion and adiabatic cooling as causes for the above observations. They explain the results in terms of energy dependent diffusion of the flare particles from the flare site through the coronal magnetic fields out to the spiral interplanetary field lines that connect to the observing site. The progressive softening of the flare particle energy spectra is attributed to the more rapid loss

of the higher energy particles onto spiral field lines leaving in the vicinity of the flare site. The lower energy particles are preferentially retained so that as the diffusing particle population ages, its average energy and spectral slope decreases.

Such observations will make it possible to specify certain physical conditions in the coronal regions, especially the particle diffusion coefficient. Experiments at lower energy can determine the total amount of matter traversed by the particles and thus a physical model of the diffusion in the high latitude corona can be built up.

The out-of-the ecliptic missions offer the possibility of doing an analogous experiment in which latitude is the variable, thus complementing the longitude studies. In the latitude case the situation is even more complex but also should be more revealing about the spatial structure and characteristics of the solar coronal magnetic fields. To reach high latitudes, the particles will have had to propagate through the transition zone as well as appreciably into the polar fields. There are bound to be great surprises in such observations too far outside our present experience to anticipate. Nonetheless, Figure 6 attempts to qualitatively indicate what might be the outcome of solar cosmic ray observations at high latitudes.

C. Origin of the Interplanetary Particle Populations

Figure 7 shows the so-called quiet time proton energy spectrum in interplanetary space. At the lowest energy end there are the solar wind

protons. At high energies (greater than 10 GeV) the protons almost certainly belong to a galactic population of particles, and at the very highest energies, the particles may even be intergalactic in distribution. In the range 30 MeV to about 10 GeV the protons are probably galactic but their intensity is strongly modulated by the Sun's magnetized plasma wind, at least near the ecliptic plane. The range from 2 to 100 MeV has recently been studied extensively by the University of Chicago and Goddard Space Flight Center Groups. A detailed study by J. Kinsey (1970) is based on the hypothesis that the protons in the energy interval come from two distinct populations. Figure 8 shows some spectra in this energy region. Those observations may be represented by

$$\frac{dJ}{dE} = F_s E^{-s} + F_g E^g \quad (1)$$

dJ/dE is the number of protons per square centimeter-steradian-second-MeV. F_s , F_g , s and g are parameters that give best fits to the observations. It is found that F_s and s are highly variable while F_g and g vary much less. The interpretation is that the first term on the right hand side of Equation (1) represents a proton component of solar origin while the other term is presumed to be galactic in origin.

No doubt the proton fluxes in this energy range will prove to be quite different when observed at high heliographic latitudes. There detectors presumably would be far removed from the solar source regions and the reduction of intensity in the galactic component by modulation should be much diminished.

Figure 9 shows the energy spectrum of electrons at times of lowest solar flare activity often referred to as the "interplanetary electron spectrum". As in the case of the protons, the highest energy electrons are presumed to fill the galaxy, while the lowest energy electrons are known to be of solar origin -- they are the solar wind electrons. Between these two components the situation is complicated, perhaps even more so than in the case of protons:

1. The solar wind electrons have a non-Maxwellian tail at energies above about 100 eV. This tail appears to extend to 1 or 2 keV. It can be described by a power law of $E^{-5.1}$.
2. The non-Maxwellian becomes submerged in a new particle population which extends to about 1 MeV. This spectrum approximately follows the power law E^{-3} .

There appears to be no spectral flattening of the 2 keV 1 MeV component as there is in the case of the protons.

The study of the complex electron spectrum would be greatly advanced by observations at high solar latitudes. Much will be learned by investigating how the electron spectrum changes relative to the proton spectrum.

Among the questions we can now pose about the interplanetary fluxes are:

1. Will the medium energy component decrease significantly as the detectors move away from the active sunspot zones?

2. From observing such a change systematically with latitude can we learn more about the sources and the transport of the particles through the coronal magnetic fields at high latitudes?
3. Can we identify a component that is generated by instabilities in the solar wind? Possibly the 100 eV to 1 keV non-Maxwellian tail arises in this way. As the solar wind flow changes as a function of latitude does the character of the non-Maxwellian tail change? Possibly even the 2 to 10 keV region originates, at least in part, from internal energy sources of the solar wind by means of plasma microinstabilities.
4. Is there an electron component, for example the 10 to 100 keV region, which is supplied, at least in part, by strong cosmic X-ray sources?

The high latitude electron and proton measurements will be free of planetary source effects: the Earth's bow shock and magnetosphere and Jupiter's magnetosphere. This is another important motivation for out-of-the ecliptic missions.

D. Shock Waves and Other Interplanetary Phenomena

A variety of complex energetic particle phenomena take place in interplanetary space. Although they must involve basic plasma processes they are not yet well understood. The motivation for further study is strong, however, since these processes must occur throughout our galaxy in systems of similar and larger scale sizes.

One such phenomenon is the acceleration of particles by shock waves of solar origin in interplanetary space. Figure 10 illustrates this effect in a particular case. The important observational features in this event are (R. E. McGuire, Ph.D. thesis, University of California, Berkeley, 1976):

1. The shock velocity was $520 \text{ km}/\mu$ and the shock normal was close to the Sun-Earth line.
2. Preceding the shock passage the electron and proton flux increased by a factor of 10 due evidently to a flare.
3. Twenty minutes before the shock passage the protons above 200 keV increased by a factor of 20. The flux maximum occurred about one gyroradius in front of the shock. A more gradual increase in the medium and high energy electron flux also occurred.
4. Electrons 0.5 to 14 keV increased 20-fold just behind the shock front. This flux increase may be associated with dissipation of energy by the shock.

Although several detailed models for shock acceleration exist, none seem completely satisfactory. By observing shock effects on particles at high solar longitudes where the characteristic of the interplanetary field are presumably much different it should be possible to arrive at a satisfactory shock acceleration model. This is a problem of first order importance to cosmic ray studies since shock acceleration occurs

in many cosmic systems. For example, shock waves probably play an important role in the production of energetic flare particles; shocks may accelerate the entire fast electron component. And it is known that shock waves carry energy into interplanetary space in amounts equal to a large fraction of the total flare energy (Hundhausen and Gentry, 1969). There is still no satisfactory theoretical solution to the problem of magnetic field line merging as an energy source for flare phenomena and it thus becomes vitally important in the study of the flare process to know as much as possible about shock acceleration.

At high solar latitudes the magnetic field will make a smaller angle with respect to the solar wind flow direction, on the average, compared to lower latitudes. Also, one expects that the power spectrum of fluctuations in the interplanetary field to be considerably reduced at high latitudes as compared to the latitude range of the activity zones. These differences can then be used to explain differences in the shock acceleration of particles as a function of heliocentric latitude.

There seem to be several solar-interplanetary phenomena which emerge clearly during part of the solar cycle but then become less apparent or disappear later in the solar cycle. In his presentation at the symposium Dr. Hundhausen (1976) mentioned such an effect in the solar wind. Another example is the abundance of long lived particle streams (recurrence events) early in the solar cycle (McDonald and Desai, 1971). Yet another example is the electron-proton "splitting" effect reported by

Lin and Anderson (1967). This effect occurs in solar co-rotating streams that appear near Earth one or two days following solar flares. The electrons in these streams are displaced to the west of the protons and thus are observed to pass over the detectors before the protons do. This time displacement is a few hours up to 10 hours (a few degrees in longitude). An example of electron-proton splitting is given in Figure 11.

None of the proposed mechanisms has been shown to quantitatively account for this effect, and no explanation has been offered for their apparent disappearance later in the solar cycle. Lin and Anderson (1967) thought that the effect could be due to the larger drift velocities of the protons compared to the electrons (the larger gyroradius of the protons means that the protons sample any gradients in the magnetic field to a greater extent). Jokipii (1969) proposed that the splitting can occur in interplanetary space due to combined gradient and curvature drift in the interplanetary magnetic field.

One expects that these phenomena and perhaps others still unexplained can be effectively studied by an out-of-the ecliptic mission.

E. Jupiter Swing-by Out of the Ecliptic Missions

For a two-spacecraft launch in late 1980 by a Titan-Centaur vehicle as described by the NASA-Ames Research Center group, Figure 12 shows when the spacecraft would reach high solar latitudes with respect to the sunspot cycle. A 1980 launch is probably not ideal for solar

cosmic ray studies since the spacecraft arrive at high latitudes near the expected decline of solar cycle 21. However, it is worth noting that several very large flares occurred in this portion of solar cycle 20 including the very great August, 1972 flares. The spacecraft remains above latitude 35° N and 35° S for somewhat more than 2 years.

Figure 13 shows where the spacecraft are positioned in solar latitude on a Maunder's butterfly diagram. This figure shows that there is some advantage in arriving at these high latitudes late in the solar cycle since the activity zones have retreated toward the equator.

Acknowledgments

This work was supported in part by National Aeronautics and Space Administration grant NGR 05-003-017.

References

- Anderson, K. A., Lifetime of solar flare particles in coronal storage regions, *Solar Phys.*, 27, 442, 1972.
- Charvin, P., Experimental study of the orientation of magnetic fields in the corona, *Solar Magnetic Fields* (ed. R. Howard), D. Reidel, p. 580, 1971.
- Hundhausen, A. J., Proceedings of this Symposium, 1976.
- Hundhausen, A. J. and G. A. Gentry, Numerical simulation of flare generated disturbances in the solar wind, *J. Geophys. Res.*, 74, 2908, 1969.
- Jokipii, J. R., Proceedings of the Cosmic Ray Conference, Budapest, 1969.
- Kinsey, J. H., Ph.D. Thesis, University of Maryland, 1970.
- Lin, R. P. and K. A. Anderson, Electrons > 40 keV and protons > 500 keV of solar origin, *Solar Phys.*, 1, 446, 1967.
- McDonald, F. B. and U. D. Desai, Recurrent solar cosmic ray events and solar M regions, *J. Geophys. Res.*, 76, 808, 1971.
- McGuire, R. E., Ph.D. Thesis, University of California, Berkeley, 1976.
- Newkirk, G., Proceedings of this Symposium, 1976.
- Stenflo, J. O., Observations of the polar magnetic fields, *Solar Magnetic Fields* (ed. R. Howard), D. Reidel, p. 714, 1971.
- Van Hollenbeke, M. A. I., L. S. MaSun and F. B. McDonald, The variation of solar proton energy spectra and size distribution with helio-longitude, *Solar Phys.*, 41, 189, 1975.

Figure Captions

Figure 1. The intermediate solar corona. This photograph was taken following solar maximum and before solar minimum. At this time the polar plumes are clearly visible. Their appearance suggests that the polar zone magnetic field lines do not close in the vicinity of the Sun. (Yerkes Observatory photograph.)

Figure 2. Synoptic charts of the polar magnetic fields $H_{\parallel}/\cos\theta$. Solid lines represent N polarity, dashed lines S polarity. The isogauss levels are 10 and 20 G. The areas covered by the observations are enclosed by curves with shadings on the outside. (a) North pole. Observations from August 1-23 1968. (b) South pole. Observations from July 31-August 23, 1968. (From J. O. Stenflo, Observations of the polar magnetic fields, in Solar Magnetic Fields (ed. R. Howard), D. Reidel Publ. IAU Symposium No. 43).

Figure 3. Schematic map of the polar coronal magnetic fields (July 26, 1970). The prominences and filaments observed on spectroheliograms are shown on the map. (From P. Charvin, Experimental study of the orientation of magnetic fields in the corona, in Solar Magnetic Fields (ed. R. Howard), D. Reidel, I. A. U. Symp. No. 43).

Figure 4. The difference ΔT_m of the time between onset of 20-80 MeV proton and maximum particle intensity is plotted as a function of the heliolongitude. The solid line is a least square fit through the data. It shows a minimum at $\sim 50^\circ \pm 30^\circ$ W of the central meridian.

Figure 5. Variation of the spectral index γ_p in the 20-80 MeV range as a function of the heliolongitude λ_{\odot} . The open circles are 'long rise time events' with a rise time longer than 24 hours. For these events, effects of interplanetary propagation may be significant. The dashed contour lines enclose 92% of all the other events. The solid line is a least square fit obtained for them. $\gamma_p(\lambda_{\odot})$ can be represented approximately by $\gamma_p(\lambda_{\odot}) = 2.7 [1 + \Delta\lambda/2]$.

Figure 6. This figure idealizes how solar flare particle fluxes might depend on latitude for various coronal magnetic field configurations which vary with heliographic latitude.

Figure 7. The interplanetary quiet time proton spectrum is made up of several components: at the lowest energy the solar wind protons and at the highest energies, the galactic cosmic rays. In between is a spectrum which probably has solar origin.

Figure 8. This figure shows the region of presumed overlap between interplanetary protons of galactic and of solar origin.

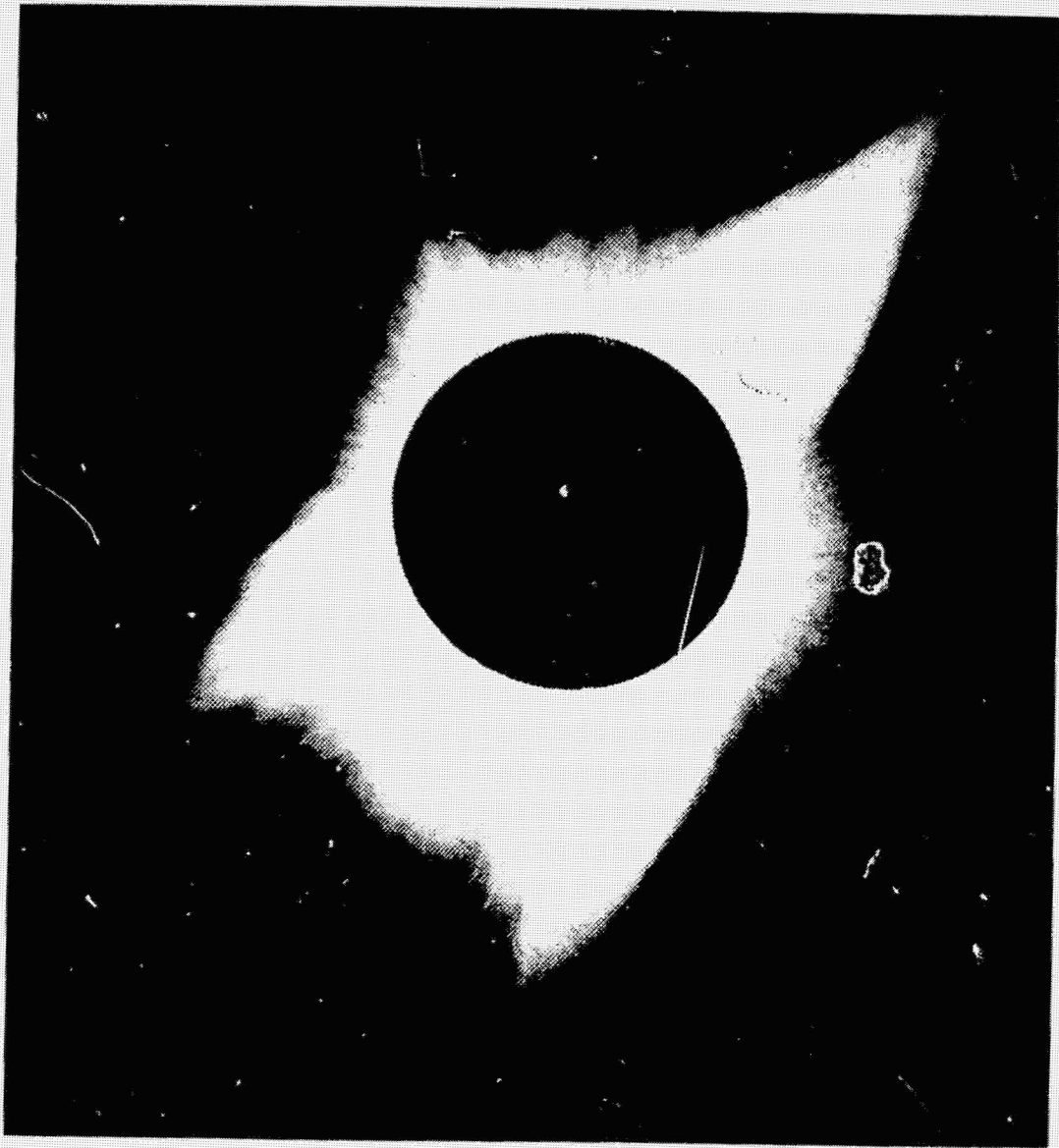
Figure 9. The interplanetary quiet time electron spectrum is also made up of several components: the solar wind electrons at the lowest energies and the galactic component at the highest. Several components appear to exist at intermediate energy. Little is known about their origin.

Figure 10. An interplanetary shock (speed 540 km/sec at 1 AU) that produced large effects on particles. Protons in the 0.3 to 0.5 MeV range are swept up or accelerated by the shock. A blanket of hot electrons appears just behind the shock possibly the result of energy dissipation by the shock.

Figure 11. This figure shows an example of electron-proton splitting early in solar cycle 20. The particles arrive at Earth in a co-rotating stream but the electrons are displaced toward the West by a few degrees. The origin of this effect is not known and it appears to become less frequent later in the solar cycle.

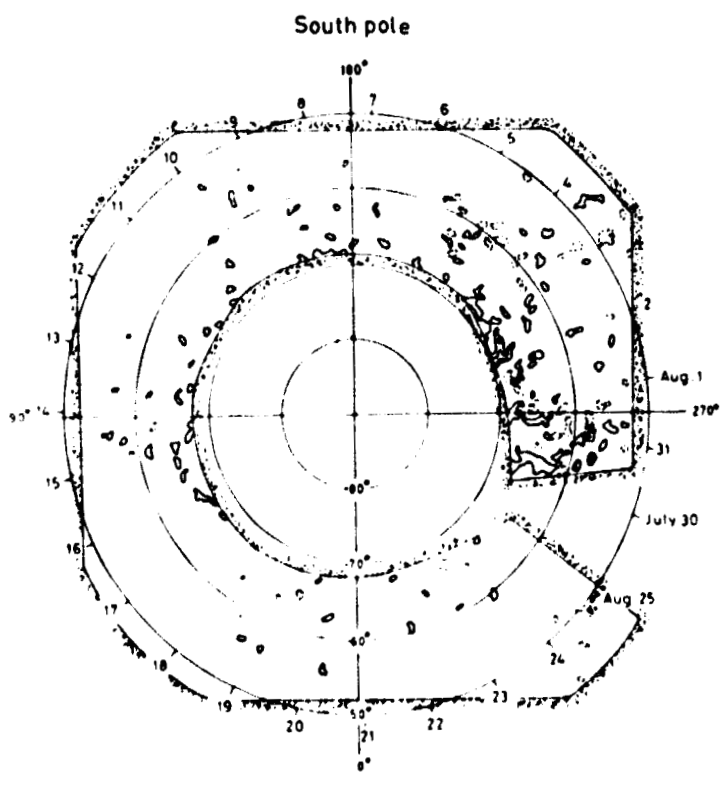
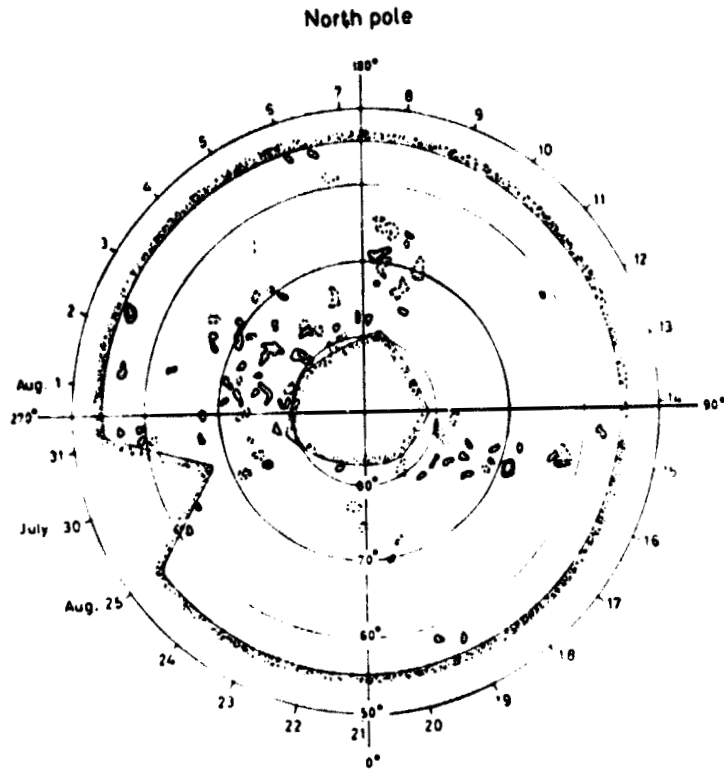
Figure 12. This figure shows that for certain Jupiter swing-by out-of-the-ecliptic missions launched in late 1980, the spacecraft will arrive at high ($> 35^\circ$) latitudes in late 1983 and remain there for somewhat over two years.

Figure 13. For the same missions the spacecraft is seen to rapidly rise past the sunspot zones which, late in the solar cycle, have moved close to the equator.



OP 111
ES FOUR

Figure 1



REPRODUCIBILITY OF THE
ORIGINAL PAGE IS POOR

Figure 2

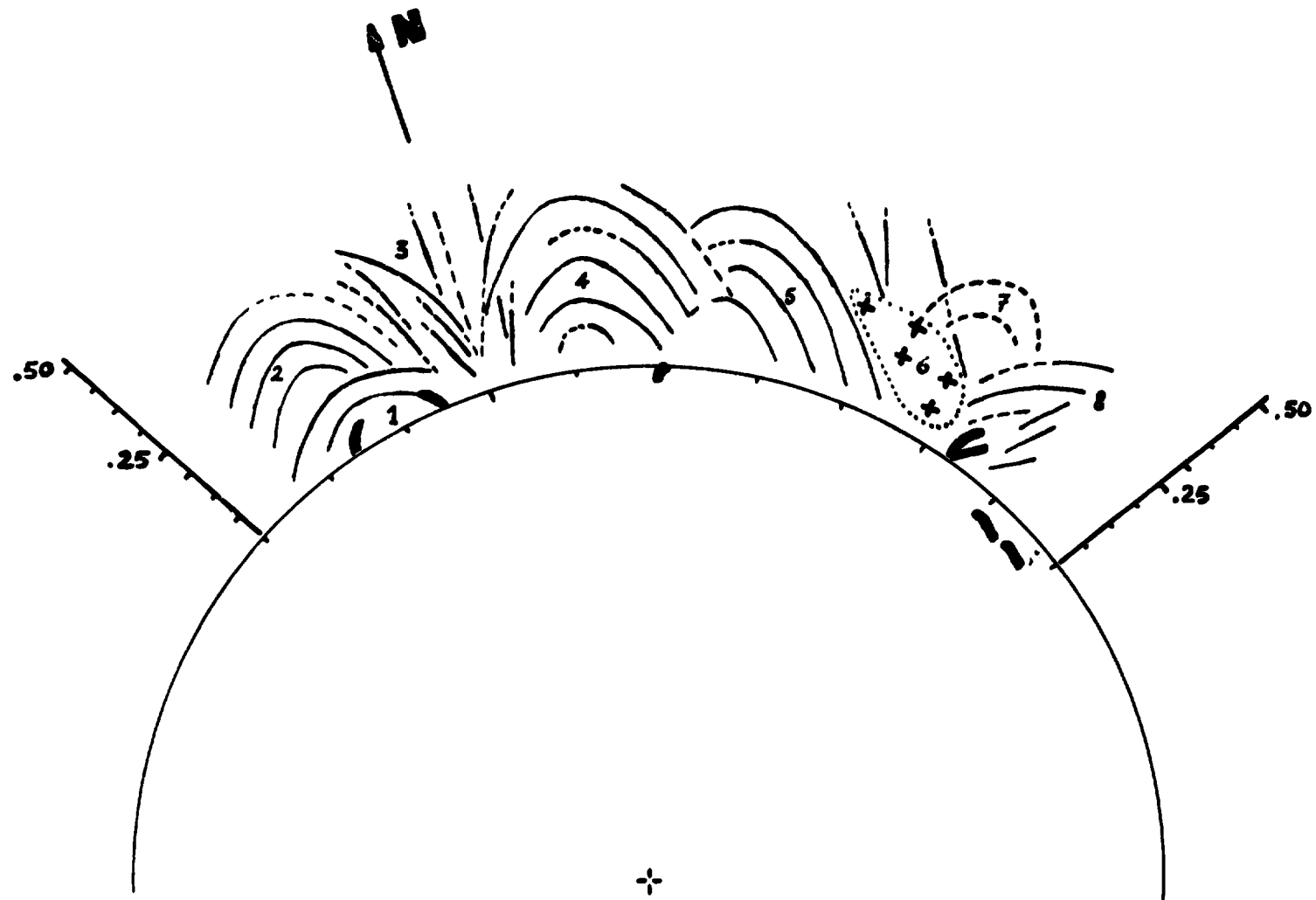


Figure 3

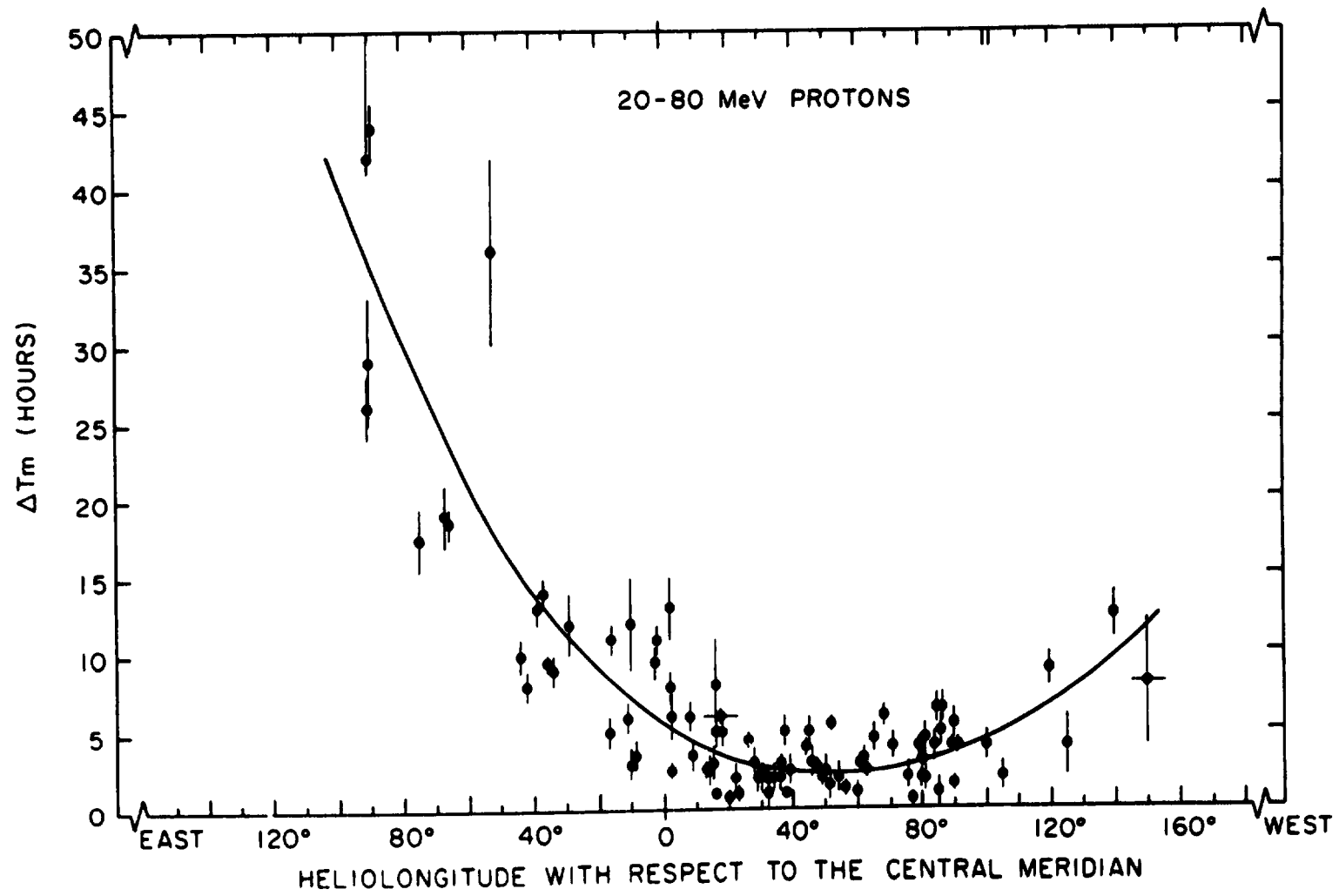


Figure 4

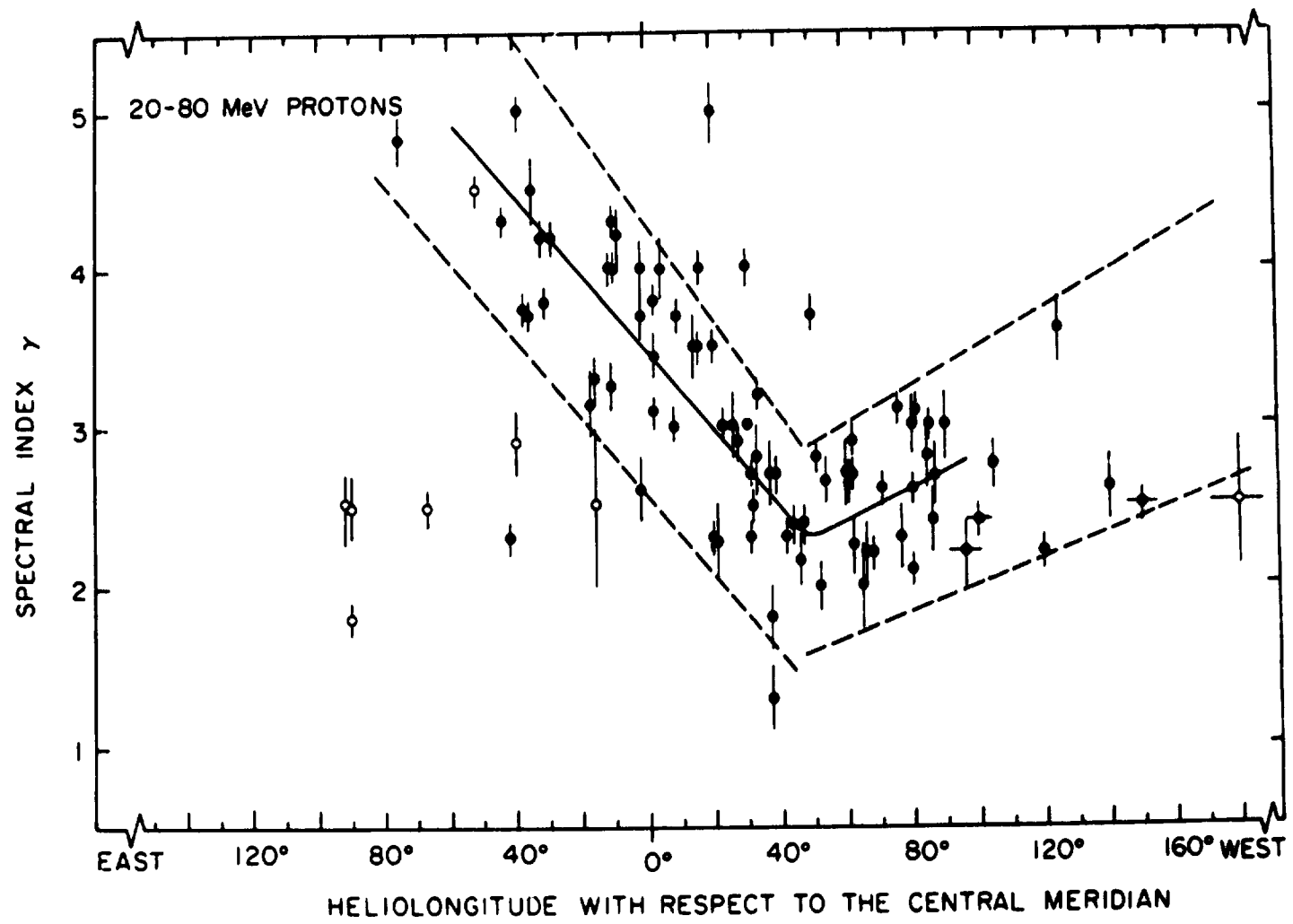


Figure 5

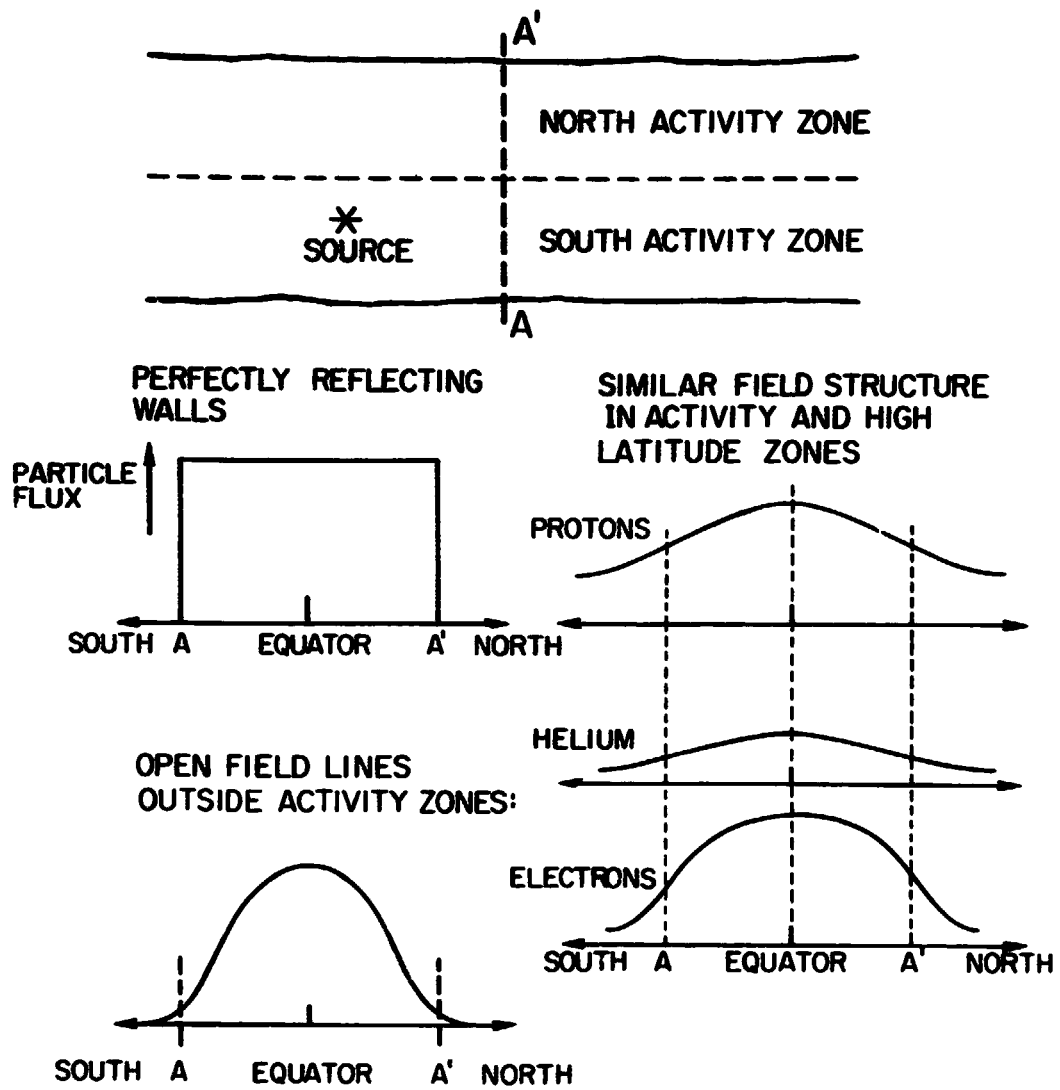


Figure 6

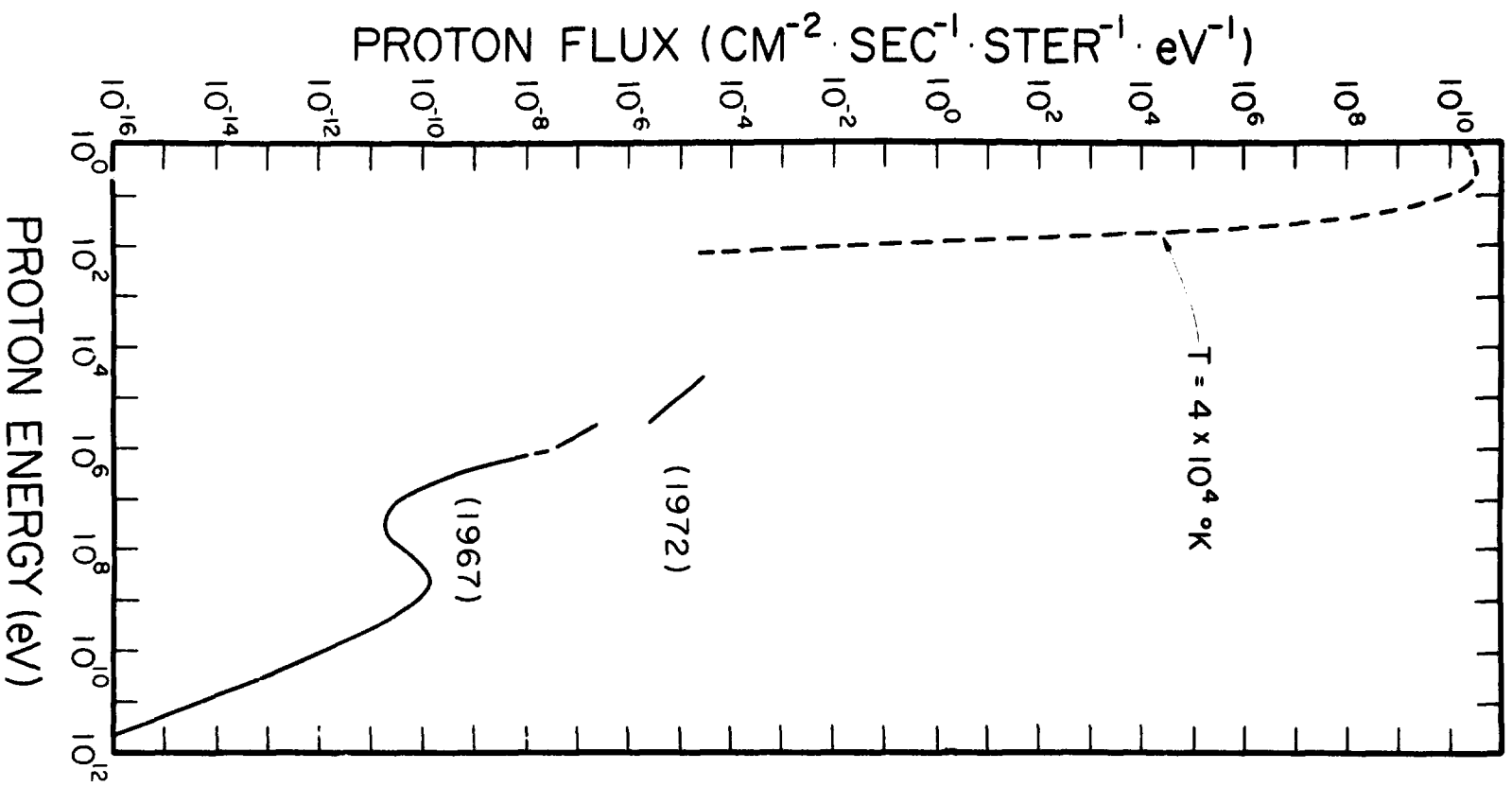


Figure 7

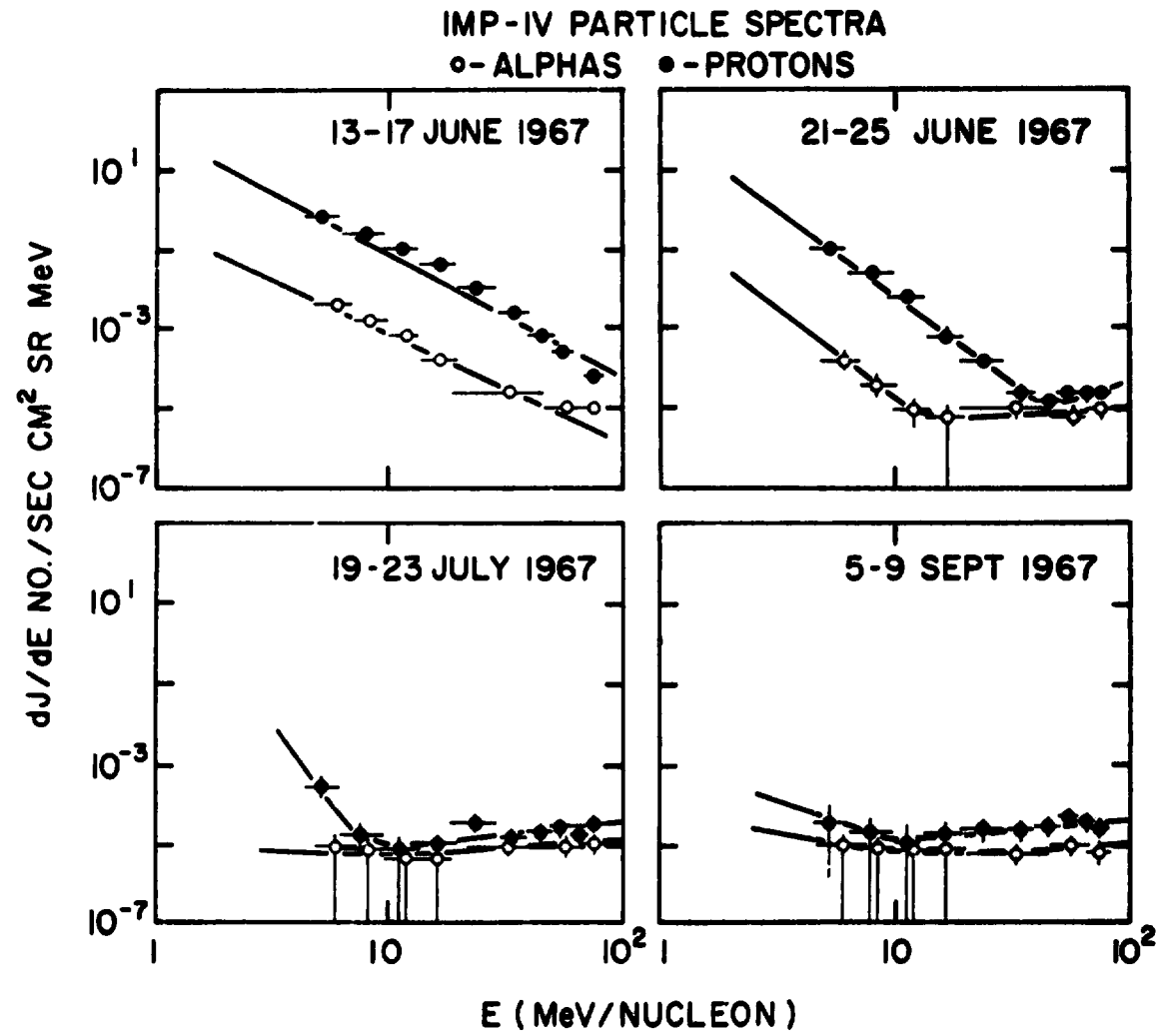


Figure 8

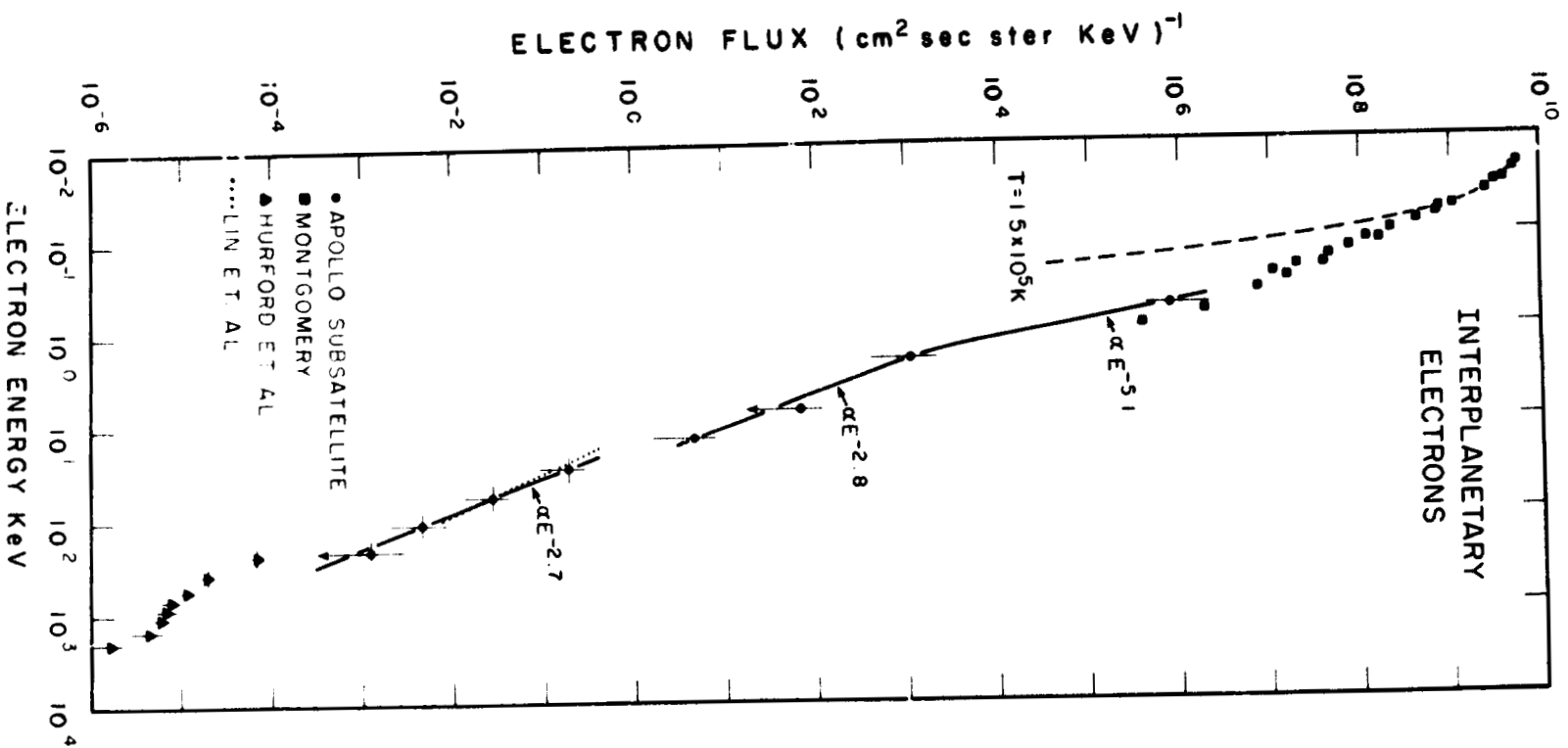


Figure 9

REPRODUCIBILITY OF THE
ORIGINAL PAGE IS POOR

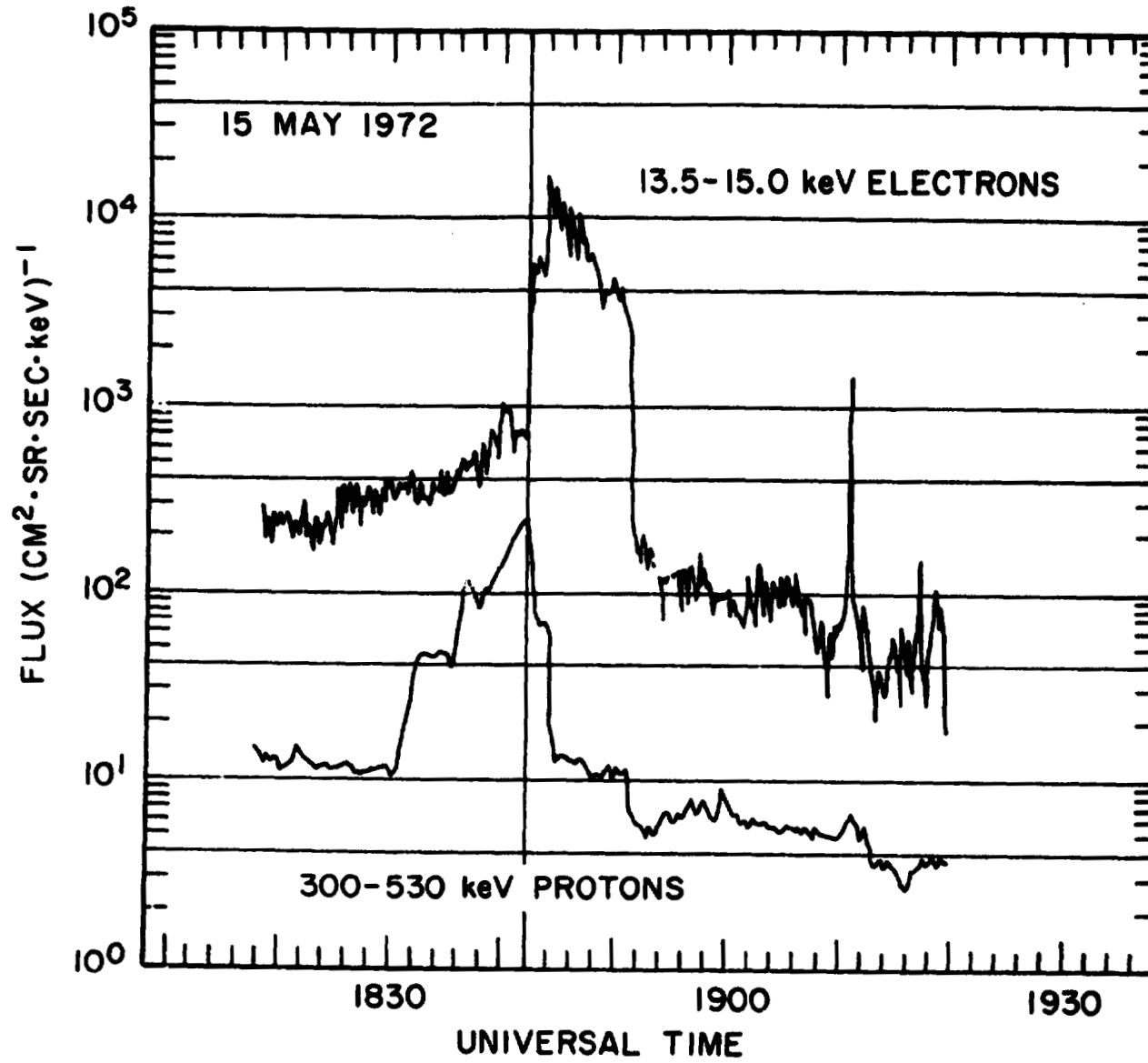


Figure 10

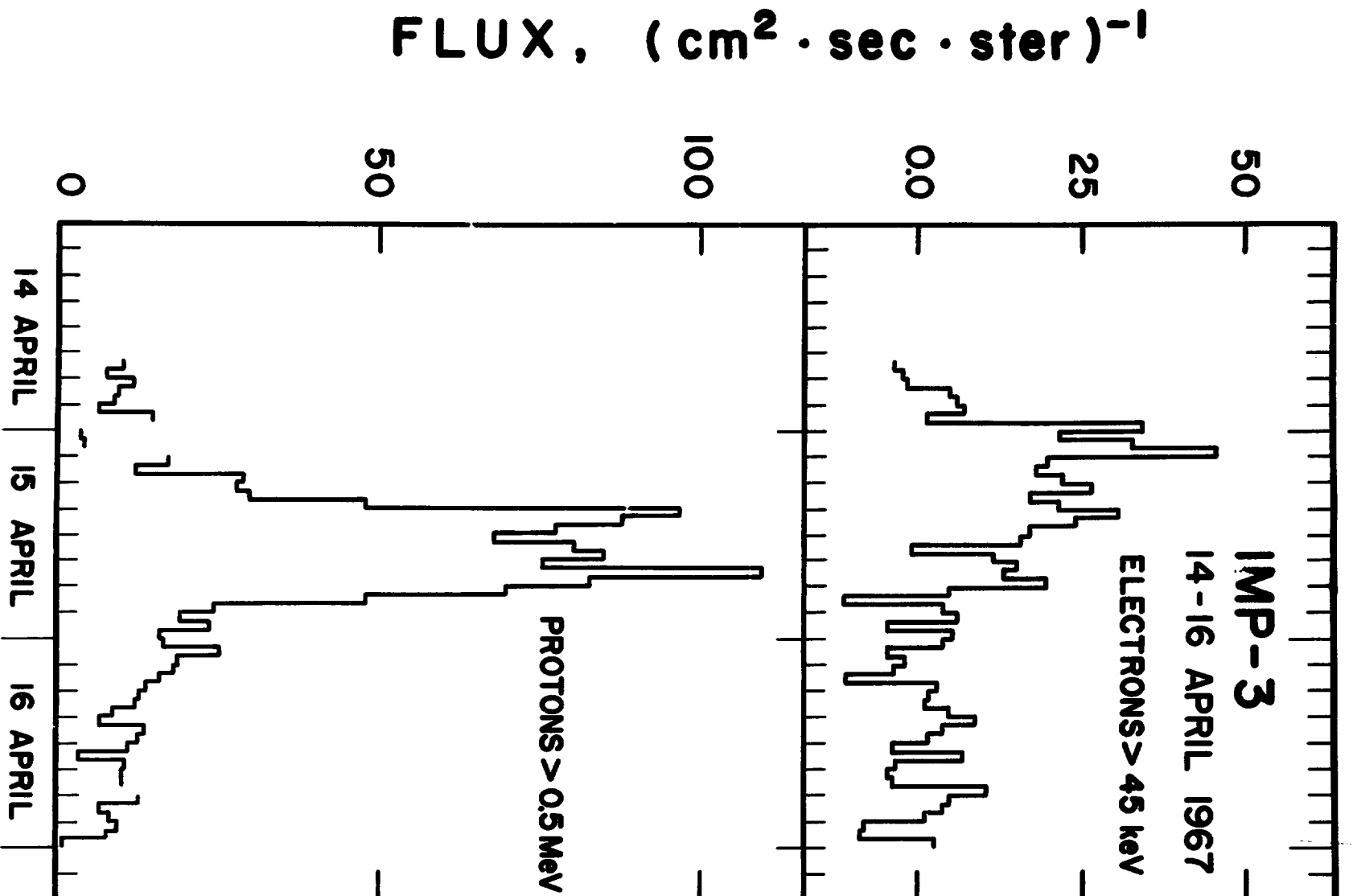


Figure 11

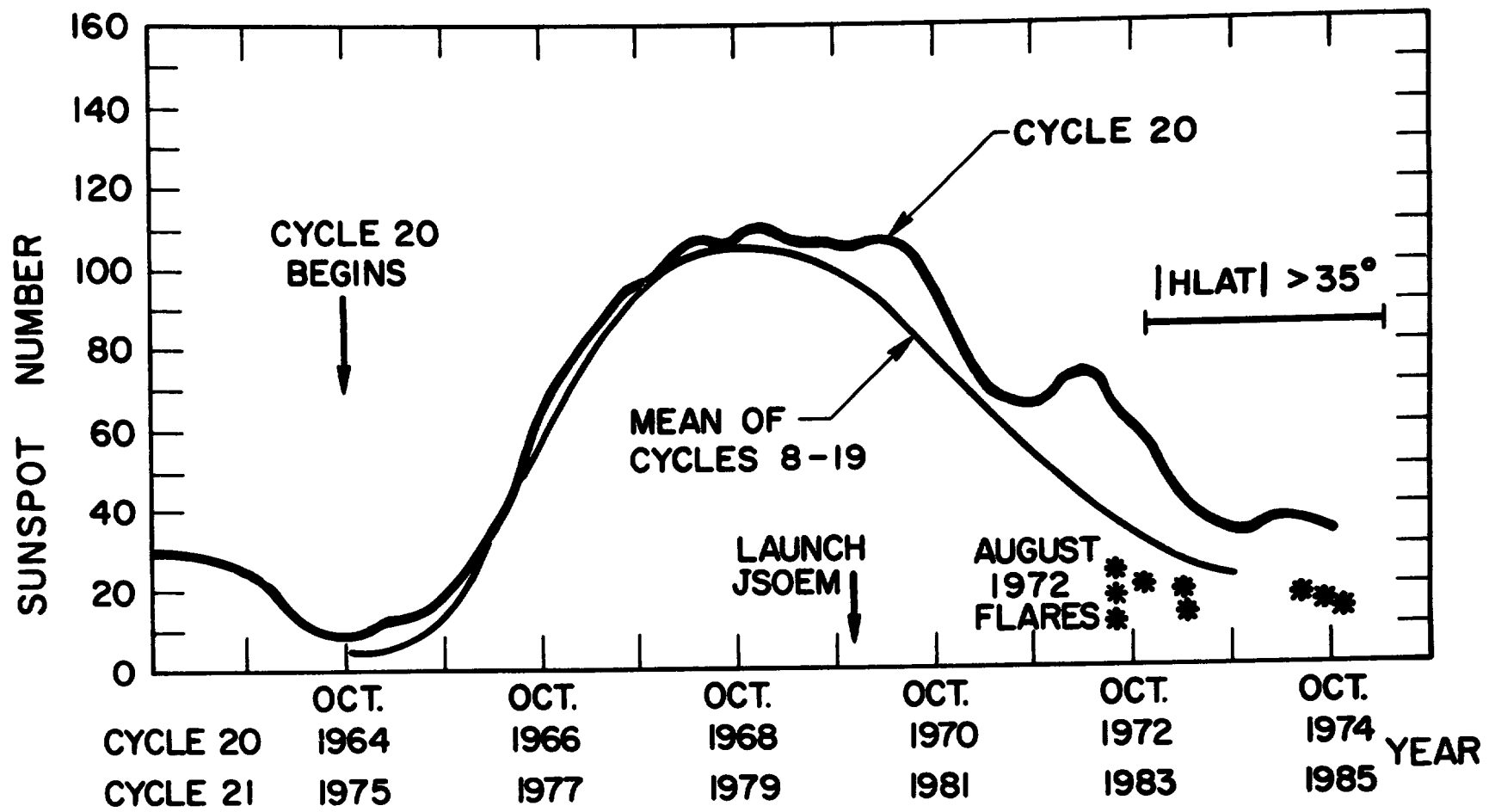


Figure 12

10
10
10

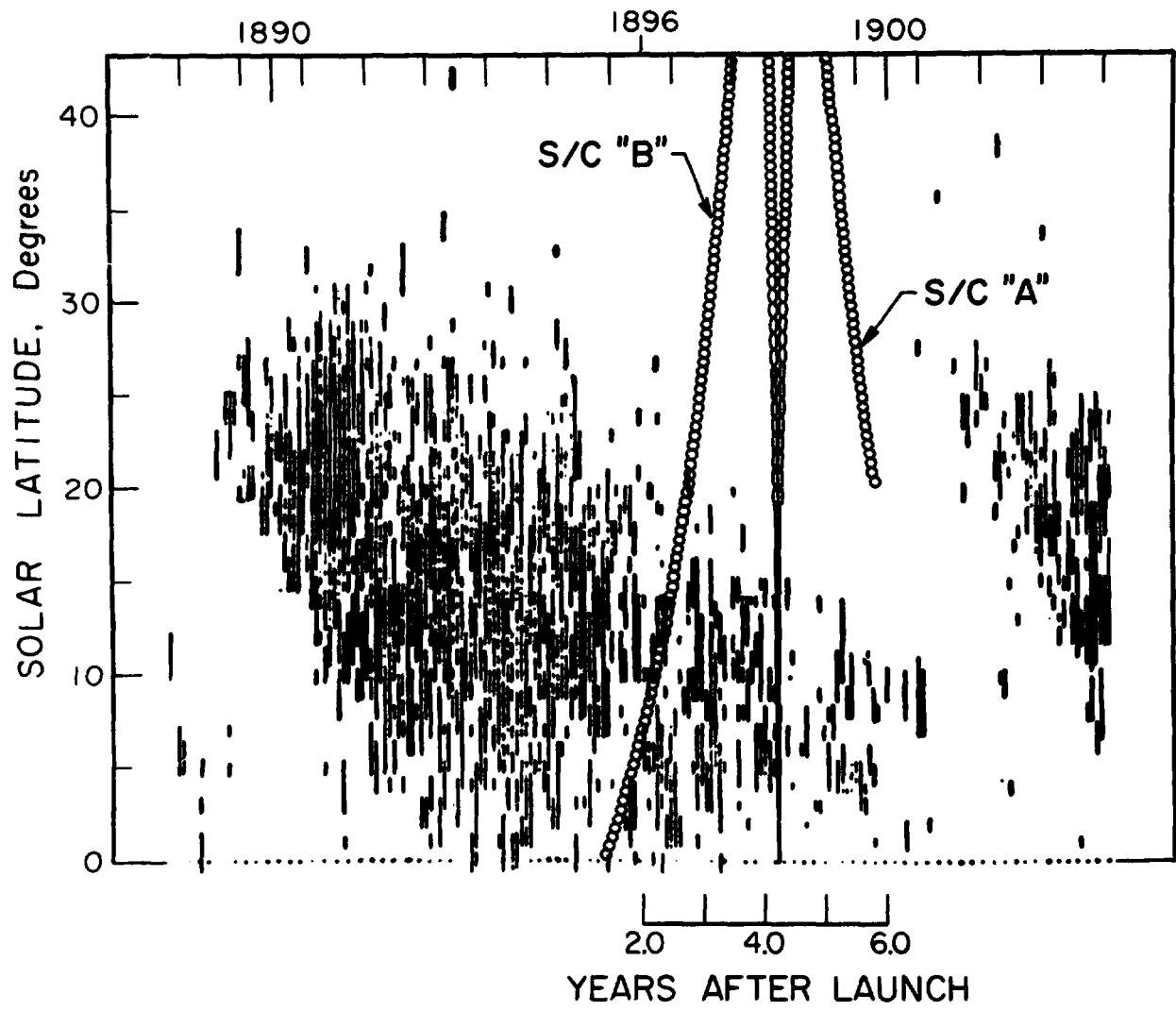


Figure 13

CORONAL PROPAGATION: VARIATIONS WITH SOLAR LONGITUDE
AND LATITUDE*

N76-24133

G. Wibberenz

Institut für Reine und Angewandte Kernphysik der
Christian-Albrechts-Universität Kiel, 23, Kiel, FRG

Abstract:

Observational results on the East-West effect are summarized and discussed in the context of existing models of coronal propagation. The variation of the number of events with solar longitude is surprisingly similar for particles covering a large interval of rigidities. Over large longitudinal distances, time delays to the event onset and maximum intensity are independent of energy and velocity. This has important implications and will require probably a transport process which is determined by fundamental properties of solar magnetic fields, e.g. reconnection processes between open and closed field configurations.

A fit of Reid's model for diffusive propagation in the corona to the observed delay times gives a (two-dimensional) diffusion coefficient κ , corresponding to $r_c^2/\kappa \approx 100$ hours (r_c = distance of the thin diffusing shell from the center of the Sun). Limitations of the diffusion model are given by the existence of a fast propagation region which may extend up to $40...50^\circ$ from the flare site, by the possible existence of an energy independent drift process, and by the influence of solar sector boundaries. The relative role of open and closed field configurations is extensively discussed. Some evidence is presented that the acceleration of protons to higher (> 10 MeV) energies is related with a shock wave traveling in the solar atmosphere.

The importance of measurements performed from spacecraft out of the ecliptic plane is stressed, in particular with respect to the fundamental problems of particle acceleration in the flare process and for understanding fundamental dynamical properties of large-scale solar magnetic fields.

*Extended version of a talk presented at the "Symposium on the Study of the Sun and Interplanetary Medium in Three Dimensions", Goddard Space Flight Center, USA, May 15/16, 1975.

1. Introduction

The story of coronal propagation begins with the East-West-effect for solar cosmic ray events: with increasing longitude of the parent flare on the Eastern hemisphere of the Sun the number of events detected at the earth decreases considerably, and, for those events which are detected, the delay between the flare and the arrival of particles at the earth increases (see Burlaga, 1967, for a summary of some earlier results). The reason for the East-West-effect is obviously the asymmetric nature of the interplanetary magnetic field with respect to the central meridian on the Sun. For average solar wind conditions, a bundle of interplanetary magnetic field (imf) lines observed near the earth connects back to a point on the Sun which is close to 60° W. However, the controlling nature of the regions close to the Sun for the azimuthal propagation of energetic particles became only clear, when it was established that the propagation of energetic particles in space occurs preferentially along the imf. The arguments for negligible particle motion perpendicular to the imf have meanwhile been summarized by various authors. In addition to the arguments presented e.g. by Roelof (1974) we wish to point out that the variation of delay times with solar longitude is independent of energy, which is another strong argument against interplanetary perpendicular diffusion (Reinhard and Wibberenz, 1974, Ma Sung et al., 1975).

These effects of "coronal propagation" which depend on the relative azimuthal distance between a parent flare on the Sun and the point in space where the energetic solar particles are observed, could be studied so far only as a function of solar longitude. It is the purpose of this paper, (i) to summarize the observational results and to order them with respect to existing models, (ii) to point out which fundamentally new results we should expect by studying variations with solar latitude, i.e. by using observations in space out of the ecliptic plane.

We shall start in section 2 to summarize the methods, by which various transport processes can be separated. In section 3 we discuss the statistical methods, where the variation of characteristic parameters of solar events with solar longitude is studied for a large number of events. Different models have been developed to describe the average longitudinal variations. An independent method described in section 4 consists in detailed studies of individual events, including multi-spacecraft observations at different heliocentric longitudes, simultaneous intensity and anisotropy measurements, and the relation to observations of solar surface structures. Some indications to the acceleration process itself are treated briefly in section 5. Finally we summarize the open questions in section 6 and try to relate them to studies of solar particle events off the ecliptic plane.

2. Separation of various transport processes

In the sequence of events between the first acceleration of particles on the Sun and their final observation in space, we can ask different questions: How is the solar atmosphere filled up with energetic particles following the original acceleration process? How do the particles escape into space? How can the interplanetary propagation be separated from the solar transport processes? Let us start with some terminology related to the different steps.

(a) The acceleration process is visualized in many models as a pulse-like process limited in spatial extent to the flare area itself, approximated by a delta-function in space and time. In principle, the acceleration could also occur over an extended area in the solar atmosphere for long periods of time (see below).

(b) The accelerated particles spend a certain time in the vicinity of the Sun. We wish to make a distinction between propagation when they move away from the acceleration region and finally occupy a large area on the Sun, and storage when the particles remain confined to a certain region. The difference is depicted schematically in Figure 1. In reality, we may have a mixture of both processes.

(c) The number of solar particles observed in space is determined by the probability per unit time that a particle will leave the solar atmosphere by finally reaching an open field line leading out into space (Reid, 1964; Newkirk, 1973). This release mechanism has a very important influence on the azimuthal distribution of particles, because it also determines how many particles are left for further propagation along the solar surface.

(d) Sufficiently far away from the solar surface we only find open field lines which lead out into the interplanetary medium. Along this "source surface" (Newkirk, 1973) the processes (a) to (c) define an injection function $K(\varphi, \theta, t)$. Measurements on a single spacecraft connect back to a certain solar longitude φ close to the solar equator ($\theta \approx 0$), and for a given solar wind velocity the connection longitude $\varphi(t)$ as a function of time may be determined (see e.g. Nolte and Roelof, 1973).

A single satellite therefore "sees" an injection profile $I(t) = N(\phi(t), 0, t)$. Roelof and Krimigis (1973) have described an effective method to separate real longitudinal changes $\partial N/\partial\phi$ from changes in the injection function $\partial N/\partial t$. Since $dI/dt = (\partial N/\partial\phi)d\phi/dt + \partial N/\partial t$, the relative contribution of the two terms to the observed dI/dt depends on the motion $d\phi/dt$ of the connection longitude. For a negative gradient in the solar wind velocity V_w , a solar wind "dwell", $d\phi/dt$ is very small, so that $dI/dt \approx \partial N/\partial t$. For a positive gradient in V_w , $d\phi/dt$ is large, the second term can be neglected, and one may directly construct the coronal distribution $N(\phi)$. A more direct method for determining $N(\phi)$ is of course the use of multi-spacecraft observations (McCracken et al., 1971; Bukata et al, 1972), in particular if combined with actual solar wind measurements for determination of the connection longitude $\phi(t)$. Results of this method are summarized by Roelof (1974).

(e) It is clear that any attempt to determine the (coronal) injection profile $I(t)$ or the related longitudinal distribution $N(\phi)$ has to start from observations in space, and, therefore, one first has to separate the effects of interplanetary propagation. Methods available to perform this separation are

- (1) statistical studies in which the properties of solar particle events (maximum particle flux, times of onset and of maximum flux, shape of energy spectrum etc.) are ordered with respect to the longitude of the parent flare;
- (2) multi-spacecraft observations, by which longitudinal and temporal changes can be separated;
- (3) simultaneous intensity and anisotropy measurements, which allow to separate long-lasting solar injection processes from long-lasting interplanetary storage;
- (4) the "mapping" of observed interplanetary particle fluxes to the high coronal source longitude, by using the simultaneously measured solar wind velocity.

use

We shall start with a summary of results obtained by method (1), since it makes use of the largest amount of observational data and gives insight into the average behaviour. Methods (2) to (4) can then be used to check predictions of models which have been developed and to provide additional insight into the relation with certain features observed on the solar surface.

3. Statistical studies of longitudinal effects

Let us first discuss how the total number of observed events varies with solar longitude. Figure 2 shows the longitudinal distribution of solar particle events for four different sets of observations. The dashed line is for non-relativistic electrons (after Lin, 1974), the dotted line for relativistic electrons (after Simnett, 1974a) plotted for longitudinal bins of 10° or 30° , respectively. The full line is the original curve of Van Hollebeke et al. (1975) for 20-80 MeV protons, and the hatched area indicates results for ground level neutron monitor data (GLEs), as taken from Pomerantz and Duggal (1974).

All four curves show the largest number of events observed when the parent flare is on the western hemisphere of the Sun, with a broad maximum somewhere between 30 and 90°W . The number of events clearly decreases as one goes to the Eastern hemisphere and beyond the West limb. Note that because of the difficulties of flare identification no electron data have been plotted beyond 90°W .

The overall similarity of the curves is rather surprising; only for the non-relativistic electrons the decrease in the number of events seems to start for a more westerly longitude. The similarity in the other three curves suggests a common propagation characteristics for the different particle species, which cover a range of Larmor radii of at least three orders of magnitude. Apart from the clear decrease of the distributions of Figure 2 east of about $W30$ solar longitude, the functional shape of the curves cannot be determined precisely. From a different set of data, Smart et al. (1975) have fitted a Gaussian distribution to the longitudinal distribution of 154 flares on the visible hemisphere of the Sun, which have produced proton events. They find the highest frequency of flares grouped between $W30$ and $W40$, and a standard deviation

REPRODUCIBILITY OF THE
ORIGINAL PAGE IS POOR

of the Gaussian of 55° . A Gaussian curve with these parameters supplies a rather good fit also to the three similar curves in Figure 2. From this fit, one can now extrapolate to the invisible hemisphere of the Sun, with the result, that roughly 20 % of all events should not be associated with a flare on the visible hemisphere of the Sun (for details see Smart et al., 1975). A similar result has been found by Van Hollebeke et al. (1975).

As we shall see below the decrease in the number of events is mainly determined by the escape rate of particles from the Sun, so that distributions of the type shown in Figure 2 can be used to determine the escape rate. We note then that the similarity in the distribution function for different particle species suggests escape rates which do not depend strongly on particle type and energy. Let us turn now to the variation of characteristic times of solar events with longitude. If the parent flare of a solar particle event is located on the Eastern hemisphere of the Sun, the arrival of energetic particles becomes more and more delayed with increasing solar longitude (Durlaga, 1967; Englade, 1971; Dattlowe, 1971; Barouch et Simnett, 1972; McKibben, 1972; Lanzerotti, 1973; Reinhard et al., 1971 and Wibberenz, 1974; Ma Sung et al., 1975).

As discussed above, azimuthal propagation of particles in the interplanetary medium cannot account for the observations. The first quantitative model for particle propagation in a surface layer around the Sun was developed by Reid (1964) and extended by Axford (1965). In Reid's model, the injection function can be written as

$$H(\chi, t) \sim \frac{1}{t \cdot \tau_L} \exp \left\{ - \frac{\chi^2 \cdot r_c^2}{4 K_c t} - \frac{t}{\tau_L} \right\} \quad (1)$$

Here τ_L is the loss time which describes the escape of particles into interplanetary space, K_c is the coronal diffusion coefficient, and r_c the distance of the diffusing layer from the center of the Sun. So $r_c^2 / K_c = \tau_c$ is a characteristic time it takes the particles to diffuse by an angular distance

of $\sqrt{2}$ rad = 81° from the flare origin. In what follows, we put the flare origin at $\chi = 0$ and measure the angular distance χ from the flare to the root of a bundle of field lines leading out into space where an observer is located at longitude ϕ_R and latitude $\theta_R \approx 0$. Note that flares occur off the solar equator, say at longitude ϕ_F and latitude θ_F , so that $\chi^2 = \theta_F^2 + (\phi_F - \phi_R)^2$. On the average $\theta_R \approx 20^\circ$; in what follows, we shall disregard the dependence on solar latitude and put $\chi = \phi_F - \phi_R$. Observationally it is not possible to find systematic differences over a 20° angular interval.

Both τ_L and τ_C are assumed independent of χ , but may vary with particle energy. Reid (1964) originally obtained an estimate of $\tau_C = 3.4$ hours and $\tau_L \geq 1.2$ hr. Applying Axford's (1965) version of the coronal diffusion model, Kirsch and Münch (1974) obtain values for the coronal diffusion coefficient of the same order of magnitude for the event of Nov 2, 1969. Lanzerotti (1973) used the Reid model to describe the variation of onset times for 0.6 to 25 MeV protons with longitude. He estimated $7 \text{ hr} \leq \tau_C \leq 16 \text{ hr}$. These values are probably underestimated because τ_C refers to the bulk of particles to diffuse and not to the "first" particles which define the event onset. It is remarkable that τ_C shows almost no energy dependence. This energy independence of the coronal transport times over large longitudinal distances is meanwhile firmly established (McKibben, 1972; Reinhard and Wibberenz, 1974; Ma Sung et al., 1975).

The most careful study so far in applying the Reid/Axford model to the East-West effect has been performed by Ng and Gleeson (1975). They have replaced the plane approximation by diffusion in a real spherical shell, and the coronal injection profile is then used as the boundary condition for interplanetary propagation, taking into account anisotropic diffusion along the spiral shaped IMF, convection, adiabatic deceleration, and corotation of the flux tubes past the observer. With their two stage propagation model they reproduce many features of solar events. They have used in particular the results by McKibben (1972) on the variation of the time-to-maximum with longitude.

Their best estimates of the coronal parameters are $50 \leq \tau_c \leq 100$ hr and $10 \leq \tau_L \leq 15$ hr. For the interplanetary propagation they obtain a value of the (radial) mean free path, which corresponds to 0.03 AU for 10 MeV protons. This value is probably too small (see Wibberenz, 1974), since in many cases even for Western hemisphere events part of the delay is due to coronal, and not to interplanetary propagation (Reinhard and Wibberenz, 1974). But for the discussion of the East-West effect this difference is not critical.

In Figure 3 we compare the computations of Ng and Gleeson (1975) with t_m -values for > 10 MeV protons (Reinhard and Wibberenz, 1974). For both curves (a) and (c) there is a well defined minimum close to W60, and a systematic increase on both sides of this ideal connection longitude. The apparent linear relation between t_m and λ results from the escape term, which largely influences the coronal injection profile (1) for $t \gtrsim \tau_L$. The minimum value of t_m is related to the interplanetary propagation and could be shifted downward by a factor of 2 or more, without changing the general conclusions. We can see now the limitations of the (modified) Reid model. For curve (a), a small value for the coronal diffusion time has been taken, $\tau_c \approx 13$ hours. This gives the desired flat longitudinal dependence for western events, but does not explain the large values of t_m for eastern events. In model (c), the larger value for the coronal diffusion time, $\tau_c = 100$ hr, gives the larger increase of t_m on the eastern hemisphere, but this increase now starts right away at W60 and is in strong disagreement with the bulk of data between 0 and W90.

It had already been pointed out by Reinhard and Wibberenz (1974) that observational evidence speaks against a well defined minimum in the propagation times somewhere between W40 and W60, and that very fast propagation with small or negligible coronal propagation times can be found for events where the parent flares are located between about 0 and W100. The horizontal lines in Figure 3 are meant to indicate the existence of a "fast propagation region" (FPR) where minimal propagation times can be found. The extent of this FPR may vary from one

event to the other. The existence of a very efficient solar propagation for certain longitude ranges had also been pointed out by Fan et al. (1968). The "open cone of propagation" for > 40 keV electrons found by Anderson and Lin (1966) and Lin (1970), which also has an extent of about 100° , may be identical with the FPR. A "region of preferred connection longitudes" ranging from about W20 to W80 is defined by the work of Van Hollebeke et al. (1975). It may indeed be more appropriate to talk about a preferred connection to the acceleration region than about a fast propagation from it. We shall return to this point in section 5.

Let us return to the slow coronal propagation outside the FPR. One will obviously get a better fit to the data (see Figure 3) if e.g. curve (c) describing the coronal propagation does not start around W60, but with the same slope on both sides of the FPR. Clues to the possible nature of this slow coronal propagation may be found by a study of the dependence of t_m on particle parameters. Reinhard and Wibberenz (1974) have studied time histories for 58 events in the energy range 10-60 MeV and found that the most probable travel distance vt_m is a linear relation of velocity, or with other words, t_m can be written as $t_m = c_1 + c_2/v$. The velocity dependent term in t_m is found to be independent of solar longitude and describes interplanetary propagation. On the average, $c_2 \approx 4.5$ AU (with variations between about 2 and 10 AU). On the other hand, c_1 increases steadily with solar longitude East of central meridian and is independent of proton energy.

These results have been confirmed by Ka Sung et al. (1975) and extended to higher velocities (near-relativistic electrons) and to the inclusion of the event onset times t_{on} . They show that for the onset times a similar relation holds, namely $t_{on} = B_{on} + A_{on}/v$, with two additional constants A_{on} and B_{on} , which have to be determined for each event in addition to c_1 ($\equiv B_{max}$) and c_2 ($\equiv A_{max}$). A_{on} and A_{max} do not vary systematically with solar longitude, so that they can be taken to describe interplanetary propagation. The numerical values ($\langle A_{on} \rangle = 2$ AU, $\langle A_{max} \rangle = 4$ AU) confirm that interplanetary

propagation plays a relatively minor role up to the time of maximum particle intensity at 1 AU. B_{on} and $B_{max} = c_1$ describe the onset time and the time of maximum of the solar injection profile, respectively. Both parameters are relative small on the Western hemisphere (of the order of 1 hour if averaged over many events), but increase systematically with increasing longitude on the Eastern hemisphere. Both parameters are independent of energy and/or velocity of the studied particles (0.5 to 1.1 MeV electrons, 4-80 MeV protons).

The energy independence of the coronal transport puts severe limits on the possible physical mechanisms. Any particle motion in a given static magnetic field configuration gives transport times with $(\text{velocity})^{-1}$ as one factor. This excludes e.g. gradient or curvature drift as one basic mechanism as well as the current sheet diffusion (Fisk and Schatten, 1972), since a diffusion mean free path λ which varies inversely with velocity (to give $K \sim v \lambda = \text{const}$) independent of the particle type is physically unrealistic. Ma Sung et al. (1975) propose a "leaky box model" with a diffusion coefficient $k_L \sim (\Delta L)^2 / \Delta \tau$, where ΔL is the scale size of the boxes which open randomly on a time scale $\Delta \tau$. The leaky boxes could be idealized models of large coronal magnetic field loops, and the process of field line reconnection provides the random opening of the boxes. In this model, the direction and speed of transport processes is not governed by the particle parameters (like velocity or rigidity), but by fundamental properties of solar magnetic fields; it is the randomness of the reconnection process which would be responsible for a diffusion-like behaviour, whereas the particle motion is deterministic. Note that this concept might also lead to non-diffusive processes, if there is only a small number of boxes or channels along which the particles propagate. A more deterministic process, namely an energy-independent drift, which should act in addition to coronal diffusion, has been proposed by Reinhard and Wibberenz (1974). One of the original supports for this idea, namely the linear relationship between t_m and χ , can no longer be maintained, since because of the escape processes a quasi-linear relation can also be simulated in a diffusion

model (Ng and Gleeson, 1975). However, the total injection time profile depends critically on the nature of the processes. Reinhard and Roelof (1975) have studied the relation between onset times and maximum times and confirmed the necessity to include solar drift processes. Their (linear) drift-diffusion model contains a drift rate τ_E , a diffusion time $\tau_C = r_C^2/K_C$, and a loss time τ_L . When the corresponding injection profile is convoluted with interplanetary diffusion processes, one gets a good description of the measured time profiles of 10-60 MeV protons. The parameters of the solar injection profile and the interplanetary scattering mean free path are independent of proton energy. From a fit to several Eastern events, Reinhard and Roelof (1975) determine average values for the coronal parameters as $\tau_E = 0.42$ hr/grad, $\tau_C = 400$ hr, $\tau_L = 13$ hr.

This choice of τ_C takes care of the observed widening of the time profiles with increasing solar longitude, whereas it is essentially the drift which determines the increase of the absolute time delay with solar longitude. The corresponding dependence $t_m(\phi)$ for the drift-diffusion model is indicated by the dashed line in Figure 3. Here an extension of the FPR of $\pm 40^\circ$ has been assumed, centered around W50 longitude, so the increase sets in East of W10 and West of W90°. The average contribution of the interplanetary propagation corresponds to a time delay of 4.4 hr for 10 MeV protons.

The loss time of 13 hours is within the range assumed to be realistic by Ng and Gleeson (1975). Let us see how the loss time τ_L can be determined observationally.

There are in general two processes by which for a given point on the solar surface the intensity is diminished. (1) the lateral spread of particles causes a corresponding decrease in surface density, (2) the injection into the interplanetary medium causes a general loss proportional to the number of particles present. These two points also determine the maximum intensity N_{\max} in the injection function. If we take the Reid/Axford model seriously, see equ. (1), we can derive the following predictions:

(a) For small distances ϕ the propagation times are small to that the escape term $\exp(-t/\tau_L)$ has no influence on the time of the intensity maximum c_m of the coronal injection function. In this case $c_m = (r^2/4\kappa_e) \cdot \chi^2$ and we get from equ.(1)

$$N_{\max}(\chi) = N(\chi, c_m) \sim \chi^{-2} \quad (2)$$

(independent of the coronal parameters). Thus, a strong dependence of N_{\max} in the coronal injection profile on angular distance from the flare is predicted by the Reid/Axford model. Its verification by observations in space is limited, (a) by the convolution with interplanetary propagation, (b) by the fact that most flares occur remote from the solar equator (see above, $\theta_F \approx 20^\circ$).

In addition, the existence of the FPR will initially fill up an extended area close to the flare site, which will preclude the sharp dependence of N_{\max} on χ as suggested by (2). In any case, the relatively flat distribution of the number of events with longitude on the western hemisphere (see Figure 2) favors a model with a moderate variation of N_{\max} over small distances from the flare.

(b) For large distances χ , it is mainly the exponential term $\exp(-t/\tau_L)$ in equ. (1) which determines the decrease of N_{\max} . (It should be noted that in the more realistic version of the Reid model treated by Ng and Gleeson (1975), at late times this is the only term in the temporal variation, because the whole solar surface is covered with particles, there is no $1/t$ -factor left).

Let us describe the average decrease of the number of particles at the maximum of the injection function with $P(\phi)$. $P(\phi)$ is allowed to vary with energy, but shall be the same for every event. Here we measure ϕ along the solar equator and let $P(\phi)$ be normalized to 1 for events close to $\phi \approx 0^\circ$. It is this variation

$$N_{\max}(\phi) = N_{\max}(0) P(\phi) \quad (3)$$

which determines how the number of events detected varies with solar longitude (Reinhard and Roelof, 1975). For normally an "event" is identified when the number of particles during the maximum phase exceeds a certain threshold, which is determined by detector background and counting rate statistics. Let the size distribution (the number W of events where the maximum intensity of particles exceeds a given value N_{\max}) be a separable function of N_{\max} and longitude, i.e. the longitudinal distribution is independent of the size of the event,

$$W(N_{\max}, \phi) = f(N_{\max}) g(\phi) \quad (4)$$

With $N_{\max} = T$ = threshold for detection of the event type under study we get $W(T, 0)$ = total number of events above threshold close to the preferred connection longitude around $W40...W60$, and $W(T, \phi) = f(T)g(\phi)$ is the longitudinal flare distribution (see Figure 2).

On the other hand, we have from equ. (3) $W(T, \phi) = W\left[\frac{T}{P(\phi)}, 0\right]$. Equating the two expressions for W , we finally obtain

$$f\left(\frac{T}{P(\phi)}\right) = f(T)g(\phi) \quad (5)$$

Relation (4) has been verified by Reinhard and Roelof (1975) for protons >10 MeV, >30 MeV, and >60 MeV, and they showed that $f(N_{\max})$ can be described by a power law $(N_{\max})^{\mu}$ with $\mu = 0.36$. Inserting this into (5) they get $g(\phi) = [P(\phi)]^{0.36}$ as relation between the longitudinal distribution g and the size variation P . Note that this relation implies that $g(\phi)$ is rather insensitive to the size variation $P(\phi)$. This is even more so, if we take an independent determination of the size spectrum from Van Hollebeke et al. (1975); they obtain for the differential size spectrum $dw/dE_{\max} \sim N_{\max}^{-\alpha}$ with $\alpha = 1.15 \pm .05$, which implies that the integral spectrum W is rather flat and $\mu \approx 0.15$ instead of 0.36 as above.

The longitudinal distribution has been determined by Reinhard and Roelof (1975) as $g(\phi) = \exp(m\phi)$ with $m = -0.01$ (degree) $^{-1}$. Insertion into the drift-diffusion model with the average

parameters cited above leads to a loss time $\tau_L = 13$ hours, independent of energy. In contrast, Van Hollebeke et al. (1975) have concluded from a variation of the observed spectral shapes of proton spectra with longitude, that the escape rate should be energy dependent. They find an average loss time of $\tau_L = 1.85$ hours for protons with a mean energy of 40 MeV, and an increase in the loss rate of 35-45% from 20 MeV to 80 MeV. The smaller loss time for the higher energies would then be responsible for the observed steepening of the spectrum with longitude.

Reinhard and Roelof (1975) do not find a systematic variation of the spectral slope with longitude. The reason for the discrepancy is not clear, it should be partly related to the use of a different set of data (difference in the threshold T for event detection; different selection criteria for "solar events"). In any case, it appears that a loss time of about 2 hours is too small to be compatible with observations; the corresponding decrease in the injection function by a factor of 10 every 4.5 hours would make events from the Eastern hemisphere of the Sun practically undetectable. Because of the intensitivity of the size distribution on τ_L (see the discussion following equ. (5) above) more direct determinations will be necessary (see section 4 for some indications).

Let us close this section on the variations of solar event parameters with solar longitude. We have discussed the delay times (onset and time-to-maximum), the general shape of the intensity-time profiles, and the distribution of the number of events with longitude. We have tried to relate the average behaviour of a large number of events to specific coronal propagation models. Let us summarize the essential aspects of the various models, in particular with respect to predictions of latitudinal solar variations.

(1) Propagation over small angular distances; existence of a fast propagation region?

In the Reid/Axford-model there is just one fundamental process acting throughout the solar surface, characterized by a diffusion coefficient k_c . We had pointed out the difficulty to describe

simultaneously, with a unique value for κ_c , the increase of t_m on the Eastern disk and the small values of t_m over the Western disk (see Figure 3). In principle, this difficulty might be overcome by assuming a large variability of κ_c and by ascribing the small t_m -values to occasional large values of κ_c . Tests of the Reid model from measurements in the ecliptic plane are partly restricted because one never scans $\chi \approx 0$. A spacecraft measuring solar equatorial latitudes in the range $20-30^\circ$ should see the strong dependence with distances from the solar flare predicted by the variation of N_{\max} (see equ. (2)) or a well defined second maximum related with the corotation for events East of the connection longitude (see Ng and Gleeson, 1975).

On the other hand, small latitudinal variations would be expected if the FPR (fast propagation region) exists. Reinhard and Wibberenz (1974) have suggested that the extent of the FPR is related to solar sector boundaries which have already been found to play an important role in determining the efficiency of coronal propagation (Roelof and Krimigis, 1973). The azimuthal distribution of the number of particles shows discontinuities at certain solar sector boundaries, so that it has become possible to assign "access probabilities" to individual unipolar solar cells (Gold and Roelof, 1974; Roelof, 1974). Studies on spacecraft off the ecliptic plane and the technique of mapping intensities back to the high solar corona (see Roelof, 1974) should allow to observe the very existence of the FPR, its latitudinal extent and the influence of the polewards sides of the unipolar solar cells.

(2) Propagation over large distances; dimensionality of transport?

A very schematic distinction between various models can be seen in Figure 4, where the broad time development over the solar surface is plotted for the pure diffusion model (left) and the drift-diffusion model (right). For simplicity, we neglect the influence of the loss term and merely indicate how a characteristic angular extent ϕ and the average particle density within ϕ are expected to vary with time.

C-4

The essential point in the "drift" process is that the transport process in the corona is not totally statistical (like in a diffusion process, where the net streaming of particles is simply proportional to the density gradient), but that there is a preferential bulk motion of particles into one direction superimposed. The filling up of one large "box" which was initially empty might be one such process (see the above discussion about the "leaky box concept"). A pure drift, where all particles move into the same direction, is depicted schematically in the outer right part of Figure 4. An $E \times B$ -drift of the required order of magnitude (corresponding to velocities of 7 km/sec if $r_c = 1$ solar radius) is not very likely. However, a very direct proof would be the systematic depletion of particles from the region close to the original flare (see Fig. 4, right part). The shift of time intensity profiles between spaceprobes separated in heliocentric longitude has been shown to be consistent with normal corotation for four individual solar events in 1968 (McKibben, 1973) and does not require an additional drift. Moreover, the azimuthal gradients are in general positive when one approaches the heliocentric longitude of the flare (see McCracken and Rao, 1970; McCracken et al., 1971).

So one should still regard the drift-diffusion model as hypothetical and a convenient mathematical description to describe coronal injection profiles at one longitude. The consequence of a depletion around $\phi \approx 0$ at late times has still to be confirmed.

Let us turn now to the question of dimensionality of transport. The distinction is shown in the two left schemes in Figure 2. The question is still open whether the coronal propagation is related to a fundamental solar process which acts similarly all over the solar surface, or if it is related to specific processes which are typical for the activity belts say. If the propagation is somehow related to large scale magnetic field loops, one should expect a preferential propagation along the East-West direction because of the preferential orientation of the loops in this way. This would favor a one-dimensional

propagation in a limited latitudinal range (see second sketch from the left in Figure 4). In this case, observations beyond about 40 or 50° in latitude would hardly show an detectable amount of solar energetic particles, and the large coronal holes found sometimes at the solar poles would be totally free of solar flare particles.

On the other hand, coronal propagation might be related to a process which is occurring all over the Sun, similar to the supergranulation, or to the numerous current sheets and minute dipoles with average strength of $500 - 1000$ Gauß and 12 hour lifetimes (see Newkirk, 1975, for discussion). In such a universal process, we should more expect a distribution sketched in the outer left part of Figure 4. It is clear that studies of particle populations at large heliocentric latitudes offer a unique opportunity to distinguish between the two fundamentally different possibilities.

4. Detailed studies of individual events

It is not intended to give a detailed account of the numerous studies of longitudinal effects for single events or for selected periods of time. We simply want to describe various methods and to describe a few results which give the necessary and important supplements to the statistical studies discussed so far.

McCracken et al. (1971) have studied data from four Pioneer spacecraft separated by $\approx 180^\circ$ in heliocentric longitude. At late times (≥ 4 days) in the events they still found strong gradients in longitude, with e-folding angles for 10 MeV protons of the order $\eta = 30^\circ$, and no temporal change in the relative gradient. This corresponds to a factor of 10 decrease every 70° . Note that this value of η has only been directly determined for two events. Van Hollebeke et al. (1975) from the study of a much larger number of events conclude that on the average the event size for protons around 40 MeV decreases by about two orders of magnitude every 60° away from the preferred connection region. This value is also consistent with an exponential gradient in longitude corresponding to a change of two orders of magnitude over a longitudinal distance of $40^\circ \dots 60^\circ$ (Roelof et al., 1975) for MeV protons and alpha particles. A comparison of these gradients with specific coronal propagation models has not yet been performed.

Persistent anisotropies along the IMF from the general solar direction have been among the first indicators that the solar source has to be described by a long-lasting injection instead of a delta-function in time (Bartley et al., 1966; Fan et al., 1968; Krimigis et al., 1971). The interpretation of these persistent large anisotropies depends on whether or not interplanetary propagation can be neglected. Schulze et al. (1974) gave an example where the simultaneous fit of intensity and anisotropy data for 22-60 MeV protons during the Nov 18, 1968, event allows to determine the approximate duration of the solar injection as well as the interplanetary mean free path. As pointed out later (Schulze et al., 1975) the interplanetary data are relatively insensitive to the form of the solar

injection profile. A change in the form (not the characteristic duration) of the solar injection profile can be canceled by a suitable change in the interplanetary scattering mean free path without changing essentially the intensities or anisotropies.

The situation is different when interplanetary scattering within the inner solar system can be neglected. For the scatter-free proton event of April 20, 1971, Palmer et al. (1975) could directly determine the solar injection profile and obtained a solar decay time of about 7 hours for 7.6-55 MeV protons. Roelof and Krimigis (1973) have pointed out that for low energy protons ($\lesssim 1$ MeV) scattering in the inner solar system is almost absent. Here the magnitude and the direction of the anisotropies are used to infer the small interplanetary scattering, and by use of the "mapping" technique conclusions can be drawn on the coronal injection profiles. Various time periods have been studied in a series of papers (Roelof, 1973; 1974; Gold et al., 1974; Krieger et al., 1975). Typical coronal profiles are ramp-like structures, which are relatively smooth as long as the observer is connected to the same unipolar cell on the Sun, and sharp changes in intensity when a neutral field line on the Sun is crossed. These results are seen with corresponding time delays at spacecraft widely different in heliocentric longitude, (Roelof and Krimigis, 1973) which confirms the spatial rather than the temporal structure of the profiles.

The ordering of solar energetic particle data by solar structures observable in H_{α} -filtergrams becomes also clear in the large solar events of August 1972, where Roelof et al. (1974) have studied flux histories for protons > 13.5 MeV from Pioneers 9 and 10 and IMP 5. The different access of particles to regions on both sides of a solar sector boundary is clearly established. The crossings of solar sector boundaries are therefore in many cases seen by abrupt changes in the intensities of solar energetic particles, but they can also lead to marked changes in the rise or decay times of the total profile (see Reinhard, 1975b). It is very

remarkable that the solar sector boundaries, which are inferred from the H_{α} -filtergrams (McIntosh, 1972) and which are found to play such an important role for the access probabilities of solar energetic particles, do not in each case coincide with interplanetary sector boundaries. A possible explanation by chromospheric neutral lines which are not continued into an interplanetary magnetic field sector boundary, has been given by Roelof (1974).

The irregularities which are related with the solar cells of different polarity certainly have to be superimposed on the overall dependence on solar longitude which we discussed in section 3. Formally this could be described by a variation of the coronal parameters with solar longitude. This scheme might offer an explanation for the observations of "anomalous" injection profiles of solar particles. Keath et al. (1971) have shown that the favored path for cosmic ray propagation in the March 12, 1969 event was about 40° east of the nominal Archimedes spiral line of force from the flare location. Palmer and Smerd (1972) also found a deviation from the "classical" picture, where the best connection into space should be close to the flare site. They explain the appearance of a prompt low energy proton component far away from the original flare by the triggering action of a shock wave travelling in the solar atmosphere. Cherki et al. (1974) find by analyzing the March 29, 1970 event that particles of different rigidity are ejected at different longitudes on the Sun. Barouch et al. (1971) studied the onset times of 6-25 MeV protons for several flares from the same active region, and conclude that the magnetic fields close to the active region should be considerably distorted from the nominal Archimedean field.

These examples show that for individual events the release mechanism from the Sun may become very complicated, and that the models and coronal parameters discussed in section 3 only describe the average characteristics over many events.

In all cases, however, the unusual particle escape from the Sun is thought to be related to processes occurring in the vicinity of the Sun, in particular in the coronal magnetic fields. As discussed already in section 3, large coronal magnetic loops probably play a prominent role. Over which longitudinal range and how far up into the corona these loops extend is not yet clear. Simnett (1974b) in case of the August 11, 1970 event has suggested the existence of a stable loop extending several solar radii above the solar surface and about 100° in longitude. Two release points should exist for solar protons on both sides of this loop, with quasi-stable trapping inside the loop.

Observations from Skylab have cast some doubt on the existence of stable loops of this extent. Chase et al. (1975) have studied one hundred loops detectable in soft X-rays and show that the number of interconnections decreases steeply for longer distances; the longest interconnecting loop extends over an angular distance of 37° .

The question how far the loops extend and which portion of the solar surface is covered with "closed" or "open" configurations is crucial for the whole propagation problem. The energetic particles perform gyrations about the field lines, and the transport of particles from one field line to the neighbouring one does not depend on whether the field lines are closed (i.e. return to the solar atmosphere) or open (i.e. lead out into interplanetary space). However, the number of closed field lines determines the amount of trapping, and once particles have been transmitted to open field lines they will escape into space. This means that an efficient storage mechanism, and a transport which finally allows to fill practically the whole solar atmosphere (see McCracken et al., 1971; McKibben, 1972) ought to be only possible if a large fraction of the solar surface is "closed". This is confirmed by observational evidence; there should be a relative amount of open field lines of the order 10-15 % in equatorial regions, 25-40 % averaged over the whole Sun (Newkirk, private communication). These figures are based on the potential (current-free) coronal field calculated from the observed-line-of-sight fields at the photospheric level (Altschuler

and Newkirk, 1969) and may have to be modified by the influence of the expanding solar wind.

Newkirk (1973) concludes that the ambient field configuration around active regions also determines whether or not protons escape from a given flare. It is found that among all flares proton flares have significantly more open field lines emerging from the vicinity of the active region. Newkirk assumes an "injection surface" of $36^\circ \times 36^\circ$ centered on the flare and finds that the spread in longitude of open field lines is characterized by a full-width-at-50 percent of 10° to 20° which is insufficient to explain the observed longitudinal distribution of energetic particle events. One possible explanation for the discrepancy is that perhaps the original injection surface must be larger. This would occur if shocks are the principal sources of energetic protons in the corona. We shall discuss this point in somewhat more detail in the next section.

5. Relation to the acceleration process in solar flares.

Let us first summarize some of the properties of coronal propagation along the ideas of Simnett (1974) or McKibben (1973). There is a "prompt component" or "phase 1" of solar particle events. This is due to particles which either have been directly accelerated on open field lines or have been injected onto open field lines shortly after the flare. The longitudinal extent where these prompt particles are found should correspond to the "fast propagation region" discussed above. These initially injected particles give rise to a relatively short decay time (McKibben, 1973).

There is a "delayed component" or "phase 2" of solar particle events. It is very probable that these delayed particles have been accelerated on closed field lines. They then propagate in the corona, from one closed configuration to the next, maybe according to the concept of the leaky boxes discussed above, and from thereon there is only a gradual release of these particles into space. If this release were instead very fast and efficient, we would never observe that flare particles have finally occupied essentially the whole inner solar system!

There are two different solar decay times for the two types of particle populations. Wibberenz and Reinhard (1975) and Reinhard (1975a) show that by convoluting the solar decay processes with interplanetary propagation one can quite naturally explain the exponential or quasi-exponential nature of the interplanetary decay, and that no "free escape boundary" around 2...3 AU is required, which would be difficult to be reconciled anyhow with the Pioneer 10 and 11 observations.

We turn now to the phase-1 particles within the FPR. It has been shown that the injection profiles for these particles are not of the delta-function type in time, but finite in width (Palmer et al., 1975; Reinhard, 1975a). It is certainly difficult to distinguish whether these finite injection profiles stem from continuous release or continuous acceleration of particles. But if the decay in phase 1 is much steeper than in phase 2 (McKibben, 1973), then the particles cannot be replenished by the neighbouring storage region through the same process as the phase-2 particles. There might be a small storage region close to the flare with a different release mechanism for the phase-1 particles (this mechanism might exist because of the high degree of disturbance in the solar atmosphere following the flare). Or we have to assume that the injection profile directly gives the number of particles as they are accelerated.

The second possibility is very interesting with respect to the two-stage acceleration process, which is discussed in detail e.g. by Lin (1974). In the first phase non-relativistic electrons are accelerated. If a sufficiently large number of electrons is damped into the chromosphere and lower corona, explosive heating occurs and produces an ejection of material and a shock wave which accelerates electrons and protons to relativistic energies. This picture is confirmed by Svestka and Fritzová-Svestková (1974). They present convincing evidence that proton acceleration to higher energies ($\gtrsim 10$ MeV) is closely connected with type II bursts, i.e. shock waves travelling in the solar atmosphere. Our above interpretation that the finite injection profiles might resemble the finite duration of the acceleration process itself would favor the shock acceleration model for protons, and it also explains,

why protons may be found on a wide longitudinal range of open field lines.

The small longitudinal variation of the slopes of the proton energy spectrum discussed in section 3 implies that the particles of phase 1 and phase 2 have the same energy spectrum, which means that the acceleration process should work in the same manner on open as well as on closed field lines. In addition, any model of the acceleration process should explain why the spectral slopes for high energy protons and relativistic electrons are roughly the same, $\gamma \approx 3$ (see Van Hollebeke et al., 1975). It would also be interesting to see if the energy dependence of the decay times, as suggested by Reinhard (1975a) can be reproduced by a shock model acceleration.

We close with a remark which emphasizes the role which the fast propagation region may play for the study of solar acceleration processes. The He³-rich events which are a novel feature of solar cosmic rays (Serlemitsos and Balasubrahmanyam, 1975) appear to be observed only for sufficiently small events and are only found when the parent flare is on the Western hemisphere (McDonald, private communication). This might indicate a specific configuration near the Sun, where the acceleration process supplies He³ nuclei only directly to open field lines.

6. Conclusions.

There are two important features of the interplanetary propagation which allow us to study coronal transport phenomena: (1) the motion of energetic particles perpendicular to the IMF is small, (2) the scattering mean free path along the IMF is large, so that details of the solar injection profiles can be regained from measurements in space.

We have tried to order the material by models for acceleration, injection, and propagation processes. None of these models has been proven to give the real physical picture, because the underlying processes could not yet be identified. In this brief summary we shall concentrate on those open points which could be further clarified by spacecraft measurements performed out of the ecliptic plane.

- (1) What is the nature of the "fast propagation region" (probably identical with the "open cone of propagation" or the "region of preferred connection longitudes")? Is there also a region of preferred connection latitudes? If the latitudinal extent is limited, what is the nature of the boundary?
- (2) If there is a transport process involved within the fast propagation region, what is the nature of this process? Could it be a diffusive process with a sufficiently large diffusion coefficient? In this case one should be able to see the relatively strong dependence of the maximum intensity on angular distance θ for small θ as discussed in section 3, because the connection point of an ex-ecliptic spacecraft comes closer to the active regions.
- (3) Is the acceleration process directly responsible for the longitudinal width of the FPR and for the fast access of particles to open field lines? If particles are accelerated on open field lines by a travelling shock and may then escape into space, the extent of this "prompt" region should be determined by the distance which the shock can travel in longitude and latitude. Will we see particles arrive very fast over the poles?
- (4) Which role do the solar sector boundaries play? Is there a similar change in the access probabilities if one leaves a unipolar cell on the northern or the southern boundary? If there is one large unipolar cell (e.g. a coronal hole) extending from the pole to the equator, is there the same access probability all over this cell, or is there a gradual or drastic change with latitude? Would one detect He⁺-rich events over the poles?
- (5) What is the nature of the energy-independent slow coronal propagation over large distances in longitude? Is there a drift process (possibly related to electric fields) involved? Are the time delays and the intensity decreases merely a function of the absolute angular distance between flare and observer, or are the variations typically different into the East-West and into the North-South direction? If the large scale magnetic loops in the corona play an important role for the propagation, one would expect such systematic differences, and then the preferred direction of the propagation and the latitudinal

extent up to which particles are transported may vary with the solar cycle, because of the difference in the average orientation and location of the loops. If the interpretation in section 3 on the importance of magnetic reconnection processes is correct, the study of large scale coronal particle transport should give insight into a fundamental solar problem.

Acknowledgements:

I wish to acknowledge stimulating discussions with R. Reinhard, C.-G. Ng, M.A.I. Van Hollebeke, G. Newkirk, Jr., G. Simnett, and D. Smart. I also thank R. Reinhard, M.A.I. Van Hollebeke, and C.-G. Ng that I could make use of their results before publication.

References:

- Altschuler, M.D. and G. Newkirk, Jr., Magnetic fields and the structure of the solar corona, Solar Phys. 9, 131, 1969
- Axford, W.I., Anisotropic diffusion of solar cosmic rays, Planet. Space Sci., 13, 1301, 1965
- Barouch, E., M. Gros, P. Masse, The solar longitude dependence of proton event delay time, Solar Phys., 19, 483-493, 1971
- Bartley, W.C., R.P. Bukata, K.G. McCracken, U.R. Rao, Anisotropic cosmic radiation fluxes of solar origin, J. Geophys. Res., 71, 3297-3304, 1966
- Bukata, R.P., U.R. Rao, K.G. McCracken, and E.P. Keath, Observation of solar particle fluxes over extended solar longitudes, Solar Phys., 26, 229, 1972
- Burlaga, L.F., Anisotropic diffusion of solar cosmic rays, J. Geophys. Res., 72, 4449, 1967
- Chase, R.C., A.S. Krieger, Z. Svestka, and G.S. Vaiana, Skylab observations of X-ray loops connecting separate active regions, Space Res., XVI (COSPAR-Meeting, Varna 1975), to be published, 1975
- Cherki, G., J.P. Mercier, A. Raviart, L. Treguer, D. Maccagni, F. Perotti, and G. Villa, Effect of solar corona condition on flare particle propagation, Solar Phys., 34, 223, 1974
- Datlowe, D., Relativistic electrons in solar particle events, Solar Phys., 17, 436, 1971
- Elliot, H., Particle diffusion in the solar corona, in Dyer (ed.), Solar Terrestrial Physics, Part I, 1, 134, 1970
- Englade, R.C., A computational model for solar flare particle propagation, J. Geophys. Res., 76, 768, 1971
- Fan, C.Y., M. Pick, R. Pyle, J.A. Simpson, and D.R. Smith, Protons associated with centers of solar activity and their propagation in interplanetary magnetic field regions corotating with the sun, J. Geophys. Res., 73, 1555, 1968
- Fisk, L.A., and K.H. Schatten, Transport of cosmic rays in the solar corona, Solar Phys., 23, 204, 1972
- Gold, R.E., and E.C. Roelof, A prediction technique for low energy solar proton fluxes near 1 AU, Space Res. XVI (Cospar-Meeting Varna 1975), to be published, 1975
- Keath, E.P., R.P. Bukata, K.G. McCracken, and U.R. Rao, The anomalous distribution in heliocentric longitude of solar injected cosmic radiation, Solar Phys., 18, 503, 1971
- Lanzerotti, L.J., Coronal propagation of low energy solar protons, J. Geophys. Res., 78, 3942, 1973
- Kirsch, E. and J.W. Münch, Intensities and anisotropies of low energy solar protons measured aboard the satellites AZUR, Explorer 35 and 41, November 1969- April 1970., Solar Phys., 39, 459, 1974

- Krieger, A.S., J.T. Nolte, J.D. Sullivan, A.J. Lazarus, P.S. McIntosh, R.E. Gold, and E.C. Roelof, Relation of large-scale coronal X-ray structure and cosmic rays: 1. Sources of solar wind streams as defined by X-ray emission and H_{α} absorption features, Proc. 14th Intern. Cosmic Ray Conf., Paper SP 4-4, München 1975
- Krimigis, S.M., E.C. Roelof, T.P. Armstrong, and J.A. Van Allen, Low energy (>0.3 MeV) solar particle observations at widely separated points (>0.1 AU) during 1967, J. Geophys. Res., 76, 5921, 1971
- Lin, R.P., Observations of scatter-free propagation of ~ 40 keV solar electrons in the interplanetary medium, J. Geophys. Res., 75, 2583, 1970
- Lin, R.P., Non-relativistic solar electrons, Space Sci. Revs., 16, 189, 1974
- Ma Sung, L.S., M.A.I. Van Hollebeke, and F.B. McDonald, Propagation characteristics of solar flare particles, preprint 1975
- McCracken, K.G., and U.R. Rao, Solar cosmic ray phenomena, Space Sci. Revs., 11, 155, 1970
- McCracken, K.G., U.R. Rao, R.P. Bukata, and E.P. Keath, The decay phase of solar flare events, Solar Phys., 18, 100, 1971
- McIntosh, P.S., Solar magnetic fields derived from hydrogen alpha filtergrams, Revs. Geophys. Space Phys., 10, 837, 1972
- McKibben, R.B., Azimuthal propagation of low energy solar-flare protons as observed from spacecraft very widely separated in solar azimuth, J. Geophys. Res., 77, 3957, 1972
- McKibben, R.B., Azimuthal propagation of low-energy solar flare protons: Interpretation of observations, J. Geophys. Res., 78, 7184, 1973
- Newkirk, G., Jr., Coronal magnetic fields and energetic particles, in High Energy Phenomena on the Sun, Symposium Proceedings, GSFC X-693-73-193, p. 453, 1973
- Newkirk, G. Jr., Solar activity, coronal observations, and composition, Proc. 14th Intern. Cosmic Ray Conf., Invited Paper, München 1975
- Ng, C.-G., and L.J. Gleeson, A complete model of the propagation of solar-flare cosmic rays, preprint 1975
- Nolte, J.T. and E.C. Roelof, Large-scale structure of the interplanetary medium. I: High coronal source longitude of the quiet-time solar wind, Solar Phys., 33, 241, 1973
- Palmer, I.D. and S.F. Smerd, Evidence for a two-component injection of cosmic rays from the solar flare of 1969, March 30, Solar Phys., 26, 460, 1972
- Palmer, I.D., R.A.R. Palmeira, and F.R. Allum, Monte Carlo Model of the highly anisotropic solar proton event of 20 April 1971, Solar Phys., 40, 449, 1975

- Pomerantz, M.A., and S.P. Duggal,
The Sun and cosmic rays,
Revs. Geophys. Space Phys. 12, 343, 1974
- Reid, G.C., A diffusive model for the initial phase of a solar
proton event, J. Geophys. Res., 69, 2659, 1964
- Reinhard, R., and G. Wibberenz, Propagation of flare protons in
the solar atmosphere, Solar Phys., 36, 473, 1974
- Reinhard, R., and E.C. Roelof, Drift and diffusion of solar flare
protons in the corona, Preprints, 1975
- Reinhard, R., The exponential decay of solar flare particles. II.
Western hemisphere events. Proc. 14th Intern. Cosmic Ray Conf.
Paper SP 4-1, München, 1975a
- Reinhard, R., Die solare Ausbreitung flareerzeugter Protonen im
Energiebereich 10 - 60 MeV, Dissertation, Kiel, 1975b
- Roelof, E.C., Coronal magnetic fields and the structure of low-
energy solar charged particle events, In: Symposium on High
Energy Phenomena on the Sun, NASA Publ. X-693-73-193, pp.
486, 1973
- Roelof, E.C., Coronal structure and the solar wind, In C.T. Russell
(Ed.), "Solar Wind Three", Proc. Asilomar Conf., Los Angeles 1974
- Roelof, E.C., and S.M. Krimigis, Analysis and synthesis of coronal
and interplanetary energetic particle, plasma, and magnetic
field observations over three solar rotations, J. Geophys. Res.,
78, 5375, 1973
- Roelof, E.C., J.A. Lezniak, W.R. Webber, F.B. McDonald, B.J. Teegarden,
and J.H. Trainor, Relation of coronal magnetic structure to
the interplanetary proton events of August 2-9, 1972,
In: D.E. Page (Ed.), Correlated Interplanetary and Magneto-
spheric Observations, Dordrecht 1974
- Roelof, E.C., R.E. Gold, S.M. Krimigis, A.S. Krieger, J.T. Nolte,
P.S. McIntosh, A.J. Lazarus, and J.D. Sullivan, Relation of
large-scale coronal X-ray structure and cosmic rays: 2. Coronal
control of interplanetary injection of 300 keV protons,
Proc. 14th Intern. Cosmic Ray Conf., Paper SP 4-5, München, 1975
- Schulze, B.-M., A.K. Richter, and G. Wibberenz, The influence of
finite injection periods on anisotropies during solar particle
events, Proceedings of the HELIOS Scientific Colloquium,
Windberg 1974
- Schulze, B.-M., A.K. Richter, and G. Wibberenz, On the influence of
injection profiles and of interplanetary propagation on the
time-intensity and time-anisotropy profiles of solar cosmic
rays at 1 AU, Proc. 14th Intern. Cosmic Ray Conf., Paper 5. 1-9,
München 1975
- Simnett, G.M., Relativistic electrons from the sun observed by Imp-4.
Solar Phys., 22, 189, 1972
- Simnett, G.M., Relativistic electrons events in interplanetary space,
Space Sci. Revs., 16, 257, 1974a
- Simnett, G.M., A correlation between time-overlapping solar flares
and the release of energetic particles, Solar Phys., 34, 337
1974b
- Serlemitsos, A.T., and V.K. Balasubrahmanyam, Solar particle
events with anomalously large relative abundance of ^3He ,
Astrophys. J., 198, 195, 1975

- Smart, D.F., M.A. Shea, H.W. Dodson, and E.P. Hedeman,
Distribution of proton producing flares around the Sun,
Space Res. XVI (COSPAR-Meeting, Varna 1975), to be published
- Svestka, Z. and L. Fritzoová-Svestková, Type II radio bursts and
particle acceleration, Solar Phys. 36, 417, 1974
- Van Hollebeke, M.A.I., L.S. Ma Sung, and F.B. McDonald, The variation
of solar proton energy spectra and size distribution with
heliolongitude, Solar Phys. 41, 189, 1975
- Wibberenz, G., Interplanetary magnetic fields and the propagation
of cosmic rays, J. Geophys. 40, 667, 1974
- Wibberenz, G., and R. Reinhard, The exponential decay of solar
flare particles. I. Eastern hemisphere events, Proc. 14th Intern.
Cosmic Ray Conf., Paper SP 4-1, München 1975

Figure Caption:

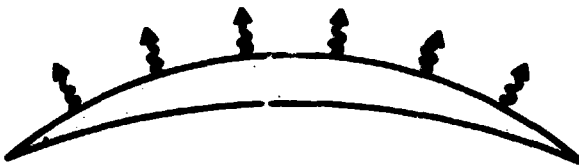
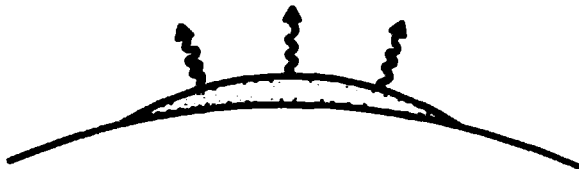
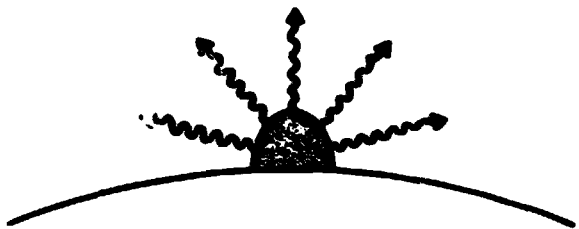
Figure 1: Schematic representation of "propagation" and "storage" processes. The main difference is in the lateral distribution of particles, whereas an observer close to the original acceleration region may see the same injection function in both cases.

Figure 2: Number of solar events as a function of solar longitude, for different particle types and energies. Data have been collected from Lin (1974), Van Hollebeke et al. (1975), Pomerantz and Duggal (1974), and Sinnott (1974).

Figure 3: The time of the intensity maximum (t_m) as a function of solar longitude. The collection of experimental points taken from Reinhard and Wibberenz (1974) is compared with calculations. Curves (a) and (c) are based on the coronal diffusion model (Reid, 1964) in the extended version of Ng and Gleeson (1975), curve (DD) is based on the combination of a fast propagation region with the drift-diffusion model (Reinhard and Roelof, 1975).

Figure 4: Angular spread over the solar surface for different coronal propagation models. Temporal development from top to bottom. The influence of the escape process is neglected. N is the average particle density within the cross-hatched area, ϕ is a characteristic maximum distance from the flare site reached after time t .

PROPAGATION
(♦RELEASE ~~~~~)



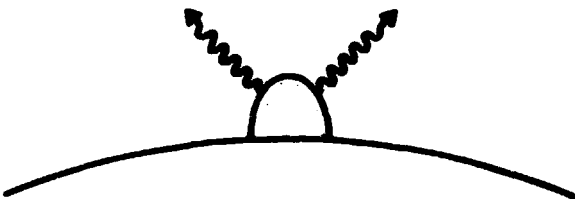
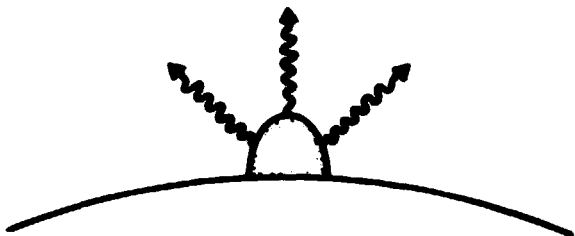
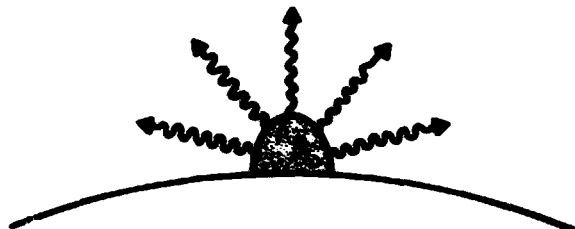
**-SMALL DENSITY GRADIENT
(APART FROM INITIAL PHASE)**

**-GRADUAL WIDENING OF
CONFINEMENT REGION**

**-REDUCTION IN DENSITY BY
LATERAL SPREAD**

♦ LEAKAGE

STORAGE
(♦RELEASE ~~~~~)

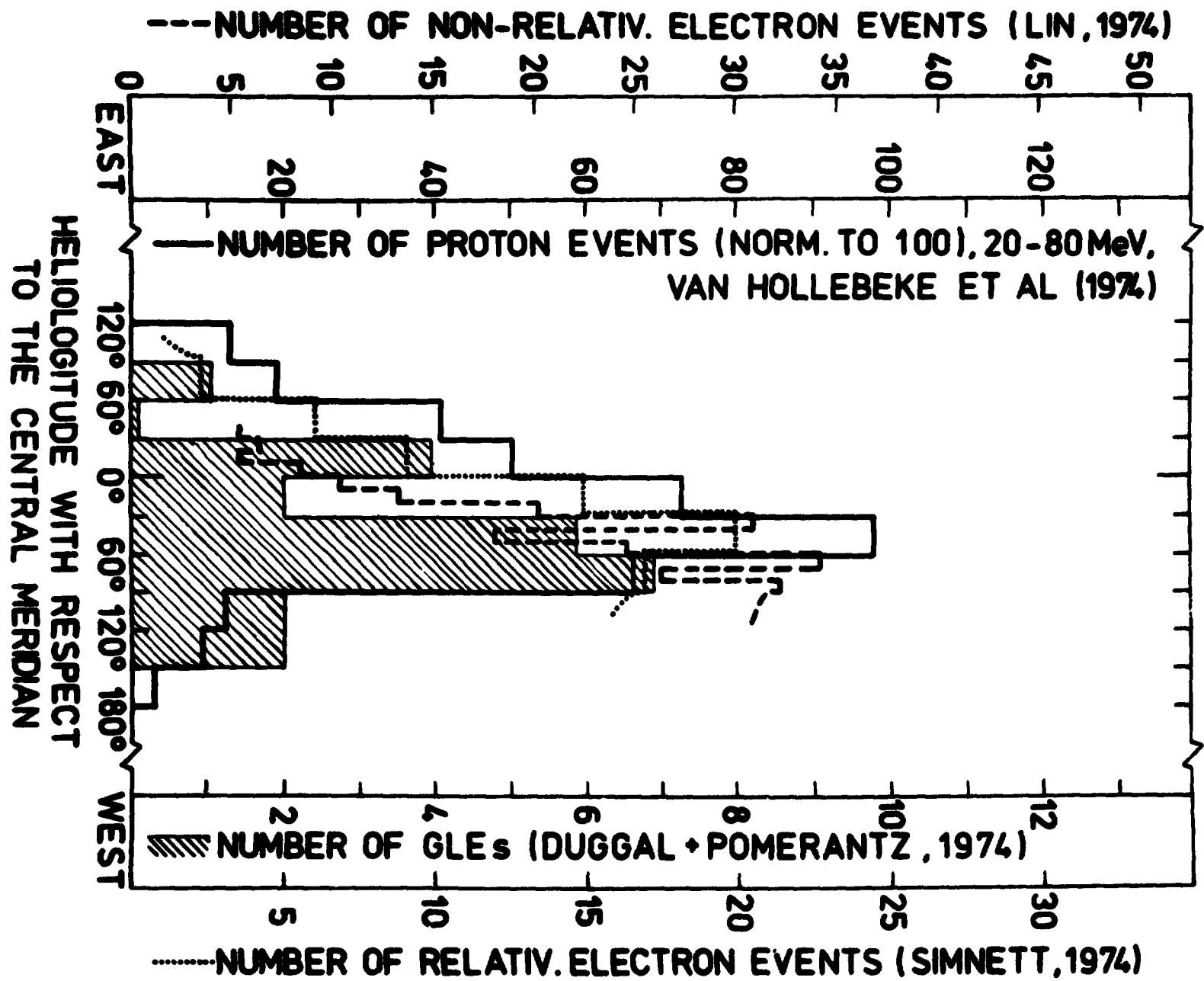


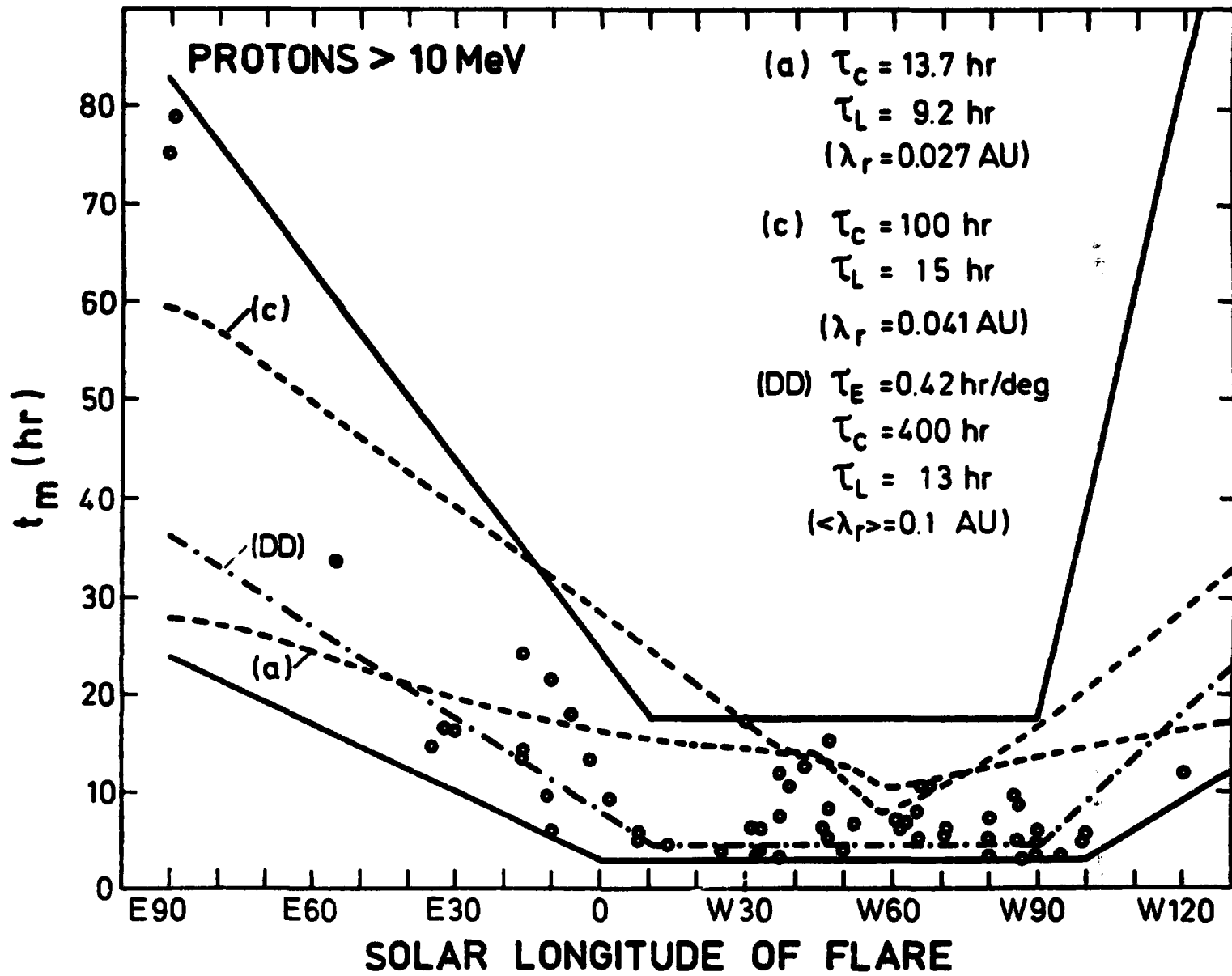
**-LARGE DENSITY GRADIENTS
AT THE BOUNDARY OF THE
STORAGE REGION**

**-NO OR SMALL WIDENING OF
CONFINEMENT REGION**

**-REDUCTION OF DENSITY BY
LEAKAGE**

REPRODUCIBILITY OF THE
ORIGINAL PAGE IS POOR





MODELS FOR PROPAGATION OVER LARGE DISTANCES IN SOLAR LONGITUDE

DIFFUSION (REID'S MODEL)		DRIFT-DIFF. (REINHARD, ROELOF, WIBBERENZ)	
TWO-DIMENS.	ONE-DIMENS.	TWO-DIMENS.	ONE-DIMENS.
<p>$t \approx 0$ (FLARE)</p> <p>TIME</p> <p>$\phi = 0$</p> <p>$N \sim \frac{1}{\phi}$ $\phi \sim \sqrt{t}$</p>	<p>$t \approx 0$ (FLARE)</p> <p>TIME</p> <p>$\phi = 0$</p> <p>$N \sim \frac{1}{\phi}$ $\phi \sim \sqrt{t}$</p>	<p>$t \approx 0$ (FLARE)</p> <p>TIME</p> <p>$\phi = 0$</p> <p>$N \sim \frac{1}{\phi}$ $\phi \sim t$</p>	<p>$t \approx 0$ (FLARE)</p> <p>TIME</p> <p>WESTWARD DRIFT</p> <p>$\phi = 0$</p> <p>$N \approx \text{const.}$ $\phi \sim t$</p>

CHAPTER VI

INTERPLANETARY DUST/INTERSTELLAR NEUTRAL GAS

INVESTIGATION OF INTERPLANETARY DUST FROM
OUT-OF-ECLIPTIC SPACE PROBES

N 76-24134

H. Fechtig

Max-Planck-Institut für Kernphysik, Heidelberg, FRG.

R.H. Giese

Bereich Extraterrestrische Physik, Ruhr-Universität
Bochum, FRG.

M.S. Hanner *

Space Astronomy Laboratory, State University of New York at
Albany, USA.

H.A. Zook

NASA Lyndon B. Johnson Center, Houston, Texas, USA.

* Now at Max-Planck-Institut für Astronomie, Heidelberg, FRG

ABSTRACT

Measurements of interplanetary dust via zodiacal light observations and direct detection are discussed for an out-of-ecliptic space probe. Particle fluxes and zodiacal light brightnesses are predicted for three models of the dust distribution. These models predict that most of the information will be obtained at space probe distances less than 1 A.U. from the ecliptic plane. Joint interpretation of the direct particle measurements and the zodiacal light data will yield the best knowledge of the three-dimensional particle dynamics, spatial distribution, and physical characteristics of the interplanetary dust. Such measurements are important for our understanding of the origin and role of the dust in relation to meteoroids, asteroids, and comets, as well as the interaction of the dust with solar forces.

Introduction

The microscopic dust particles are an important constituent of our solar system. A knowledge of the physical and dynamical properties of these dust particles in three dimensions should aid our understanding of the origin and evolution of the planetary system and furthermore of circumstellar dust clouds as detected by infrared astronomy. In this paper we discuss the type of dust measurements suitable for an out-of-ecliptic mission and the information which could be expected from these measurements.

The interplanetary dust can be explored from space probes by two complementary methods:

1. Direct detection of individual particles intercepted by a sensor. Velocity and mass parameters can be derived and, depending on the specific experiment, information on the chemical composition. Recent experiments have extended the limiting sensitivity down to masses of about 10^{-16} g at impact velocities of approximately 20 km/s (Hoffman et al. 1975).
2. Zodiacal light observations. Measurements of the brightness, color, and polarization of sunlight scattered by the dust particles give information on the average scattering properties and the spatial distribution of the dust along the line of sight (ref. Leinert 1975).

Direct detection has the advantage of defining a complete set of parameters for individual particles but the drawback of

sampling only a small number of particles. The zodiacal light observations sample a large volume of space, but the information on the physical properties of the particles is indirect.

Combined data from these two methods can be valuable especially if the direct detection instrument is sensitive enough to cover the entire mass range which may contribute to the zodiacal light. The combined data can in principle specify particle velocities, orbits, size, mass range, spatial distribution, and the general physical composition of the dust grains (structure, density etc.). These parameters are necessary for an understanding of the dynamical history of the dust particles, their relation to cometary and asteroidal material, and their interaction with it.

Extensive ground-based photometry and polarimetry of the zodiacal light has been carried out (see for example Weinberg 1964, Dumont and Sánchez 1975). However, observations from the earth alone have the fundamental drawback that the spatial distribution and the particle scattering function can not be uniquely separated, unless some assumptions are made about the decrease of particle number density with solar distance and about the independence of dust composition from the position in the solar system (Dumont and Sánchez 1975). Information about the validity of such assumptions can be obtained by zodiacal light photometry and polarimetry from space probes still in the ecliptic plane but far from the earth's orbit (Giese and Dziembowski 1969, Hanner and Leinert 1972).

The zodiacal light experiments on Pioneer 10/11 and Helios provide the brightness and polarization of the zodiacal light as a function of heliocentric distance in the ecliptic plane, (Manner et al. 1975, Link et al. 1975) from which the large-scale spatial distribution in the ecliptic between 0.3 and 3.3 A.U. can be derived.

Impact detectors with increasing sophistication have been used to measure particle fluxes and velocities by experiments on the space missions of Pioneer 8/9, Prospero, HEOS 2, Pioneer 10/11, and Helios (Berg et al. 1971, Bedford 1975, Dietzel et al. 1973, Hoffmann et al. 1975, Humes et al. 1974, Soberman et al. 1974). Pioneer 8/9 and submicron-sized impact craters on lunar surface samples showed the existence of a component of small particles moving outward from the sun under the influence of non-gravitational forces (Berg and Grun 1973, Fechtig et al. 1974).

The interplanetary dust forms a non-stable dust cloud in the solar system. The continuous sources are mainly comets, asteroids, and space erosion processes. It is, however, unknown which of these processes contribute to which extent. The main dust sink is, besides impacts on planets and their satellites, undoubtedly the sun: dust particles spiralling into the sun according to the Poynting-Robertson effect (Wyatt and Whipple 1950) presumably lead to a vaporisation near the sun (Sekanina 1975) and hence to a dust stream of submicron-sized remnants

leaving the solar system as a result of the radiation pressure force. These so-called beta meteoroids (Zook and Berg 1975; Zook, in press) are also produced by mutual collisions of meteoroids. Hemenway has suggested that a component of these beta meteoroids is being formed directly at and ejected by the sun (Hemenway et al 1972). In addition to these interplanetary particles, a component of interstellar origin can possibly be expected.

Models of Out-of-Ecliptic Dust Distribution

To predict the particle flux and the zodiacal light brightness which might be observed from an out-of-ecliptic probe, we chose three models for the spatial distribution of the dust, as described by Giese (1975).

$$I : n(r) = n_0 \cdot r^{-\gamma} \left(1 + (\gamma \sin \beta_0)^2 \right)^{-\gamma/2}; \gamma = 9.0 \text{ (Ellipsoid model)}$$

$$II : n(r) = n_0 \cdot r^{-\gamma} \exp \left[-(\gamma z)^2 \right]; \quad \gamma = 2.5 \text{ (Gauss model)}$$

$$III : n(r) = n_0 \cdot r^{-\gamma} \exp \left[-|\gamma \sin \beta_0| \right]; \quad \gamma = 3.0 \text{ (Fan model)}$$

Here $n(r)$ is the particle number density as a function of distance r (A.U.) from the sun, n_0 is the number density at 1 A.U. in the ecliptic plane, z (A.U.) is the distance above or below the ecliptic plane, and β_0 is the heliocentric ecliptic latitude

($\sin \beta_0 = z/r$). We have set the parameter $v = 1.0$, consistent with the Pioneer 10/11 and Helios zodiacal light data. The flattening parameter γ was adjusted for each model to give the ratio 0.32 for the brightness of the zodiacal light at the ecliptic pole to the brightness in the plane at elongation 90° , as observed by Dumont (1973).

Contours of equal dust density are illustrated in Figures 1a, 1b, and 1c respectively for the three examples. All three models predict that the dust is considerably concentrated toward the ecliptic plane. In comparison, the spatial distribution of radio meteors derived by Southworth and Sekanina (1973) shows a similar z -dependence at a x -distance of 1 A.U., but an increasing number density beyond 1 A.U. in the ecliptic plane.

The 0.5 contour in our examples ranges from $z = 0.2$ to 0.4 A.U. at $x = 1.0$ A.U.. The spatial density at 1 A.U. away from the ecliptic is at most $0.1 n_0$. Thus, observations of the zodiacal light and direct detection of particles will take place mainly at space probe distances less than 1 A.U. from the ecliptic.

Direct Detection

Direct measurements from an out-of-ecliptic mission could help to identify the various sources and sinks of the non-stable dust cloud. On the basis of the results of Pioneers 8/9 and HEOS 2

missions in the ecliptic at 1 A.U. and on the basis of the three models referred to above, the number of events per orbit were computed for a detector surface of 100 cm^2 and a space probe on a circular orbit of 1 A.U. radius having an ecliptic inclination of 30° or 60° or 90° respectively. Two cases of vehicle stabilisations (spinner with axis perpendicular to the orbital plane and three-axis stabilisation) were considered. The results are presented in Table 1 excluding or including the case of particles coming directly from the sun (marked 'no sun particles' or 'sun particles').

From these data it is evident that, while such a particle detection experiment is not able to differentiate among the various models of the spatial distribution directly, it could provide information on the role of the sun as a possible dust sink or source. Furthermore, the event rate is sufficient to continue analysis of enough individual particles to look for differences in composition between particles with low- and high-inclination orbits.

Zodiacal Light

The brightness and polarization of the zodiacal light can be predicted theoretically as a function of observing direction and observer's position in the solar system for any spatial distribution. If one assumes, that the average scattering properties of the particles are independent of location in the

solar system, then the brightness variation with spacecraft position is directly related to the spatial distribution of the dust (Hanner and Leinert 1972). Models for the zodiacal light distribution over the sky as seen from an out-of-ecliptic space probe were discussed by Giese (1971). By use of the same program we have computed for our three dust models the variation of zodiacal brightness for an out-of-ecliptic space probe on a circular orbit of 1 A.U. radius as a function of the z distance between the spaceprobe and the ecliptic plane. The maximum value z_m of z is related to orbital inclination i by $z_m = (1 \text{ A.U.}) \cdot \sin i$. For the scattering function a simple diffraction plus isotropic reflection form (albedo = 1) was chosen. The size distribution adopted was a 3-part power law $n(a)da \propto a^{-\kappa}$ with $\kappa = 2.7$; 2; or 4.33 in the regions of particle radii from 0.008 to 0.16; 0.16 to 29; or 29 to 189 μm , and $n_0 = 3.7 \cdot 10^{-13}$; $4.3 \cdot 10^{-15}$; or $7.4 \cdot 10^{-18}$ particles/cm³ in each regime, respectively. This is a fair approximation taking into account both the distribution of particle radii as derived by Grün (1975) from direct measurements (Fechtig et al. 1974), and the brightness of 200 stars of tenth magnitude per square degree ($200 S_{10}$) found by Dumont and Sánchez (1975) at $\epsilon = 90^\circ$ elongation in the ecliptic.

Figs. 2a through 2c present the decrease of zodiacal light brightness with increasing orbital altitude z of the probe for the three models of Fig. 1. The viewing direction from the

probe is parallel to the ecliptic plane and perpendicular to the sun (Fig. 2a); in the positive z direction (Fig. 2b); or parallel to the negative x direction (Fig. 2c). In all cases the models predict brightness values easily observable ($\geq 10 S_{10}$) at space probe z distances up to 0.4 A.U. (Model II) or up to approximately 1 A.U. (Models I and III), and at the same time observable differences between the models, particularly in the case of Model II with its flattened outer contours. Even if the density does not follow the functional forms we have chosen as examples, the brightness variation with space probe z distance at a constant observing direction will give a measure of the rate of dust decrease away from the ecliptic plane. To look for any systematic changes in the average scattering properties of the particles (size, composition) with z distance, polarization measurements as a function of elongation are necessary, in addition to brightness observations (see Giese and Dziembowski 1969).

Interstellar Dust

The existence of an interstellar component in the solar system dust cloud has been proposed by Greenberg (1969) and others. Even if such small particles are excluded from the inner solar system by radiation pressure, they might be observable with a sensitive detector at large heliocentric distance, during the

transfer orbit of an out-of-ecliptic probe. If we take, for example, a number density of $3 \cdot 10^{-13}$ particles/cm³ of interstellar origin and a relative velocity of 30 km/sec between the particles and a 100 cm² detector, 8 such particles should be detectable each day.

Conclusion

A joint dust experiment which combines direct detection of the velocity and mass of individual particles with measurements of the zodiacal light brightness and, if possible, polarization will best serve the purpose of an out-of-ecliptic mission.

These two complementary methods together will give a picture of the three-dimensional dynamics and spatial distribution of the interplanetary dust. Such a picture will help to clarify the relation of dust particles to cometary and asteroidal material as well as the interaction of the dust with the solar radiation field. The influence of the sun on particle motions and physical characteristics has a significance for the role of the dust in the early evolution of the solar nebula and early phases of stellar evolution.

Acknowledgements

We are grateful to Dr. J. Dachs for providing some useful references and to Mrs. K. Flotow for programming. Part of the work contains material obtained by investigations supported by the Bundesminister für Wissenschaft und Technologie (FRG).

References

- Bedford, P. K., Proc. Roy. Soc. A 343, 277, 1975.
- Berg, O. E. and U. Gerloff, More than two years of micrometeorite data from two pioneer satellites, Space Res. XI, 225-235, 1971.
- Berg, O. E. and E. Grün, Evidence of hyperbolic cosmic dust particles, Space Res. XIII, 1047, 1973.
- Dietzel, H., G. Eichhorn, H. Fechtig, E. Grün, H. J. Hoffmann and J. Kissel, The HEOS 2 and HELIOS micrometeoroid experiments, Scientif. Instr. 6, 209-217, 1973.
- Dumont, R. and F. Sánchez-Martínez, Photométrie de la lumière zodiacale hors de l'ecliptique en quadrature et en opposition avec le soleil, Astron. and Astrophys. 22, 321-328, 1973.
- Dumont, R. and F. Sánchez-Martínez, Zodiacal light photometry, II gradients along the ecliptic and phase functions of interplanetary matter, Astron. and Astrophys. 38, 405-412, 1975.
- Fechtig, H., W. Gentner, J. B. Hartung, K. Nagel, G. Neukum, E. Schneider and D. Storzer, Microcraters on lunar samples, Soviet-American Conference on Cosmochemistry of the Moon and the Planets Moscow, 1974.
- Giese, R. H. and C. V. Dziembowski, Suggested zodiacal light measurements from space probes, Planet.Space Sci. 17, 949-956, 1969.

- Giese, R. H., Model computations concerning zodiacal light measurements by space probes, *Space Res.* XI, 255-260, 1971.
- Giese, R. H., Out-of-ecliptic dust, *Eldo-Cecles/Esro-Cers Scient. and Techn. Rev.* 7, 43-51, 1975.
- Greenberg, J. M., A possible interrelation between interstellar and interplanetary cosmic dust, *Space Res.* IX, 111-113, 1969.
- Grün, E., Personal communication 1975.
- Hanner, M. S. and C. Leinert, The zodiacal light as seen from the pioneer F/G and helios probes, *Space Res.* XII, 445-455, 1972.
- Hanner, M. S., J. G. Sparrow, J. L. Weinberg, D. E. Beeson, Pioneer 10 observations of zodiacal light brightness near the ecliptic: changes with heliocentric distance, IAU Colloquium No. 31, Heidelberg June 1975.
- Hemenway, C. L., D. S. Hallgreen and D. C. Schmalberger, Stardust, *Nature* 238, 256-260, 1972.
- Hoffmann, H. J., H. Fechtig, E. Grün, J. Kissel, First results of the micrometeoroid experiment S 215 on the HEOS 2 - satellite, *Planet. Space Sci.* 23, 215-224, 1975.
- Humes, D. H., J. M. Alvarez, W. H. Kinard and R. L. O'Neil, The interplanetary and near-Jupiter meteoroid environment, *JGR* 79, 3677-3684, 1974.
- Leinert, C., The zodiacal light - a measure of the interplanetary environment, *Space Sci. Rev.* (in print).

- Link, H., C. Leinert, E. Pitz, N. Salm, Preliminary results of the helios a zodiacal light experiment, IAU Colloquium No. 31, Heidelberg June 1975.
- Sekanina, Z., Modelling of the orbital evolution of vaporizing dust particles near the sun, IAU Colloquium No. 31, Heidelberg June 1975.
- Soberman, R. K., S. L. Nester and K. Lichtenfeld, Optical measurement of interplanetary particulates from pioneer 10, JGR 79, 3685-3694, 1974.
- Southworth, R. B. and Z. Sekanina, Physical and dynamical studies of meteors, NASA Contractor Rep. CR - 2316, 1973.
- Weinberg, J. I., The zodiacal light at 5300 Å, Annales d'Astrophys. 27, No. 6, 718-738, 1964.
- Wyatt, S. P. and F. L. Whipple, The Poynting-Robertson effect on meteor orbits, Astrophys. J. 111, 134-141, 1950.
- Zook, H. A. and O. E. Berg, A source of hyperbolic dust particles, Plan. Space Sci. 23, 183-203, 1975.
- Zook, H. A., Hyperbolic cosmic dust: its origin and its astrophysical significance, Plan. Space Sci. (in press).

T A B L E 1

	0°, 1 AU	30°, 1 AU			60°, 1 AU			90°, 1 AU		
		F	E	G	F	E	G	F	E	G
<u>Spinner</u> no sun p.	156	68	64	84	43	44	44	37	40	37
<u>Spinner</u> sun p.	156	119	117	125	108	109	109	106	107	106
<u>3 Ax. Stab.</u> Apex point.	120	53	49	64	33	34	34	29	31	29
<u>3 Ax. Stab.</u> sun point. no sun p.	300	132	122	161	83	84	85	72	76	72
<u>3 Ax. Stab.</u> sun point. sun p.	300	300	300	300	300	300	300	300	300	300

Numbers of events per orbit per year and per 100 cm² sensor surface
=====

F = Fan Model ($\gamma=2.9$)
E = Ellipsoid Model
G = Gauss Model

Figures

Fig. 1 Surfaces of equal number density of dust particles in the interplanetary cloud

n_0 number density in the ecliptic plane at 1 A.U.
from the sun

x solar distance in the ecliptic plane (A.U.)

z height above the ecliptic plane (A.U.)

a) Ellipsoid Model (ref. text case I, $\nu = 1; \gamma = 9$)

b) Gauss Model (case II; $\nu = 1; \gamma = 2.5$)

c) Fan Model (case III; $\nu = 1; \gamma = 3$).

Fig. 2 Brightness of the zodiacal light as seen by a spaceprobe ascending to an altitude of z (A.U.) above the ecliptic plane on a circular orbit of 1 A.U. radius.

S_{10} : Stars of 10th magnitude per square degree

dashed curve: Ellipsoid-model

dots : Gauss-model

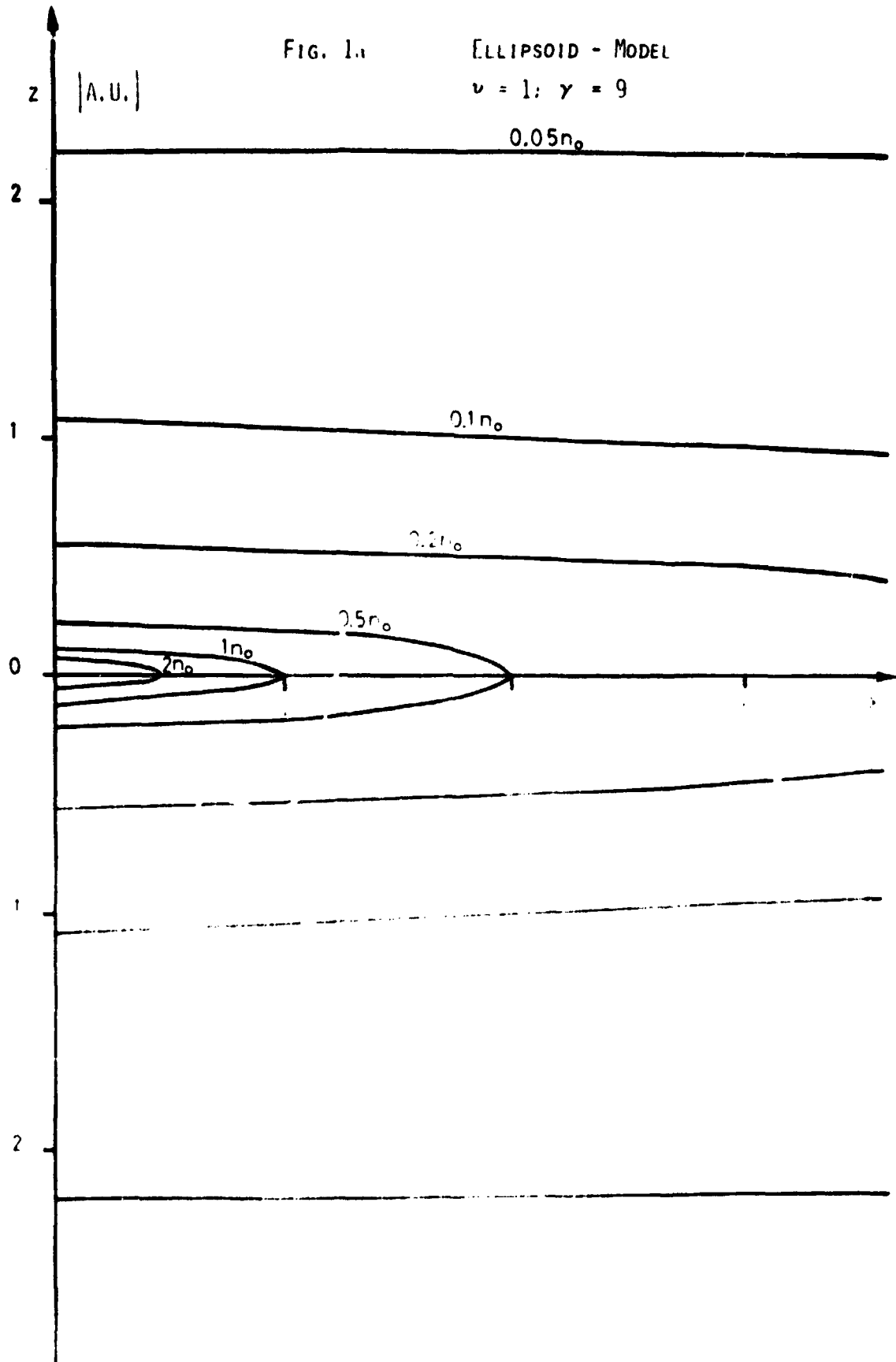
solid curve : Fan-model

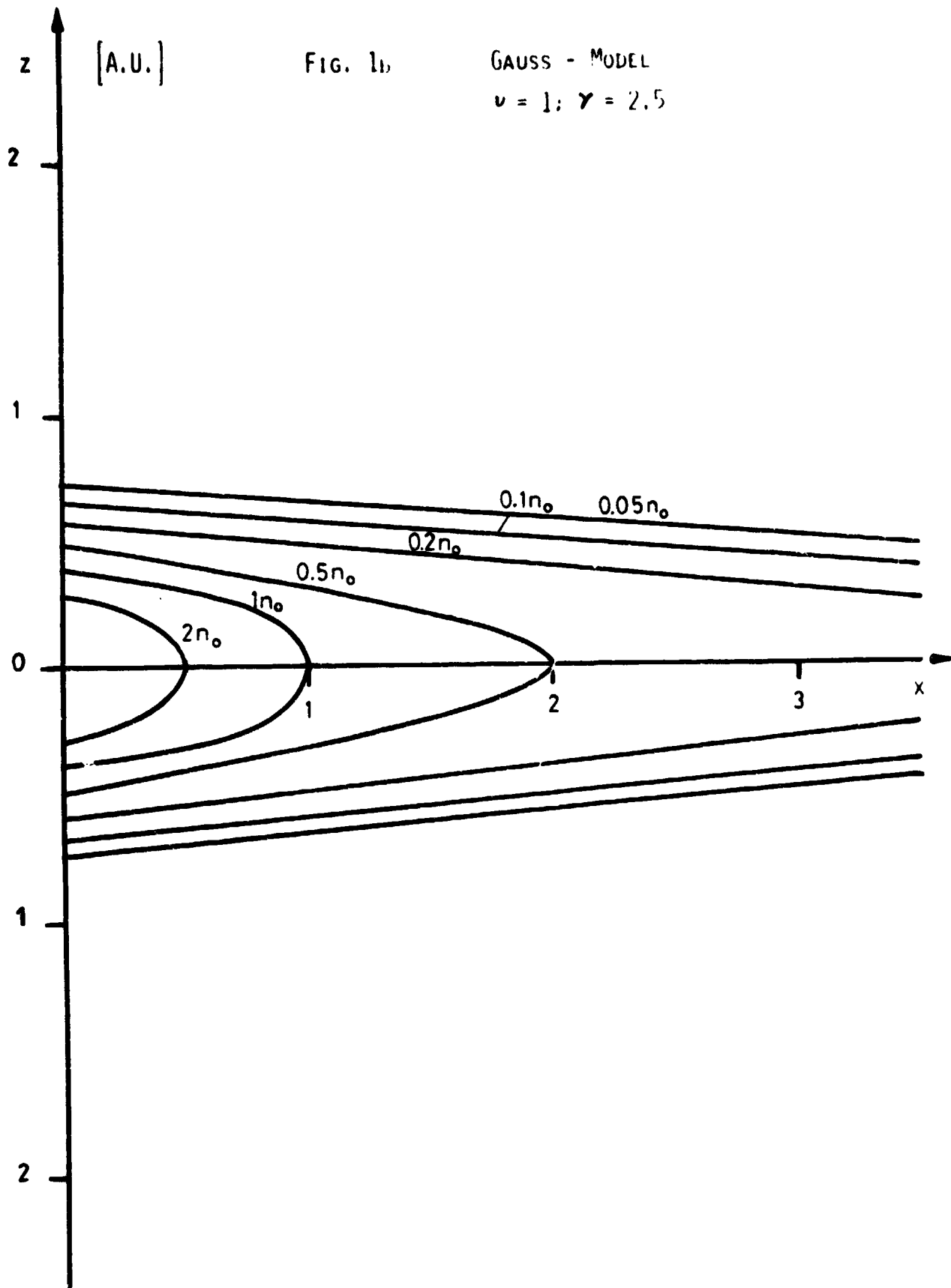
a) direction parallel to the ecliptic plane at right
angle to the solar direction ($\epsilon = 90^\circ$)

b) direction towards the ecliptic pole (+ z direction)

c) direction parallel to the ecliptic plane and
parallel to the earth's sun direction (- x axis).

FIG. 1.1 ELLIPSOID - MODEL
 $\nu = 1; \gamma = 9$





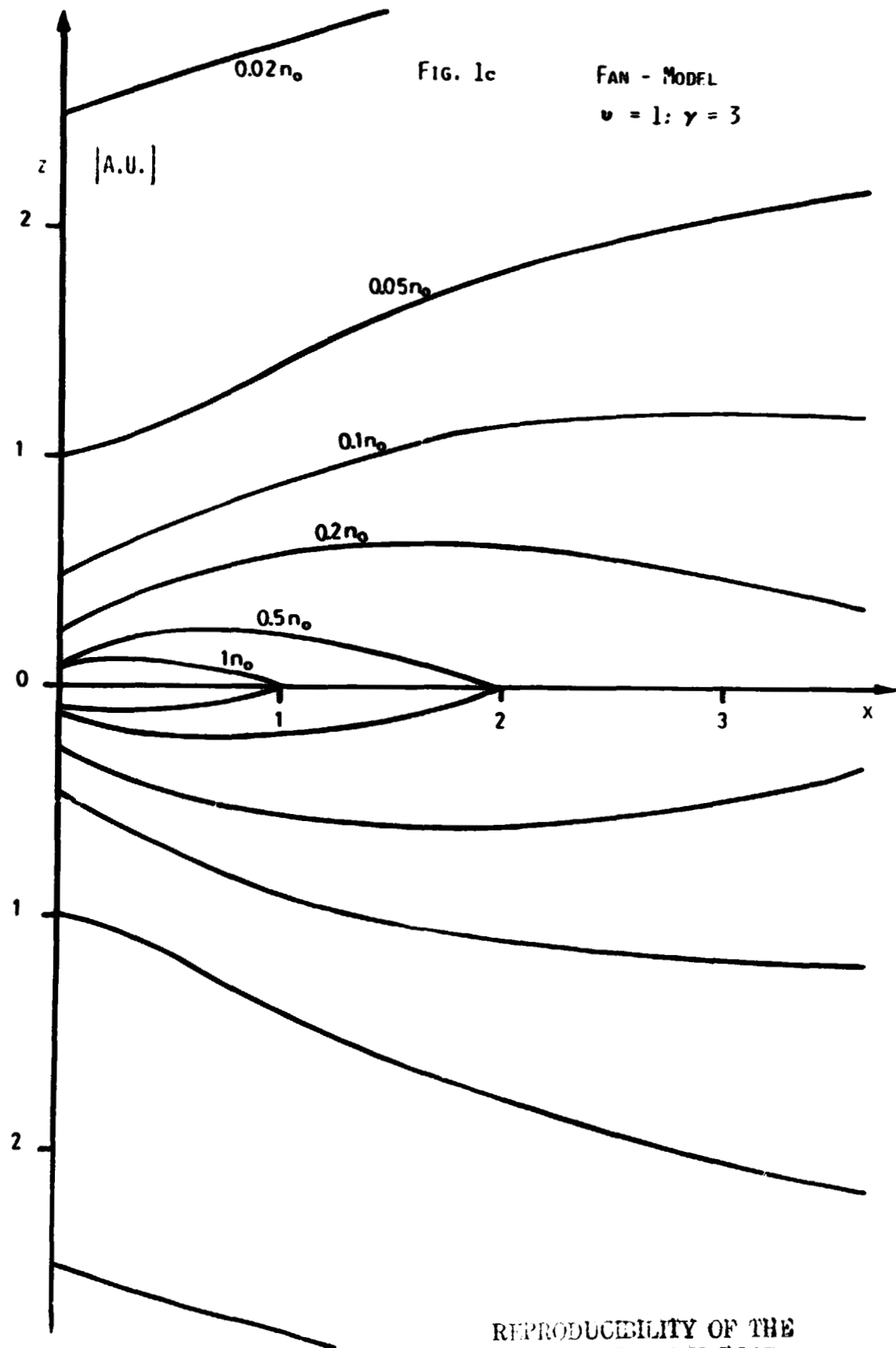


FIG. 1c

FAN - MODEL

$\nu = 1; \gamma = 3$

REPRODUCIBILITY OF THE ORIGINAL PAGE IS POOR

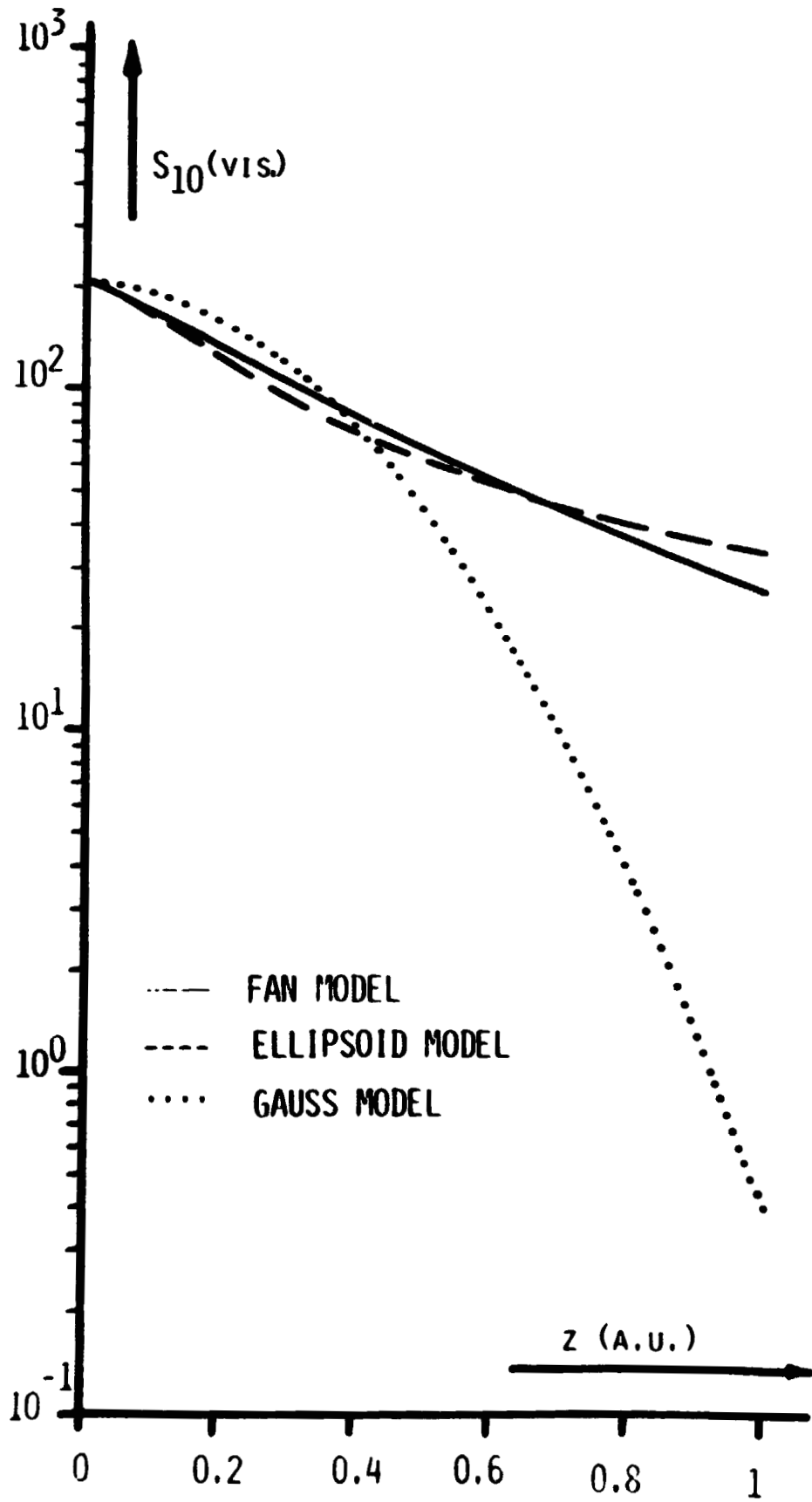


FIG. 2b

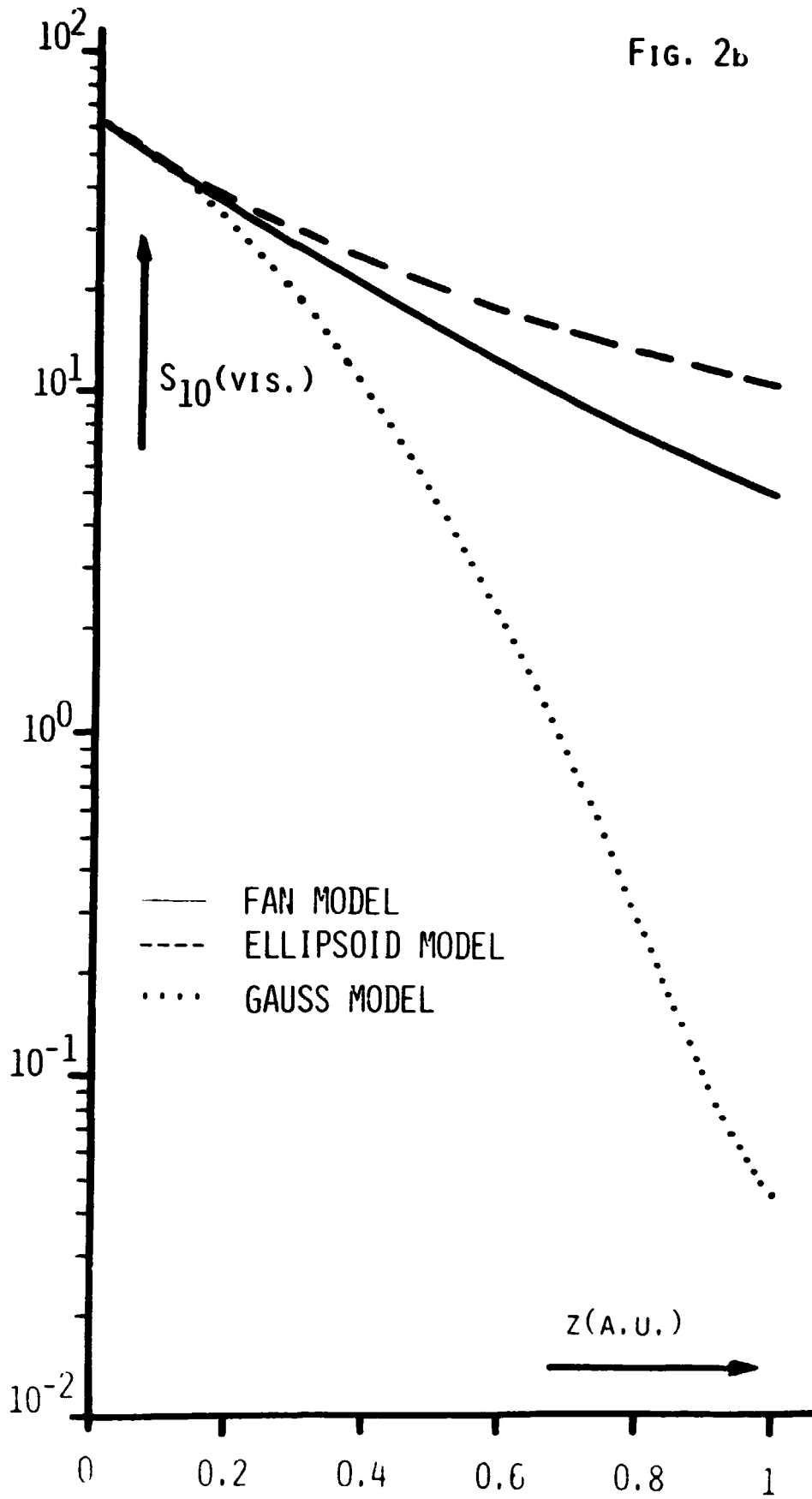
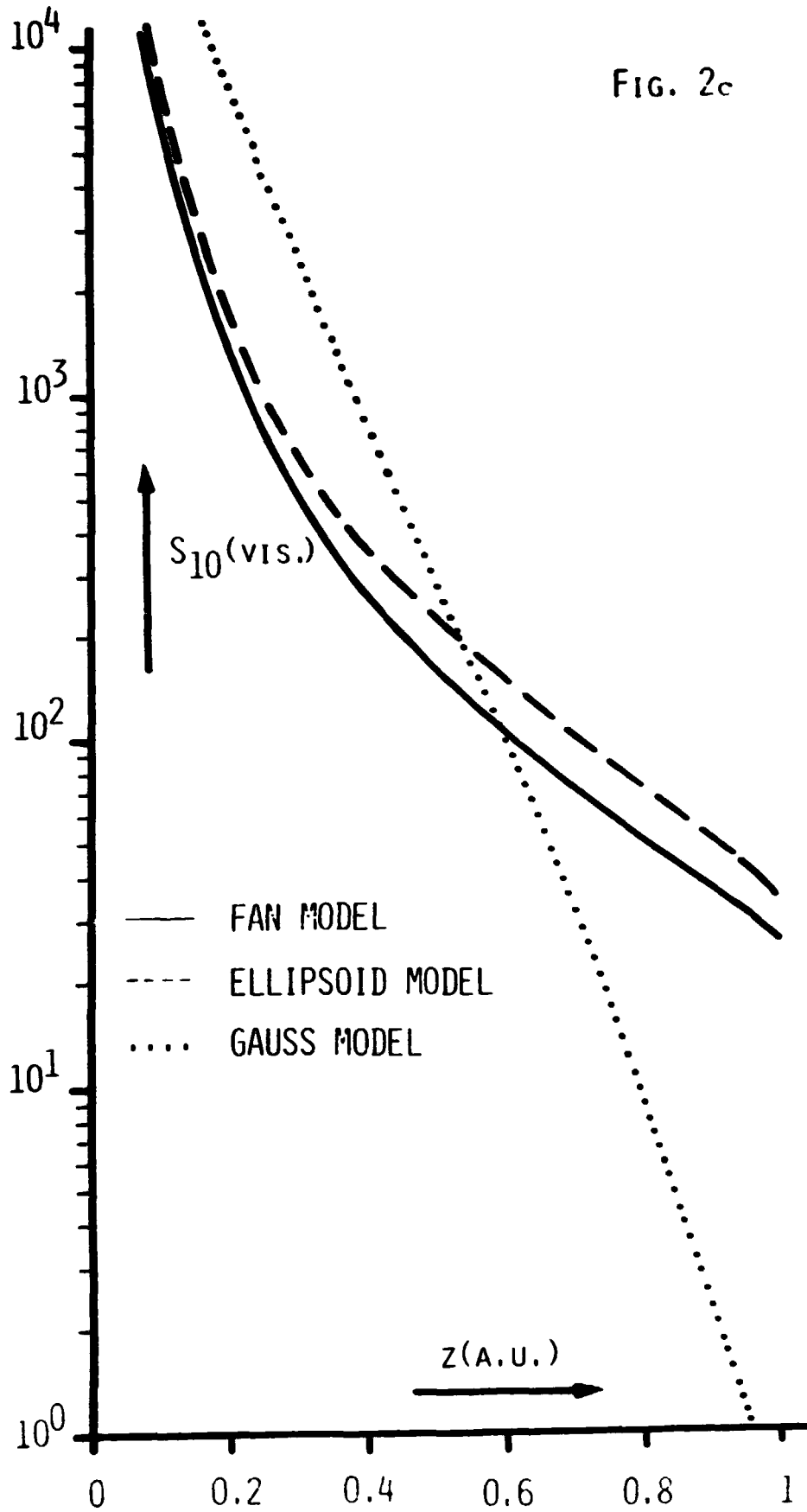


FIG. 2c



N 76-24135

A MEANS OF IN SITU MEASUREMENTS OF NEUTRAL
H AND HE ON AN OUT-OF-THE-ECLIPTIC MISSION

K. C. Hsieh

Department of Physics
University of Arizona
Tucson, Arizona 85721

ABSTRACT

On an out-of-the-ecliptic mission, in situ measurements of densities and temperature of interstellar neutral H and He in the heliosphere should complement observations based on backscattered Lyman-alpha intensities. A means of performing the in situ measurements is briefly described.

The experiments performed by the groups at the University of Paris (Bertaux and Blamont, 1971) and at the University of Colorado (Thomas and Krassa, 1971) have provided us the first glimpse of the presence and the distributions of interstellar neutral H and He in the heliosphere. Like all optical observations, the observations of neutral H and He by backscattered Lyman-alpha photons are indirect and integral in nature. Therefore, their results are constrained by the assumptions one must make about the properties of the solar wind and those of the solar H and He Lyman-alpha emissions as well as the temperature of the interstellar H and He. To complement the optical measurements, in situ direct determination of the densities and temperature of the H and He will be necessary. An out-of-the-ecliptic mission would provide the unique opportunity for such an effort since the relative velocity of the sun to the interstellar medium points out of the ecliptic.

The necessary in situ measurements can be performed with an instrument of low power (1 W), low mass (< 3 kg) and single-particle counting capability such as the field-ionization neutral detector (FIND) being developed at the University of Arizona (Curtis et al., 1975). Figure 1 illustrates the principal parts of FIND. The ionization tips, the grid and the surface-barrier Si detector are encased in a chamber with an entrance aperture. Neutral H and He enter the chamber and as they reach the vicinity of the tips, they are field-ionized to become H^+ and He^+ , respectively. These +1 ions are immediately accelerated towards the detector and their electrical signals analyzed.

Although all the ions arrive at the detector with essentially identical kinetic energies acquired in acceleration, He^+ , being more

massive, will interact with the crystal lattice of the detector more and thus provide a smaller electrical signal than an H^+ of same energy. Figure 2 is a composite plot showing that the He^+ peak is shifted by 2.8 KeV from the H^+ peak which appears at 26 keV, corresponding to the accelerating potential of 26 kV. We note that each pulse-height distribution is gaussian and has well defined peak position and FWHM. Therefore, using only one detector and one pulse-height analyzer the two species can be separated.

Our laboratory results also indicate that with a bundle of 200 needles at +26 kV facing a 1 cm^2 detector at a distance of 1 cm, sensitivities of 3×10^{-7} counts sec^{-1} per unit flux (1 unit flux = $1 \text{ cm}^{-2} \text{ sec}^{-1}$) for H and 4×10^{-8} for He in the same units can be attained. Assuming an H flux of $10^4 \text{ cm}^{-2} \text{ sec}^{-1}$, e.g., $n = 0.01 \text{ cm}^{-3}$ and $v = 10 \text{ km sec}^{-1}$, a detector background of $1.4 \times 10^{-2} E^{-1.2} \text{ sec}^{-1} \text{ keV}^{-1}$ (G. Gloeckler, private communication, 1974) and an FWHM of 3 keV, then H signals can be well separated from the background in one day's accumulation. (Actual background can be determined in flight by turning off the high voltage supply to the ionization tips.) Figure 3 is a computer simulation based on the above assumptions. In addition to H, He of three different relative abundances are also included. The varied $n(He)/n(H)$ are due to the different values the parameter μ might take (see review by Axford, 1972). A least-square fit of two gaussian distributions of known peak positions and FWHM's to any of the three curves shown in Figure 3 will yield the corresponding $n(H)$, $n(He)$ and $n(He)/n(H)$.

The above description of FIND leaves little doubt that in situ determination of neutral H and He concentrations can be performed. In addition, if the aperture of FIND scans the part of the sky surrounding the direction of maximum flux, the angular distribution of the neutral flux would then

be a measure of the temperature of the neutral gas at the point of observation. With an instrument such as FIND complementing a Lyman-alpha spectrometer on a spacecraft that covers large heliocentric distances and latitudes, the local interstellar medium and its interactions with the solar wind can be examined fully.

ACKNOWLEDGEMENT: For the work on FIND I thank my colleagues C. C. Curtis, C. Y. Fan and also L. W. Swanson at the Oregon Graduate Center. The work on FIND is supported by NASA grant NGR 03-002-107 and my travel to this Symposium is made possible by the support of the University of Arizona.

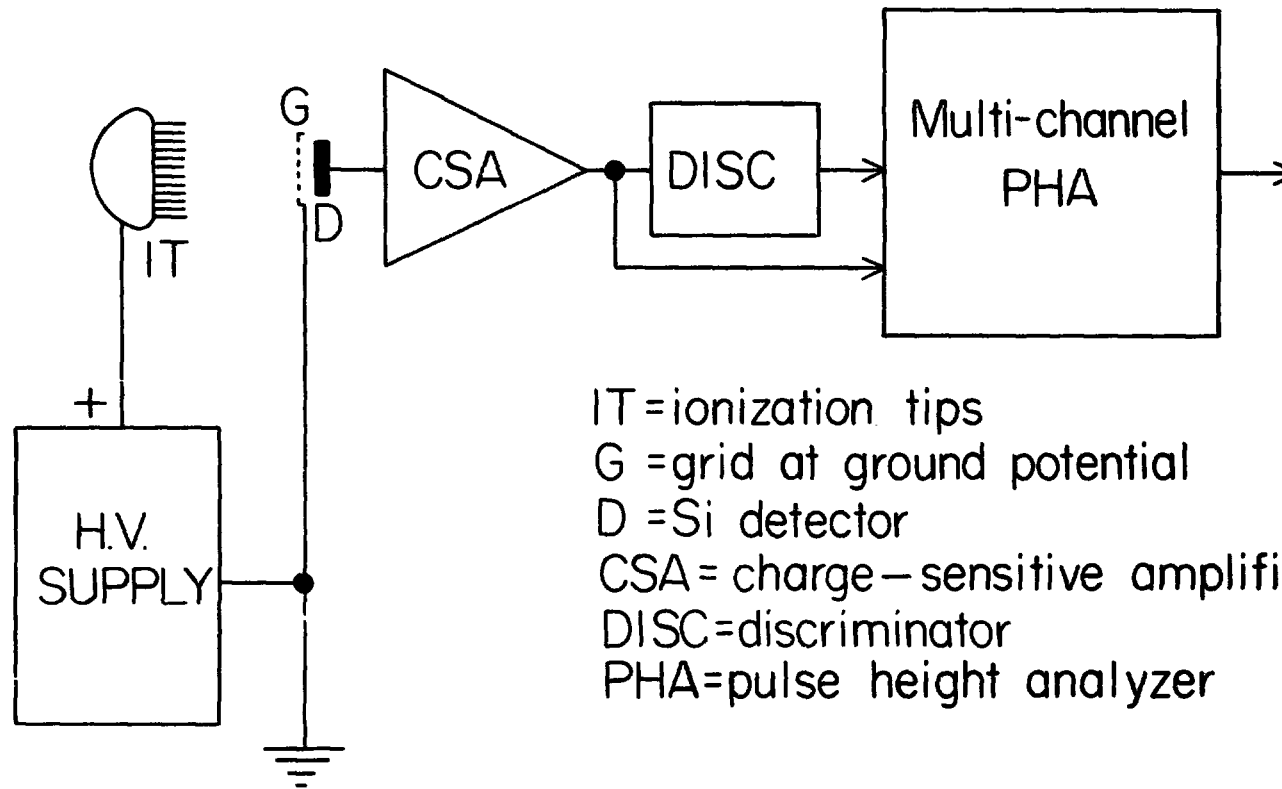
REFERENCES

- Bertaux, J. L., and J. E. Blamont, Evidence for a Source of an Extra-terrestrial Hydrogen Lyman-alpha Emission: the Interstellar Wind, *Astron. & Astrophys.*, 17, 200-217, 1971.
- Curtis, C. C., K. C. Hsieh, C. Y. Fan, and L. W. Swanson, A Field-Ionization Neutral Detector: FIND, Proceedings of the 14th International Cosmic Ray Conference, T6-1, 1975.
- Thomas, G. E., and R. F. Krassa, OG05 Measurements of the Lyman Alpha Sky Background, *Astron. & Astrophys.* 17, 218-233, 1971.

FIGURE CAPTIONS

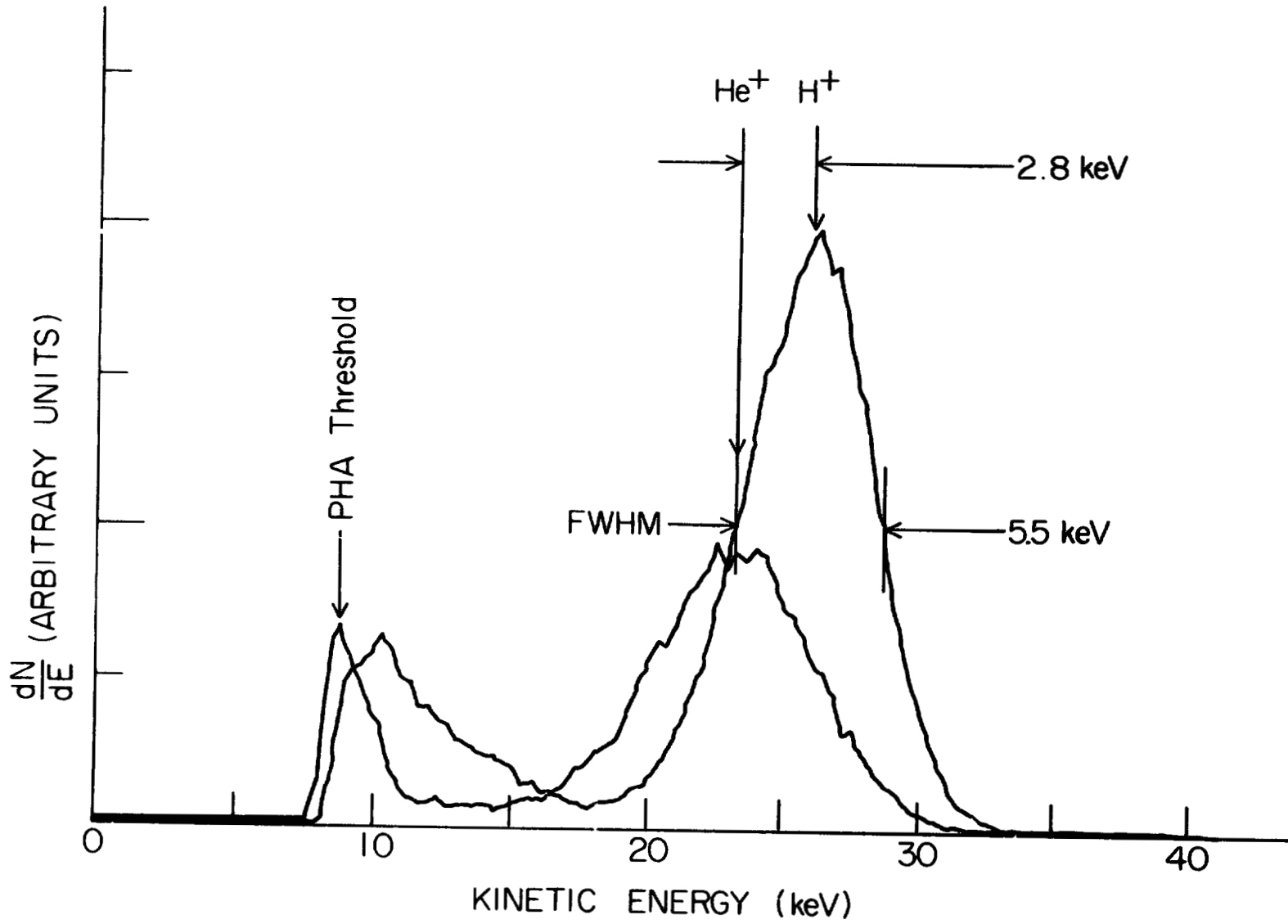
- Figure 1. An over-simplified diagram of FIND. For actual space missions, the ionization tips and the detector assembly should be protected from low energy charged particles by the use of repelling grids at the entrance aperture and from γ -rays and secondary particles by the use of an anti-coincidence guard counter immediately behind and surrounding the ion detector.
- Figure 2. Laboratory results showing the difference in the pulse-height distributions of H^+ and He^+ signals by a 2.8 keV shift. Both ion species have an average kinetic energy of 26 keV. The noise of the detector is 5.5 keV (FWHM).
- Figure 3. Predicted pulse-height distributions of an H flux of $1 \times 10^4 \text{ cm}^{-2} \text{ sec}^{-1}$ and He fluxes of 10^3 , 10^4 and $10^5 \text{ cm}^{-2} \text{ sec}^{-1}$ as seen in one day's accumulation by a FIND having an accelerating potential of 26 kV, a detector noise of 3 keV (FWHM) and a background following the distribution $1.4 \times 10^{-2} E^{-1.2} \text{ sec}^{-1} \text{ keV}^{-1}$. The sensitivities to H and He used in this calculation are $3 \times 10^{-7} \text{ counts sec}^{-1}$ per unit flux and $4 \times 10^{-8} \text{ counts sec}^{-1}$ per unit flux, respectively.

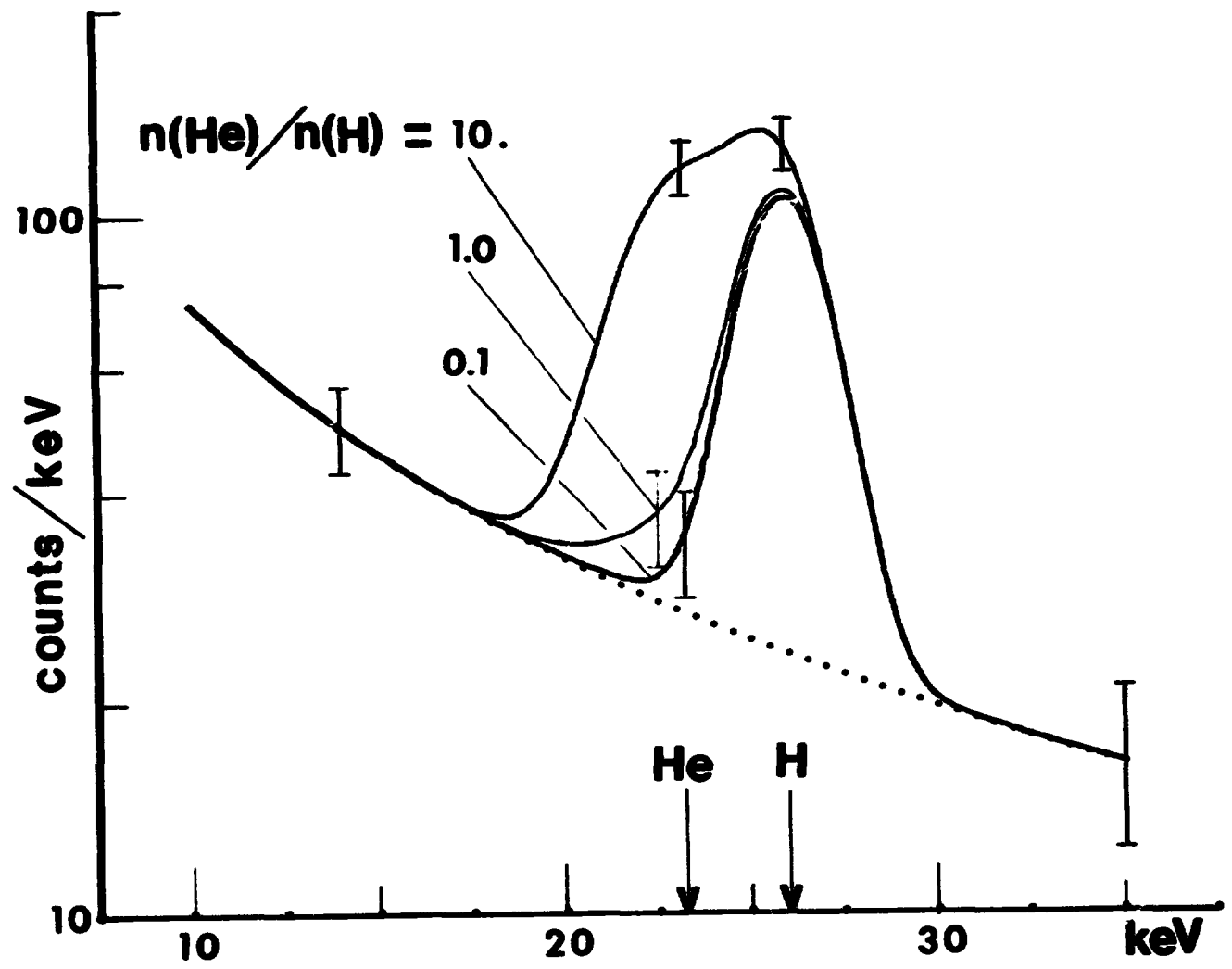
SCHMATIC DIAGRAM
FIND:Field-Ionization Neutral Detector



IT=ionization tips
G =grid at ground potential
D =Si detector
CSA= charge-sensitive amplifier
DISC=discriminator
PHA=pulse height analyzer

REPRODUCIBILITY OF THE
IMAGE IS POOR





APPENDIX A

THE PROGRAM

A SYMPOSIUM ON THE STUDY OF THE SUN
AND INTERPLANETARY MEDIUM IN THREE DIMENSIONS

GODDARD SPACE FLIGHT CENTER

May 15-16, 1975

THE PROGRAM

P. A. Sturrock, Stanford Solar Structure and Activity:
Do We Need a New Viewpoint?

MISSION OPTIONS

J. A. Simpson, Chairman

J. A. Simpson, U. of Chicago A Preview of Mission Alternatives and Their Scientific Opportunities

D. H. Herman, NASA/Hdqtrs. . . . NASA's Position on an Out-of-the-Ecliptic Mission

G. Haskell, ESRO/Hdqtrs. . . . ESRO's Position on an Out-of-the-Ecliptic Mission

H. Matthews, E. Tindle and L. Manning, NASA/Ames Jupiter Swing-By Out-of-the-Ecliptic Missions

M. Schuyer, ESTEC A Possible Approach for Low-Cost Jupiter Swing-By Out-of-the-Ecliptic Spacecraft

J. H. Duxbury, JPL Low-Cost Missions for the Future

SOLAR PHYSICS

A. F. Timothy, Chairman

R. W. Noyes, SAO Solar EUV/X-ray Studies

- G. A. Newkirk, HAO Solar Magnetic Fields
- J. D. Bohlin, R. A. Howard Tentative Ideas About Coronograph Instrumentation
and M. J. Koomen, NRL
- E. C. Roelof, APL Coronal Structure Inferred
from Interplanetary Field and
Particle Observations
- A. Riddle, U. of Colorado The Need for Out-of-the-
Ecliptic Radio Observations
- J. L. Steinberg, Meudon Obs. . . . Three-Dimensional Solar Radio
Astronomy

SOLAR WIND

A. J. Lazarus, Chairman

- B. J. Rickett, UCSD The Solar Wind Velocity in
1972-1974 as Measured by Radio
Scintillations
- J. C. Brandt, NASA/GSFC Latitudinal Properties of the
Solar Wind from Studies of Ion
Comet Tails
- A. J. Hundhausen, HAO Solar Wind Dynamics
- W. C. Feldman, LASL Solar Wind Chemistry
- M. D. Montgomery, LASL Solar Wind Plasma Processes

INTERPLANETARY MAGNETIC FIELDS

P. Hedgecock, Chairman

- L. F. Burlaga and N. F. Ness, . . . The Large-Scale Interplanetary
NASA/GSFC Magnetic Field
- H. Volk, MPI/Heidelberg The Microstructure of the Field

- G. L. Siscoe, MIT Three-Dimensional Aspects of
Discontinuities, Shocks and
Fluctuations in the Heliosphere
- E. J. Smith, JPL Scientific Objectives Associ-
ated With the Jupiter Swing-By

COSMIC RAYS

R. Vogt, Chairman

- K. A. Anderson, UCB Solar Cosmic Rays
- G. Wibberenz, Kiel U. Coronal Transport and Storage
- J. R. Jokipii, U. of Arizona . . . Cosmic-Ray Propagation
- J. J. Quenby, Imperial College . . Galactic Cosmic-Ray Modulation

DUST/ZODIACAL LIGHT/
INTERSTELLAR GAS

O. Berg, Chairman

- M. S. Hanner, SUNYA Optical Measurements of Inter-
planetary Dust
- H. Fechtig, MPI/Heidelberg . . . Direct Measurements of Inter-
planetary Dust
- J. Blamont, CNES/Paris Interstellar Neutral Gas

APPENDIX B

ATTENDEES

**A SYMPOSIUM ON THE STUDY OF THE SUN
AND INTERPLANETARY MEDIUM IN THREE DIMENSIONS**

**Goddard Space Flight Center
May 15-16, 1975**

List of Participants

M. M. Abbas Code 692 NASA/GSFC Greenbelt, MD 20771	Kenneth L. Atkins Mail Stop 156-220 Jet Propulsion Lab. Pasadena, CA	John Belcher 37-695 M.I.T. Cambridge, Mass. 02139
Mario H. Acuna Code 692 NASA/GSFC Greenbelt, MD 20771	Siegfried Auer Code 923 NASA/GSFC Greenbelt, MD 20771	Otto E. Berg Code 672 NASA/GSFC Greenbelt, MD 20771
J. K. Alexander Code 693 NASA/GSFC Greenbelt, MD 20771	W. I. Axford Max Planck Institut 3411 Lindau/Harz West Germany	Dave Bertsch Code 662 NASA/GSFC Greenbelt, MD 20771
C. Alissandrakis Astronomy Program Univ. of Maryland College Park, MD 20742	Taeil Bai Code 660 NASA/GSFC Greenbelt, MD 20771	T. J. Birmingham Code 602 NASA/GSFC Greenbelt, MD 20771
James L. Allen 1237-10th St., N.W. Washington, DC 20001	V.K. Balasubrahmanyan Code 661 NASA/GSFC Greenbelt, MD 20771	J. B. Blake Aerospace Corp. 120/1825 Box 95085 Los Angeles, CA 90045
Jose Alvarez Langley Research Center Mail Stop 323 Hampton, VA 23665	Sam Bame Mail Stop 436 Los Alamos Scientific Lab. Los Alamos, NM 87544	J. Blamont CNES, 129 rue de l'Universite Paris 7e FRANCE
S.P.S. Anand Code 680 NASA/GSFC Greenbelt, MD 20771	E. Barouch Code 690 NASA/GSFC Greenbelt, MD 20771	J. D. Bohlin Code 61418 Naval Research Laboratory Washington, DC 20375
Kinsey A. Anderson Space Sciences Lab. Univ. of California Berkeley, CA 94720	S. J. Bauer Code 600 NASA/GSFC Greenbelt, MD 20771	Carl O. Bostrom Applied Physics Lab. Johns Hopkins Univ. 8621 Georgia Avenue Silver Spring, MD 20910
Thomas P. Armstrong Dept. of Physics Univ. of Kansas Lawrence, Kansas 66045	K. W. Behannon Code 692 NASA/GSFC Greenbelt, MD 20771	

List of Participants (continued)

J. Brandt Code 680 NASA/GSFC Greenbelt, MD 20771	Carol Jo Crannell Code 682 NASA/GSFC Greenbelt, MD 20771	Igor J. Eberstein Code 912 NASA/GSFC Greenbelt, MD 20771
Herbert S. Bridge 37-241 M.I.T. Cambridge, Mass. 02139	Nancy Crooker Bldg. 37-415 M.I.T. Cambridge, Mass. 02139	John A. Eddy High Altitude Observatory Box 3000 Boulder, CO 80303
Thomas E. Burke Code SL NASA Headquarters Washington, DC 20546	G. Dalu Code 911 NASA/GSFC Greenbelt, MD 20771	Robert Edelson M.S. 114-B13 Jet Propulsion Lab. 4800 Oak Grove Dr. Pasadena, CA 91103
David P. Cauffman Code SG NASA Headquarters Washington, DC 20546	Ulrich Denskat Institut fur Geophysik der T U Braunschweig D 33 Braunschweig Mendelssohusk 1A Germany	Joseph Fainberg Code 693 NASA/GSFC Greenbelt, MD 20771
Mac Chapman TRW 01/1010 1 Space Park Redondo Beach, CA 90278	Upendra D. Desai Code 663 NASA/GSFC Greenbelt, MD 20771	D. H. Fairfield Code 692 NASA/GSFC Greenbelt, MD 20771
Gloria Chen 11 Min-Der New Village Tah-Si, Tan-Yuan Taiwan Rep. of China	Murray Dryer Space Environment Lab. NOAA-ERL Boulder, CO 80302	C. Y. Fan Max Planck Institut 8046 Garching b Munchen WEST GERMANY
Thomas L. Cline Code 661 NASA/GSFC Greenbelt, MD 20771	Maurice Dubin Code 680 NASA/GSFC Greenbelt, MD 20771	Dr. Hugo Fechtig Max Planck Institut 69 Heidelberg 1 Postfach 10 3980 WEST GERMANY
K. D. Cole Code 621 NASA/GSFC Greenbelt, MD 20771	S. P. Duggal Bartol Res. Foundation Swarthmore, PA	William C. Feldman Los Alamos Scientific Lab. Group P-4, Box 1663 Los Alamos, NM 87544
William A. Coles University of California La Jolla, CA 92037	John H. Duxbury 4800 Oak Grove Drive Pasadena, CA 91103	Joseph F. Fennell Aerospace Corp. 120/1813, Box 92957 Los Angeles, CA 90009
G. Colombo Harvard Smithsonian Center 60 Garden Street Cambridge, Mass. 02138	Clive S. Dyer Code 682 NASA/GSFC Greenbelt, MD 20771	L. A. Fisk Code 660 NASA/GSFC Greenbelt, MD 20771

List of Participants (continued)

Richard J. Fitzenreiter
Code 693
NASA/GSFC
Greenbelt, MD 20771

Miriam A. Forman
State Univ. of New York
Stony Brook, NY 11794

L. Friedman
Jet Propulsion Lab.
4800 Oak Grove Drive
Pasadena, CA 91103

J. F. Friichtenicht
TRW Systems
1 Space Park
Redondo Beach, CA 90278

George Gloeckler
Dept. Physics & Astronomy
Univ. of Maryland SS 1215A
College Park, MD 20742

Robert E. Gold
APL/JHU
8621 Georgia Ave.
Silver Spring, MD 20910

M. L. Goldstein
Code 692
NASA/GSFC
Greenbelt, MD 20771

Douglas E. Greiner
Lawrence Berkeley Lab.
50-245
Berkeley, CA 94720

Martha S. Hanner
Space Astronomy Lab.
Executive Park East
Stuyvesant Plaza
Albany, NY 12203

Richard Hart
Space Science Board
Natl. Academy Science
2101 Constitution Avenue
Washington, DC 20418

George Haskell
ESRO Headquarters
114 Ave. Charles DeGaulle
92522 Neuill sur-Seine
Paris, FRANCE

Mike Hauser
Code 661
NASA/GSFC
Greenbelt, MD 20771

P. C. Hedgecock
Physics Dept.
Imperial College
London SW7
ENGLAND

J. C. Henoux
Observatoire de Paris
92190 Meudon
FRANCE

Daniel H. Herman
Code SL
NASA Headquarters
Washington, DC 20546

Noel W. Himmers
Code S, NASA Headquarters
400 Maryland Ave.
Washington, DC 20546

V. D. Hopper
Physics (RAAF) Dept.
University of Melbourne
Victoria
AUSTRALIA 3052

John Hornstein
Code 693
NASA/GSFC
Greenbelt, MD 20771

Dietrich Hovestadt
Max Planck Institut
F. Extra-Terr. Physik
8046 Garching
Munich
GERMANY

Robert F. Howard
Hale Observatories
813 Santa Barbara St.
Pasadena, CA 91103

Russell A. Howard
Code 7141 H
Naval Research Lab.
Washington, DC 20375

K. C. Hsieh
Dept. of Physics
Univ. of Arizona
Tucson, AZ 85721

A. J. Hundhansen
High Altitude Observatory
Boulder, CO 80302

Takesi Iijima
Applied Physics Lab.
Johns Hopkins Univ.
8621 Georgia Ave.
Silver Spring, MD 20910

Devrie Intriligator
171 Stauffer Hall Sci.
Physics Dept.
Univ. So. Calif.
University Park
Los Angeles, CA 90007

F. M. Ipavich
Dept. Physics & Astro.
Univ. of Maryland
College Park, MD 20742

Bruno J. Jambor
Martin Marietta Corp.
PO Box 179
Denver, CO 80201

Jacque Johnson
Hughes Aircraft Co.
Space & Commun. Group
El Segundo, CA

J. R. Jokipii
Dept. Interplanetary Sci.
Univ. of Arizona
Tucson, AZ 85721

List of Participants (continued)

Frank C. Jones
Code 602
NASA/GSFC
Greenbelt, MD 20771

Tom Kaiser
Code 602
NASA/GSFC
Greenbelt, MD 20771

S. O. Kastner
Code 682
NASA/GSFC
Greenbelt, MD 20771

E. Keppler
Max Planck Institut
Lindau
3411 Lindau/Harz
WEST GERMANY

Joseph H. King
Code 601
NASA/GSFC
Greenbelt, MD 20771

Alexander J. Klimas
Code 692
NASA/GSFC
Greenbelt, MD 20771

Martin J. Koomen
Code 7141
Naval Research Lab.
Washington, DC 20375

R. S. Kraemer
Code SL
NASA Headquarters
Washington, DC 20546

A. S. Krieger
American Science and
Engineering, Inc.
955 Massachusetts Ave.
Cambridge, Mass. 02139

S. M. Krimigis
Applied Phys. Lab,
Johns Hopkins Univ.
Silver Spring, MD 20910

M. R. Kundu
Astronomy Program
Univ. of Maryland
College Park, MD 20742

L. J. Lanzerotti
Bell Laboratories
Murray Hill, NJ 07974

Howard Laster
Dept. Physics & Astro.
Univ. of Maryland
College Park, MD 20742

Alan Lazarus
Code SGP
NASA Headquarters
Washington, DC 20546

Lou-Chuang Lee
Theoretical Studies
NASA/GSFC
Greenbelt, MD 20771

Martin A. Lee
Physics Dept.
Box 1105
Washington Univ.
St. Louis, MO 63130

Joseph Lemaire
Code 692
NASA/GSFC
Greenbelt, MD 20771

Ronald P. Lepping
Code 692.3
NASA/GSFC
Greenbelt, MD 20771

Eugene H. Levy
Bartol Res. Foundation
Swarthmore, PA 19081

Jerry Lezniak
Dept. Physics
Univ. N. H.
Durham, NH 03824

Don Lind
NASA/JSC
Code TE
Houston, TX 77058

Sou-Yang Liu
Astronomy Program
Univ. of Maryland
College Park, MD 20742

John A. Lockwood
Physics Dept.
Univ. of New Hampshire
Durham, NH 03824

Kaichi Maeda
Code 602
NASA/GSFC
Greenbelt, MD 20771

Ron Maehl
Code 661
NASA/GSFC
Greenbelt, MD 20771

Harriet H. Malitson
Code 693
NASA/GSFC
Greenbelt, MD 20771

H. F. Matthews
1998 Colleen Dr.
Los Altos, CA 94022

Billy M. McCormac
Lockheed (Dept. 52-60)
3251 Hanover
Palo Alto, CA 94304

F. B. McDonald
Code 660
NASA/GSFC
Greenbelt, MD 20771

Richard W. McEntire
Applied Physics Lab/J.H.U.
8621 Georgia Ave.
Silver Spring, MD 20910

List of Participants (continued)

Rosalind B. Mendell
Dept. of Physics
N.Y.U.
4 Washington Place
New York, NY 10003

L. H. Meredith
Code 100
NASA/GSFC
Greenbelt, MD 20771

Peter Meyer
Univ. of Chicago
Enrico Fermi Institute/IASR
933 E. 56th Street
Chicago, IL 60637

A. G. Michalitsanos
Code 683
NASA/GSFC
Greenbelt, MD 20771

M. A. Mitz
Code SL
NASA Headquarters
Washington, DC 20546

M. Montgomery
Los Alamos Sci. Lab.
Los Alamos, NM 87544

Dermott Mullas
Bartol Res. Foundation
Swarthmore, PA 19081

N. F. Ness
Code 690
NASA/GSFC
Greenbelt, MD 20771

Werner Neupert
Code 682
NASA/GSFC
Greenbelt, MD 20771

Gordon Newkirk, Jr.
High Altitude Observatory
Boulder, CO 80302

T. G. Northrop
Code 602
NASA/GSFC
Greenbelt, MD 20771

Robert Noyes
Center for Astrophysics
60 Garden Street
Cambridge, Mass. 02138

Robert R. Nunamaker
Pioneer Project
MS 244-8
NASA/Ames Research Center
Moffett Field, CA 94035

T. Obayashi
Code 601
NASA/GSFC
Greenbelt, MD 20771

Joseph J. O'Gallagher
Dept. Physics & Astron.
Univ. of Maryland
College Park, MD 20742

J. F. Ormes
Code 661
NASA/GSFC
Greenbelt, MD 20771

Stephen Paddack
Code 405.3
NASA/GSFC
Greenbelt, MD 20771

D. Edgar Page
Space Science Dept.
ESTEC
Domeinweg, Noordwijk
NETHERLANDS

S. I. Pai
Inst. for Fluid Dy. &
Applied Math.
Univ. of Maryland
College Park, MD 20742

Andy Park
Hughes Aircraft Co.
Space & Commun. Group
El Segundo, CA

Carl D. Parker
3410 Duraleigh Road
Raleigh, NC 27612

E. N. Parker
Laboratory for Astrophysics
and Space Research
Univ. of Chicago
933 E. 56th Street
Chicago, IL 60637

V. L. Patel
Dept. of Physics
Univ. of Denver
Denver, CO 80210

G. A. Paulikas
Aerospace Corp.
P.O. Box 92957
Los Angeles, CA 90009

Dennis Peacock
National Science Foundation
1800 G St., N.W.
Washington, DC

Charles Pellerin
Code 662
NASA/GSFC
Greenbelt, MD 20771

Dr. Peytremann
ESRO Headquarters
114 Ave. Charles DeGaulle
92522 Neuilly-sur-Seine
Paris, FRANCE

Monique Pick
D.A.S.O.P. Radioastronomy
Meudon Observatory
Meudon 92190
FRANCE

George F. Pieper
Code 600
NASA/GSFC
Greenbelt, MD 20771

Martin A. Pomerantz
Bartol Research Foundation
Swarthmore, PA 19081

J. Puget
Code 641
NASA/GSFC
Greenbelt, MD 20771

List of Participants (continued)

J. J. Quenby
Physics Dept.
Imperial College
Prince Consort Road
London S.W. 7
UNITED KINGDOM

John P. Rahlf
Bldg. 01, Rm. 1050
TRW Systems
One Space Park
Redondo Beach, CA 90278

I. S. Rasool
Code AAD-1
NASA Headquarters
400 Maryland Ave.
Washington, DC 20546

Don Reames
Code 662
NASA/GSFC
Greenbelt, MD 20771

John W. Rhee
Code 672
NASA/GSFC
Greenbelt, MD 20771

Barney J. Rickett
Applied Physics & Info.
Science Dept.
Univ. Calif. San Diego
P.O. Box 109
La Jolla, CA 92037

Anthony C. Riddle
Dept. Astrogeophysics
Univ. of Colorado
Boulder, CO 80302

Paul Rodriguez
Univ. of Iowa
Iowa City, Iowa

E. C. Roelof
Applied Physics Lab./J.H.U.
8621 Georgia Avenue
Silver Spring, MD 20911

Edward D. Rothe
Code 683
NASA/GSFC
Greenbelt, MD 20771

Richard Rothschild
Code 661
NASA/GSFC
Greenbelt, MD 20771

Pamela Rothwell
Physics Dept.
Univ. of Southampton
Southampton SO95NH
ENGLAND

C. T. Russell
Inst. of Geophysics
Univ. of California
Los Angeles, CA 90024

Charles Ryter
Code 660
NASA/GSFC
Greenbelt, MD 20771

Jack Saba
Astronomy Program
Univ. of Maryland
College Park, MD 20740

Kunitomo Sakurai
Inst. Fluid Dynamics &
Applied Math.
Univ. of Maryland
College Park, MD 20742

Emmanuel T. Sarris
Applied Physics Lab./J.H.U.
8621 Georgia Avenue
Silver Spring, MD 20910

Frank Scherb
Physics Dept.
Univ. of Wisconsin
Madison, Wis. 53706

E. R. Schmerling
Code SG
NASA Headquarters
Washington, DC 20546

Wolfgang Schmidt
Code 661
NASA/GSFC
Greenbelt, MD 20771

Maurice Schuyer
ESTEC
Noordwyk
THE NETHERLANDS

Richard K. Sciambi
Dept. of Physics
Univ. of Maryland
College Park, MD 20742

Art Serlemitsos
Code 661
NASA/GSFC
Greenbelt, MD 20771

M. M. Shapiro
Code 7020
Naval Research Laboratory
Washington, DC 20375

J. A. Simpson
Enrico Fermi Institute
Univ. of Chicago
Chicago, IL 60637

George L. Siscoe
37-651
M. I. T.
Cambridge, Mass. 02139

Edward J. Smith
183-401
Jet Propulsion Lab.
4800 Oak Grove Drive
Pasadena, CA 91103

Henry Smith
Code SS
NASA Headquarters
Washington, DC 20546

Robert Alan Smith
Code 602
NASA/GSFC
Greenbelt, MD 20771

List of Participants (continued)

William C. Snoddy
Code ES-11
NASA/Marshall Space Flt. Ctr.
Alabama 35812

Robert K. Soberman
General Electric Space
Sciences Lab.
POB 8555 (M9161)
Philadelphia, PA 19101

Jean-Louis Steinberg
Observatoire De Meudon
92220 Meudon
FRANCE

David P. Stern
Code 602
NASA/GSFC
Greenbelt, MD 20771

Edward Stone
Calif. Inst. of Technology
Downs Lab. of Physics 220-47
Pasadena, CA 91125

L. R. O. Storey
C.R.P.E./C.N.R.S.
45 Orleans-La-Source
FRANCE

Peter A. Sturrock
Institute for Plasma Research
Stanford University
Stanford, CA 94305

Linda Ma Sung
Code 664
NASA/GSFC
Greenbelt, MD 20771

Leif Svalgaard
Stanford University
Stanford, CA 94305

Bonnard Teegarden
Code 661
NASA/GSFC
Greenbelt, MD 20771

Adrienne F. Timothy
Code SG
NASA Headquarters
Washington, DC 20546

R. Tousey
Code 7140
Naval Research Lab.
Washington, DC 20375

James Trainor
Code 663
NASA/GSFC
Greenbelt, MD 20771

S. K. Trehan
Code 680
NASA/GSFC
Greenbelt, MD 20771

Will Turk
Hughes Aircraft
P.O. Box 92919
Los Angeles, CA 90009

M. Van Hollebeke
Code 660
NASA/GSFC
Greenbelt, MD 20771

Vytenis M. Vasylivnas
Room 37-675
M. I. T.
Cambridge, Mass. 02139

D. Venkatesan
Dept. of Physics
University of Calgary
Calgary, Alberta T2N1N4
CANADA

James I. Vette
Code 601
NASA/GSFC
Greenbelt, MD 20771

Giorgio Villoresi
Laboratorio Di Ricerca E
Tecnologia
Per Lo Studio Del Plasma
Nello Spazio
C.P. No. 27, 00044 Frascati
(Roma) ITALY

R. Vogt
Calif. Institute of Tech.
Downs Laboratory of Physics
220-47
Pasadena, CA 91125

H. Volk
Max Planck Institut
Fur Kernphysik
69 Heidelberg 1
Postfach 103980
GERMANY

Tycho Von Rosenvinge
Code 661
NASA/GSFC
Greenbelt, MD 20771

Hugo D. Wahlquist
Bldg. 183-601
Caltech - JPL
4800 Oak Grove Drive
Pasadena, CA 91103

Peter Wasilewski
Code 691.2
NASA/GSFC
Greenbelt, MD 20771

Katherine Watts
Code 664
NASA/GSFC
Greenbelt, MD 20771

William R. Webber
Physics Dept.
Univ. of New Hampshire
Durham, NH 03824

Charles Wende
Code 601
NASA/GSFC
Greenbelt, MD 20771

Y. C. Whang
Dept. Aerospace &
Atmospheric Sciences
Catholic Univ. of America
Washington, DC 20064

List of Participants (continued)

G. Wibberenz
Institut Fur Kernphysik
Olshausen St. 40
2300, Kiel
WEST GERMANY

John M. Wilcox
Institute for Plasma Research
Via CRESPI
Stanford University
Stanford, CA 94305

Klaus Wilhelm
Max Planck Institut
3411 Katlenburg
Lindau 3
GERMANY

Donald J. Williams, Director
NOAA/Space Environment Lab., R43
Boulder, CO 80302

Richard Woo
Jet Propulsion Laboratory
MS 238/737
4800 Oak Grove Drive
Pasadena, CA 91103

Bruce E. Woodgate
Code 683
NASA/GSFC
Greenbelt, MD 20771

Shi Tsan Wu
Univ. of Alabama
P.O. Box 1247
Huntsville, Alabama 35807

Herbert A. Zook
1703 Bowline
Houston, TX 77058